The Effect of Plenum Configuration on the Performance of Air-Cooled Heat Exchangers

Carlos Antonio Salta

Thesis presented in partial fulfilment of the requirements for the degree of
Master of Mechanical Engineering at the University of Stellenbosch.

Thesis Supervisor : Prof. D. G. Kröger

Department of Mechanical Engineering
University of Stellenbosch
January 1995

Declaration

I, Carlos Antonio Salta, the undersigned hereby declare that the work contained in this thesis is my own original work and has not previously, in its entirety or in part, been submitted at any university for a degree.

17...... day of ....February........ 1995

Abstract

The main objective of this study is to determine the effect of plenum configuration on the performance of an air-cooled heat exchanger (particularly the fan system's operating point). Various plenum configurations, ranging from simple box-shaped plenums to plenums incorporating round-to-rectangular transition pieces, are tested for a normal flow heat exchanger, a delta heat exchanger and an experimental compact heat exchanger referred to as a double delta heat exchanger. The performance of the various heat exchangers relative to each other is also evaluated. The most important conclusions are as follows :

The plenum losses (and hence the fan system performance) of a normal flow heat exchanger having a box-shaped plenum are not very sensitive to plenum length. However, a minimum plenum length of 0.4 fan diameters is advised. The plenum losses occurring in the abovementioned fan system result in approximately 28% of the kinetic energy introduced by the fan being dissipated within the plenum. It is also shown that in a well designed air-cooled heat exchanger the reduction in thermal efficiency due to a distortion of the air velocity distribution through it, is small.

For the case of a delta heat exchanger system, the plenum losses result in approximately 70% of the kinetic energy introduced by the fan being dissipated within the plenum. Plenum losses occurring within a double delta heat exchanger system result in approximately 95% of the kinetic energy being lost. In both cases the incorporation of a round-to-round diffuser in the plenum configuration results in a decrease in plenum losses and hence a noticeable increase in the fan system performance. The incorporation of a round-to-rectangular diffuser in the plenum configuration also leads to a decrease in the plenum losses. However, due to the poor static pressure recovery characteristics of the round-to-rectangular diffuser, the increase in the fan system performance is not as large as that achieved with a round-to-round diffuser.

Keywords : Plenum, air-cooled heat exchanger, fan, fan system.

Opsomming

Die hoofdoel van hierdie ondersoek is om die invloed van die plenum konfigurasie op die vermoë van 'n lugverkoelde warmteuitruiler (veral op die waaierstelsel se bedryfspunt) te bepaal. Verskillende plenum konfigurasies, van eenvoudige reghoekige plenums tot dié wat rond-tot-reghoekige oorgangstukke insluit, word getoets vir 'n normaal-vloei warmteuitruiler, 'n delta warmteuitruiler en 'n dubbel-delta warmteuitruiler. Die werkverrigting van die verskillende warmteuitruilers word ook met mekaar vergelyk. Die belangrikste gevolgtrekkings is die volgende :

Die plenumverliese (en dus die waaierstelsel se werkverrigting) van 'n normaal-vloei wartmeuitruiler met 'n reghoekige plenum is nie baie sensitief vir plenumlengte nie. 'n Minimum plenumlengte van 0.4 waaier deursnitte word egter aanbeveel. Die plenumverliese wat voorkom in bogenoemde waaierstelsel veroorsaak dat ongeveer 28% van die kinetiese energie wat deur die waaier opgewek word, verkwis word binne in die plenum. Dit word ook getoon dat vir 'n goed-ontwerpte lugverkoelde warmteuitruiler die afname in termiese doeltreffendheid as gevolg van 'n distorsie in die lug snelheidsverdeling deur die wamteruitruiler, klein is.

Met 'n delta warmteuitruiler word ongeveer 70% van die kinetiese energie wat deur die waaier opgewek word, weens plenumverliese verkwis. Vir die geval van 'n dubbel-delta konfigurasie veroorsaak plenumverliese dat bykans 95% van die kinetiese energie verkwis word. In beide gevalle veroorsaak die insluiting van 'n rond-tot-rond diffusor in die plenumopstelling 'n afname in plenumverliese en gevolglik 'n merkbare toename in waaierstelselwerkverrigting. Die insluiting van 'n rond-tot-reghoekige diffusor in die plenum lei ook na 'n afname in plenumverliese. Weens die swak statiese drukherwinnings eienskappe van die rond-tot-reghoekige diffusor is die toename in waaiersteselwerkverigting egter nie so groot as die van die rond-tot-rond diffusor nie.

Sleutelwoorde : Plenum, lugverkoelde warmteuitruiler, waaier, waaierstelsel.

Acknowledgements

The author wishes to express his sincere gratitude towards the following persons and institutions for their assistance and/or contributions during the course of this study :

- The Foundation for Research and Development and the Water Research Commision for financial support in the form of bursaries.
- Prof. D. G. Kröger for his constant guidance, assistance and insight as promoter.
- Kobus Zietsman for his help with the assembly of the apparatus, practical insight and generally helpful nature.

Contents

Declaration ... i

Abstract ... ii

Opsomming ... iii

Acknowledgements ... iv

Contents ... v

Nomenclature ... ix

1. Introduction ... 1.1

2. Experimental Equipment

2.1. Fan Testing Facility ... 2.1

2.2 Instrumentation ... 2.3

2.3 The Fan ... 2.4

2.4 Heat Exchangers ... 2.4

2.5 Diffusers ... 2.7

3. Normal Flow Heat Exchanger

3.1 Experimental Equipment ... 3.1

3.2 Experimental Procedure ... 3.2

3.3 Experimental and Calculated Results ... 3.3

3.4 Discussion ... 3.5

4. Delta Heat Exchanger

4.1 Experimental Equipment........ 4.1
4.2 Experimental Procedure........ 4.3
4.3 Experimental and Calculated Results........ 4.4
4.4 Discussion........ 4.8

5. Double Delta Heat Exchanger

5.1 Experimental Equipment........ 5.1
5.2 Experimental Procedure........ 5.4
5.3 Experimental and Calculated Results........ 5.5
5.4 Discussion........ 5.9

6. Conclusions and Recommendations

6.1 Conclusions........ 6.1
6.2 Recommendations........ 6.4

References........ R.1

A. Experimental and Calculated Results for Normal Flow Heat Exchanger Tests........ A.1

B. Experimental and Calculated Results for Delta Heat Exchanger Tests........ B.1

C. Experimental and Calculated Results for Double Delta Heat Exchanger Tests........ C.1

D. Fan and Diffuser Characteristics

D.1 S-fan Characteristics D.2

D.2 S-fan with Round-to-Round Diffuser D.13

D.3 S-fan with Round-to-Rectangular Diffuser D.25

E. K-values of Heat Exchangers

E.1 K-values of Normal Flow Heat Exchanger E.2

E.2 K-values of Delta Heat Exchanger E.7

E.3 K-values of Double Delta Heat Exchanger E.18

F. Sample Calculations

F.1 Fan and Fan System Characteristic Calculations F.2

F.2 Heat Transfer Rate in a Normal Flow Heat Exchanger F.6

G. Calibration of Instrumentation

G.1 Calibration of the Pressure Transducers G.2

G.2 Calibration of the Torque Transducer G.4

G.3 Calibration of the Propeller Anemometers G.6

Nomenclature

Symbols

A	Area	[m^2]
c_p	Specific heat capacity at constant pressure	[J/kg K]
c_{pr}	Static pressure recovery coefficient	[-]
d	Diameter	[m]
E	Voltage	[V]
e	Surface effectiveness	[-]
G	Mass velocity	[kg/m^2s]
g	Gravitational acceleration	[m/s^2]
h	Heat transfer coefficient	[W/m^2 K]
K	Pressure loss coefficient	[-]
k	Thermal conductivity	[W/m K]
L	Length	[m]
M	Mass	[kg]
m	Mass flow rate	[kg/s]
N	Rotational speed	[rpm]
n	Number	[-]
P	Pitch	[m]
P	Power consumption	[W]
p	Pressure	[Pa]
Q	Heat transfer rate	[W]
R	Universal gas constant	[J/kg K]
T	Temperature	[K]
T	Torque	[N.m]

t	Thickness	[m]
U	Overall heat transfer coefficient	[W/m^2 K]
V	Volume flow rate	[m^3/s]
v	Velocity	[m/s]
x	Plenum lengths	[m]

Greek Symbols

α	Flow coefficient	[-]
α	Kinetic energy coefficient	[-]
ε	Expansibility factor	[-]
ε	NTU effectiveness	[-]
Δ	Differential	[-]
η	Efficiency	[-]
μ	Dynamic viscosity	[Ns/m^2]
ρ	Density	[kg/m^3]
θ	Semi-apex angle	[°]
θ_m	Mean angle of attack	[°]

Subscripts

a	Air or air-side area
actual	Actual static pressure differential
atm	Atmospheric
amb	Ambient
avg	Average
b	Bundle

bar	Barometric
bell	Bellmouth
c	Condensate, contraction or minimum flow area
D	Diffuser
d	Dynamic pressure
dj	Downstream jetting
duct	Rectangular duct
e	Exit
F	Fan
f	Fin or frictional
fr	Frontal
h	Hydraulic
he	Heat exchanger
i	Inlet
iθ	Inlet losses due to oblique flow
id	Ideal
ideal	Ideal
o	Outlet or outside
l	Longitudinal
pl	Plenum
r	Root or rows
S	System
s	Static pressure or steam process duct
sett	Settling chamber
sys	System operating point
t	Tip or total pressure or tube length
tot	Total

tr	Transverse rows
uniform	Uniform velocity distribution
w	Wet bulb
x	Axial
θ	Oblique flow conditions

Groups

Pr	Prandtl number	[-]
Re	Reynolds number	[-]
Ry	Characterisitic flow parameter	[m^{-1}]

1. Introduction

Forced draught air-cooled heat exchangers (ACHE's) as found in the petro-chemical, process and power industries use axial flows fans to force air over finned tube bundles. There are predominantly two main configurations for forced draught ACHE's viz. the normal flow heat exchanger and the delta (or A-frame) heat exchanger. In the normal flow heat exchanger, the finned tube bundles are mounted perpendicular to the impeller shaft of the fan (as shown in figure 1.1). In the delta heat exchanger the tube bundles are placed so that they form an oblique angle relative to the impeller shaft of the fan.

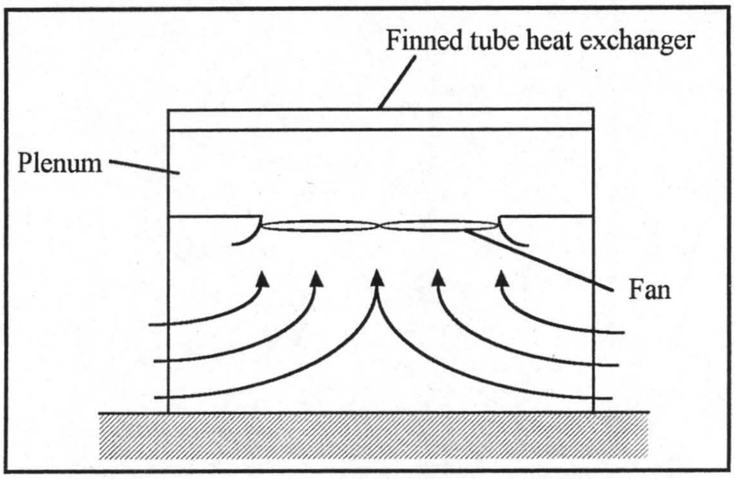

Figure 1.1 : Normal flow heat exchanger.

The section of ducting between the fan outlet and the heat exchanger inlet is referred to as the plenum. Plenum configurations range from being quite simple (box-shaped plenums with rectangular cross sections) to quite complex (round-to-rectangular transitions pieces between the fan and the finned tube bundles). The configuration of the plenum affects not only the velocity distribution at the inlet to the tube bundles but also the pressure losses that occur within the plenum and thus the fan system (fan, plenum and heat exchanger) performance. By decreasing the pressure losses that occur within the plenum, the fan system's operating point (the volume flow rate at which the fan system operates) can be increased and thus the cooling capacity of the ACHE can be increased using the same fan configuration.

When designing the ACHE, the fan selection is based upon matching the fan static pressure rise characteristics (as determined using certain standards e.g. BS 848) to the empirical pressure loss correlations for the various components present in the system. The operating point (volumetric flow rate) of the fan system is calculated by determining the intercept between the fan static pressure rise curve and the pressure drop across the heat exchanger. This method of predicting the fan system's operating point thus assumes that all of the kinetic energy introduced by the fan rotor to the plenum is dissipated within the plenum.

Research conducted on normal flow heat exchangers and specifically on the plenums of normal flow heat exchangers include work by Lambert et al [72LA1], Turner [75TU1], Russel and Berryman [88RU1] and Beiler[91BE1]. Lambert et al [72LA1] concerned themselves with the flow characteristics within a box-shaped plenum having a square cross-section and found that a central core of rotating air exists which expands from the inlet to reattach within the plenum and then continues to move upwards and out of the plenum. Turner [75TU1] concluded much the same in tests conducted with a box-shaped plenum having a rectangular cross-section. Russel and Berryman [88RU1] collated data on plenum losses from various sources. Beiler[91BE1] conducted tests on a normal flow heat exchanger having a round-to-rectangular plenum and found that a non-uniform air flow distribution, due to airflow distortions caused by the fan, exists at the tube bundle inlet. Furthermore, he found that approximately 63% of the kinetic energy leaving the fan is dissipated within the plenum. It should be noted that Beiler employs a round-to-rectangular type of diffuser having a relatively high mean expansion angle.

Research conducted on delta heat exchangers includes work by Venter [90VE1] and Van Aarde and Kröger [93VA1]. Venter [90VE1] compared theoretically and experimentally determined system effects of individual components, as well as the combination of different components, within delta plenums. He found good agreement between the predicted and actual fan system's operating point (volumetric flow rate) when assuming all of the kinetic energy introduced by the fan is dissipated within the plenum. Van Aarde and Kröger [93VA1] provide correlations to predict the total oblique flow loss coefficient for delta heat exchangers given the geometry of the delta heat exchanger and the isothermal heat exchanger loss coefficient under normal flow conditions.

It is the objective of this study to determine the effect of plenum configuration on plenum losses and hence on the fan system performance (in particular the fan system's operating point). Furthermore, the accuracy of the assumption that all of the kinetic energy introduced by the fan rotor is dissipated within the plenum will be investigated.

Various plenum configurations will be tested for a normal flow heat exchanger, a delta heat exchanger and a new experimental compact heat exchanger referred to as a double delta heat exchanger. Plenum configurations that will be tested include box-shaped plenums, plenums incorporating round-to-round diffusers and plenums incorporating round-to-rectangular diffusers.

For the case of the normal flow heat exchanger, a theoretical analysis will be performed to determine what effect the distorted velocity profile through the finned tube heat exchanger has on the thermal performance of the heat exchanger.

A secondary objective will be to compare the fan system performances of the normal flow heat exchanger, the delta heat exchanger and the double delta heat exchanger relative to each other.

2. Experimental Equipment

2.1. Fan Testing Facility

To evaluate the performance characteristics of different plenum and heat exchanger configurations use was made of an existing fan test facility.The fan testing facility, designed according BS 848 specifications, is shown schematically in figure 2.1.1.

A calibrated inlet bellmouth is used to determine the volumetric flow rate of air through the system. The inlet diameter of the bellmouth section in which the static pressure tappings are installed is 1.008 m. Venter [90VE1] calibrated the bellmouth against pitot static tube traverses performed at different volumetric flow rates.

Immediately downstream of the bellmouth is the throttling device, consisting of a set of variable angle louvres. Two flow straightners are located on either side of the throttling device. To accommodate the throttling device, two transformation pieces convert the round duct to square and back to round.

An auxiliary fan is installed downstream of the throttling device and is used to overcome pressure losses due to the different components in the test facility. The auxiliary fan has an outer diameter of 1.54 m and its six blades are set at 24°. An 11 kW electric motor powers the fan with the fan rotor directly attached to the motor's shaft. Two transformation pieces are placed on either side of the auxiliary fan to enlarge the duct diameter from 1.5 m to 1.55 m and then back to 1.5 m in order to accommodate the auxiliary fan.

The last transformation piece is a diffuser. A set of guide vanes are installed at the exit of the diffuser in order to distribute the air flow more evenly as it enters the settling chamber.

The settling chamber (having inside dimensions of 4 m x 4 m x 7 m) has a set of three stainless steel mesh screens installed at the locations specified by BS 848. Two air-tight access doors on either side of the screens ensure access to the settling chamber. The outlet of the settling chamber is fitted with an elliptical bellmouth having an inside dimension of 1.542 m.

The hydraulic motor used to power the test fan is mounted inside the settling chamber. The motor has a maximum power output of 10 kW at 750 rpm. The motor's rotational speed can be varied by changing the flow rate of the hydraulic oil.

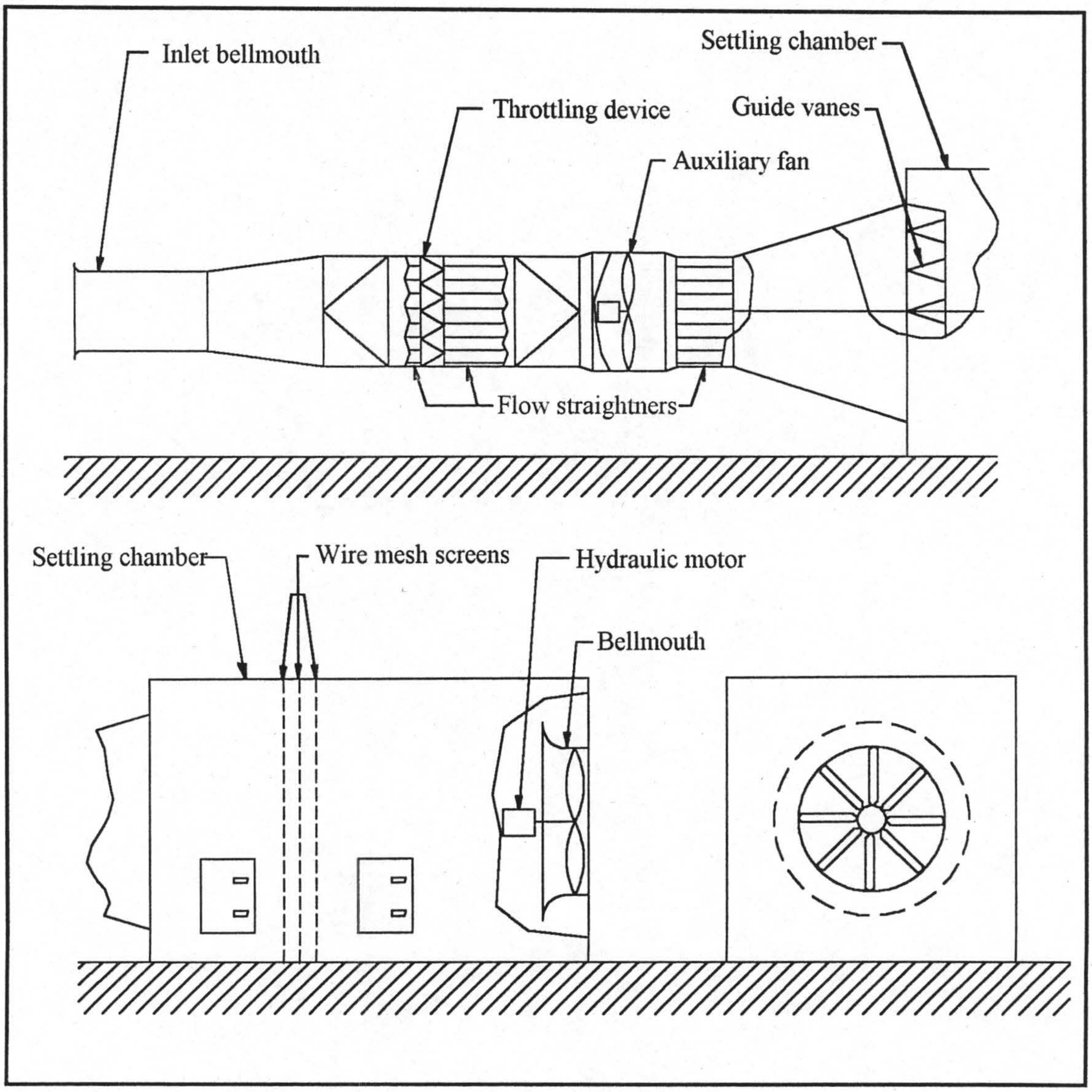

Figure 2.1.1 : The fan testing facility.

2.2 Instrumentation

For the purpose of determining fan and system characteristics, it is necessary to measure four values. They are : the pressure drop over the inlet bellmouth, the pressure differential between the settling chamber and atmosphere, the torque transmitted by the hydraulic motor and the rotational speed of the fan.

Höttinger type PD1 inductive pressure transducers, having a range of -1000 and 1000 Pa, are used to measure the pressure drop over the inlet bellmouth and the pressure differential between the settling chamber and atmosphere. The torque transmitted by the hydraulic motor is measured using a Höttinger type T2 torque transducer, having a range of -500 and 500 Nm. The torque transducer is a resistive full bridge instrument. All three transducers are connected to a Höttinger KWS 3073 bridge amplifier which amplifies the input signals to give output signals between -10 and 10 V. The calibration of the above instruments is discussed in Appendix G.

The rotational speed of the fan is measured using a magnetic speed pick up sensor connected to a frequency counter. As well as having a digital display, the frequency counter has a linear voltage output which can be read by a computer.

Output voltages from the bridge amplifier as well as the linear voltage output from the frequency counter are read by an analogue-to-digital converter card mounted in an Olivetti M21 personal computer. Real time input voltage readings are displayed in graphical form on the computer's screen. Once steady state conditions have been achieved, 3000 data points per channel are sampled at a sampling frequency of 100 Hz. The average of these data points is saved to disk.

Seven propeller anemometers mounted on a 1.9 m staff are used to perform axial velocity traverses at the heat exchanger exit. The anemometers have a linear voltage output and are also connected via the analogue-to-digital converter to the computer. When measuring the velocity profile, 1000 data points per anemometer are sampled at a sampling frequency of 100 Hz. The average of these data points is saved to disk.

Ambient temperature is measured using a mercury thermometer having an accuracy level of 0.5 °C. A mercury barometer having an accuracy level 0.05 mm Hg is used to measure ambient pressure.

2.3 The Fan

The eight-bladed variable pitch axial flow fan (referred to as the S-fan from hereon) used for all the tests conducted is shown in figure 2.3.1. The fan performance characteristics for blade angles varying between 10° and 26° are given in Appendix D.

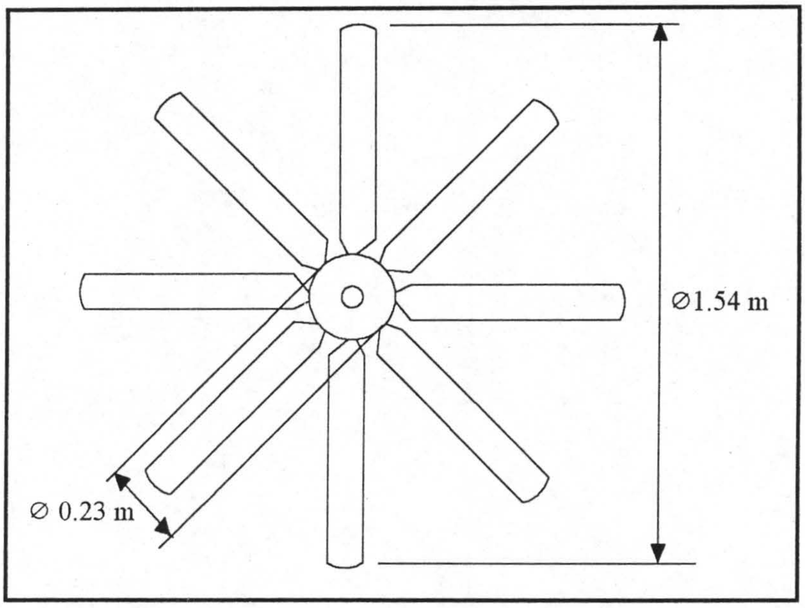

Figure 2.3.1 : The S-fan.

2.4 Heat Exchangers

Three different types of heat exchanger configurations were tested, viz. : normal flow, delta and double delta. The three types of heat exchanger configuration are shown in figure 2.4.1 All three made use of the same 1.6 m long elliptical tubes with wound on galvanised elliptical fins. The finned tubes had the following geometrical dimensions :

Tube length	L_t	= 1.6 m
Transversal tube pitch	P_t	= 36 mm
Fin pitch	P_f	= 2.5 mm
Fin thickness	t_f	= 0.48 mm
Tube inside diameter	d_i	= 33 x 11 mm
Tube outside diameter	d_o	= 36 x 14 mm
Fin diameter	d_f	= 54 x 34 mm

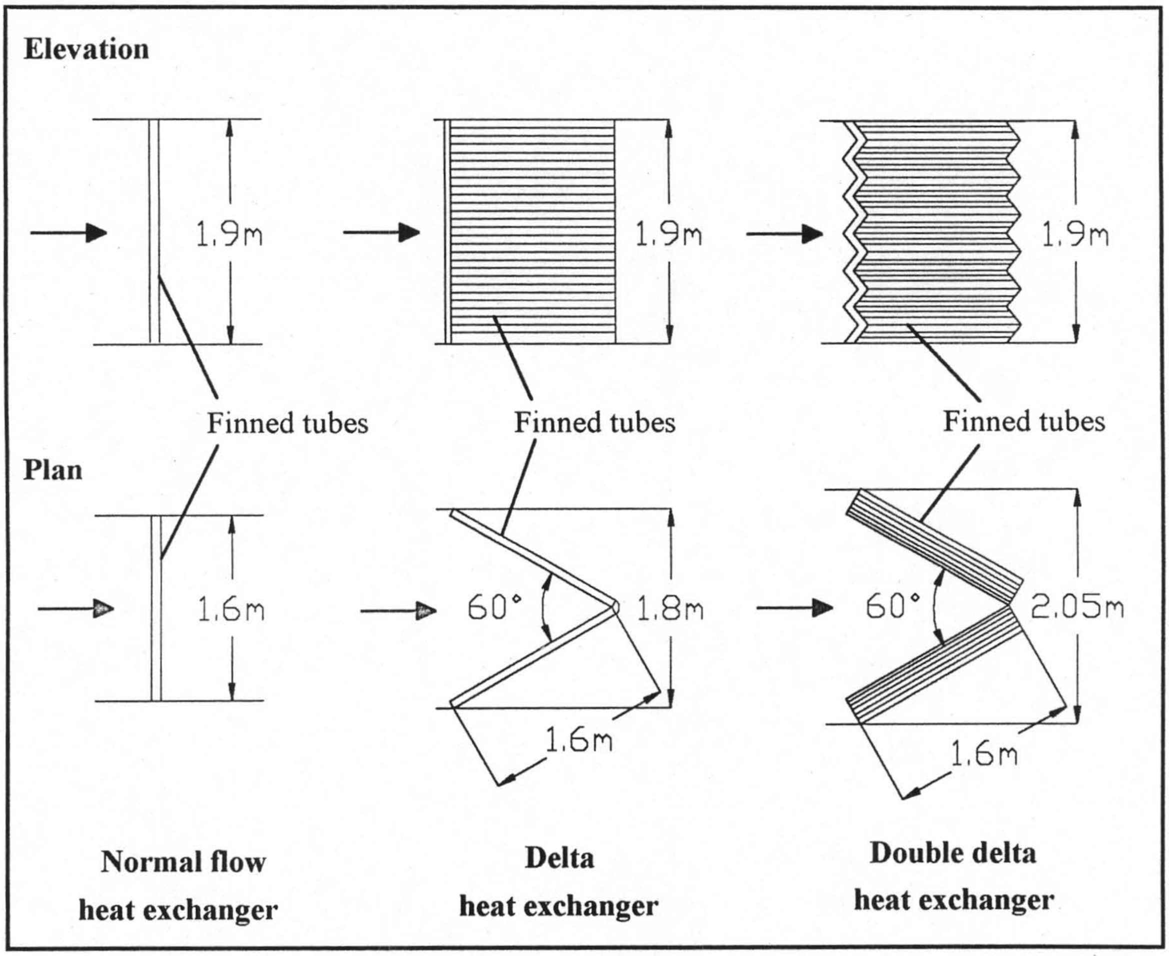

Figure 2.4.1 : The normal flow, delta and double delta heat exchanger.

The normal flow heat exchanger consists of one row of finned tubes having 54 tubes. The delta heat exchanger, which consists of two normal flow heat exchangers placed so as to form two sides of an equilateral triangle, has 108 finned tubes. The double delta is a further development on the delta heat exchanger. Instead of using normal flow heat exchangers to form the two sides of the triangle, a heat exchanger consisting of six smaller (secondary) deltas is used. Figure 2.4.2 shows a detail sketch of a secondary delta. The apex angle of these secondary deltas is also 60°. There are 14 finned tubes per secondary delta (each side of the delta has 7 finned tubes and is thus 252 mm wide) and hence the double delta has a total of 168 finned tubes.

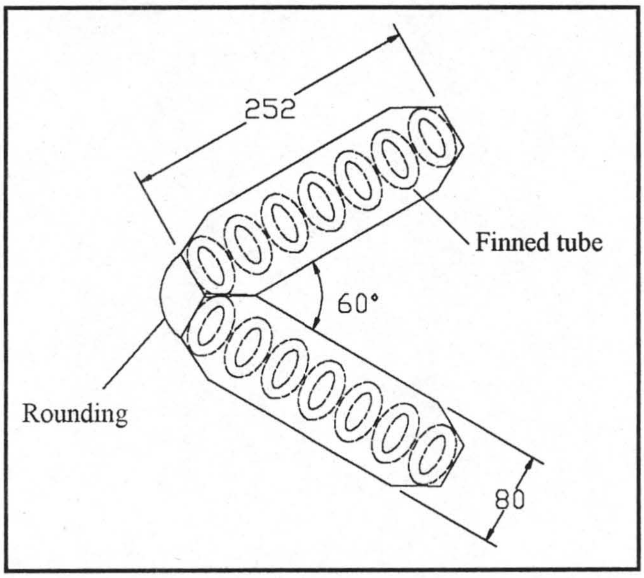

Figure 2.4.2 : Detail sketch of a secondary delta of the double delta heat exchanger.

From the above it follows that the surface area of the delta heat exchanger is double that of the normal flow heat exchanger and that the surface area of double delta heat exchanger is exactly 1.55 times that of the delta.

Lengths of pine quarter rounds, placed upstream between the finned tube rows (as shown in figure 2.4.3), are used to alter the flow resistance of the heat exchanger in order to simulate the flow resistance of a heat exchanger having four rows of finned tubes. The loss coefficients (K-values) of each of the heat exchangers are determined experimentally as described in Appendix E.

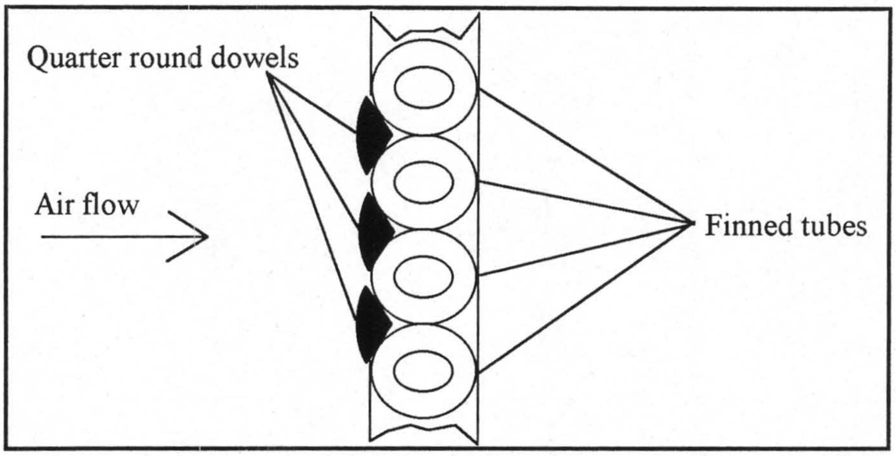

Figure 2.4.3 : The placement of pine quarter-round dowels between the finned tubes.

It must be noted that the test heat exchanger bundles are not operated in a heat transfer mode but are merely employed to evaluate fan system characteristics.

2.5 Diffusers

Two types of diffusers are used in the tests conducted, viz : a round-to round diffuser and a round-to-rectangular diffuser. Both types and their dimensions are shown in figure 2.5.1.

The round-to-round diffuser (having an included angle of 14°) is designed in accordance with guide lines given by Ventilatoren Stork Hengelo [85ST1] which specify that the included angle should lie between 12° and 17°. The round-to-round diffuser is thus representative of diffusers used in air-cooled heat exchangers in industry.

As the round-to-rectangular diffuser is intended for use exclusively with the double delta heat exchanger, its dimensions are mainly determined by the geometry of the fan and the double delta heat exchanger, the only variable being the length of the diffuser. In an effort to further improve the performance of the round-to-rectangular diffuser, two other flow devices were constructed specifically for use with round-to-rectangular diffuser viz : the flow director and the flow straightner. The purpose of the flow director (shown in figure

2.5.2) is to guide the airflow smoothly from the fan outlet to the secondary deltas of the double delta heat exchanger. The flow straightner (shown in figure 2.5.3) is used to remove the strong rotational component in the airflow exiting the fan.

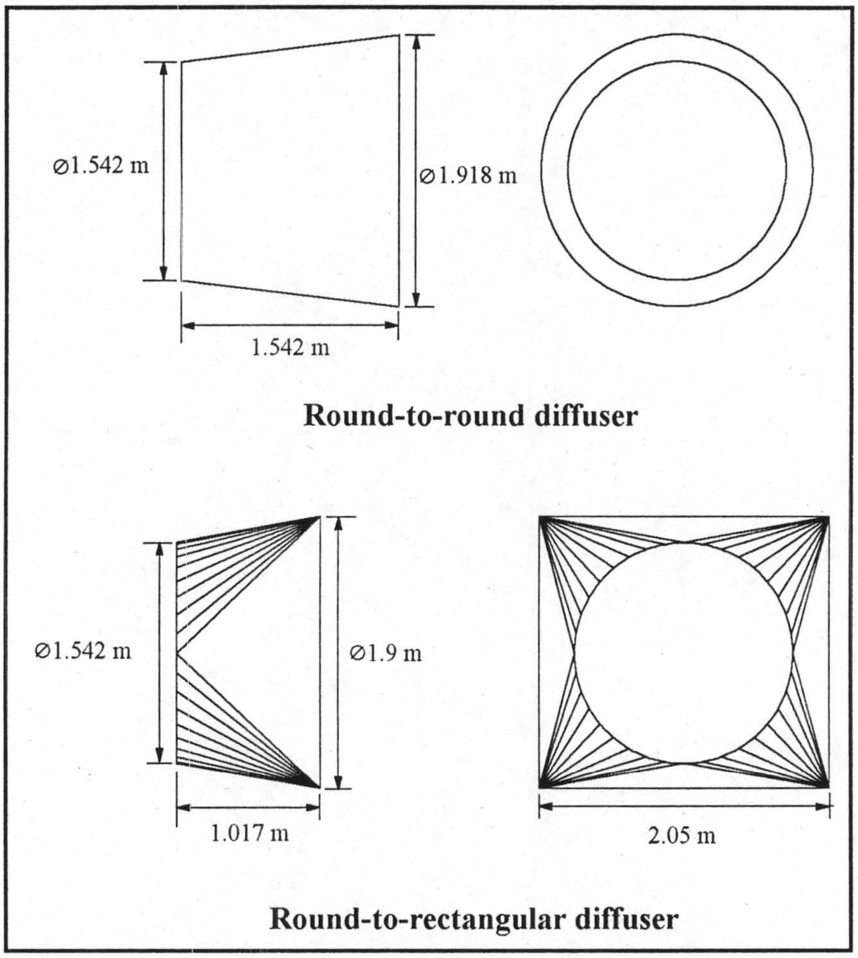

Round-to-round diffuser

Round-to-rectangular diffuser

Figure 2.5.1 : Round-to-round and round-to-rectangular diffuser.

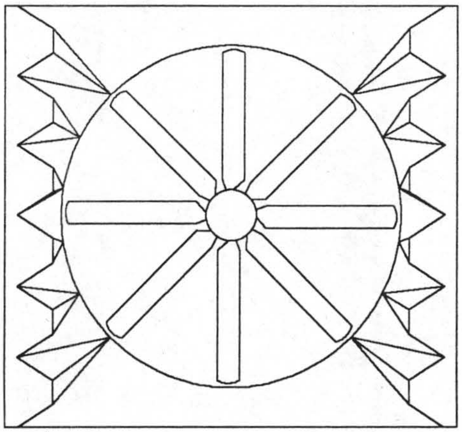

Figure 2.5.2 : The flow director.

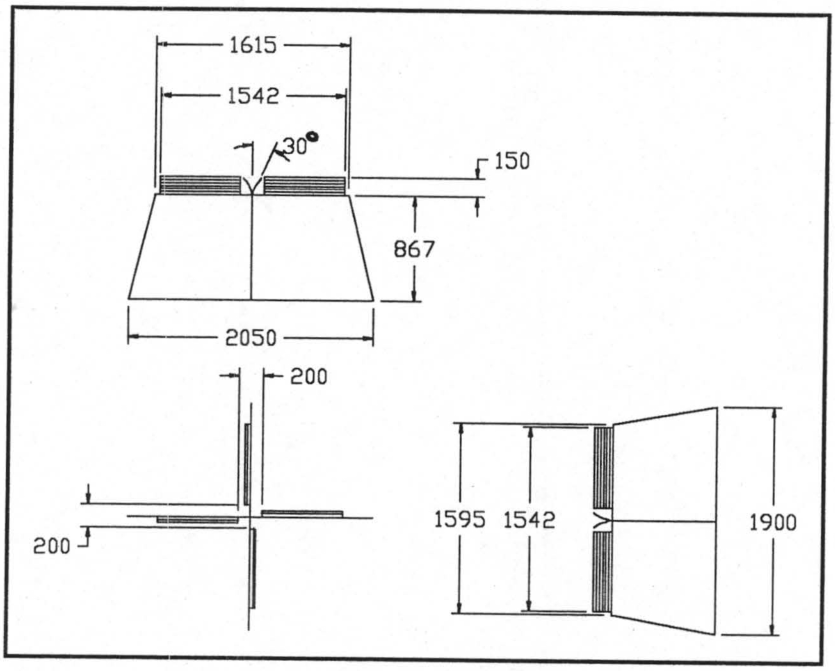

Figure 2.5.3 : The flow straightner.

3. Normal Flow Heat Exchangers

3.1 Experimental Equipment

A rectangular duct (plenum) having a cross sectional area of 1.6 m x 1.9 m is attached to the downstream or outlet side of the S-fan which is mounted in the settling chamber of the code tunnel. A normal flow finned tube heat exchanger having a frontal area that corresponds to the cross-sectional dimensions of the duct is placed in the plenum as shown in figure 3.1.1. By varying the distance between the downstream edge of the fan blade and the heat exchanger, the plenum length (x) is varied.

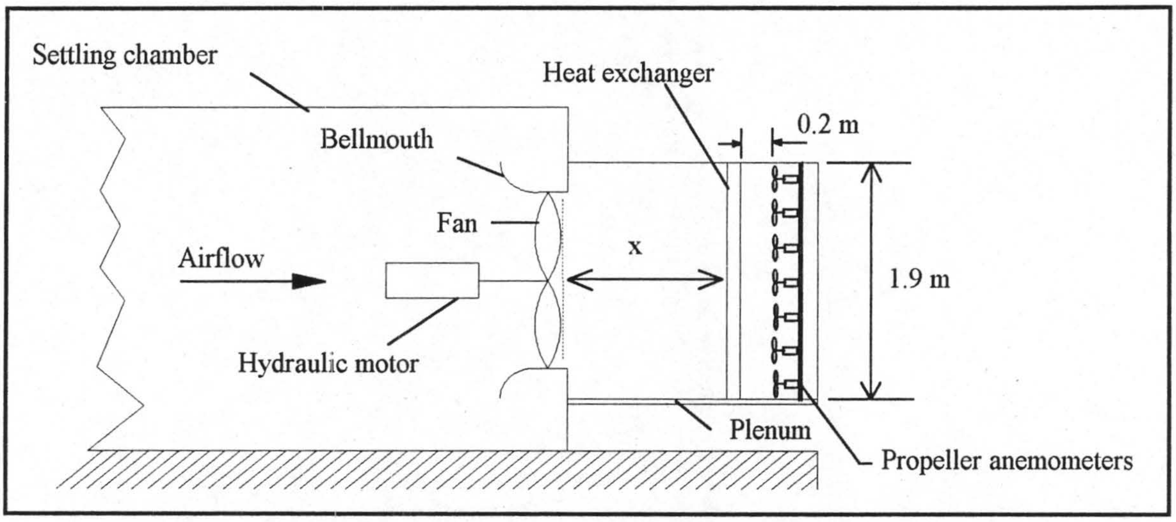

Figure 3.1.1 : Experimental set-up for normal flow heat exchanger tests.

The normal flow heat exchanger consists of one row of finned tubes having 54 tubes. To alter the flow resistance of the heat exchanger, lengths of pine quarter rounds are placed upstream between the finned tubes (as shown in figure 2.4.2). All tests are conducted using a fan blade angle of 10°. This value was chosen such that the fan would operate near its point of maximum efficiency in the presence of the normal flow heat exchanger.A fan speed of 750 rpm is used in order to obtain a tip speed of 60 m/s. This is in keeping with conventional design practice which advises a fan tip speed of 60 m/s or less in order to limit the noise levels generated by the fan.

3.2 Experimental Procedure

The fan system (fan, plenum and heat exchanger) characteristics are determined for the following plenum lengths : 0.05 m, 0.3 m, 0.57 m, 1.08 m and 1.56 m. The "operating point" of the system is defined as the volume flow rate for which the system's static pressure rise is zero and represents the volumetric flow rate that would be achieved through the system were it to be constructed and operated under normal conditions (i.e. in the absence of the auxiliary fan and the other upstream flow devices incorporated in the fan testing facility). As the cooling capacity of an ACHE is directly proportional to the volumetric flow rate of the fan system, the system operating point is a dominant parameter when measuring the performance of an ACHE. The system operating point for each of the configurations tested is determined from the system characteristics by interpolating between data points for which the system static pressure rise are just above and below 0 Pa..

In addition to determining the system characteristic for each of these plenum configurations, a velocity traverse is performed approximately 200 mm downstream from the heat exchanger bundle while the fan is operating at the system's operating point. This is done by manually traversing a 1.9 m staff with propeller anemometers attached at various points (as shown in figure 3.1.1) across the width of the heat exchanger. The distance of 200 mm is a compromise value selected so as to minimise the effect of small scale flow distortions immediately downstream of the heat exchanger but not so far as to allow substantial flow mixing to occur. The grid of the velocity traverse is shown in figure A1.1. The propeller anemometers were calibrated beforehand. Appendix G demonstrates the calibration process as well as listing the calibration constants.

An additional test without a heat exchanger in the plenum is performed in order to quantify the amount of pressure recovery obtained from attaching the rectangular duct to the outlet of the fan. Certain tests are repeated in order to determine the repeatability of the results obtained.

3.3 Experimental and Calculated Results

Tables A1.1 to A1.8 list the experimental readings taken to determine the system characteristics for various plenum lengths. The system characteristics calculated from these readings are listed in tables A2.1 to A2.8 and are shown graphically in figures A2.1 and A2.2. Appendix F contains a sample calculation of how the system characteristics are determined.

Table 3.3.1 provides a summary of how the system's power requirements and operating point vary for each of the plenum lengths tested as determined from figures A2.1 and A2.2. Also listed in table 3.3.1 are two parameters which will be used to compare the normal flow, the delta and the double delta heat exchanger with each other viz. V_{sys}/P and V_{sys}/A_{he}. The former, V_{sys}/P, reflects the volumetric flow rate achieved per unit of fan power supplied to the system and hence provides a measure of the "economic efficiency" of the system. The lower the value of V_{sys}/P, the more power that has to be supplied to achieve the same system operating point (volume flow rate) and hence the higher the operating costs. As the cooling capacity of the system is directly related to the average velocity over the finned tubes, the ratio V_{sys}/A_{he} provides a measure of the cooling capacity of the system per unit heat exchanger area. For the normal flow heat exchange $A_{he} = 3.04\ m^2$.

Table 3.3.1 : System operating point and power requirement for various plenum lengths.

x (m)	**V_{sys}** (m^3/s)	**P** (kW)	**V_{sys} / P** ($m^3/s/kW$)	**V_{sys} / A_{he}** (m/s)
0.05	12.915	4.789	2.697	4.248
0.30	13.770	4.827	2.853	4.530
0.57	13.951	4.828	2.882	4.589
1.08	13.787	4.887	2.821	4.535
1.56	13.913	4.747	2.931	4.577

Figures A2.3 to A2.5 compare the system characteristics obtained with a rectangular duct attached to the outlet of the fan to the fan characteristics with a blade angle of 10°. Also shown in figure A2.4 is the static pressure drop characteristic of the normal flow heat exchanger system.

Conventional design practice matches the fan to the system by determining the intercept between the fan static pressure curve and the empirically determined static pressure loss over the heat exchanger as shown in figure A2.4. Using this method, the predicted (or expected) operating point of the normal flow heat exchanger system is 13.15 m^3/s. It must be noted that in determining the operating point in this way, it is implied that the kinetic energy introduced by the fan to the inlet of the plenum is dissipated in its entirety in the plenum. Furthermore, it is assumed that the outlet kinetic energy losses to atmosphere are negligible.

Tables A3.1 through to A3.6 list the velocity profile readings taken downstream of the heat exchanger and are shown in graphical form in figures A3.1 to A3.6. The relatively distorted velocity distribution is noted.

The kinetic energy after the heat exchanger lost to the atmosphere differs for the various plenum configurations. As can be seen from figures A3.1 and A3.5, the velocity distribution downstream of the heat exchanger varies between -0.76 m/s and 6.15 m/s for a plenum length of 0.05 m and between 2.03 m/s and 6.056 m/s for a plenum length of 1.08 m. In order to estimate the kinetic energy correctly, the kinetic energy coefficient is introduced :

$$\alpha = \frac{\int_A |\overline{v}|^2 \, \overline{v}.d\overline{A}}{v_{avg}^2 \int_A \overline{v}.d\overline{A}}$$

From tables A3.1 to A3.5, the values of the kinetic energy coefficient after the heat exchanger ,α_{he} (the flow is essentially axial thus $\alpha_{he} = \alpha_{he_x}$), for plenum lengths (x) of 0.05 m, 0.30 m, 0.57 m and 1.08 m are 1.312, 1.189, 1.149 and 1.107 respectively. With no heat exchanger in the plenum, the axial kinetic energy coefficient, α_x, is found to be

1.743 (determined from table A3.6). The actual kinetic energy coefficient is higher due to tangential and radial velocity components.

The high degree of distortion in the velocity distribution after the heat exchanger raises the question as to what effect this distortion has on the overall heat transfer rate from the heat exchanger to the air. Appendix F provides a sample calculation to illustrate as to how the total heat transfer rate from an arbitrary round finned tube heat exchanger to the air (Q_{tot}) and the heat transfer rate that would be achieved with a uniform velocity distribution and the same air mass flow rate ($Q_{uniform}$) can be calculated for the case of x = 1.08. The same procedure is used to determine Q_{tot} and $Q_{uniform}$ for the other plenum lengths tested. The results are listed in Table 3.3.2.

Table 3.3.2 : Calculated total heat flux and uniform heat flux for various plenum lengths.

x (m)	**Q_{tot} (W)**	**$Q_{uniform}$ (W)**	**% difference**
0.05	461261	466426	1.107
0.30	499380	501348	0.392
0.57	495555	499161	0.723
1.08	499566	501747	0.435

3.4 Discussion

Figure A2.1 shows that the fan shaft power (P) remains fairly constant for a given volume flow rate (V) as the plenum length (x) is increased. The largest fluctuations in P are approximately 4% and as such does not merit further attention.

It can be seen from table 3.3.1 that the operating point varies very little except when the plenum is very short (0.05 m). Assume that the ideal volume flow rate (V_{id}) is that flow rate at which the system would operate, were the heat exchanger sufficiently far away from the fan so as not to have any system effect on it. The ideal volume flow rate thus corresponds with the maximum volume flow rate possible through the fan system (fan, plenum and heat exchanger). From the above data it can be assumed that V_{id} is 13.96

m^3/s for this case as the highest volume flow rate measured was 13.95 m^3/s (for $x = 0.57$ m).

The above data is displayed in the non-dimensionalised form of system performance (V_{sys}/V_{id}) versus x/d_F (where d_F is the fan diameter) in figure 3.4.1. Also shown in the graph is a fitted exponential curve giving a general correlation between system performance and plenum length. It would appear from the graph that a plenum length of about $0.4d_F$ should be used to ensure maximum system performance of normal flow heat exchangers if $A_F/A_{he} = 0.61$. Russell and Berryman [88RU1] collate plenum loss data from Hart [78HA1] and Spiers [80SP1]. Due to insufficient information concerning the experimental set-ups used by Hart and Spiers, comparison between the data published by Russell and Berryman and the experimental results obtained during this project are inconclusive and are hence not shown in figure 3.4.1.

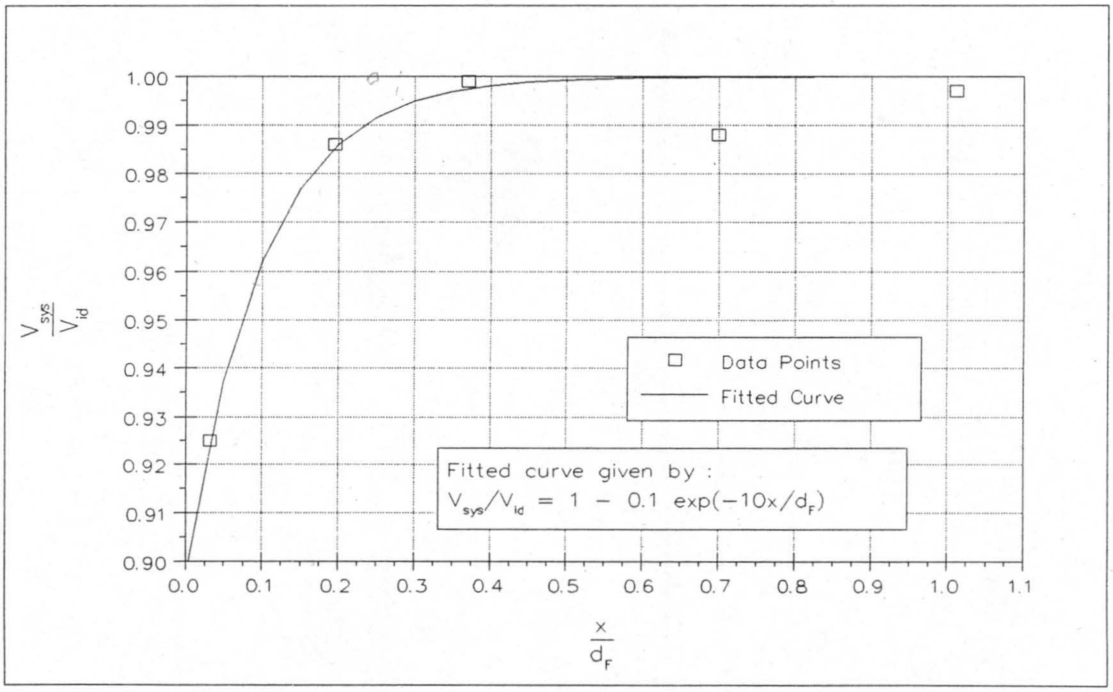

Fitted curve given by :

$V_{sys}/V_{id} = 1 - 0.1 \exp(-10x/d_F)$

Figure 3.4.1 : Effect of plenum length on system performance. ($A_F/A_{he} = 0.61$ and bell type inlet to fan)

It can be seen from table 3.3.1 that the average volume flow rate achieved per unit of fan power for the normal flow heat exchanger is 2.837 $m^3/s/kW$ and the average volume flow rate achieved per unit heat exchanger area is 4.496 m/s.

From figure A2.4 it can be seen that the predicted operating point of the system is 13.15 m^3/s. However, Table 3.3.1 shows that for $x \geq 0.3$ m ($x/d_F \geq 0.19$) the system operating point is greater than or equal to 13.77 m^3/s. This would indicate that there is a certain amount of pressure recovery occurring in the plenum.

If the case of $x = 0.57$ m is studied in further detail, it can be seen from figure A2.4 that at a volumetric flow rate of 13.951 m^3/s the static pressure rise over the fan (Δp_{s_F}) is 211.376 Pa and the static pressure drop over the heat exchanger ($\Delta p_{s_{he}}$) is 246.261 Pa. This would indicate that an increase of 34.885 Pa in the static pressure occurs within the plenum. The dynamic pressure head of the air just after leaving the fan is given by :

$$p_{d_F} = \alpha_F \cdot \frac{1}{2} \cdot \rho \cdot v_F^2$$

where

$$v_F = \frac{V_{sys}}{A_F} = \frac{13.951}{\pi \cdot 0.771^2} = 7.472 \text{ m/s}$$

Beiler [91BE1] shows that the kinetic energy coefficient at fan outlet (α_F) for a fan very similar to the S-fan with a free outlet (BS 848 type A test) is 1.8 at a volume flow rate of 18.5 m^3/s and 1.498 at a volume flow rate of 24 m^3/s. Due to a lack of relevant data, the above values will be used although it must be stressed that the values of the kinetic energy coefficient for a system incorporating a plenum may differ from the α_F for the case of a free outlet after the fan (as given above).

In calculating the fan dynamic pressure, it is assumed that α_F varies linearly between these two volume flow rates. Thus, for a volume flow rate of 13.951 m^3/s, $\alpha_F = 2.05$.

$$p_{d_F} = 2.05 \cdot \frac{1}{2} \cdot 1.2 \cdot 7.472^2 = 68.665 \text{ Pa}$$

The dynamic pressure head of the air just before it flows through the heat exchanger is given by :

$$p_{d_{he}} = \alpha_{he} \cdot \frac{1}{2} \cdot \rho \cdot v_{he}^2$$

where

$$v_{he} = \frac{V_{sys}}{A_{he.}} = \frac{13.951}{1.6 \cdot 1.9} = 4.589 \text{ m/s}$$

As mentioned previously, α_{he}= 1.149 for a plenum length of 0.57 m. Thus

$$p_{d_{he}} = 1.149 \cdot \frac{1}{2} \cdot 1.2 \cdot 4.589^2 = 14.518 \text{ Pa}$$

The static pressure upstream of the fan and downstream of the heat exchanger both equal atmospheric pressure. Thus under ideal circumstances, we have from Bernoulli that :

$$\Delta p_{s_F} + p_{d_F} = \Delta p_{s_{he}} + p_{d_{he}}$$
$$\Delta p_{s_{he}} - \Delta p_{s_F} = p_{d_F} - p_{d_{he}} = 68.665 - 14.518 = 54.147 \text{ Pa}$$

Thus, under ideal circumstances, the static pressure recovery within the plenum is 54.147 Pa. The actual static pressure recovery measured is 34.885 Pa. Hence, 34.885/68.665 = 50.8% of the dynamic pressure head leaving the fan is converted to static pressure head within the plenum. The diffuser efficiency is defined as follows

$$\eta_D = \frac{\Delta p_{s_{actual}}}{\Delta p_{s_{ideal}}} x100 \ \%$$

Since the actual static pressure recovery is 34.885 Pa and the ideal static pressure recovery is 54.147 Pa for this case, the diffuser efficiency of the plenum is

$$\eta_D = \frac{34.885}{54.147} x100 = 64.4\%$$

Taking the energy loss within the plenum into consideration, an energy balance between the fan outlet and the heat exchanger inlet (within the plenum) yields

$$\Delta p_{s_F} + p_{d_F} = \Delta p_{s_{he}} + p_{d_{he}} + K_{pl} \cdot \frac{\rho \cdot v_F^2}{2}$$

$$K_{pl} = \frac{\left(\Delta p_{s_F} + p_{d_F}\right) - \left(\Delta p_{s_{he}} + p_{d_{he}}\right)}{\frac{\rho \cdot v_F^2}{2}}$$

$$= \frac{(211.376 + 68.655) - (246.261 + 14.518)}{0.5 \cdot 1.2 \cdot 7.472^2}$$

$$= 0.575$$

where K_{pl} is the plenum loss coefficient. It should be noted that K_{pl} is based upon the reference area A_F (the area of the fan shroud). Furthermore, due to the fact that the actual values of α_F may differ for a fan exhausting into a plenum when compared with the free outlet case used here to determine p_{d_F}, the actual value of K_{pl} may differ from that calculated above.

This result indicates that (K_{pl}/α_F)x100 = (0.575/2.05)x100 = 28% of the kinetic energy leaving the fan is dissipated within the plenum. This strongly contradicts conventional design practice which assumes that all of the kinetic energy introduced by the fan is dissipated within the plenum.

The above tendencies of static pressure recovery within the plenum are not reflected in figure A2.4, which compares the system static pressure rise of the S-fan with the rectangular duct attached but with no heat exchanger present, to the fan static pressure rise characteristic of the S-fan. As can be seen from the graph, there is an increase in static pressure in both the low (0 m^3/s to 9 m^3/s) and the high (>15m^3/s) flow rate range. However, there is no discernible increase in static pressure in the medium flow rate range (9 m^3/s to 15 m^3/s) and it is in this range that the system (fan, plenum and heat exchanger) operates. This would seem to suggest that the normal flow heat exchanger has a fairly extensive system effect on the air flow within the plenum and that this effect works to the advantage of the system by causing considerable static pressure recovery within the plenum.

As can be seen from figure A2.3, the fan power consumption is slightly lower if the fan outlet is ducted. Due to the diffuser-like action of the rectangular ducting at the fan outlet, figure A2.5 shows a corresponding increase in static efficiency of the fan and plenum combination at higher volume flow rates. The static efficiency curve moves up and to the right on the graph of η_s versus V with the increased maximum efficiency of 64 % now being achieved at 17 m^3/s instead of 59% at 15 m^3/s. However ,as V_{id} for this system is 14 m^3/s it would seem to indicate that either a lower blade angle or a heat exchanger which has a lower pressure drop should be used if the system is to be operated at its maximum static efficiency.

Figures A3.1 through to A3.6 show the variation of the exit velocity profile as the normal flow heat exchanger is moved further away from the fan. The dead spot behind the hub of the fan is clearly visible when the heat exchanger is very close to the fan (figures A3.1 and A3.2). A certain amount of reverse flow is visible in these figures. Also noticeable is the low velocities in the corners of the heat exchanger. As the heat exchanger is moved further away (figures A3.3 to A3.5), the severity of the dead spot decreases and the corner velocities increase, thus the velocity profile tends to become flatter (as to be expected). This tendency is also reflected in the kinetic energy coefficient which decreases from 1.312 (for a plenum length of 0.05 m) to 1.107 (for a plenum length of 1.08 m).

The velocity distribution measured by Turner [75TU1] above a full-sized normal flow heat exchanger in a forced draught configuration having a $x/d_F = 0.5$ is shown in figure A3.7. This velocity distribution has the same general features as those shown in figures A3.1 to A3.5 : a dead spot downstream of the fan hub and low velocities in the corners.

Figure A3.6 shows the velocity distribution measured without a heat exchanger in the test section. The dead spot is noticeably larger in this figure than in any other. It would thus seem that the normal flow heat exchanger tends to flatten the velocity profile.

As can be seen from table 3.3.2, the flow maldistribution does not have too adverse an effect on the thermal performance of the heat exchanger (the largest decline in heat transfer rate is approximately 1.1 %). This is in general agreement with work done by Beiler [91BE1].

4. Delta Heat Exchanger

4.1 Experimental Equipment

A rectangular duct having a cross sectional area of 1.8 m x 1.9 m is used to house a delta heat exchanger having a frontal area corresponding to the cross-sectional area of the duct. The delta heat exchanger consists of two normal flow finned tube heat exchangers placed so as to form two sides of an equilateral triangle. To alter the flow resistance of the heat exchanger, lengths of pine quarter rounds are placed upstream between the finned tubes (as shown in figure 2.4.2).

The rectangular duct is attached either directly to the downstream (outlet) side of the S-fan, which is mounted in the settling chamber of the code tunnel, or downstream of the round-to-round diffuser which in turn is attached to the outlet of the S-fan. Figure 4.1.1 shows the two possibilities for mounting the rectangular duct. Furthermore, the side walls of the rectangular duct are removable thus enabling tests to be conducted with or without sides.

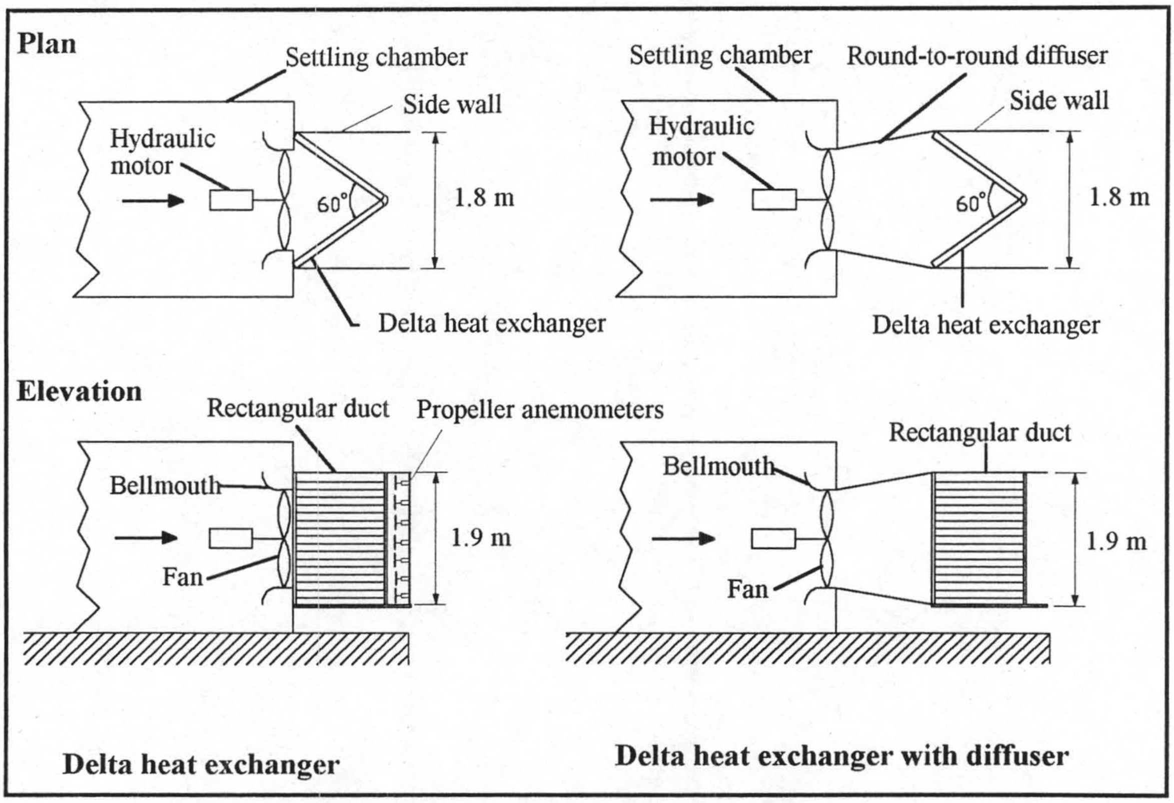

Figure 4.1.1 : Experimental set-up for delta heat exchanger tests.

The various delta heat exchanger configurations to be tested are shown in figure 4.1.2.

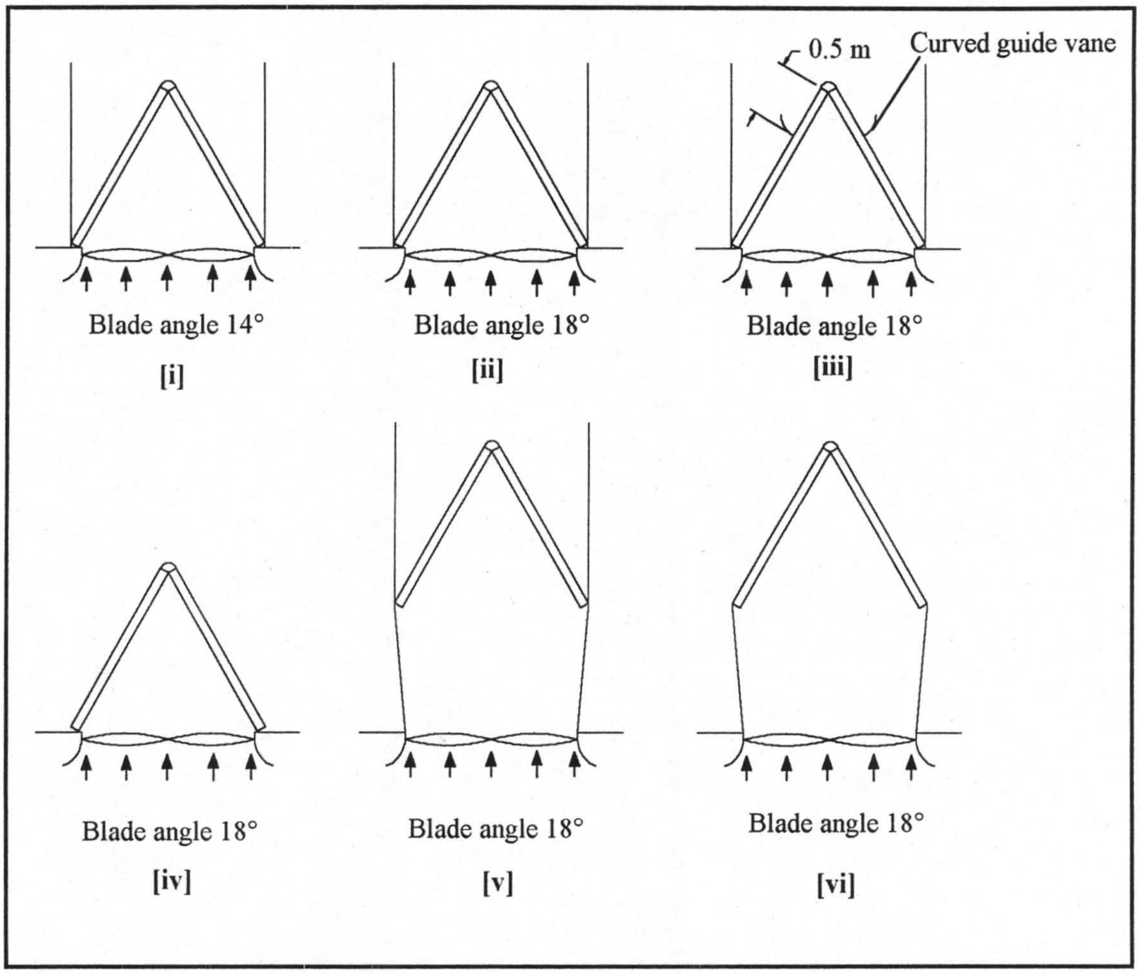

Figure 4.1.2 : Delta heat exchanger test configurations.

A fan speed of 750 rpm is used during all tests in order to maintain a tip speed of 60 m/s. This is in keeping with conventional design practice which recommends a fan tip speed of 60 m/s or less to limit noise levels generated by the fan. Blade angles of 14° and 18° are used in order to obtain predicted system operating points (volumetric flow rates) that are between 40 % and 50 % greater than those obtained with the normal flow heat exchanger. The motivation for this is the fact that the delta heat exchanger has double the surface area of the normal flow heat exchanger, and thus a greater volumetric flow rate is required in order to try and obtain the same volumetric flow rate per unit frontal area (V_{sys}/A_{he}) ratio of the normal flow heat exchanger. The fan operates near its point of maximum efficiency in the presence of the delta heat exchanger for both the 14° and the 18° blade angle.

The round-to-round diffuser is only used in tests conducted with a blade angle of 18° as the diffuser performs better at the higher volumetric flow rates (as shown in section D.2) obtained by using a greater blade angle. The curved guide vanes used in configuration [iii] are tested as a matter of interest to see if such flow devices improve the velocity distribution downstream of the heat exchanger. A more uniform outlet velocity distribution would lead to a decrease in the outlet energy coefficient (and outlet kinetic energy losses) and hence an increase in the system performance. The guide vanes used in configuration [iii] have a radius of curvature of 200 mm and an included angle of 60° (so chosen that the air flow leaving the guide vane flows in the axial direction).

Tests conducted with the side walls present are representative of delta heat exchangers which have wind walls mounted. Without the side walls present, the gain in system performance obtained by removing the wind walls can be investigated. The side walls can further be used to simulate the effect of adjacent fans blowing through delta heat exchangers into a common area above the heat exchangers as is the case with an array of delta heat exchangers.

4.2 Experimental Procedure

The fan system (fan, plenum and heat exchanger) characteristics are determined for each of the configurations shown in figure 4.1.2. From the system characteristics it is possible to determine the system's operating point (as defined is section 3.2) for each configuration. This is done by either linearly interpolating between data points whose fan system static pressure rise are just above and below 0 Pa or (for those cases where the system characteristic curves do not extend below 0 Pa) by linearly extrapolating from the given data. In cases where extrapolation is used, great care must be taken that the data points used are representative of the gradient of the fan system static pressure rise curve.

In addition to determining the system characteristics for each of the configurations, a velocity traverse is performed near the exit of the rectangular duct (approximately 100 mm downstream of the apex of the delta heat exchanger) for configurations [i], [ii], [iii] and [v]. This is done by manually traversing a 1.9 m staff with propeller anemometers attached at various points (as shown in figure 4.1.1) across the width of the duct. The grid of the velocity traverse is shown in figure B1.1. The calibration constants of the anemometers are given in Appendix G.

4.3 Experimental and Calculated Results

Table B1.1 to B1.7 list the experimental readings taken to determine the system characteristics for the various configurations. The system characteristics calculated from these readings are listed in tables B2.1 to B2.7 and are shown graphically in figures B2.1 and B2.2. Appendix F contains a sample calculation of how the system characteristics are determined.

Table 4.3.1 lists the system operating point for each of the configurations tested as determined from figure B2.2. Also listed is the fan static pressure rise (Δp_{s_F}), the dynamic pressure immediately downstream of the fan rotor (p_{d_F}), the total pressure drop over the heat exchanger system (Δp_{t_S}), the total pressure drop within the plenum ($\Delta p_{t_{pl}}$) and the plenum loss coefficient (K_{pl}) at the system operating point. The calculation procedure for each of these parameters is shown below.

Table 4.3.1 : System operating point and plenum losses for various configurations tested.

Config.	V_{sys} **(m^3/s)**	Δp_{s_F} **(Pa)**	α_F	p_{d_F} **(Pa)**	Δp_{t_S} **(Pa)**	$\Delta p_{t_{pl}}$ **(Pa)**	K_{pl}	**% p_{d_F} lost**
i	20.111	174.609	1.712	119.094	208.436	85.266	1.225	71.6
ii	21.702	205.166	1.624	131.604	241.289	95.480	1.178	72.6
iii	22.063	199.178	1.604	134.358	239.766	93.771	1.120	69.8
iv	23.317	176.789	1.536	143.625	204.246	116.168	1.242	80.9
v	23.041	225.024	1.551	141.629	270.725	95.928	1.050	67.7
vi	26.161	177.654	1.379	162.411	254.029	86.036	0.731	53.0

The fan static pressure rise (Δp_{s_F}) is determined from the fan characteristics whilst the dynamic pressure immediately downstream of the fan is calculated as follows :

$$p_{d_F} = \alpha_F \cdot \frac{1}{2} \cdot \rho \cdot v_F^2 \tag{4.3.1}$$

where α_F is the kinetic energy coefficient at fan outlet and

$$v_F = \frac{V_{sys}}{A_F} = \frac{V_{sys}}{\pi \cdot 0.771^2}$$

As mentioned in section 3.4, Beiler [91BE1] shows that the value of the kinetic energy coefficient at fan outlet (α_F) for a fan with a free outlet (BS 848 type A test) is 1.8 at a volume flow rate of 18.5 m^3/s and 1.498 at a volume flow rate of 24 m^3/s. The values of the kinetic energy coefficient for a fan system incorporating a plenum may differ from the values of α_F for the case of a free outlet after the fan. In calculating the fan dynamic pressure rise, it is assumed that α_F varies linearly between these two volume flow rates.

The total pressure drop over the heat exchanger is determined from the total oblique flow isothermal loss coefficient, K_θ, for the delta heat exchanger as determined in Appendix E. Van Aarde and Kröger [93VA1] provide correlations to calculate (or predict) K_θ for delta heat exchangers given the geometry of the delta heat exchanger and the isothermal heat exchanger loss coefficient under normal flow conditions (K_{he}). As shown in section E.2, there is good agreement between the calculated (or predicted) values of K_θ and the experimentally determined values of K_θ in the high volume flow rate range where the heat exchanger operates. Hence, the correlations provided by Van Aarde and Kröger will be used to calculate K_θ.

In section E.2 it is shown how the correlations provided by Van Aarde and Kröger are reduced to equations (E2.17) and (E2.18) for the delta heat exchanger with side walls and without side walls respectively :

Delta heat exchanger with side walls

$$K_\theta = 90.613844 \cdot Ry^{-0.121771} + 12.117 \tag{4.3.2}$$

Delta heat exchanger without side walls

$$K_\theta = 90.613844 \cdot Ry^{-0.121771} + 3.873 \tag{4.3.3}$$

As is shown later in this section, the use of the guide vanes in configuration [iii] reduces the outlet kinetic energy coefficient to 1.615. This differs quite considerably from the assumption that the outlet kinetic energy coefficient is 1.9874 used to derive equation (4.3.2), hence equation (4.3.2) cannot be used to calculate K_θ for configuration [iii]. If the outlet kinetic energy coefficient is 1.615 then the value of K_θ (as predicted by Van Aarde's method) for configuration [iii] is given by

$$K_\theta = 90.613844 \cdot Ry^{-0.121771} + 10.940 \tag{4.3.4}$$

In equations (4.3.2), (4.3.3) and (4.3.4) the characteristic flow parameter (Ry) is given by

$$Ry = \frac{\rho \cdot v_{he}}{\mu} \qquad \text{where } v_{he} = \frac{V_{sys}}{A_{he}} = \frac{V_{sys}}{2 \cdot 1.6 \cdot 1.9}$$

With the value of K_θ known, the total pressure drop over the heat exchanger is calculated as follows :

$$\Delta p_{t_S} = K_\theta \cdot \frac{1}{2} \cdot \rho \cdot v_{he}^2 \tag{4.3.5}$$

The static pressure upstream of the fan and downstream of the heat exchanger both equal atmospheric pressure, hence an energy balance between the fan outlet and the heat exchanger inlet (within the plenum yields)

$$\begin{aligned} \Delta p_{sF} + p_{d_F} &= \Delta p_{t_S} + \Delta p_{t_{pl}} \\ \Delta p_{t_{pl}} &= \Delta p_{sF} + p_{d_F} - \Delta p_{t_S} \end{aligned} \tag{4.3.6}$$

The plenum loss coefficient (based upon the fan cross-sectional area) is defined as

$$K_{pl} = \frac{\Delta p_{t_{pl}}}{\frac{1}{2} \cdot \rho \cdot v_F^2} \tag{4.3.7}$$

The amount of kinetic energy introduced by the fan rotor which is dissipated within the plenum can be calculated as follows

$$\%\ \text{of}\ p_{d_F}\ \text{lost in plenum} = \frac{K_{pl}}{\alpha_F} \times 100 \tag{4.3.8}$$

Table 4.3.2 provides a summary of the system operating point and the fan power requirements for each of the configurations tested as determined from figures B2.1 and B2.2. Also shown in table 4.3.2 is the volumetric flow rate per unit fan power and the volumetric flow rate per unit frontal area of the heat exchanger for each of the configurations tested. The frontal area for the delta heat exchanger is given by $A_{he} = 2 \times 1.6 \times 1.9 = 6.08\ m^2$.

Table 4.3.2 : System operating point and power requirement for configurations tested.

Config.	**V_{sys} (m^3/s)**	**P (kW)**	**V_{sys} / P ($m^3/s/kW$)**	**V_{sys} / A_{he} (m/s)**
i	20.111	6.416	3.135	3.308
ii	21.702	8.446	2.570	3.569
iii	22.063	8.421	2.597	3.629
iv	23.317	8.494	2.745	3.835
v	23.041	8.538	2.699	3.790
vi	26.161	8.560	3.056	4.303

Tables B3.1 to B3.4 list the velocity distribution readings taken and are shown in graph form in figures B3.1 to B3.4. Figures B3.5 and B3.6 show the velocity profiles measured at the outlet of the delta heat exchanger by Venter [90VE1] and Van Aarde and Kröger [93VA1]. Note that the velocity profiles measured by Venter and Van Aarde and Kröger are measured between the steam ducts atop of the apexes of two adjacent delta heat exchangers

The kinetic energy lost to the atmosphere differs for the various configurations. In order to correctly estimate the kinetic energy that is lost, the kinetic energy coefficient α (as defined in section 3.3) is calculated from tables B3.1 to B3.4. The value of α for configurations [i], [ii], [iii] and [v] are 1.865, 1.955, 1.615 and 1.920 respectively.

4.4 Discussion

It is common fan design practice that the fan is matched to the system by determining the intercept between the fan static pressure curve and the total pressure loss of the system (heat exchanger inlet losses due to oblique flow, frictional losses, exit losses, jetting losses and the outlet kinetic energy loss). Figure B1.2 shows the fan static pressure rise characteristics for blade angles of 14°, 18° and 18° with the round-to-round diffuser attached the fan outlet. The heat exchanger total pressure drop characteristics for the delta heat exchanger with and without side walls are also shown in the figure. From this, the predicted (or expected) operating point can be determined for each of the configurations tested. Table 4.4.1 provides a summary of the predicted operating point, the actual operating point and the % difference between the two for each of the configurations tested.

From table 4.4.1 it can be seen that the actual operating point is on average 5.9% higher than the predicted operating point. This can be attributed to the fact that in determining the predicted operating point, it is assumed that all of the kinetic energy introduced by the fan rotor is dissipated within the plenum whilst it can be seen from table 4.3.1 that on average only 69 % of this kinetic energy is lost within the plenum.

Table 4.4.1 : The design point for each of the configurations tested.

Config.	**Predicted** $V_{sys}\left(m^3/s\right)$	**Actual** $V_{sys}\left(m^3/s\right)$	**%** **difference**
i	19.208	20.111	4.701
ii	20.709	21.702	4.795
iii	20.709	22.063	6.538
iv	22.522	23.317	3.530
v	21.792	23.041	5.731
vi	23.836	26.161	9.784

Venter [90VE1] compared theoretically and experimentally determined system effects of individual components, as well as the combination of different components, within A-frame plenums. His work included tests conducted with a safety grid at the inlet of the fan, a walkway and support beams placed in the plenum and with windwalls present. He found good agreement between the predicted and the actual operating point when assuming that all of the kinetic energy introduced by the fan is dissipated within the plenum.

Test configurations [i] and [ii] most closely approximate the delta configurations investigated by Venter. From table 4.3.1 it can be seen that the amount of kinetic energy dissipated within the plenum is 71.6% and 72.6% for configurations [i] and [ii] respectively. The discrepancy between the results obtained in this thesis and those obtained by Venter may be due to the absence of the inlet safety grid, the walkway and the support beams in the plenum in tests conducted by the author. All of these components have the tendency to increase pressure losses occurring before and in the plenum and thus lower the actual operating point. It has been found that the presence of a walkway immediately downstream of the fan is especially detrimental to the amount of kinetic energy which is dissipated within the plenum as it has the tendency to increase the kinetic energy coefficient at the fan outlet ($\alpha_{F_{pl}}$) to a value as high as 5 or 6. This increase in $\alpha_{F_{pl}}$ leads to an increased amount of flow distortion within the plenum and hence increased losses.

Thus it would seem that in practical installations these secondary losses account for the remaining ±30% of the kinetic energy and that the conventional method of predicting the system operating point gives good results. However this good agreement between the predicted and actual operating point can be regarded as being coincidental. Often these secondary losses are not taken into account when determining the system operating point and it just so happens that the 30% of the dynamic head leaving the fan that is converted to static head cancels out these secondary losses.

It can be seen from table 4.3.1 that when the diffuser is placed between the fan and the delta heat exchanger, the total pressure drop within the plenum remains fairly constant (95.480 Pa for configuration [ii] and 95.928 Pa for configuration [v]). However, the increase in the system operating point (from 21.702 m^3/s to 23.041 m^3/s) leads to a 10.9% decrease in the plenum loss coefficient from 1.178 (for configuration [ii]) to 1.050 (for configuration [v]). This decrease in K_{pl} is reflected in the decrease in the percentage of fan kinetic energy lost in the plenum from 71.6% to 67.7%. Thus, apart from increasing the amount of the static pressure available to the fan system, the diffuser helps to slightly decrease the pressure losses occurring within the plenum.

Furthermore, table 4.3.1 shows that the plenum loss coefficient decreases by 30% from 1.050 (for configuration [v]) to 0.731 (for configuration [vi]) when the side walls are removed with the diffuser mounted downstream of the fan. This large decrease in the plenum loss coefficient is reflected in the percentage of fan kinetic energy lost in the plenum which decreases from 67.7% to 53.0%. In contrast to this, there is a 5.4% increase in the plenum loss coefficient from 1.178 (for configuration [ii]) to 1.242 (for configuration [iv]) when the side walls are removed for the case where the fan exhausts directly into the delta heat exchanger. Further detailed studies would be required to derive a method to account for the conflicting tendicies observed above.

From table 4.4.1 it can be seen that the system operating point increases from 21.702 m^3/s (for configuration [ii]) to 23.041m^3/s (for configuration [v]) with the introduction of the diffuser into the fan system. This increase of 1.339 m^3/s (which represents an increase of 6.2%) in the operating point is slightly higher than the predicted increase of 1.083 m^3/s, but is still in good agreement. The slight discrepancy between the two is due to the decrease in the plenum loss coefficient brought about by the introduction of the diffuser.

Furthermore, table 4.4.1 shows that when the side walls are removed without a diffuser present in the fan system, the system operating point increases by 7.4% from 21.702 m^3/s (for configuration [ii]) to 23.317 m^3/s (for configuration [iv]). This increase of 1.615 m^3/s is 11% less than the predicted increase of 1.82 m^3/s. This slight discrepancy between the actual and predicted increase is due to the increase in the plenum loss coefficient. This increase of 7.4% in the operating point represents the increase that would be obtained if the windwalls were to be removed from delta heat exchangers having windwalls.

When the diffuser is mounted downstream of the fan (as in test configurations [v] and [vi]), the actual increase in the system operating point when the side walls are removed is 3.12 m^3/s , which is 53% higher than the predicted 2.044 m^3/s increase. This discrepancy between the actual and predicted increase in the system operating point can be attributed to the decrease in the plenum loss coefficient when the side walls are removed.

The velocity distributions at the heat exchanger outlet shown in figures B3.1 to B3.4 compare well to those measured by Venter [90VE1] (figure B3.5) and Van Aarde and Kröger [93VA1] (figure B3.6). Van Aarde and Kröger found the value of the kinetic energy coefficient (α) at the heat exchanger outlet to be 1.9874. This compares well to the values of 1.865, 1.955 and 1.920 determined for test configurations [i], [ii] and [v] respectively.

The guide vanes installed in configuration [iii] have the effect of decreasing α to 1.615. As a result of this, less kinetic energy is lost at the heat exchanger outlet and the system operating point increases from 21.702 m^3/s to 22.063 m^3/s. Thus, a 18.7% decrease in α translates to an increase of 1.7% in the system volume flow rate.

From table 4.3.2 it can be seen that the volumetric flow rate per unit fan power decreases by 18% and the volumetric flow rate per unit frontal area increases by 7.9% as the blade angle is increased from 14° to 18° (configurations [i] and [ii]). The addition of the round-to-round diffuser leads to a 4.7% increase in V_{sys}/P from 2.578 $m^3/s/kW$ (for configuration [ii]) to 2.699 $m^3/s/kW$ (for configuration [v]) along with a 6.2% increase V_{sys}/A_{he} from 3.569 m/s to 3.790 m/s.

Removing the side walls results in a 6.5% increase in V_{sys}/P from 2.578 $m^3/s/kW$ (for configuration [ii]) to 2.699 $m^3/s/kW$ (for configuration [iv]) and a 7.4% increase in V_{sys}/A_{he} from 6.346 m/s to 6.818 m/s. The highest values for V_{sys}/P and V_{sys}/A_{he} are obtained with a round-to-round diffuser and no side walls (configuration) and they are 3.056 $m^3/s/kW$ and 7.649 m/s respectively.

5. Double Delta Heat Exchanger

5.1. Experimental Equipment

A rectangular duct having a cross-sectional area of 2.05 m x 1.9 m is used to house a double delta heat exchanger having a frontal area corresponding to the cross-sectional area of the duct. The double delta heat exchanger consists of two finned tube heat exchanger placed end to end so as to have a 60° included angle between them. Each of these finned tube heat exchangers contains six smaller (secondary) deltas. The apex angle of these secondary deltas is also 60°. There are 7 finned tubes on each side of the secondary delta, thus making each side 252 mm long and giving a total of 14 finned tubes per secondary delta and 168 finned tubes for the entire double delta heat exchanger. To alter the flow resistance of the heat exchanger, lengths of pine quarter rounds are placed upstream between the finned tubes (as shown in figure 2.4.2).

The rectangular duct is attached either directly to the downstream (outlet) side of the S-fan, which is mounted in the settling chamber of the code tunnel, or downstream of a diffuser which in turn is attached the outlet of the S-fan. Either the round-to-round diffuser or the round-to-rectangular diffuser can be used. Figure 5.1.1 shows the various possibilities for mounting the rectangular duct. Furthermore, the side walls of the rectangular duct are removable thus enabling tests to be conducted with or without sides.

For tests conducted with the round-to-rectangular diffuser, it is possible to make use of two other flow devices specifically designed for use with the round-to-rectangular diffuser viz. : the flow director and the flow straightner. The purpose of the flow director (shown in figure 2.5.2) is to guide the airflow smoothly from the fan outlet to the secondary deltas of the double delta heat exchanger. The flow straightner (shown in figure 2.5.3) is used to remove the rotational component in the airflow exiting the fan.

The various double delta heat exchanger configurations to be tested are shown in figure 5.1.2.

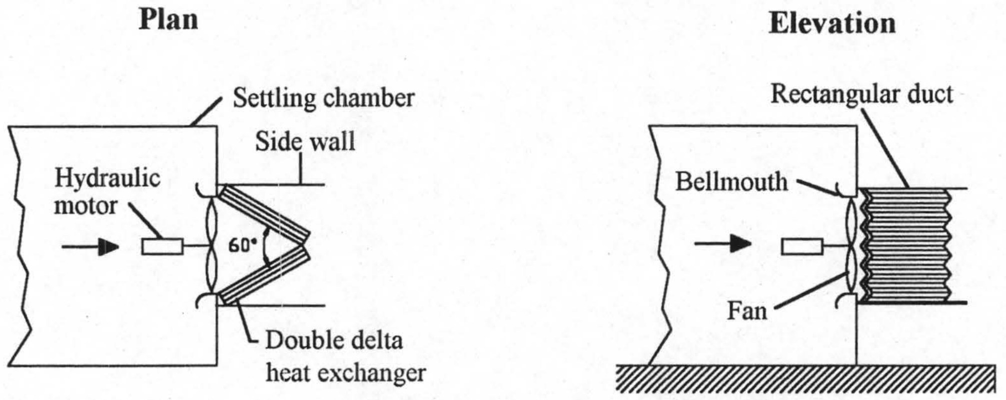

Double delta heat exchanger

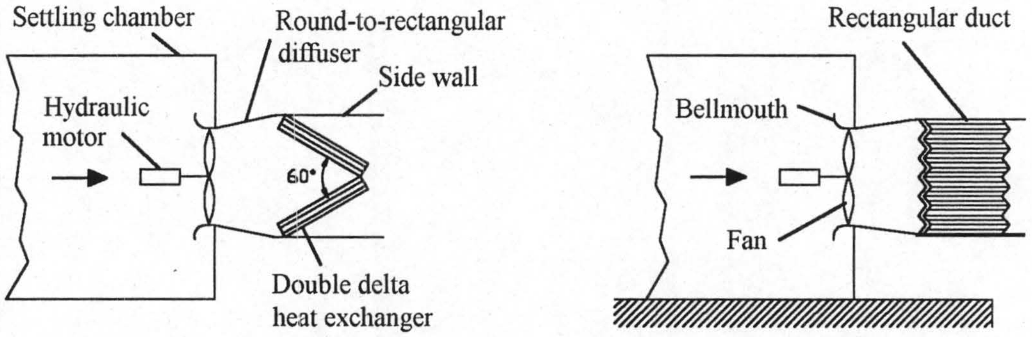

Double delta heat exchanger with round-to-rectangular diffuser

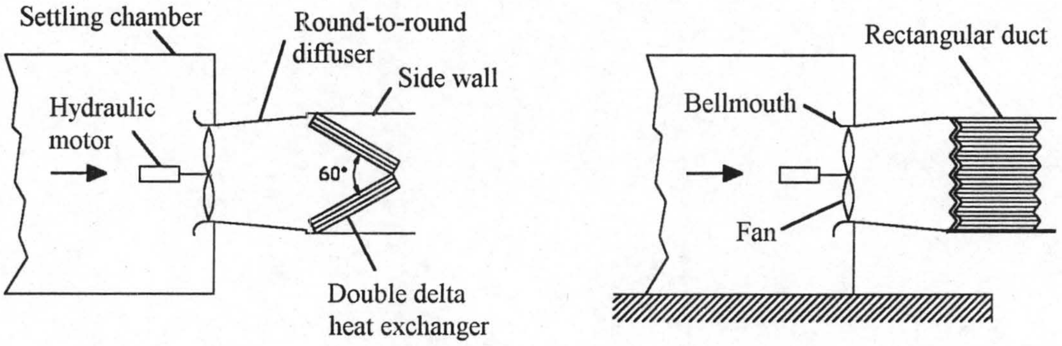

Double delta heat exchanger with round-to-round diffuser

Figure 5.1.1 : Experimental set-up for double delta heat exchanger tests.

A fan speed of 750 rpm is used during all tests conducted in order to obtain a fan tip speed of 60 m/s. This is in keeping with conventional design practice which advises a fan tip speed of 60 m/s or less in order to limit the noise levels generated by the fan. In cases where it is not possible to maintain a fan speed of 750 rpm due to increased fan power requirements, a fan speed of 650 rpm or 700 rpm is to be used and the results extrapolated for a fan speed of 750 rpm using the fan laws (as discussed later in section 5.2).

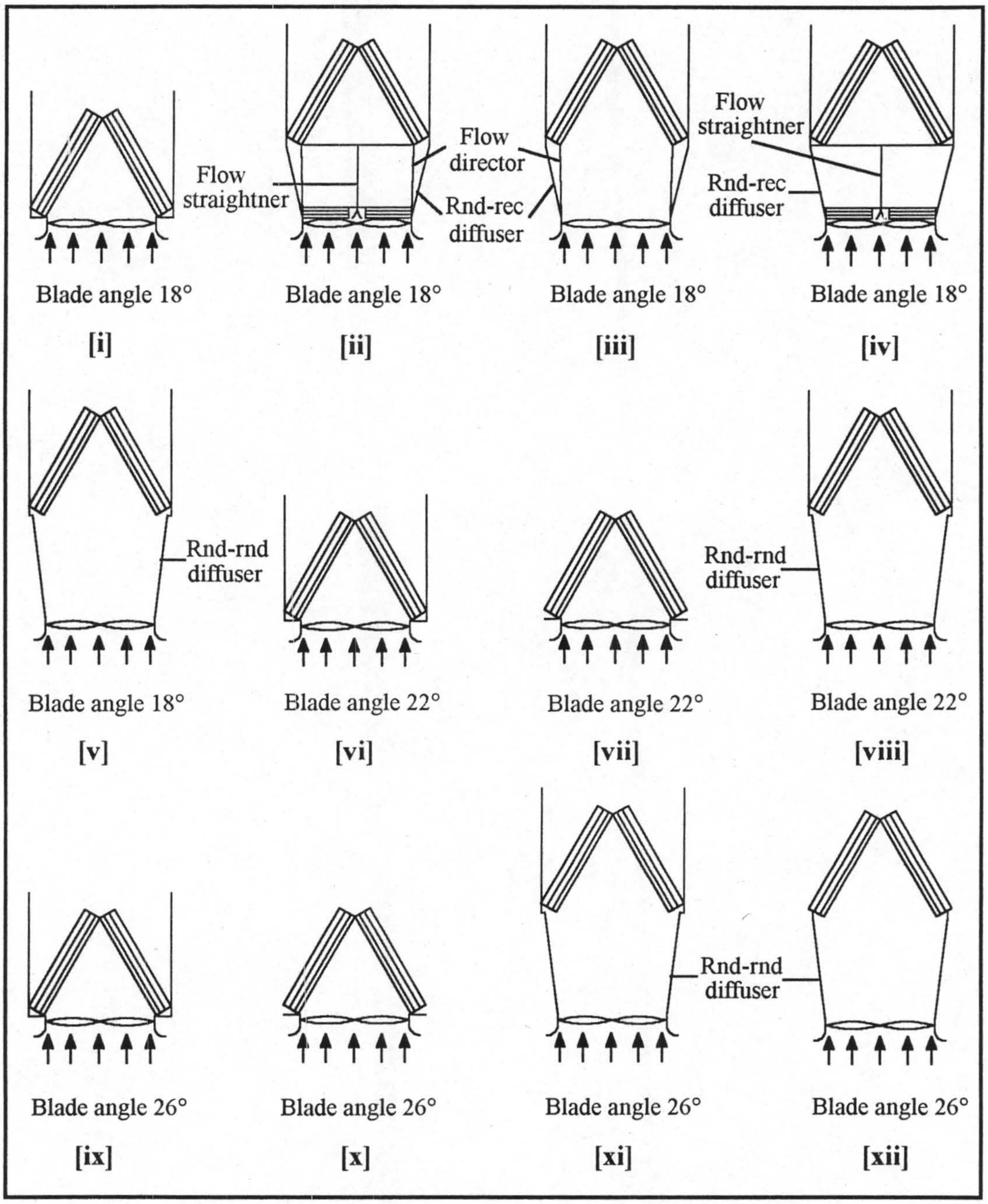

Figure 5.1.2 : Double delta heat exchanger test configurations.

Fan blade angles of 18°, 22° and 26° are used to obtain predicted system volumetric flow rates that are between 70% and 90% higher than that obtained with the normal flow heat exchanger. Such high volumetric flow rates are required in order to try and obtain the same volumetric flow rate per unit frontal area (V_{sys}/A_{he}) as obtained with the normal flow heat exchanger. Unfortunately, the high volumetric flow rates used result in the fan operating to the right of its maximum static efficiency in the presence of the double delta heat exchanger (especially with the blade angle set to 26°). Furthermore, as the blade angle is increased, the maximum possible static efficiency decreases. Hence testing of higher blade angles is considered unnecessary as the greatly increased power requirements would make such a system economically unviable.

The round-to-rectangular diffuser is used to investigate what advantage is to be obtained by incorporating such a transition piece in the plenum configuration. It is expected to perform poorly when compared to the round-to-round diffuser due to its poor pressure recovery characteristics (see section D.3). Attempts to improve the performance of the round-to-rectangular diffuser by adding flow components such as the flow director and the flow straightner are also to be tested. For tests conducted with the higher blade angles (and hence higher volumetric flow rates) of 22° and 26° only the round-to-round diffuser is used as its static pressure recovery performance is superior to that of the round-to-rectangular diffuser.

Tests conducted with side walls present simulate a heat exchanger having wind walls present. Without the side walls present, the gain in system performance obtained by removing the wind walls can be investigated. The side walls can further be used to simulate the effect of adjacent fans blowing through double delta heat exchangers into a common area above the heat exchangers as is the case with an array of double delta heat exchangers.

5.2 Experimental Procedure

The fan system (fan, plenum and heat exchanger) characteristics are determined for each of the configurations shown in figure 5.1.2. From the system characteristics it is possible to determine the system's operating point (as defined in section 3.2) for each configuration. As the fan system static pressure characteristics do not extend to 0 Pa, the system operating point is determined by linearly extrapolating the static pressure characteristics to 0 Pa (taking care that the data points used are representaive of the gradient of the static pressure curve).

The power requirements for operating the S-fan at a blade angle of 22° or 26° at 750 rpm exceed the hydraulic motor's maximum power output of 10 kW. Hence, when determining the system characteristics for configurations [vi] to [xii] it is necessary to perform the tests at 650 rpm or 700 rpm and extrapolate the results for a fan speed of 750 rpm using the fan laws (as given in section F.1).

In addition to determining the system characteristics for each of the configurations, a velocity traverse is performed approximately 100 mm downstream of the apex of the double delta heat exchanger for configurations [i], [ii], [iii], [iv] and [v]. This is done by manually traversing a 1.9 m staff with propeller anemometers attached at various points across the width of the duct. The grid of the velocity traverse in shown in figure C1.1. The calibration constants of the anemometers are given in Appendix G.

5.3 Experimental and Calculated Results

Tables C1.1 to C1.12 list the experimental readings taken to determine the system characteristics for the various configurations tested. The system characteristics calculated from these readings are listed in tables C2.1 to C2.12 and are shown in graph form in figures C2.1 to C2.6. Appendix F contains a sample calculation showing how the system characteristics are determined.

Table 5.3.1 lists the system operating point for each of the configurations tested as determined from figures C2.2, C2.4 and C2.6. Also listed is the fan static pressure rise (Δp_{s_F}), the dynamic pressure immediately downstream of the fan rotor (p_{d_F}), the total pressure drop over the heat exchanger (Δp_{t_S}), the total pressure drop within the plenum ($\Delta p_{t_{pl}}$) and the plenum loss coefficient (K_{pl}) at the system operating point. The calculation procedure for each of these parameters is shown below.

The fan static pressure rise (Δp_{s_F}) is determined from the fan characteristics whilst the dynamic pressure immediately downstream of the fan is calculated as follows :

$$p_{d_F} = \alpha_F \cdot \frac{1}{2} \cdot \rho \cdot v_F^2 \tag{5.3.1}$$

where α_F is the kinetic energy coefficient at fan outlet and

$$v_F = \frac{V_{sys}}{A_F} = \frac{V_{sys}}{\pi \cdot 0.771^2}$$

As mentioned is section 3.4, Beiler [91BE1] shows that the value of the kinetic energy coefficient at fan outlet (α_F) for a fan with a free outlet is 1.8 at a volume flow rate of 18.5 m^3/s and 1.498 at a volume flow rate of 24 m^3/s. In calculating the fan dynamic pressure rise, it is assumed that α_F varies linearly between these two volume flow rates.

The total pressure drop over the heat exchanger is determined from the total oblique flow isothermal loss coefficient, K_θ, for the double delta heat exchanger as determined in section E.3. Figure E.3.2 shows that K_θ for the double delta heat exchanger is given by :

Double delta heat exchanger with side walls

$$K_\theta = 131.756958 \cdot Ry^{-0.077146} \tag{5.3.2}$$

Delta heat exchanger without side walls

$$K_\theta = 229.872544 \cdot Ry^{-0.149352} \tag{5.3.3}$$

In equations (4.3.2) and (4.3.3), the characteristic flow parameter (Ry) is given by

$$Ry = \frac{\rho \cdot v_{he}}{\mu} \qquad \text{where } v_{he} = \frac{V_{sys}}{A_{he}} = \frac{V_{sys}}{2 \cdot 12 \cdot 0.252 \cdot 1.6}$$

With the value of K_θ known, the total pressure drop over the heat exchanger is calculated as follows :

$$\Delta p_{t_S} = K_\theta \cdot \frac{1}{2} \cdot \rho \cdot v_{he}^2 \tag{5.3.4}$$

The static pressure upstream of the fan and downstream of the heat exchanger both equal atmospheric pressure, hence an energy balance between the fan outlet and the heat exchanger inlet (within the plenum yields)

$$\begin{aligned} \Delta p_{sF} + p_{dF} &= \Delta p_{ts} + \Delta p_{t_{pl}} \\ \Delta p_{t_{pl}} &= \Delta p_{sF} + p_{dF} - \Delta p_{ts} \end{aligned} \tag{5.3.5}$$

The plenum loss coefficient (based upon the fan cross-sectional area) is defined as

$$K_{pl} = \frac{\Delta p_{t_{pl}}}{\frac{1}{2} \cdot \rho \cdot v_F^2} \tag{5.3.6}$$

The amount of kinetic energy introduced by the fan rotor which is dissipated within the plenum can be calculated as follows

$$\% \text{ of } p_{dF} \text{ lost in plenum} = \frac{K_{pl}}{\alpha_F} \text{ x } 100 \tag{5.3.7}$$

Table 5.3.1 : System operating point and plenum losses for various configurations tested.

Config	**V_{sys} (m^3/s)**	**Δp_{sF} (Pa)**	**α_F**	**p_{dF} (Pa)**	**Δp_{ts} (Pa)**	**$\Delta p_{t_{pl}}$ (Pa)**	**K_{pl}**	**% p_{dF} lost**
i	23.330	176.544	1.535	143.738	182.400	137.882	1.472	95.9
ii	24.094	140.526	1.493	149.112	194.059	95.579	0.957	64.1
iii	24.375	136.408	1.477	150.975	198.434	88.949	0.870	58.9
iv	23.380	150.451	1.532	144.073	183.152	111.372	1.184	77.3
v	25.469	187.913	1.417	158.135	215.914	130.134	1.166	82.3
vi	25.200	210.042	1.432	156.451	211.550	154.943	1.418	99.0
vii	26.731	182.528	1.348	165.712	172.404	175.836	1.430	106.1
viii	27.556	216.697	1.303	170.220	251.218	135.699	1.039	79.7
ix	26.409	234.495	1.366	163.904	231.497	166.902	1.391	101.8
x	28.321	204.184	1.261	174.007	191.861	186.330	1.350	107.1
xi	30.233	237.736	1.156	181.783	300.244	119.275	0.758	65.6
xii	32.731	201.325	1.019	187.813	250.785	138.353	0.751	73.7

Table 5.3.2 provides a summary of the system operating point and fan power consumption for each of the configurations tested as determined from figures C2.1 to C2.6. Also shown in table 5.3.2 is the volumetric flow rate per unit fan power and the volumetric flow rate per unit frontal area of the heat exchanger. The frontal area for the double delta heat exchanger is given by $A_{he} = 24 \times 0.252 \times 1.6 = 9.6768\ m^2$.

Table 5.3.2 : System operating point and fan power consumption for double delta heat exchanger test configurations.

Config.	**V_{sys} (m^3/s)**	**P (kW)**	**V_{sys} / P ($m^3/s/kW$)**	**V_{sys} / A_{he} (m/s)**
i	23.330	8.359	2.791	2.411
ii	24.094	8.201	2.938	2.490
iii	24.375	8.166	2.985	2.519
iv	23.380	8.150	2.931	2.416
v	25.469	8.093	3.147	2.632
vi	25.200	10.665	2.363	2.604
vii	26.731	10.867	2.460	2.762
viii	27.556	10.860	2.537	2.848
ix	26.409	12.978	2.035	2.792
x	28.321	13.250	2.137	2.927
xi	30.233	13.075	2.312	3.124
xii	32.731	13.418	2.439	3.382

Tables C3.1 to C3.5 list the velocity distribution readings taken and are shown in graph form in figures C3.1 to C3.5. In order to estimate the kinetic energy that is lost to the atmosphere at the heat exchanger outlet, the kinetic energy coefficient α (as defined in section 3.3) is calculated from tables C3.1 to C3.5. The value of α for configurations [i], [ii], [iii], [iv] and [v] are 1.482, 1.451, 1.504, 1.483 and 1.531.

5.4 Discussion

According to common fan design practice, the fan is matched to the system by determining the intercept between the fan static pressure curve and the total pressure loss of the system. The total pressure loss of the system includes inlet losses due to oblique flow, frictional and exit losses in the heat exchanger, downstream jetting losses and outlet kinetic energy losses. Thus, this method of predicting the fan system's operating point assumes that all of the kinetic energy introduced by the fan is dissipated within the plenum and that the total pressure available to overcome the pressure losses downstream of the fan is given by the fan's static pressure rise.

Figures C1.2 , C1.3 and C1.4 show the fan static pressure rise characteristics for blade angles of 18°, 22° and 26°. Also shown in these graphs are the double delta heat exchanger total pressure drop characteristics. From these graphs the predicted operating point can be determined for each of the configurations tested. Table 5.4.1 provides a summary of the predicted operating point, the actual operating point and the percentage difference between the two for each of the configurations tested.

Table 5.4.1 : The predicted operating point for each of the double delta configurations tested.

Config.	**Predicted** V_{sys} **(m^3/s)**	**Actual** V_{sys} **(m^3/s)**	**% difference**
i	23.156	23.330	0.8
ii	22.185	24.094	8.6
iii	22.185	24.375	9.9
iv	22.185	23.380	5.4
v	24.574	25.469	3.6
vi	25.154	25.200	0.2
vii	27.056	26.731	-1.2
viii	26.466	27.556	4.1
ix	26.504	26.409	-0.4
x	28.735	28.321	-1.4
xi	28.221	30.233	7.1
xii	31.010	32.731	5.5

From table 5.4.1 it can be seen that the actual operating point is on average 3.5% higher than the predicted operating point. This would indicate that the assumption that all of the kinetic energy is dissipated within the plenum gives fairly accurate results when predicting the operating point of a double delta heat exchanger.

Table 5.3.1 shows that on average 84.3 % of the kinetic energy introduced by the fan is dissipated within the plenum. In all the tests where a diffuser was not used (configuration [i], [vi], [vii], [ix] and [x]) the amount of kinetic energy dissipated within the plenum always exceeds 95%. It will be noted that in certain cases (configurations [vii], [ix] and [x]) the amount of kinetic energy lost exceeds 100%. This apparent error can be attributed to two factors. Firstly, as explained earlier, the fan characteristics for blade angles in excess of 18° and operating at 750 rpm have to be extrapolated (using the fan laws) from fan characteristics for the same blade angle but operating at a lower speed. This extrapolation process introduces a certain margin for error. Secondly, the values for the kinetic energy coefficient at the fan outlet (α_F) have to be extrapolated from data provided by Beiler [91BE1]. Unfortunately, this data only extends to a maximum flow rate of 24 m^3/s and as the operating point for all of the above mentioned test configurations is in excess of 26 m^3/s, a small degree of uncertainty arises as to the precise value of α_F. Nonetheless, the general tendency that most, if not all, of the kinetic energy (as determined during a BS 848 type A test) is dissipated within the plenum can still be concluded from these results.

From table 5.4.1 it can be seen that according to the predicted values, the system operating point decreases with the introduction of the round-to-rectangular diffuser for configurations [ii], [iii] and [iv]. However it can be seen that the system operating point actually increases from 23.330 m^3/s (for configuration [i]) to 24.094 m^3/s, 24.375 m^3/s and 23.380 m^3/s for configurations [ii], [iii] and [iv] respectively. This is due to the fact that the introduction of the round-to-rectangular diffuser lowers the plenum loss coefficient from 1.472 for configuration [i] to 0.957, 0.870 and 1.184 for configurations [ii], [iii] and [iv] respectively. The largest of these reductions represents a decrease of 41%. This reduction in the plenum loss coefficient is reflected by a decrease in the percentage of kinetic energy lost within the plenum. However this drastic decrease in the plenum loss coefficient translates to only a 3.3% increase in the system operating point (volume flow rate)as it is offset by the poor static pressure recovery characteristics of the round-to-rectangular diffuser. Furthermore, it is interesting to note that relative to the plenum loss coefficient for configuration [ii], the plenum loss coefficient decreases for configuration [iii] (to 0.870) but increases for configuration [iv] (to 1.184). From this it can be concluded that the flow straightner has an adverse effect on the plenum loss coefficient whilst the flow director has a beneficial effect. The use of the round-to-round diffuser in configuration [v] also leads to a decrease in the plenum loss coefficient but not as large a decrease as is possible with the round-to-rectangular diffuser. This, however, is more than compensated for by the better static pressure recovery characteristics of the round-to-round diffuser resulting in the highest operating point of all the configurations having a blade angle of 18°.

It can be noted from the plenum loss coefficients for configurations [vi] to [xii] that the removal of the side walls does not have a significant affect on the plenum loss coefficient. In contrast to this, the introduction of the round-to-round diffuser leads to a significant reduction in the plenum loss coefficient, the extent of which increases as the system operating point increases. For example, there is a 27% decrease in the plenum loss coefficient for configurations [vi] and [viii], whilst there is a 46% decrease for configurations [ix] and [xi].

The system operating points for configurations [vi] to [xii] show that the removal of the side walls increases the system operating point. As is to be expected, the extent of the increase is dependant on the system operating point : the higher the operating point, the greater the increase. For example, there is 3.1% increase in the system operating point for configuration [vi] and [vii], whilst there is a 8.3% increase for configurations [xi] and [xii].

The improvements in system operating point brought about by the introduction of the round-to-round diffuser are more substantial than those brought about by the removal of the side walls. The increases in the system operating point are 9.3% for configurations [vi] and [viii], 14.5% for configurations [ix] and [xi] and 15.6% for configurations [x] and [xii]. The predicted increases were 5.2% for configurations [vi] and [viii], 6.5% for configurations [ix] and [xi] and 7.9% for configurations [x] and [xii]. As can be seen, the actual increases are much larger than predicted increases. This is due to the decrease in the plenum loss coefficient brought about by the introduction of the round-to-round diffuser.

From table 5.3.2 it can be seen that the highest volumetric flow rate per unit frontal area of all of the configurations tested without a diffuser and with windwalls present is 2.792 m/s for configuration [ix]. Unfortunately it has a fairly low volumetric flow rate per unit fan power ratio of 2.035 m^3/s/kW. With the windwalls removed (as for configuration [x]), V_{sys}/P increases by 5% to 2.137 m^3/s/kW and V_{sys}/A_{he} increases by 4.8% to 2.927 m/s. Similarly, the addition of the round-to-round diffuser results in a 13.6% increase in V_{sys}/P from 2.035 m^3/s/kW (for configuration [ix]) to 2.312 m^3/s/kW (for configuration [xi]) and a 11.9% increase in V_{sys}/A_{he} from 2.792 m/s to 3.124 m/s.

From figures C3.1 to C3.5 it can be seen that velocity distribution downstream of the double delta heat exchanger is slightly more uniform than that of the delta heat exchanger. The dead spot downstream of the apex of the double delta heat exchanger is more pronounced due to the extra width of the heat exchanger bundles used. The greater uniformity in the velocity distribution is reflected in the decrease in the outlet kinetic energy coefficient from 1.9 for the delta heat exchanger to 1.5 for the double delta heat exchanger.

6. Conclusions and Recommendations

6.1 Conclusions

Contrary to expectations, the plenum length for a normal flow heat exchanger does not have as great an effect on the system operating point as thought. It is only for very small plenum lengths ($<0.05\ d_F$) that the system operating point (volume flow rate) decreases noticeably. From figure 3.4.1 it can be seen that a plenum length of $0.4\ d_F$ should be used to ensure maximum system performance of the normal flow heat exchanger for a ratio of fan cross-sectional area to heat exchanger frontal area of $A_F/A_{he} = 0.61$. However, it can be further noted from figure 3.4.1 that a plenum length as short as $0.1\ d_F$ only leads to a ± 4% decrease in system performance. For smaller ratios of A_F/A_{he} the required minimum plenum length as well as the sensitivity of the system to variations in plenum length will undoubtedly differ.

Furthermore, decreasing the plenum length has the effect of increasing the distortion in the velocity distribution downstream of the heat exchanger and hence the kinetic energy coefficient at the outlet of the heat exchanger increases and so too the kinetic energy losses to the atmosphere. Table 3.3.2 shows that this distortion in the velocity distribution has very little effect on the thermal performance of the normal flow heat exchanger. As can be seen the maximum percentage difference between total heat transfer rate from the heat exchanger to the air and the heat transfer rate that would be achieved with a uniform velocity distribution is 1.107 %. Thus, even if a very short plenum length (less than the suggested $0.4\ d_F$) is used, the deterioration in the system's volumetric performance is small and the decline in the system's thermal performance is negligible.

According to conventional fan design practice, the system's operating point (volumetric flow rate) is determined by calculating the intersection point between the fan static pressure rise characteristic and the predicted total system pressure losses (as shown in figure 6.1.1). This method effectively assumes that all of the kinetic energy introduced by the fan is dissipated within the plenum and hence that the total pressure available to overcome the total pressure losses of the system is given by the fan static pressure rise. From the results of this study, it would appear that this is a very poor assumption for the case of the normal flow heat exchanger. It is found that typically only approximately 28% of the kinetic energy is lost within the plenum.

In practice, other secondary losses such as supports, screens, louvres etc. which are present in the plenum are not taken into account when determining the total pressure losses of the system (in order to predict the system operating point). These secondary losses decrease the system operating point and hence decrease the discrepancy between the predicted (as determined by the conventional method) and the actual operating points. An advantage of using the conventional design method is that it errs on the conservative side (under predicting the system operating point by ±8%) and hence the air-cooled heat exchanger is slightly over designed. Thus, the air-cooled heat exchanger will at worst perform at the predicted operating point (if not all the secondary losses are taken into account) and in all likelihood slightly better than expected.

For the case of the delta heat exchanger, the amount of kinetic energy lost within the plenum is approximately 2.5 times greater than for the normal flow heat exchanger at 69%. This increase in the amount of kinetic energy lost within the plenum is due to the additional oblique flow losses which now occur within the plenum. Venter [90VE1] observed in tests conducted with a delta heat exchanger having walkways, support structures and fan inlet grid present that exists good agreement between the conventionally predicted operating point (volumetric flow rate) and the actual operating of the system. Thus it would seem that the secondary losses due to the walkway, support structures and fan inlet grid account for the loss of the remaining 31% of the kinetic energy entering the plenum. In view of the above, it is advised that the conventional method of predicting the system operating point (volumetric flow rate) be used.

The introduction of a round-to-round diffuser downstream of the fan and upstream of the delta heat exchanger has two effects : (i) the amount of static pressure recovery downstream of the fan is increased, and (ii) the plenum loss coefficient is decreased. The combination of these two effects leads to a 6.2% increase in the system operating point. A higher system operating (obtained by increasing the fan blade angle for example) would lead to a greater increase in the system operating point when a round-to-round diffuser is added.

If the downstream jetting losses are eliminated by removing the side walls, then there is a 7.4% increase in the system operating point. Thus, a greater improvement in the system operating point is achieved by eliminating the downstream losses than by adding the diffuser. The danger of plume air recirculation however increases if the side walls or windwalls are removed in a practical system.

When compared to the normal flow heat exchanger, the volumetric flow rate per unit fan power for a delta heat exchanger is approximately 9% lower and the volumetric flow rate per unit frontal area is approximately 21% lower. With a round-to-round diffuser present, the volumetric flow rate per unit fan power is 4.3% lower than that for a normal flow heat exchanger whilst the volumetric flow rate per unit frontal area is 16.3% lower. By increasing the fan blade angle the discrepancy between the volumetric flow rate per unit frontal area for the delta and normal flow heat exchangers can be eliminated. However, this would lead to a further decrease in the volumetric flow rate per unit fan power due to decreased fan static efficiency. Hence the advantage that the delta heat exchanger has in requiring less ground surface area as compared to a normal flow heat exchanger is offset by the increased power requirements to obtain the same cooling capacity.

Tests conducted with the double delta heat exchanger indicate that in excess of 95% of the kinetic energy introduced by the fan is dissipated within the plenum. This represents a 38% increase in the amount of kinetic energy lost within the plenum when compared to the delta heat exchanger. The introduction of a round-to-rectangular diffuser downstream of the fan and upstream of the double delta heat exchanger decreases the amount of kinetic energy lost to 59%. Unfortunately, due to the poor pressure recovery characteristics of the round-to-rectangular diffuser this translates to only a 4.5% increase in the system operating point.

If, however, a round-to-round diffuser is used, improvements of up to 14.5% in the system operating point can be achieved in spite of the fact that the round-to-round diffuser only reduces the amount of kinetic energy lost within the plenum to 76% on average. This is due to the fact that the round-to-round diffuser has good pressure recovery characteristics. As the amount of static pressure recovered by the round-to-round diffuser increases with increasing volume flow, the higher the system operating point, the greater the improvement in the operating point when the round-to-round diffuser is introduced.

If the downstream jetting losses are eliminated then the system operating point of the double delta heat exchanger increases by 8.3%. This improvement in the system operating point when the downstream jetting losses are eliminated is slightly higher than that obtained for the delta heat exchanger. This can be attributed to the fact that the double delta heat exchanger has a higher operating point and thus the downstream jetting losses (which are directly proportional to the square of the average velocity through the heat exchanger) are of greater magnitude.

Relative to that of a normal flow heat exchanger, the double delta heat exchanger has a volumetric flow rate per unit fan power that is typically 28% lower and a volumetric flow rate per unit frontal area that is 38% lower. The use of a round-to-round diffuser with the double delta heat exchanger results in a volumetric flow rate per unit fan power ratio that is 18% lower than that for a normal flow heat exchanger and a volumetric flow rate per unit frontal area ratio that is 31% lower. Thus, like the delta heat exchanger, the advantage that the double delta heat exchanger has of requiring less surface area than the normal flow heat exchanger (and the delta heat exchanger) is offset by the greatly increased power requirements to achieve the same cooling capacity. In all likelihood, these substantial decreases in the volumetric flow rate per unit fan power and volumetric flow rate per unit frontal area ratios rule out the double delta heat exchanger as a economically viable option.

6.2 Recommendations

Based upon the results obtained during the course of this project, the following topics are recommended for future research :

- Investigations into how the kinetic energy coefficient at the fan outlet (α_F) varies for various plenum configurations, especially those where obstructions such as support beams and walkways are present within the plenum. Furthermore, tests should be conducted to determine if the assumption that α_F is a function of volumetric flow rate alone is indeed a sound assumption. The exact determination of α_F is important as all the plenum loss coefficients (and hence the percentage kinetic energy lost in the plenum) are based upon the value of this parameter.

- Research to determine the influence of plenum length on the system performance of normal flow heat exchangers having various fan area to heat exchanger area (A_F/A_{he}) ratios and different pressure loss coefficients for the heat exchanger bundles. Data from Russel and Berryman [88RU1] seems to suggest that the system performance of normal flow heat exchangers having smaller A_F/A_{he} ratios than those tested here are slightly more sensitive to plenum length.

References

46SC1 Schmidt, T.E., La Production Calorifique des Surfaces Munies Dailettes, Annexe Du Bulletin De L'Institut International Du Froid, Annex G-5, 1945 - 1946

72LA1 Lambert, P.C., Cowan, G.H., and Bott, T.R., Flow Characteristics in a Box-Shaped Plenum Chamber Associated with an Air-Cooled Heat Exchanger, Atomic Energy Research Establishment, Chemical Engineering Division, Harwell, Berkshire, England, 1972.

73EC1 Eck, B., Fans - Design and Operation of Centrifugal, Axial-flow and Cross-flow Fans, Pergamon Press Ltd, Germany 1973.

73ES1 Engineering Sciences Data Unit, Performance of Conical Diffusers in Incompressible Flow, Item Number 73024, 1973

75TU1 Turner, J.T., The Aerodynamics of Forced Draught Air Cooled Heat Exchangers, International Symposium on Cooling Systems, BHRA Fluid Engineering, paper 6, pp 81-99, Cranfield, Bedford, England, February 1975.

77OS1 Osborne, W.C., Fans, International Series on Heating, Ventilation and Refrigeration, Volume 1, Pergamon Press Ltd., 1977.

78DA1 Daly, B.B., Woods Practical Guide to Fan Engineering, Woods of Colchester Ltd., Third edition, 1978.

80BS1 British Standards Institute, Fans for General Purposes, Part 1, Methods of Testing Performance, BS 848, 1980.

83WA1 Wallis, R.A., Axial Flow Fans and Ducts, John Wiley & Sons, New York, pp 82 - 100, 1983.

85GA1 Ganguli, A., Tung, S.S., Taborek, J., Parametric Study of Air Cooled Heat Exchanger Finned Tube Geometry, Heat Transfer Research, Inc., Vol. 81, No. 245, 1985

85ST1 Ventilatoren Stork Hengelo, General Instructions for E-Type Fans, V.960874, 1985.

88RU1 Russell, C.M.B. and Berryman, R.J., The Calculation of Pressure Losses in Air-Cooled Heat Exchanger Air Inlets and Plenum Losses, American Soceity of Mechanical Engineers, Heat Transfer Division, HTD volume 96, ASME New York, USA, pp 429-434, 1988.

89HO1 Holman, J.P., Heat Transfer, McGraw-Hill Book Company, pp 545 - 559, 1989.

89ID1 Idelchik, I.E. and Fried, E., Flow Resistance : A Design Guide for Engineers, Hemisphere Publishing Corporation, 1989.

89KR1 Kröger, D.G., Cooling Towers Performance Evaluation and Design, Unpublished class note, Department of Mechanical Engineering, University of Stellenbosch, South Africa, 1989.

90VE1 Venter, S.J., The Effectiveness of Axial Flow Fans in A-frame Plenums, M. Eng thesis, Department of Mechanical Engineering, University of Stellenbosch, Republic of South Africa, March 1990.

91BE1 Beiler, M.G., Effect of Flow Maldistribution on Performance of Induced and Forced Draft Air-Cooled Heat Exchangers, M. Eng thesis, Department of Mechanical Engineering, University of Stellenbosch, Republic of South Africa, January 1991.

93VA1 Van Aarde, D.J. and Kröger, D.J., Flow Losses Through an Array of A-Frame Heat Exchangers, Heat Transfer Engineering, Vol. 14, No. 1, pp 43 - 51, 1993.

Appendix A

Experimental and Calculated Results for Normal Flow Heat Exchanger Tests

Table A1.1 : Experimental readings of normal flow heat exchanger with plenum length of 0.05m.

Δp_{sett} (Pa)	Δp_{bell} (Pa)	T (N.m)	N (rpm)
326.914	8.042	48.234	748.120
310.280	11.414	48.810	749.338
283.047	18.204	49.096	746.896
259.888	27.557	50.925	749.079
233.451	43.851	52.838	750.445
196.530	58.989	54.487	748.831
166.505	81.716	56.687	751.699
129.725	102.648	58.589	751.975
86.886	120.393	59.977	750.850
49.699	143.354	60.993	749.854
9.052	162.050	61.843	749.847
-25.575	179.244	62.465	750.001
-50.450	191.224	62.594	748.654
-77.041	204.839	62.700	747.925
-101.058	216.057	63.470	751.580
-107.549	219.489	63.273	750.331

Table A1.2: Experimental readings of normal flow heat exchanger with plenum length of 0.05m (repeat).

Δp_{sett} (Pa)	Δp_{bell} (Pa)	T (N.m)	N (rpm)
339.012	5.358	50.019	752.214
320.287	9.606	50.116	751.687
290.754	17.080	50.067	748.728
267.802	28.372	52.149	752.775
236.063	42.328	53.627	750.785
200.486	59.509	55.472	751.431
165.504	79.861	57.606	752.271
126.161	101.676	58.765	748.717
85.557	122.999	60.636	751.178
48.714	140.936	61.427	749.589
10.694	160.890	62.624	752.100
-25.722	178.917	62.936	750.161
-49.282	190.915	63.120	749.552
-70.371	201.769	63.455	751.165
-88.975	210.629	63.591	751.563
-97.100	213.835	63.445	750.637
-102.602	216.697	63.565	751.264

Table A1.3 : Experimental readings of normal flow heat exchanger with plenum length of 0.3m.

Δp_{sett} (Pa)	Δp_{bell} (Pa)	T (N.m)	N (rpm)
331.156	6.682	49.259	751.617
313.523	11.635	49.454	750.630
293.094	17.274	49.967	750.240
270.763	29.703	51.992	751.030
244.336	44.290	54.129	752.119
213.467	61.541	56.032	750.758
180.017	81.626	57.879	751.401
141.227	105.310	59.602	751.503
101.734	128.408	60.990	751.068
65.221	151.427	62.067	751.521
27.838	174.189	62.736	751.172
-11.074	197.990	63.221	750.680
-31.186	211.505	63.461	750.620
-58.008	227.727	63.502	750.348
-69.451	234.524	63.524	750.416
-86.764	244.607	63.553	751.120
-92.481	247.786	63.313	749.964

Table A1.4 : Experimental readings of normal flow heat exchanger with plenum length of 0.57m.

Δp_{sett} (Pa)	Δp_{bell} (Pa)	T (N.m)	N (rpm)
323.706	5.857	50.014	752.028
307.311	9.723	50.376	752.011
282.483	18.064	51.185	750.137
264.695	28.970	53.225	750.930
240.267	43.370	55.143	750.817
211.573	60.328	56.841	749.745
179.129	81.543	58.516	748.915
145.005	103.748	60.293	751.488
105.777	127.170	60.989	749.144
68.848	151.556	62.203	751.077
31.959	176.570	63.004	752.394
3.006	194.505	63.172	751.543
-26.623	212.758	62.922	748.885
-53.194	228.490	62.937	749.617
-67.279	238.371	63.020	750.607
-79.825	246.497	62.894	750.244
-86.013	251.015	62.943	751.546

Table A1.5: Experimental readings of normal flow heat exchanger with plenum length of 1.08m.

Δp_{sett} (Pa)	Δp_{bell} (Pa)	T (N.m)	N (rpm)
301.535	5.615	49.169	750.646
285.954	9.802	49.616	749.659
267.355	17.563	51.125	749.975
247.252	29.115	53.012	748.948
226.738	42.597	55.045	749.958
198.739	60.567	57.025	750.166
170.140	78.773	58.503	749.159
135.349	102.588	60.329	751.133
98.326	127.493	61.407	750.135
63.744	149.897	62.377	750.267
27.447	172.207	63.079	749.928
-4.662	192.866	63.295	750.117
-32.474	212.558	63.429	750.217
-57.762	228.053	63.309	750.715
-74.475	237.722	62.932	749.232
-85.224	244.188	62.830	749.893
-94.343	250.894	62.745	750.757

Table A1.6 : Experimental readings of normal flow heat exchanger with plenum length of 1.56m from fan.

Δp_{sett} (Pa)	Δp_{bell} (Pa)	T (N.m)	N (rpm)
298.677	5.304	49.629	751.346
283.300	9.837	49.745	750.086
268.130	16.671	50.513	748.443
248.656	27.838	52.593	750.275
226.301	40.809	54.224	749.248
197.412	59.579	56.052	748.899
169.173	79.123	57.772	750.420
132.489	103.181	59.207	750.746
100.756	125.416	59.974	750.130
66.037	151.000	60.937	751.094
33.694	170.943	61.020	748.866
-1.231	193.980	61.330	749.758
-35.721	214.069	61.276	748.694
-52.354	226.678	61.180	748.837
-72.678	238.257	61.110	749.649
-80.780	245.981	61.077	749.982
-93.399	252.608	60.722	748.728

Table A1.7 : Experimental readings of fan system with no normal flow heat exchanger in plenum.

Δp_{sett} (Pa)	Δp_{bell} (Pa)	T (N.m)	N (rpm)
323.250	5.318	53.842	751.865
310.851	9.751	54.214	749.897
303.305	18.549	56.026	750.018
296.187	30.303	56.682	750.451
288.670	48.095	58.258	751.791
276.860	68.717	60.284	750.055
257.060	94.106	62.625	750.462
241.787	128.057	64.008	751.430
224.141	170.971	64.383	750.336
206.900	215.707	64.394	751.410
186.175	281.682	62.938	748.778
161.736	348.244	61.222	751.107
128.711	416.199	57.177	748.999
101.290	476.703	53.411	750.633
77.335	521.176	49.558	750.924
63.863	548.653	46.883	748.998
50.747	574.693	44.540	750.817

Table A1.8 : Experimental readings of fan system with no normal flow heat exchanger in plenum (repeat).

Δp_{sett} (Pa)	Δp_{bell} (Pa)	T (N.m)	N (rpm)
321.850	7.181	53.418	751.733
309.905	11.552	53.614	748.838
300.904	19.119	55.039	748.139
295.680	31.775	56.135	750.562
287.473	47.694	57.857	751.620
276.339	70.224	59.975	750.900
261.695	95.346	62.192	750.999
238.766	127.395	63.402	749.704
224.744	171.817	64.380	751.596
203.944	214.959	63.582	748.164
186.207	285.010	62.824	748.420
158.128	357.502	60.805	751.373
125.325	420.500	56.578	749.093
97.734	478.114	52.600	750.842
76.036	521.116	48.821	748.000

Table A2.1 : Calculated fan system characteristics for normal flow heat exchanger with plenum length of 0.05m.

V (m^3/s)	Δp_{sFS} (Pa)	P (W)	η_{sFS} %
2.856	324.091	3755.799	24.647
3.397	306.541	3787.688	27.491
4.303	281.373	3833.810	31.578
5.277	256.764	3952.589	34.281
6.643	229.700	4085.023	37.354
7.719	194.084	4229.154	35.422
9.047	163.058	4365.115	33.796
10.133	126.808	4506.634	28.511
10.985	85.030	4625.282	20.195
11.999	48.573	4714.413	12.362
12.752	8.524	4778.291	2.275
13.404	-25.562	4822.727	-7.105
13.866	-50.211	4848.845	-14.359
14.362	-76.599	4865.261	-22.611
14.675	-99.356	4876.077	-29.902
14.814	-106.060	4876.835	-32.218

Table A2.2 : Calculated fan system characteristics for normal flow heat exchanger with plenum length of 0.05m. (repeat).

V (m^3/s)	Δp_{sFS} (Pa)	P (W)	η_{sFS} %
2.319	332.362	3851.588	20.008
3.106	314.375	3863.699	25.274
4.157	287.543	3889.375	30.733
5.328	261.915	4006.783	34.826
6.523	231.985	4140.856	36.542
7.725	196.560	4274.474	35.521
8.935	161.772	4427.494	32.649
10.126	124.345	4557.721	27.627
11.097	83.614	4670.214	19.867
11.899	47.625	4749.521	11.931
12.666	10.078	4807.931	2.655
13.387	-25.685	4855.170	-7.082
13.836	-48.922	4876.168	-13.882
14.191	-69.377	4879.947	-20.175
14.488	-87.506	4884.354	-25.957
14.615	-95.688	4884.803	-28.629
14.700	-100.914	4885.558	-30.363

Table A2.3 : Calculated fan system characteristics for normal flow heat exchanger with plenum length of 0.3 m.

V (m^3/s)	$\Delta p_{s_{FS}}$ (Pa)	P (W)	$\eta_{s_{FS}}$ %
2.583	323.035	3774.079	22.106
3.412	306.573	3798.378	27.538
4.159	286.821	3840.969	31.055
5.446	264.320	3987.319	36.104
6.639	237.730	4138.098	38.141
7.833	208.331	4297.863	37.993
9.016	175.257	4430.445	35.665
10.235	137.307	4559.319	30.825
11.304	98.864	4669.127	23.936
12.264	63.121	4744.109	16.318
13.155	26.701	4797.901	7.321
14.029	-11.254	4839.444	-3.262
14.498	-30.886	4857.678	-9.218
15.045	-57.092	4863.040	-17.663
15.265	-68.245	4863.269	-21.421
15.572	-84.970	4855.518	-27.251
15.696	-90.814	4851.885	-29.379

Table A2.4 : Calculated fan system characteristics for normal flow heat exchanger with plenum length of 0.57m.

V (m^3/s)	$\Delta p_{s_{FS}}$ (Pa)	P (W)	$\eta_{s_{FS}}$ %
2.417	315.488	3828.580	19.916
3.114	299.465	3855.804	24.181
4.253	276.559	3936.399	29.883
5.380	258.524	4083.890	34.056
6.582	234.639	4231.338	36.498
7.772	207.098	4372.838	36.806
9.042	175.601	4510.278	35.206
10.161	141.042	4613.886	31.062
11.281	103.370	4694.624	24.839
12.279	66.751	4761.688	17.213
13.225	30.620	4804.430	8.429
13.893	2.472	4826.744	0.711
14.577	-26.574	4840.382	-8.003
15.088	-52.520	4830.849	-16.403
15.388	-66.124	4823.763	-21.094
15.654	-78.437	4818.224	-25.483
15.768	-84.185	4804.955	-27.627

Table A2.5 : Calculated fan system characteristics for normal flow heat exchanger with plenum length of 1.08m.

V (m^3/s)	$\Delta p_{s_{FS}}$ (Pa)	P (W)	$\eta_{s_{FS}}$ %
2.379	296.994	3803.716	18.572
3.146	282.336	3847.874	23.087
4.209	263.681	3960.800	28.022
5.426	244.445	4117.423	32.212
6.553	223.478	4262.999	34.351
7.809	195.664	4412.650	34.628
8.915	167.847	4537.882	32.976
10.144	132.684	4653.413	28.924
11.319	96.487	4747.405	23.006
12.267	62.350	4819.021	15.872
13.150	26.608	4875.971	7.176
13.908	-5.038	4888.621	-1.433
14.595	-32.417	4896.301	-9.663
15.104	-57.217	4879.384	-17.711
15.449	-73.920	4868.726	-23.455
15.642	-84.365	4851.723	-27.200
15.836	-93.124	4833.637	-30.509

Table A2.6 : Calculated fan system characteristics for normal flow heat exchanger with plenum length of 1.56m.

V (m^3/s)	$\Delta p_{s_{FS}}$ (Pa)	P (W)	$\eta_{s_{FS}}$ %
2.311	293.997	3836.940	17.708
3.152	279.744	3858.258	22.854
4.112	265.871	3934.459	27.787
5.300	245.281	4075.697	31.893
6.424	223.756	4212.691	34.120
7.763	195.262	4357.527	34.787
8.926	166.540	4471.807	33.242
10.185	130.169	4577.246	28.964
11.234	99.012	4642.695	23.959
12.307	64.544	4703.454	16.888
13.129	32.896	4736.418	9.119
13.964	-1.671	4747.526	-0.491
14.686	-35.801	4755.222	-11.056
15.107	-52.236	4745.185	-16.630
15.468	-72.163	4728.550	-23.605
15.708	-80.086	4721.417	-26.645
15.943	-92.820	4709.130	-31.425

Table A2.7 : Calculated characteristics of fan system without normal flow heat exchanger in plenum.

V (m^3/s)	Δp_{sF} (Pa)	P (W)	η_{sF} %
2.300	314.242	4111.061	17.581
3.122	303.729	4160.712	22.793
4.305	296.216	4298.058	29.672
5.499	288.882	4343.063	36.579
6.915	280.483	4447.592	43.610
8.284	270.171	4623.053	48.411
9.687	250.458	4796.435	50.584
11.284	234.843	4889.000	54.202
13.055	218.178	4931.135	57.762
14.640	200.652	4917.040	59.744
16.786	181.582	4838.718	62.991
18.601	156.490	4676.520	62.246
20.386	124.873	4390.726	57.978
21.764	97.468	4082.587	51.960
22.743	73.976	3784.246	44.458
23.391	61.119	3597.932	39.735
23.879	48.003	3401.142	33.702

Table A2.8 : Calculated characteristics of fan system without normal flow heat exchanger in plenum (repeat).

V (m^3/s)	Δp_{sFS} (Pa)	P (W)	η_{sFS} %
2.675	313.491	4086.673	20.522
3.406	304.148	4133.000	25.064
4.385	295.822	4250.384	30.522
5.635	288.767	4306.901	37.781
6.893	279.900	4426.139	43.592
8.372	269.488	4596.434	49.083
9.752	255.036	4764.455	52.202
11.290	233.348	4872.809	54.063
13.076	218.388	4922.380	58.014
14.690	199.819	4905.105	59.842
16.906	182.075	4842.445	63.567
18.855	153.095	4648.809	62.093
20.505	121.714	4350.570	57.365
21.807	94.102	4024.743	50.987
22.848	73.402	3763.268	44.565

Table A3.1 : Velocity distribution downstream of normal flow heat exchanger with plenum length of 0.05 m. Velocities are given in m/s.

	1	2	3	4	5	6	7	8
A	2.384	4.098	5.434	5.262	5.213	5.000	4.174	2.219
B	4.315	5.789	4.670	3.244	2.903	3.653	4.799	4.035
C	4.649	5.258	4.501	1.948	1.403	3.185	3.850	3.765
D	5.056	5.743	5.258	2.170	-0.760	4.042	6.026	6.153
E	2.462	4.025	3.982	3.855	3.251	4.110	5.084	4.466
F	1.633	3.264	4.094	4.052	4.157	4.473	3.848	1.872
G	2.217	3.068	2.231	3.267	3.890	3.842	3.143	3.205

Table A3.2 : Velocity distribution downstream of normal flow heat exchanger with plenum length of 0.05m (repeat). Velocities are given in m/s.

	1	2	3	4	5	6	7	8
A	2.102	2.363	1.317	3.286	4.043	3.974	2.673	1.909
B	2.214	3.749	4.056	4.192	4.308	4.349	4.581	3.149
C	4.112	4.932	4.303	2.238	0.470	4.388	5.293	4.423
D	5.549	5.840	5.235	2.290	-0.417	3.699	4.460	4.960
E	4.750	5.283	4.089	2.767	3.677	4.530	5.390	4.786
F	2.505	5.760	5.402	4.368	4.178	4.994	5.718	2.983
G	3.191	3.678	5.522	5.433	5.193	4.487	3.136	2.951

Table A3.3 : Velocity distribution downstream of normal flow heat exchanger with plenum length of 0.3m.

	1	2	3	4	5	6	7	8
A	5.165	5.041	5.454	4.959	4.931	4.656	5.131	5.021
B	5.222	5.338	4.186	3.074	2.903	3.401	4.029	4.220
C	4.494	4.946	4.218	3.242	1.863	3.383	3.164	3.645
D	4.684	6.086	5.936	1.917	-0.589	4.602	6.011	6.108
E	3.435	3.656	3.705	3.258	2.632	3.521	4.558	5.112
F	4.016	3.869	3.855	3.953	4.249	4.551	4.776	4.825
G	3.239	3.596	3.671	3.890	3.870	3.925	3.644	4.130

Table A3.4 : Velocity distribution downstream of normal flow heat exchanger with plenum length of 0.57m. Velocities in m/s.

	1	2	3	4	5	6	7	8
A	5.110	5.200	4.890	4.683	4.814	4.952	4.924	5.372
B	5.202	5.066	3.947	3.381	3.258	3.817	4.001	4.192
C	4.649	5.095	4.239	1.729	2.026	3.150	3.362	3.426
D	5.191	5.511	4.699	0.217	2.044	4.661	5.482	5.720
E	3.357	4.032	4.039	3.066	3.172	3.648	4.309	4.480
F	3.869	4.199	4.431	4.241	4.185	4.424	4.466	4.466
G	3.472	3.650	3.808	3.980	3.753	4.096	3.945	4.034

Table A3.5 : Velocity distribution downstream of normal flow heat exchanger with plenum length of 1.08m. Velocities are given in m/s.

	1	2	3	4	5	6	7	8
A	4.793	5.213	4.883	4.470	4.683	4.573	4.704	4.800
B	4.731	5.045	4.547	3.831	3.476	3.763	3.967	3.933
C	4.374	5.067	4.770	2.337	2.033	3.277	3.475	3.348
D	4.885	5.526	5.504	2.879	2.834	5.355	6.056	5.862
E	3.322	3.592	3.435	3.286	3.513	3.819	4.103	4.096
F	3.960	3.918	3.925	3.834	3.981	4.382	4.565	4.333
G	3.520	3.534	3.808	3.774	3.822	4.076	4.082	3.904

Table A3.6 : Axial velocity distribution 1.5m downstream of S-fan without normal flow heat exchanger present in plenum. Velocities are given in m/s.

	1	2	3	4	5	6	7	8
A	4.683	6.625	7.671	6.955	6.941	0.016	4.972	3.967
B	8.060	5.884	2.016	2.664	3.094	5.359	7.037	6.880
C	7.294	4.260	-0.089	-0.054	-0.054	2.549	5.951	7.188
D	7.577	3.819	-0.097	-0.373	0.038	2.111	6.376	8.002
E	7.266	4.977	1.360	1.346	1.254	3.535	7.180	7.799
F	6.154	6.477	5.057	5.247	5.479	6.998	8.129	6.934
G	4.021	5.097	7.668	6.482	6.036	6.071	5.694	3.376

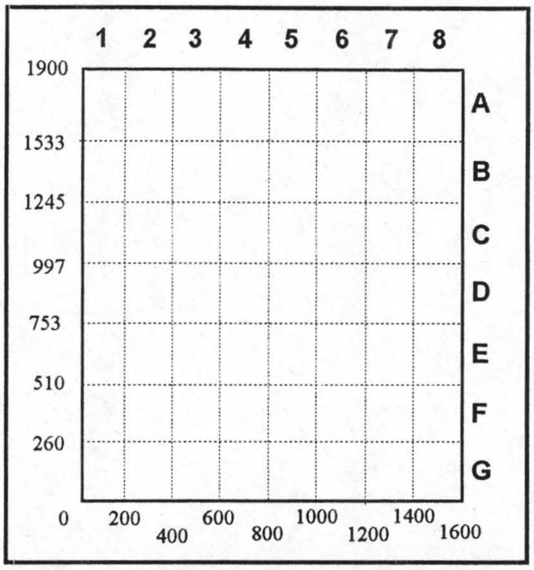

Figure A1.1 : Velocity traverse grid for normal flow heat exchanger (dimensions in mm).

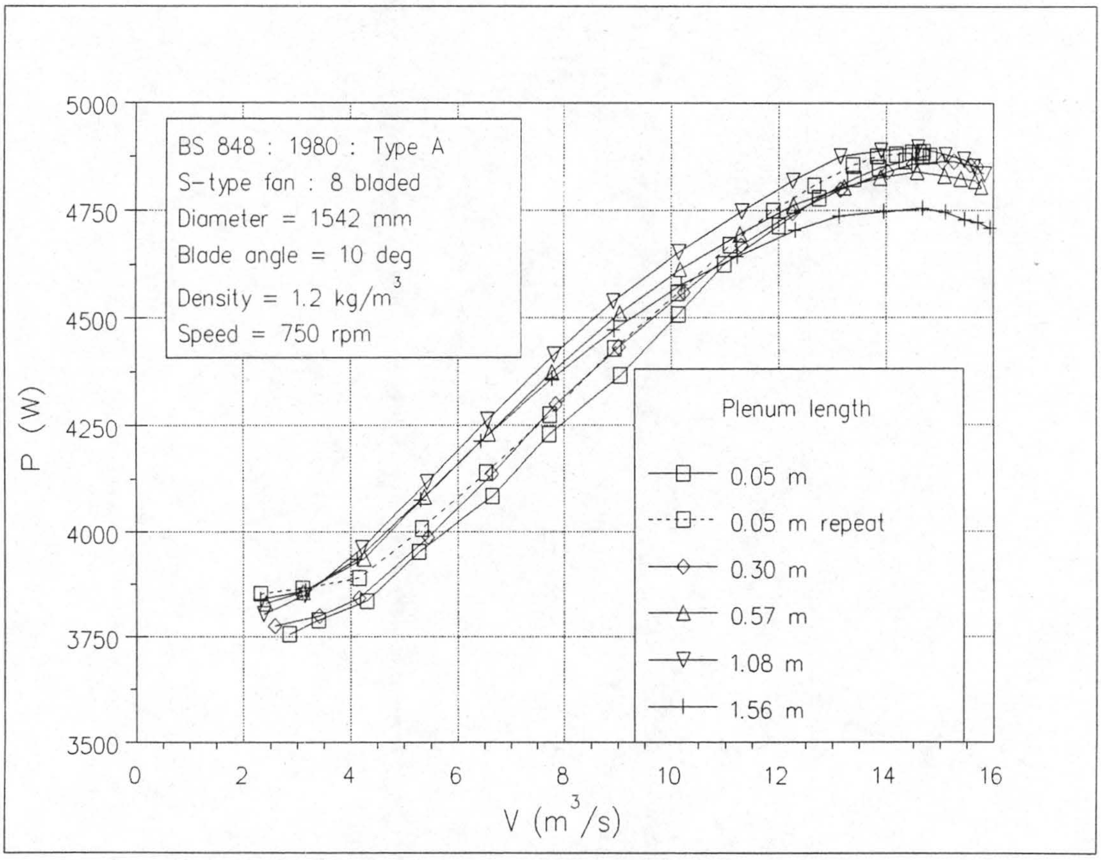

Figure A2.1 : P versus V for normal flow heat exchanger

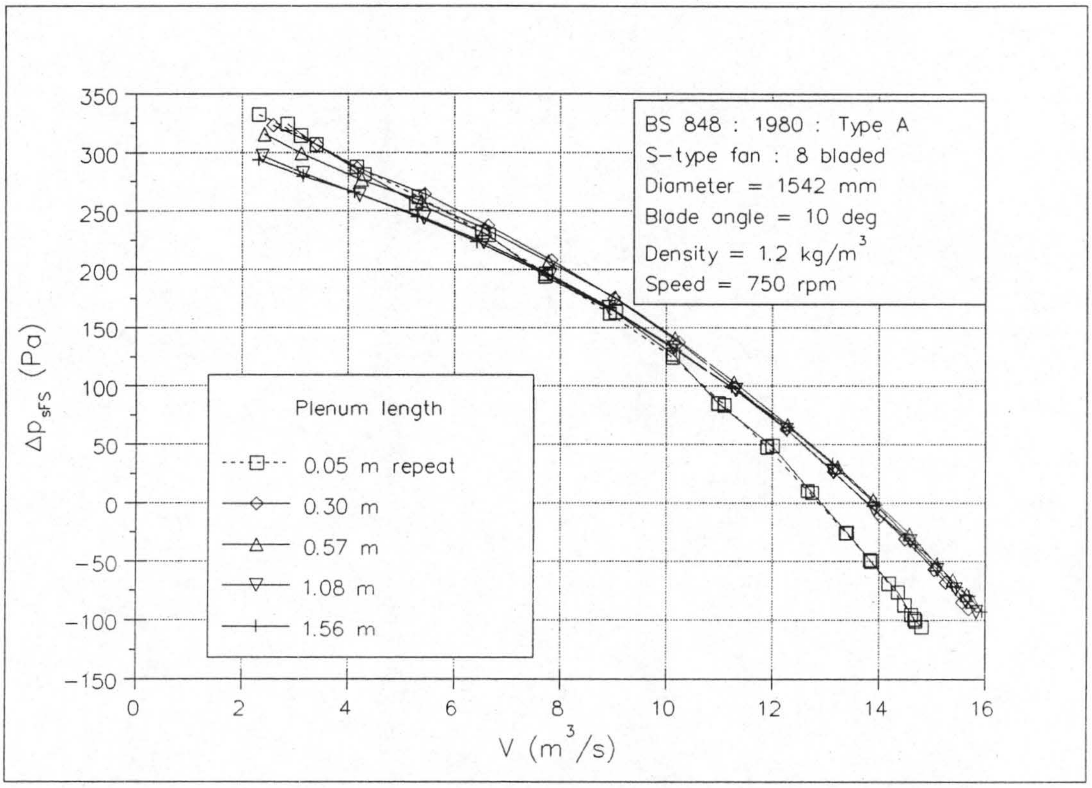

Figure A2.2 : Δp_{sFS} versus V for S-fan with normal flow heat exchanger.

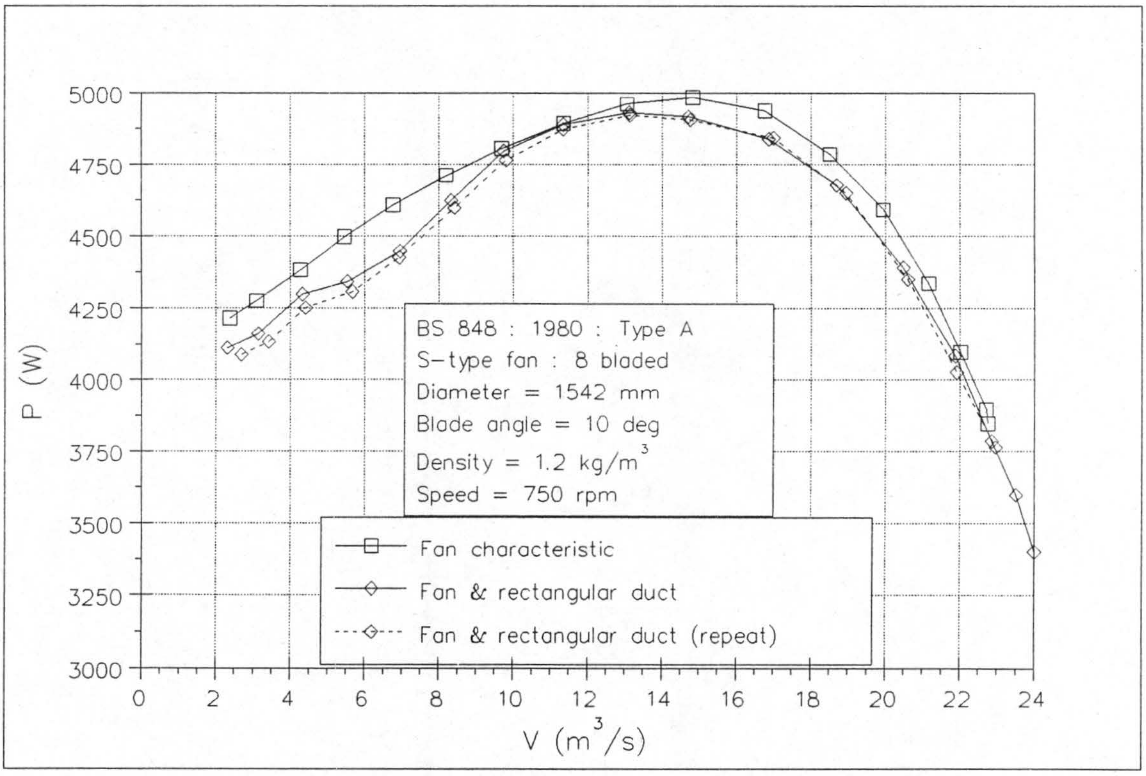

Figure A2.3 : P versus V for S-fan without a heat exchanger in the plenum.

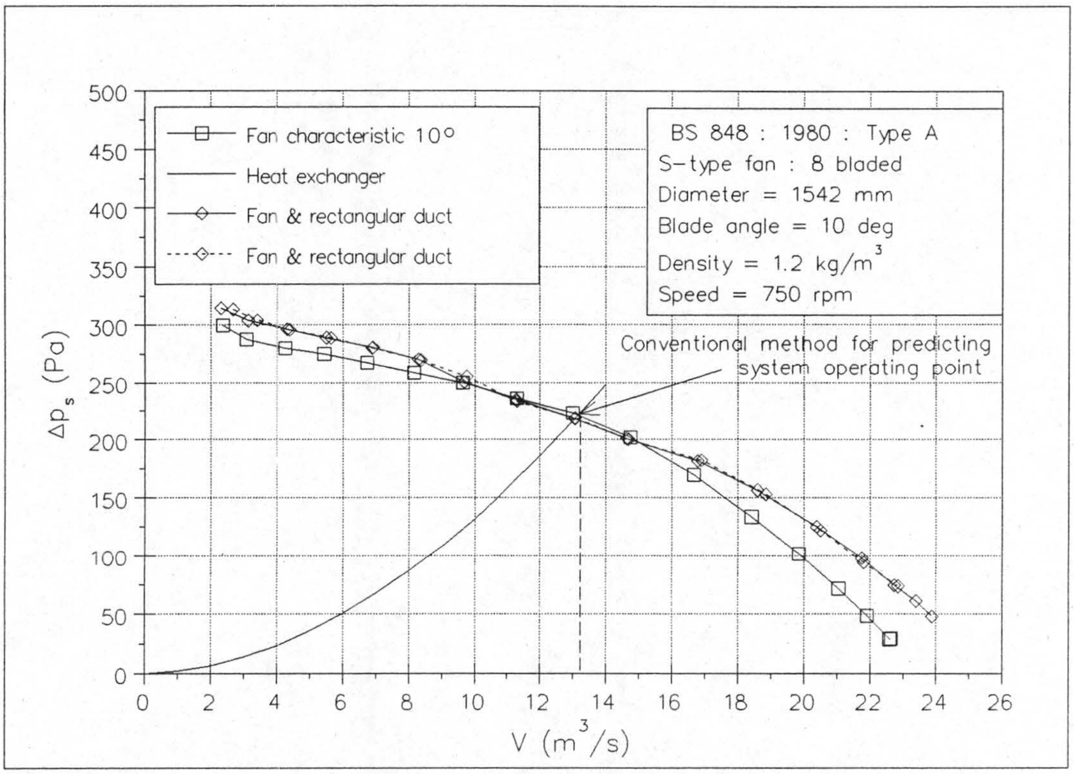

Figure A2.4 : Δp_S versus V for S-fan without a heat exchanger in the plenum.

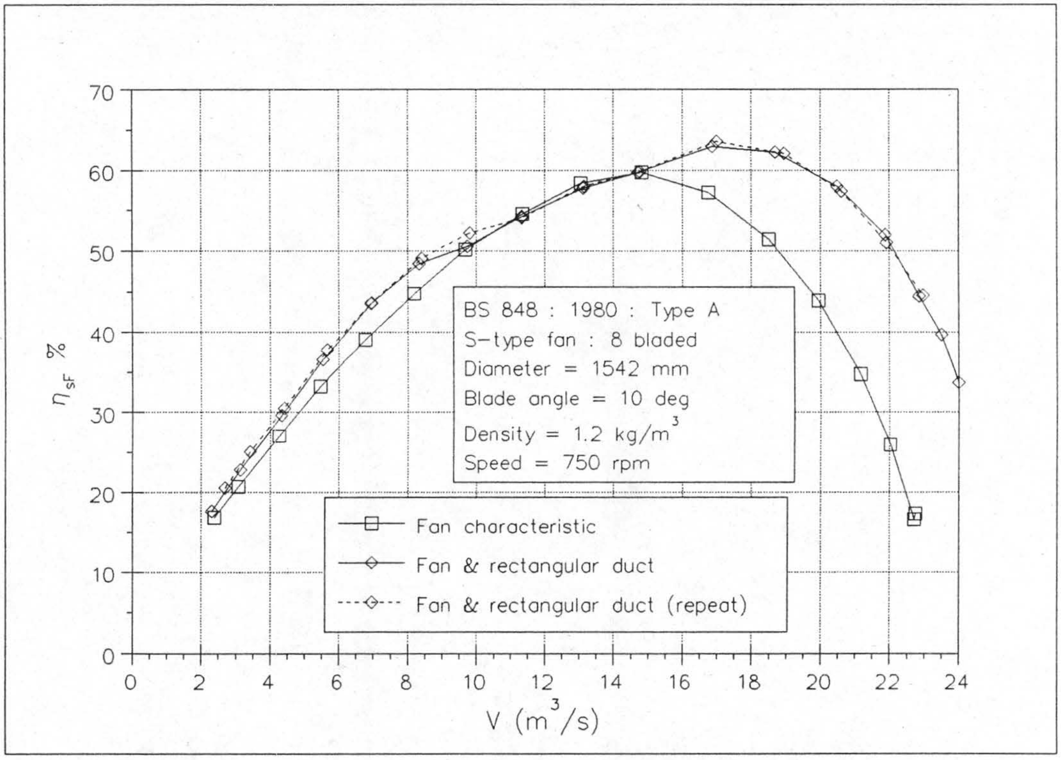

Figure A2.5 : η_S versus V for S-fan without a heat exchanger in the plenum.

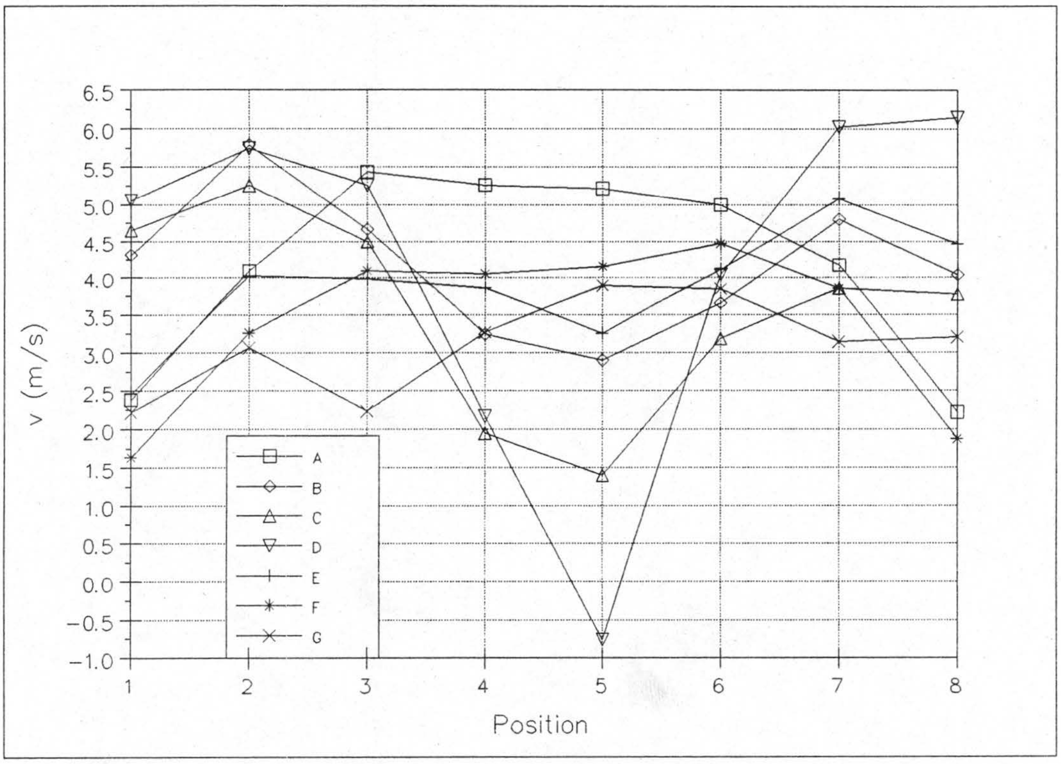

Figure A3.1 : Velocity distribution downstream of normal flow heat exchanger with plenum length of 0.05m.

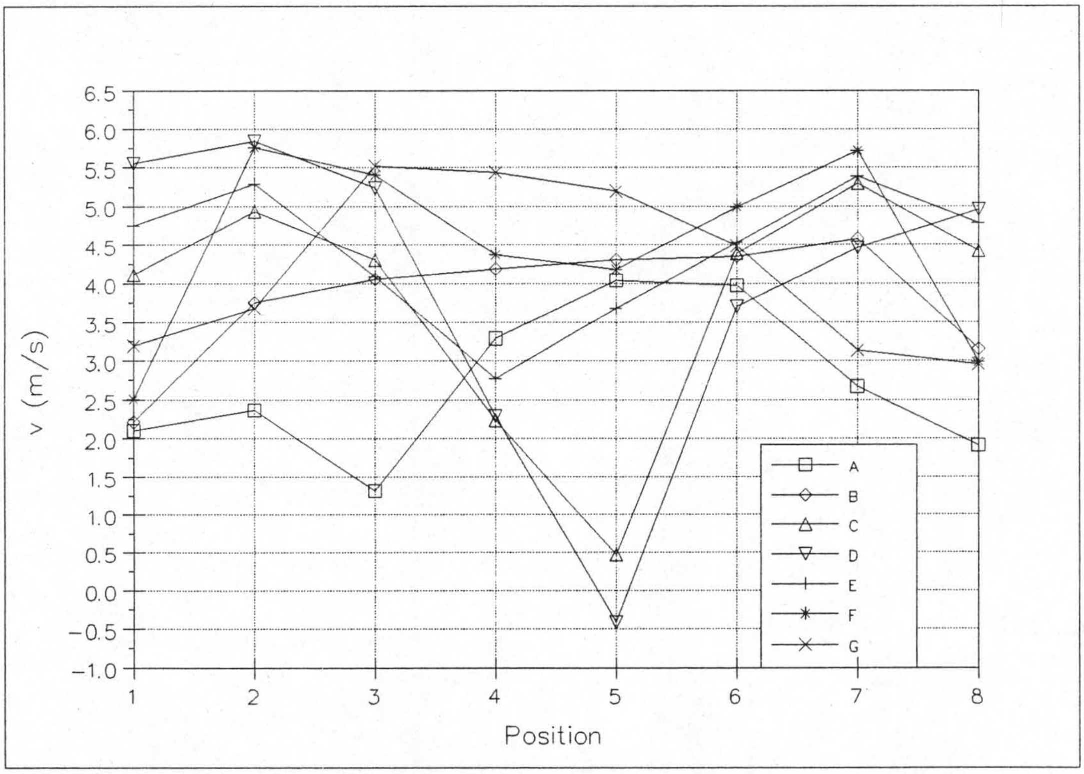

Figure A3.2 : Velocity distribution downstream of normal flow heat exchanger with plenum length of 0.05m (repeat).

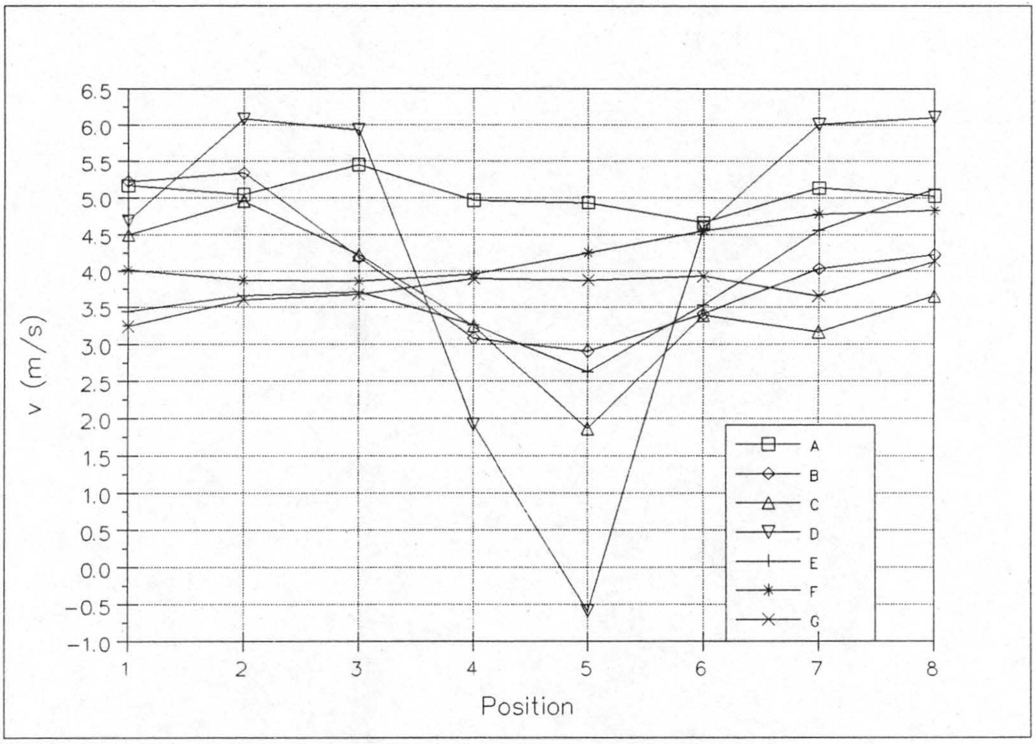

Figure A3.3 : Velocity distribution downstream of normal flow heat exchanger with plenum length of 0.3m.

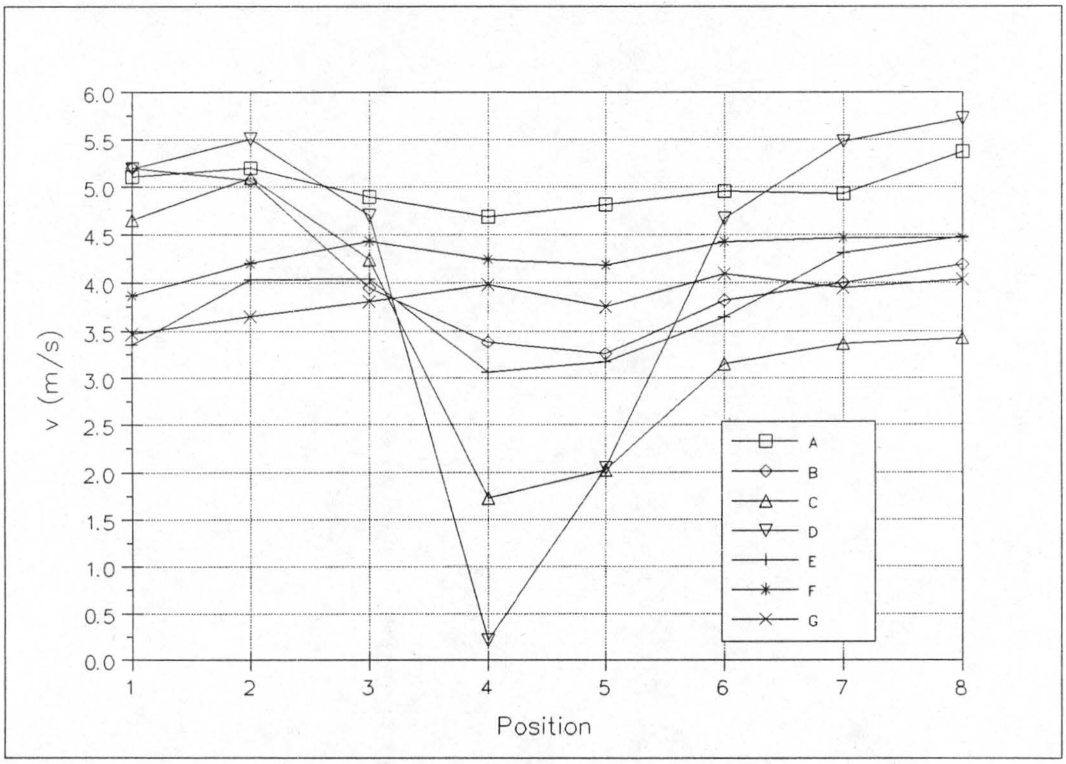

Figure A3.4 : Velocity distribution downstream of normal flow heat exchanger with plenum length of 0.57 m.

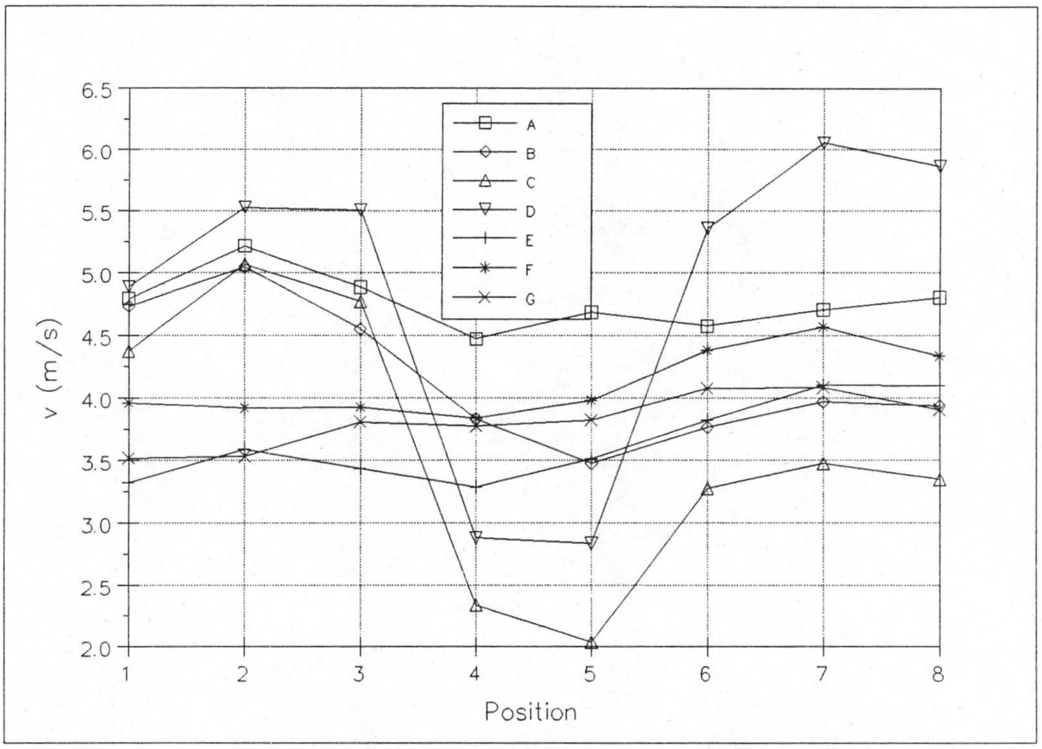

Figure A3.5 : Velocity distribution downstream of normal flow heat exchanger with plenum length of 1.08 m.

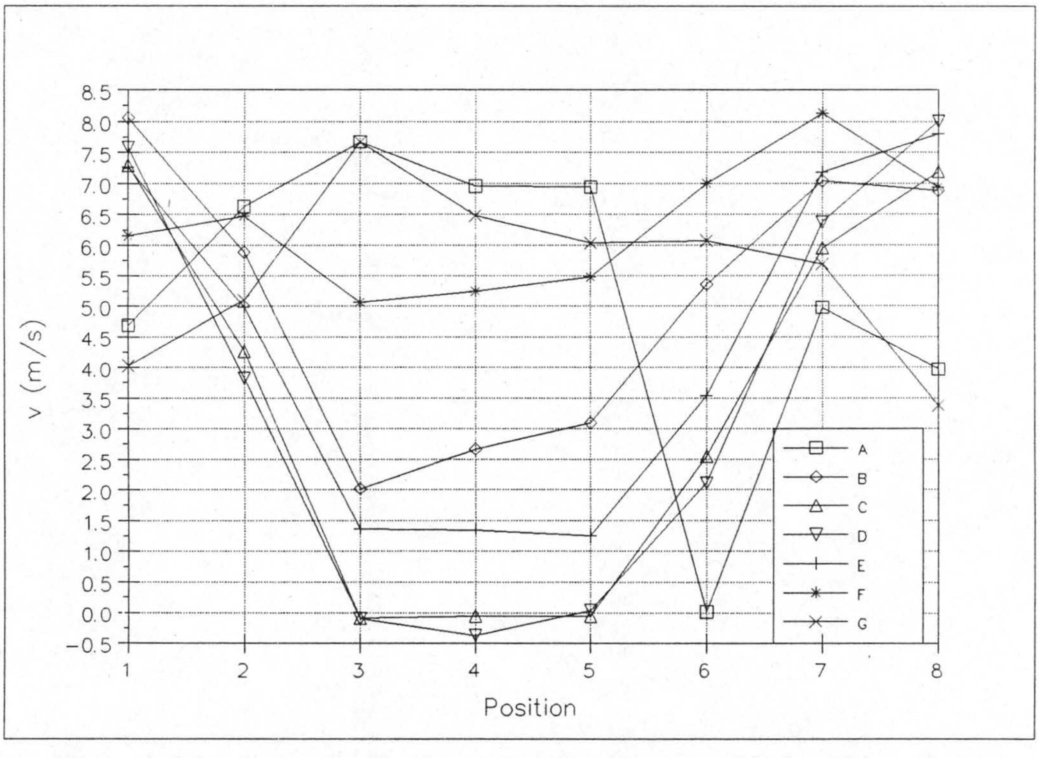

Figure A3.6 : Axial velocity distribution 1.5 m downstream of S-fan with no heat exchanger in plenum.

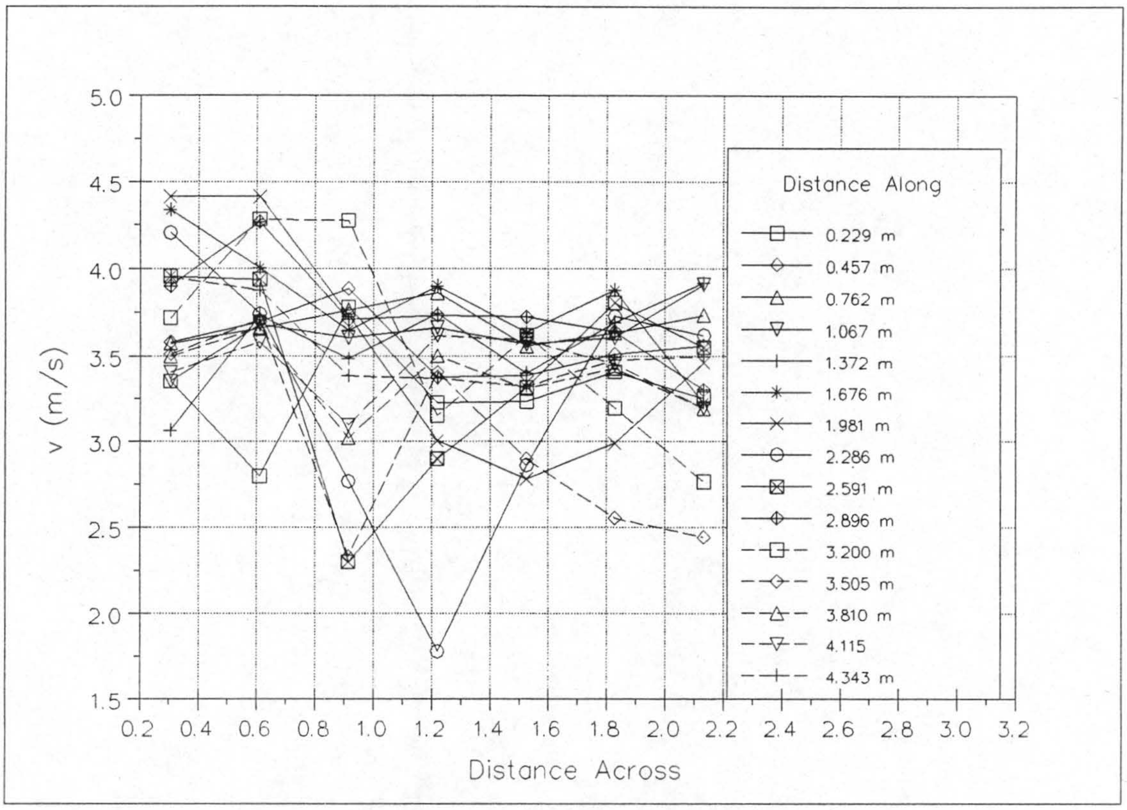

Figure A3.7 : Velocity distribution as measured by Turner [75TU1].

Appendix B

Experimental and Calculated Results for Delta Heat Exchanger Tests

Table B1.1 : Experimental readings of the delta heat exchanger with the S-fan blade angle set to 14°. (Configuration [i] in figure 4.1.2)

Δp_{sett} (Pa)	Δp_{bell} (Pa)	T (N.m)	N (rpm)
333.021	6.533	71.661	750.321
321.612	10.072	71.388	750.251
305.974	18.867	71.343	750.495
294.933	31.596	71.705	749.928
282.633	48.163	74.194	749.814
266.932	70.153	76.779	750.128
247.401	94.890	78.655	748.511
224.697	122.299	80.630	749.629
197.653	157.774	82.006	749.413
170.851	197.580	83.748	750.946
136.394	243.333	84.563	749.592
92.561	296.977	84.994	749.142
59.106	338.802	85.055	749.988
29.939	371.523	84.350	748.055
7.688	400.646	84.289	750.388
-14.390	423.170	83.108	747.492
-21.960	435.013	83.133	748.998
-23.481	434.446	83.346	749.115

Table B1.2 : Experimental readings of the delta heat exchanger with the S-fan blade angle set to 18°. (Configuration [ii] in figure 4.1.2)

Δp_{sett} (Pa)	Δp_{bell} (Pa)	T (N.m)	N (rpm)
358.701	5.734	97.880	751.361
346.442	10.314	96.329	751.218
330.567	17.293	94.895	751.679
314.724	30.279	93.796	751.903
301.768	47.605	94.267	751.481
290.178	69.175	96.840	751.871
272.767	96.344	99.766	751.386
253.933	128.815	102.005	751.118
222.375	169.376	104.194	750.299
198.128	210.722	106.452	751.437

Table B1.2 : continued.

Δp_{sett} (Pa)	Δp_{bell} (Pa)	T (N.m)	N (rpm)
161.367	265.886	108.398	750.525
120.069	325.459	110.424	751.878
82.034	375.602	111.022	750.334
51.851	412.762	111.213	749.728
28.401	444.735	111.917	751.529
14.136	464.103	112.015	751.362
6.550	473.307	112.202	752.232
-0.413	483.016	111.912	751.445
-4.506	487.745	111.936	751.696

Table B1.3 : Experimental readings of the delta heat exchanger with the S-fan blade angle set to 18°. (repeat, configuration [ii] in figure 4.1.2)

Δp_{sett} (Pa)	Δp_{bell} (Pa)	T (N.m)	N (rpm)
340.424	5.415	94.759	750.383
328.769	9.663	93.635	749.658
312.944	17.477	91.495	747.354
295.315	29.044	90.080	749.385
279.937	45.054	89.500	750.048
268.158	66.080	91.689	747.476
254.220	92.414	95.124	748.991
232.601	121.342	97.144	747.689
209.754	161.089	100.169	750.101
183.896	197.603	101.516	747.980
151.505	246.561	103.538	746.909
113.662	301.647	105.480	747.932
80.169	347.143	106.465	748.166
49.620	386.426	106.712	746.920
27.817	413.725	107.185	747.781
10.739	439.167	107.265	747.762
6.329	442.186	107.315	748.251
1.916	451.388	107.598	748.413
-5.369	460.495	107.663	748.493

Table B1.4 : Experimental readings of delta heat exchanger with a pair of curved guide vanes positioned as shown in figure 4.1.2 and the S-fan blade angle set to 18°. (Configuration [iii] in figure 4.1.2)

Δp_{sett} (Pa)	Δp_{bell} (Pa)	T (N.m)	N (rpm)
337.938	8.002	92.678	749.148
327.734	10.779	91.393	749.190
310.676	19.401	89.914	751.055
294.734	30.647	88.286	748.513
284.029	49.191	88.921	748.473
274.595	70.273	91.808	748.548
260.561	97.773	94.953	750.273
240.855	125.766	97.012	748.983
214.739	164.157	99.254	748.392
192.567	202.544	101.319	750.067
158.384	256.340	103.524	749.295
119.044	314.586	105.446	750.789
85.527	361.599	105.709	748.424
51.786	409.146	106.704	749.611
33.055	434.545	106.729	749.664
24.515	448.422	106.845	749.323
14.426	460.480	106.818	749.076
0.147	476.124	106.724	749.229

Table B1.5 : Experimental readings of the delta heat exchanger with no side walls and the S-fan blade angle set to 18°. (Configuration [iv] in figure 4.1.2)

Δp_{sett} (Pa)	Δp_{bell} (Pa)	T (N.m)	N (rpm)
348.491	5.781	96.981	749.369
337.012	9.548	95.941	748.107
320.492	18.633	94.579	747.991
306.296	29.746	92.941	747.799
294.005	46.708	93.258	750.144
283.671	69.579	95.897	748.779
269.679	95.262	98.937	750.039
249.565	126.457	100.830	747.446
226.963	165.749	104.078	749.730

Table B1.5 : continued

Δp_{sett} (Pa)	Δp_{bell} (Pa)	T (N.m)	N (rpm)
200.977	211.874	105.951	748.549
167.653	269.154	108.141	749.719
131.406	333.014	109.335	748.285
97.303	385.139	110.121	748.659
67.795	434.222	110.568	748.535
43.121	472.930	110.756	749.480
32.743	489.307	110.424	748.673
24.208	501.930	110.419	749.315
12.761	522.058	110.264	749.031
11.362	524.229	110.386	749.512

Table B1.6 : Experimental readings of the delta heat exchanger with a round-to-round diffuser and the S-fan blade angle set to 18°. (Configuration [v] in figure 4.1.2)

Δp_{sett} (Pa)	Δp_{bell} (Pa)	T (N.m)	N (rpm)
348.284	5.927	93.596	750.703
336.349	4.682	92.220	749.870
321.054	19.495	91.014	749.200
304.722	27.889	90.316	750.073
286.413	46.448	89.418	749.181
287.911	69.684	92.097	748.555
283.239	98.012	95.963	748.900
267.859	129.846	99.195	748.388
244.177	169.415	102.779	750.276
207.368	211.408	104.650	748.226
165.771	269.357	106.472	747.827
127.382	326.324	107.747	747.571
91.191	385.633	108.854	747.686
61.911	432.648	109.019	746.821
39.286	459.852	109.108	747.804
17.940	488.612	109.047	748.533
16.074	493.597	109.241	749.040
12.196	501.608	109.295	749.310

Table B1.7 : Experimental readings of the delta heat exchanger with a round-to-round diffuser, no side walls and the S-fan blade angle set to 18°. (Configuration [vi] in figure 4.1.2)

Δp_{sett} (Pa)	Δp_{bell} (Pa)	T (N.m)	N (rpm)
342.889	6.088	92.193	749.728
332.184	7.446	90.667	747.523
315.465	16.115	89.755	747.718
300.396	28.092	89.767	751.015
283.738	44.091	88.008	746.276
288.354	69.986	91.495	748.963
287.102	99.516	95.116	750.071
274.628	135.192	98.431	747.696
255.038	182.234	102.128	749.860
233.290	225.094	104.084	749.553
191.008	283.238	105.838	747.632
156.428	357.907	107.797	748.151
116.549	412.256	107.991	747.162
87.582	470.667	108.067	747.223

Table B2.1 : Calculated fan system characteristics for the delta heat exchanger with the S-fan blade angle set to 14°. (Configuration [i] in figure 4.1.2)

V (m^3/s)	Δp_{sFS} (Pa)	P (W)	η_{sFS} %
2.552	324.463	5483.849	15.101
3.169	313.362	5463.348	18.176
4.335	297.863	5455.575	23.669
5.614	287.486	5490.924	29.391
6.931	275.506	5682.547	33.604
8.360	259.885	5874.687	36.984
9.742	241.795	6043.080	38.980
11.041	218.818	6175.036	39.125
12.541	192.424	6282.348	38.412
14.002	165.466	6387.913	36.268
15.561	132.328	6471.188	31.821
17.194	89.563	6509.238	23.658
18.338	56.697	6497.067	16.003
19.247	28.392	6474.684	8.440
19.921	6.536	6428.411	2.025
20.548	-15.068	6386.130	-4.848
20.790	-22.410	6361.977	-7.323
20.773	-23.883	6376.177	-7.781

Table B2.2 : Calculated fan system characteristics of the delta heat exchanger with the S-fan blade angle set to 18°. (Configuration [ii] in figure 4.1.2)

V (m^3/s)	Δp_{sFS} (Pa)	P (W)	η_{sFS} %
2.379	345.927	7414.007	11.101
3.191	334.179	7298.346	14.612
4.129	318.408	7179.776	18.311
5.461	302.887	7091.308	23.325
6.850	290.664	7134.013	27.911
8.253	279.125	7320.241	31.467
9.744	262.598	7549.880	33.891
11.269	244.505	7723.410	35.674
12.932	214.387	7903.835	35.076
14.399	190.250	8048.768	34.034

Table B2.2 : continued.

V (m^3/s)	$\Delta p_{s_{FS}}$ (Pa)	P (W)	$\eta_{s_{FS}}$ %
16.188	155.053	8212.863	30.561
17.870	114.615	8332.792	24.579
19.229	78.248	8409.285	17.893
20.168	49.118	8434.876	11.744
20.880	26.267	8445.624	6.494
21.331	12.520	8455.587	3.159
21.515	5.195	8449.516	1.323
21.756	-1.506	8444.785	-0.388
21.854	-5.446	8440.545	-1.410

Table B2.3 : Calculated fan system characteristics for the delta heat exchanger with the S-fan blade angle set to 18°. (repeat, configuration [ii] in figure 4.1.2)

V (m^3/s)	$\Delta p_{s_{FS}}$ (Pa)	P (W)	$\eta_{s_{FS}}$ %
2.372	345.605	7555.914	10.849
3.171	334.368	7479.875	14.177
4.278	320.168	7352.844	18.626
5.498	300.413	7198.683	22.945
6.841	284.180	7138.605	27.233
8.312	274.011	7362.760	30.935
9.809	258.609	7606.674	33.348
11.257	237.301	7793.546	34.276
12.926	212.444	7982.819	34.398
14.353	187.125	8134.018	33.019
16.050	154.353	8317.154	29.786
17.722	115.154	8446.803	24.160
18.999	80.816	8517.448	18.027
20.072	49.754	8563.111	11.663
20.741	27.341	8579.412	6.610
21.366	9.873	8584.797	2.457
21.424	5.365	8577.210	1.340
21.640	0.851	8595.682	0.214
21.854	-6.579	8598.421	-1.672

Table B2.4 : Calculated fan system characteristics of the delta heat exchanger with a pair of curved guide vanes positioned as shown in figure 4.1.2 and the S-fan blade angle set to 18°. (Configuration [iii] in figure 4.1.2]

V (m^3/s)	Δp_{sFS} (Pa)	P (W)	η_{sFS} %
2.874	340.697	7338.707	13.340
3.334	330.331	7235.447	15.223
4.462	311.510	7081.805	19.626
5.626	297.459	6999.817	23.907
7.127	286.607	7050.126	28.973
8.517	276.951	7276.922	32.414
10.021	261.478	7490.548	34.982
11.383	242.403	7677.893	35.938
13.012	216.279	7865.657	35.778
14.418	192.906	7991.735	34.802
16.231	158.720	8179.666	31.495
17.938	118.484	8295.190	25.622
19.286	85.307	8365.686	19.667
20.476	51.016	8414.919	12.413
21.096	32.136	8414.093	8.057
21.438	23.551	8430.232	5.989
21.729	13.394	8432.777	3.451
22.088	-0.996	8420.760	-0.261

Table B2.5 : Calculated fan system characteristics of the delta heat exchanger with the side walls removed and the S-fan a blade angle set to 18°. (Configuration (iv) in figure 4.1.2)

V (m^3/s)	Δp_{sFS} (Pa)	P (W)	η_{sFS} %
2.413	342.947	7495.978	11.041
3.106	332.723	7439.823	13.891
4.339	316.437	7335.257	18.718
5.483	302.505	7210.364	23.002
6.848	288.475	7189.473	27.479
8.373	279.264	7419.097	31.516
9.779	264.494	7627.513	33.911
11.304	246.327	7825.956	35.580
12.899	222.486	8027.086	35.753

Table B2.5 : continued.

V (m^3/s)	Δp_{sFS} (Pa)	P (W)	η_{sFS} %
14.603	197.431	8195.215	35.181
16.428	163.910	8335.801	32.303
18.302	128.632	8457.109	27.837
19.666	94.795	8506.556	21.915
20.879	65.660	8541.398	16.050
21.756	41.186	8532.230	10.502
22.152	31.032	8524.186	8.064
22.414	22.573	8508.440	5.947
22.865	11.303	8501.959	3.040
22.898	9.911	8500.365	2.670

Table B2.6 : Calculated fan system characteristics of the delta heat exchanger with a round-to-round diffuser and the S-fan blade angle set to 18°. (Configuration [v] in figure 4.1.2)

V (m^3/s)	Δp_{sFS} (Pa)	P (W)	η_{sFS} %
2.456	346.204	7307.374	11.634
2.185	335.045	7215.062	10.145
4.461	320.297	7132.429	20.035
5.329	303.224	7060.085	22.888
6.884	285.584	7005.253	28.065
8.439	287.506	7227.288	33.572
10.004	282.497	7523.377	37.563
11.520	267.392	7786.262	39.562
13.123	242.348	8025.129	39.629
14.694	206.706	8213.008	36.982
16.588	165.110	8361.440	32.756
18.257	126.626	8464.172	27.313
19.837	90.226	8545.412	20.945
21.030	60.971	8575.669	14.952
21.647	38.137	8558.185	9.646
22.288	16.713	8534.903	4.364
22.385	14.822	8538.431	3.886
22.557	10.935	8536.138	2.890

Table B2.7 : Calculated fan system characteristics of the delta heat exchanger with a round-to-round diffuser, no side walls and the S-fan blade angle set to 18°. (Configuration [vi] in figure 4.1.2)

V (m^3/s)	$\Delta p_{s_{FS}}$ (Pa)	P (W)	$\eta_{s_{FS}}$ %
2.501	344.093	7266.526	11.841
2.773	335.281	7187.744	12.936
4.078	318.165	7110.509	18.248
5.360	300.237	7048.139	22.833
6.757	287.110	6996.868	27.725
8.482	289.645	7222.371	34.018
10.100	287.460	7485.908	38.784
11.808	276.588	7795.152	41.896
13.667	255.192	8039.709	43.380
15.192	233.431	8198.665	43.255
17.078	191.787	8376.151	39.104
19.178	156.491	8516.460	35.239
20.602	116.507	8550.950	28.070
22.004	87.124	8553.143	22.414

Table B3.1 : Velocity distribution (in m/s) downstream of the delta heat exchanger with S-fan blade angle set to 14°. (Configuration [i] in figure 4.1.2)

	1	2	3	4	5	6	7	8	9
A	8.670	6.776	5.592	4.064	-0.342	2.632	4.663	7.809	9.448
B	10.134	7.085	5.325	3.578	-0.658	3.026	5.229	7.139	8.988
C	9.402	6.750	5.625	3.284	-0.853	3.023	4.748	6.856	9.359
D	10.262	7.130	5.243	3.677	-0.410	4.035	5.191	7.212	9.516
E	9.597	7.024	5.198	2.781	-1.056	3.556	5.539	7.223	9.767
F	9.212	6.505	4.593	2.892	-0.919	3.454	5.177	7.026	9.444
G	10.527	7.387	4.713	2.985	-0.299	3.767	5.824	7.620	9.238

Table B3.2 : Velocity distribution (in m/s) downstream of the delta heat exchanger with S-fan blade angle set to 18°. (Configuration [ii] in figure 4.1.2)

	1	2	3	4	5	6	7	8	9
A	9.806	5.716	5.282	4.126	-0.377	1.840	5.296	7.885	10.260
B	11.423	7.630	5.782	3.701	-0.821	2.091	5.618	7.869	9.950
C	10.597	7.457	6.234	3.490	-1.058	3.009	5.194	7.507	10.399
D	11.395	7.764	5.802	3.945	-0.134	4.542	5.690	7.778	10.523
E	10.464	7.600	5.752	3.016	-1.092	3.826	6.164	7.827	10.883
F	10.091	7.047	5.015	2.941	-1.158	3.595	5.732	7.672	10.886
G	11.412	7.977	5.173	3.150	-0.333	4.000	6.475	8.189	9.238

Table B3.3 : Velocity distribution (in m/s) downstream of the delta heat exchanger with a pair of guide vanes positioned as shown in figure 4.1.2 and the S-fan blade angle set to 18 °. (Configuration [iii] in figure 4.1.2)

	1	2	3	4	5	6	7	8	9
A	9.041	8.229	6.287	4.429	-0.398	3.706	3.713	4.869	4.725
B	10.502	7.037	6.403	4.342	-0.508	4.035	7.105	8.224	4.588
C	9.883	7.202	6.693	4.317	-0.952	4.239	6.608	8.320	4.854
D	10.739	7.361	6.794	4.863	-0.082	5.452	6.958	8.390	4.930
E	10.066	7.330	6.576	3.826	-0.893	5.247	6.960	8.488	5.013
F	9.557	7.054	6.231	4.059	-1.341	4.923	6.773	8.460	4.973
G	11.042	7.257	7.010	4.076	-0.292	5.687	7.209	8.560	4.466

Table B3.4 : Velocity distribution (in m/s) downstream of delta heat exchanger with a round-to-round diffuser and the S-fan blade angle set to 18°. (Configuration [v] in figure 4.1.2)

	1	2	3	4	5	6	7	8	9
A	10.012	8.277	5.737	3.017	-0.232	3.823	5.096	8.153	11.065
B	11.041	8.804	6.259	3.176	-0.719	3.981	5.332	7.760	9.820
C	10.392	8.009	5.647	3.277	-0.633	4.232	5.767	7.146	9.763
D	10.739	9.024	5.765	3.207	-0.313	3.572	6.078	8.591	11.410
E	12.027	8.488	5.518	3.343	-0.772	3.016	6.079	8.381	10.712
F	10.611	9.311	6.400	3.595	-0.764	3.644	6.730	8.952	11.919
G	12.811	9.561	5.440	3.033	-0.546	4.048	5.982	8.745	9.664

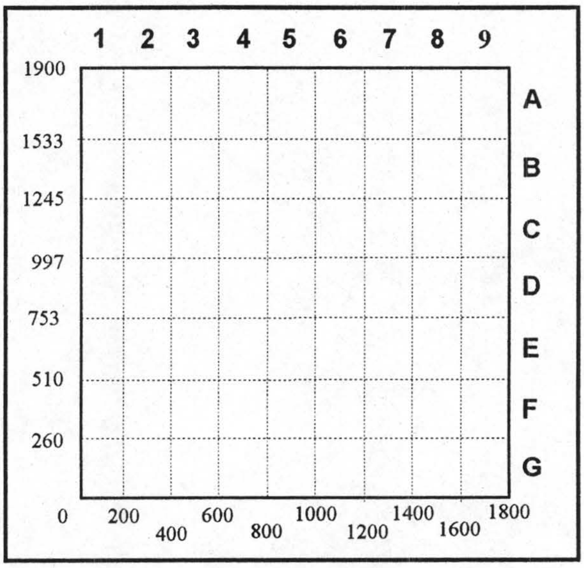

Figure B1.1 : Velocity traverse grid downstream of delta heat exchanger (dimensions in mm).

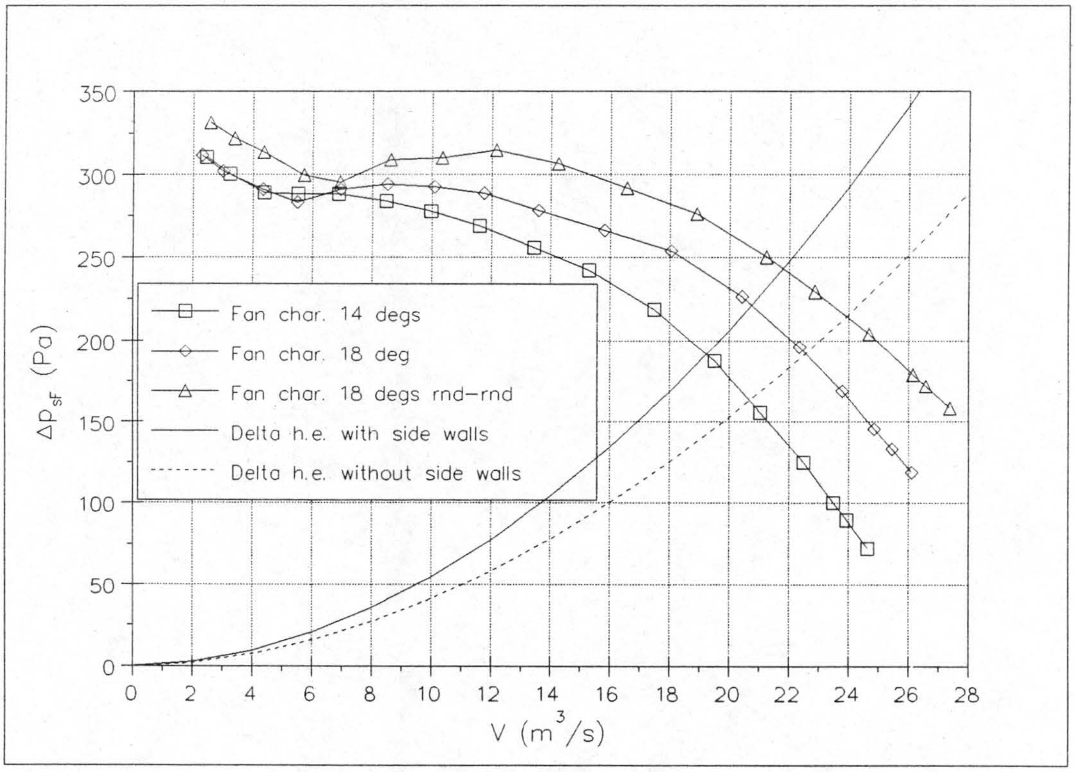

Figure B1.2 : S-fan and delta heat exchanger characteristics.

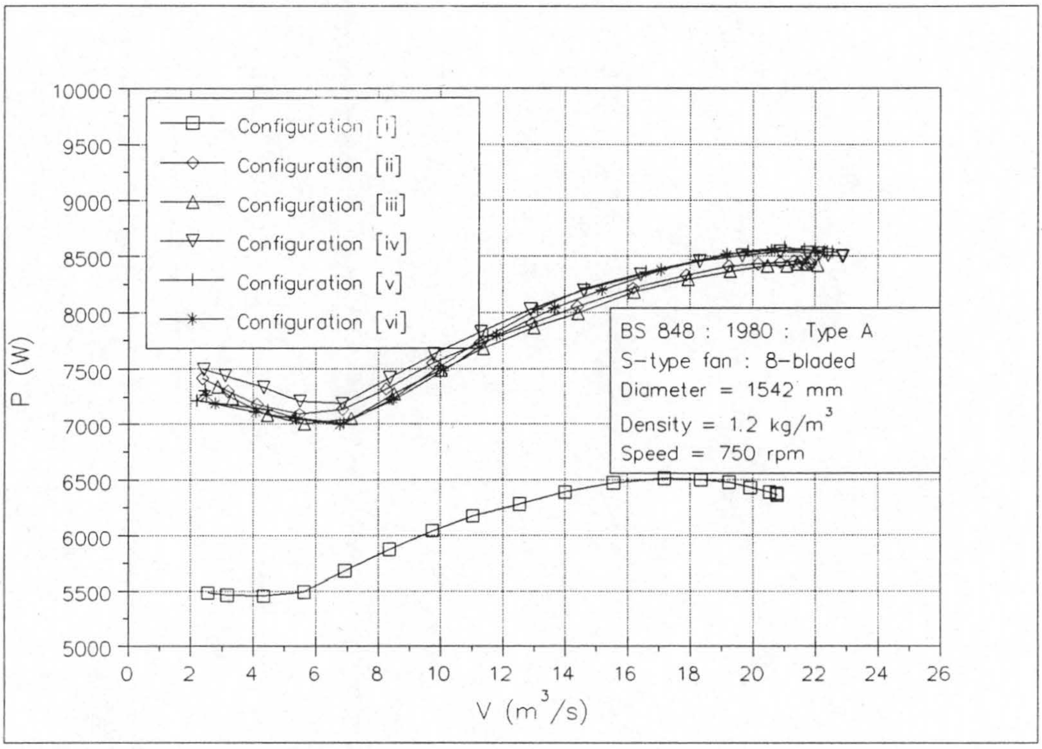

Figure B2.1 : P versus V for the delta heat exchanger.

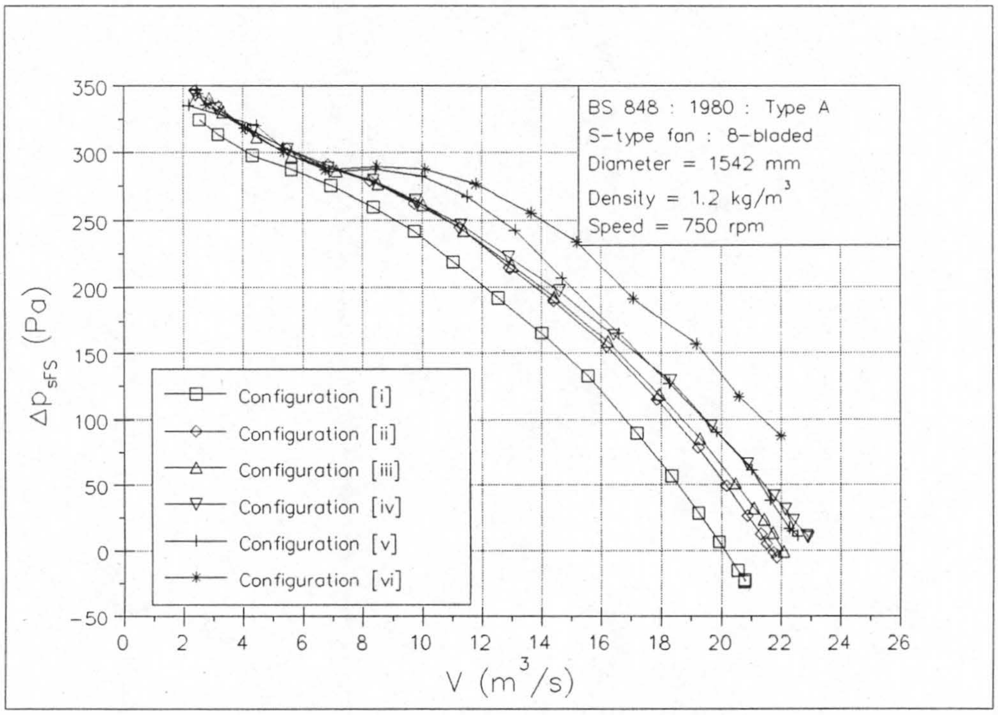

Figure B2.2 : Δp_{SFS} versus V for the delta heat exchanger.

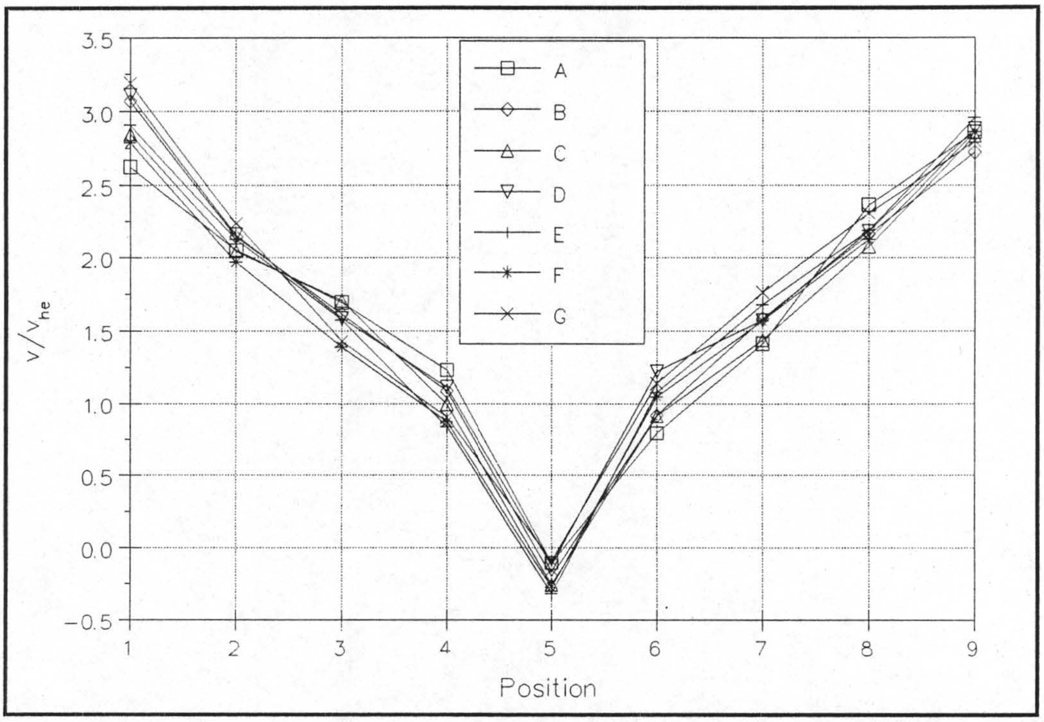

Figure B3.1 : Velocity distribution downstream of the delta heat exchanger with a blade angle of 14°. (Configuration [i] in figure 4.1.2)

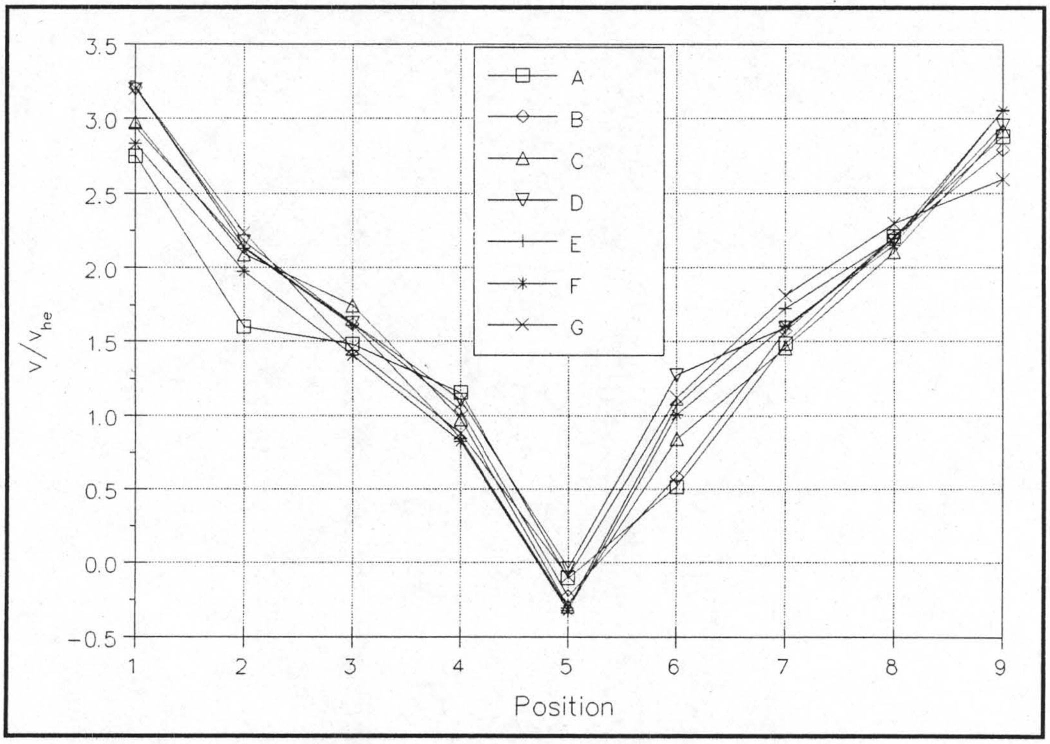

Figure B3.2 : Velocity distribution downstream of the delta heat exchanger with a blade angle of 18°. (Configuration [ii] in figure 4.1.2)

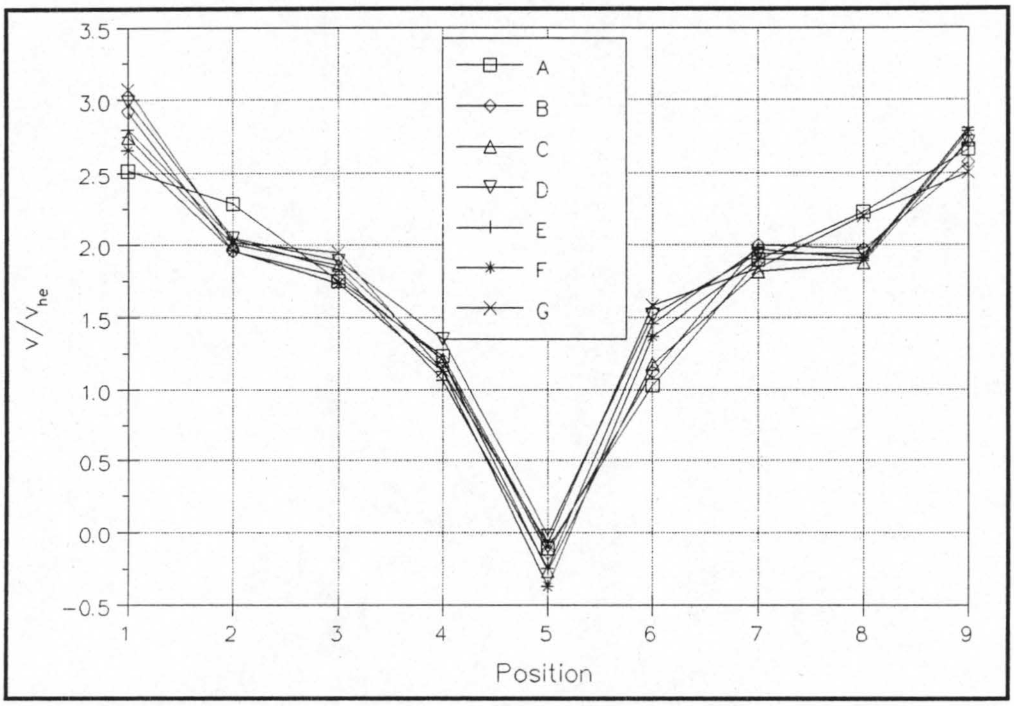

Figure B3.3 : Velocity distribution downstream of the delta heat exchanger with a blade angle of 18° and curved guide vanes placed as shown in figure 4.1.2. (Configuration [iii] in figure 4.1.2)

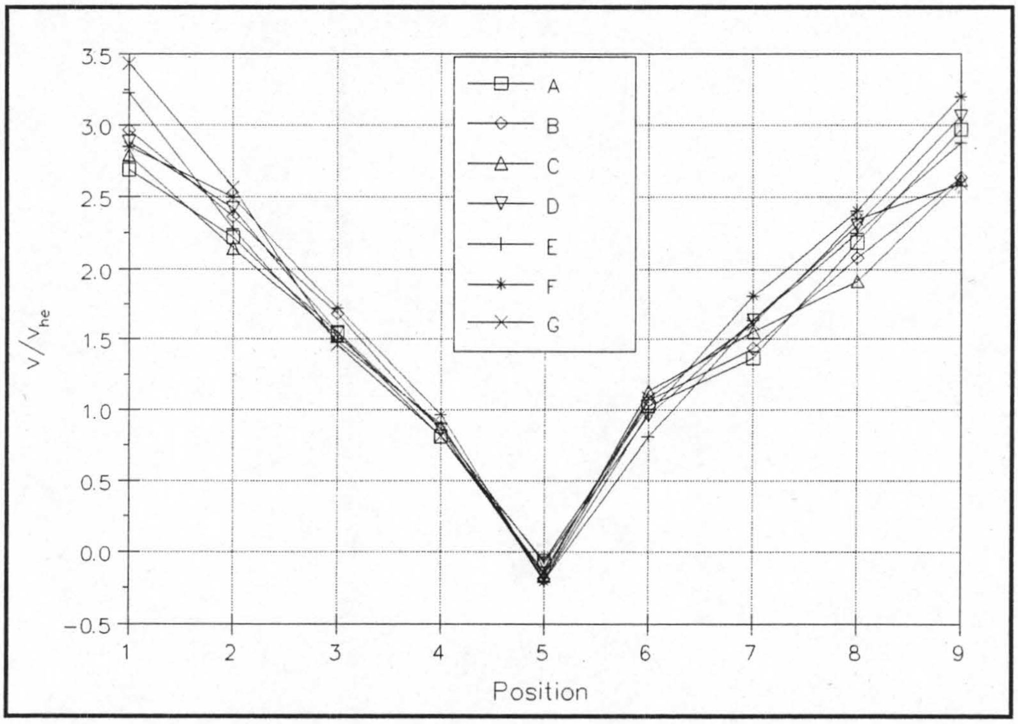

Figure B3.4 : Velocity distribution downstream of the delta heat exchanger with a blade angle of 18° and a round-to-round diffuser. (Configuration [v] in figure 4.1.2)

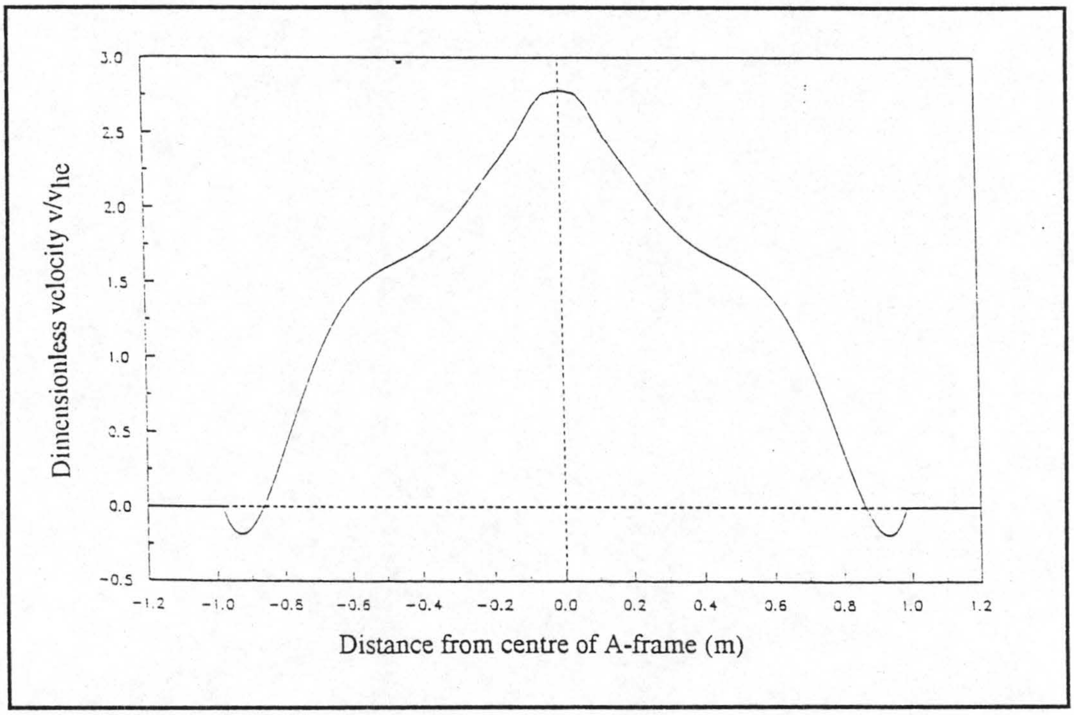

Figure B3.5 : Velocity distribution downstream of delta heat exchanger as measured by Venter [90VE1].

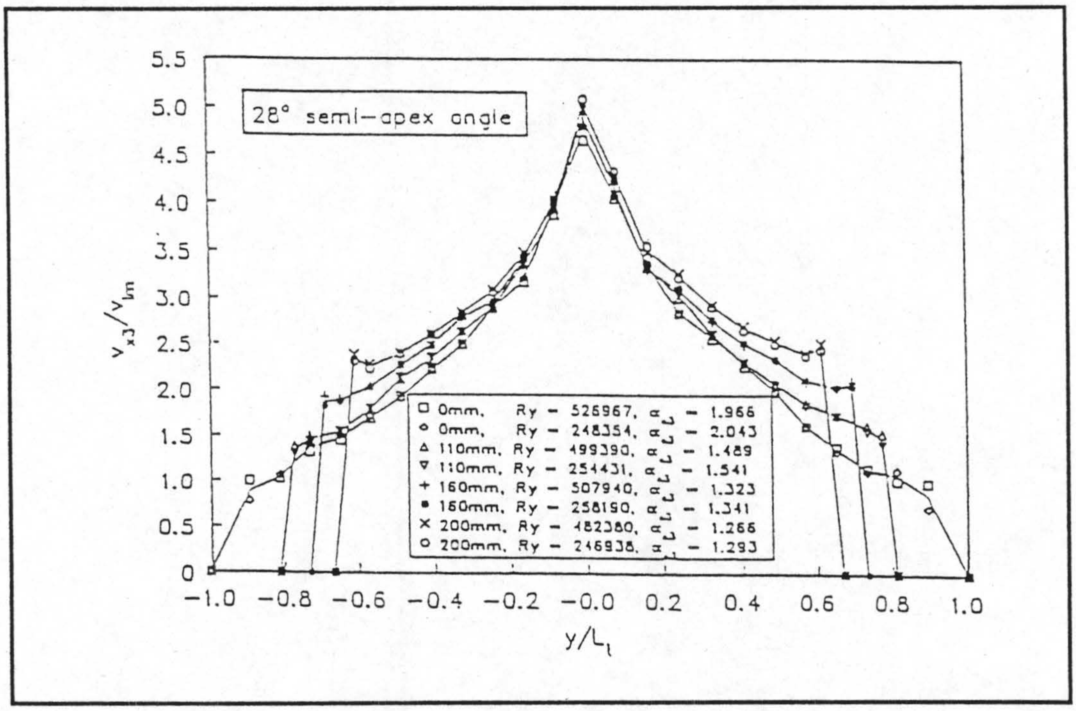

Figure B3.6 : Velocity distribution downstream of delta heat exchanger as measured by Van Aarde and Kröger [93VA1].

Appendix C

Experimental and Calculated Results for Double Delta Heat Exchanger Tests

Table C1.1 : Experimental readings of double delta heat exchanger with blade angle set to 18°. (Configuration [i])

Δp_{sett} (Pa)	Δp_{bell} (Pa)	T (N.m)	N (rpm)
351.775	6.431	96.247	752.427
337.451	11.205	94.323	751.022
322.814	17.899	93.078	751.541
306.805	31.928	93.286	751.680
299.759	47.946	95.342	751.122
285.030	70.720	97.146	749.957
267.328	97.461	99.484	750.632
247.565	128.073	101.334	750.476
226.178	168.280	103.663	751.181
198.950	208.513	105.430	750.594
165.083	264.093	107.107	750.197
129.080	325.615	108.476	750.387
97.906	382.104	109.625	751.330
73.782	423.578	109.791	750.031
47.477	467.395	110.092	751.210
37.409	488.566	109.657	750.789
21.160	520.518	109.793	751.137
20.867	520.618	109.821	751.630
18.888	520.364	109.822	751.563

Table C1.2 : Experimental readings for double delta heat exchanger with round-to-rectangular diffuser, flow director, flow straightner and blade angle set to 18°. (Configuration [ii])

Δp_{sett} (Pa)	Δp_{bell} (Pa)	T (N.m)	N (rpm)
338.972	6.089	91.967	749.859
332.320	9.257	90.964	749.652
317.612	19.097	89.585	749.425
299.016	32.272	88.262	747.323
294.480	49.621	90.398	747.670
286.174	71.755	94.178	748.920
267.893	96.542	96.793	749.584
249.504	126.051	99.192	751.072
222.761	166.630	101.115	749.090
197.888	207.794	103.030	749.787
164.869	265.399	105.170	750.866
134.756	326.580	106.025	749.667
100.274	386.710	106.775	750.015
70.958	440.453	106.883	749.934
54.231	477.928	106.885	750.840
40.663	504.408	106.443	750.236
33.488	516.488	106.347	751.018
21.727	535.338	105.639	749.429

Table C1.3 : Experimental readings of double delta heat exchanger with round-to-rectangular diffuser, flow director and blade angle set to 18°. (Configuration [iii])

Δp_{sett} (Pa)	Δp_{bell} (Pa)	T (N.m)	N (rpm)
289.525	30.594	90.302	752.037
285.652	47.928	93.001	750.629
277.299	69.948	95.737	749.065
265.665	96.681	98.800	751.511
247.329	127.267	100.534	750.197
224.760	167.040	102.392	749.545
200.262	208.877	104.036	749.235
168.177	268.101	105.807	749.186
132.434	334.073	106.842	749.239
103.037	396.294	107.370	749.449
79.888	440.688	107.452	749.889
60.754	480.308	107.489	749.952
44.751	505.520	106.934	749.926
33.573	524.999	106.935	751.022
27.907	537.812	106.350	749.445

Table C1.4 : Experimental readings of double delta heat exchanger with round-to-rectangular diffuser, flow straightner and blade angle set to 18°. (Configuration [iv])

Δp_{sett} (Pa)	Δp_{bell} (Pa)	T (N.m)	N (rpm)
299.215	30.658	90.850	749.204
291.302	47.639	92.198	749.406
281.646	70.051	95.436	748.933
268.270	98.186	97.475	748.807
248.049	128.499	99.810	749.567
222.208	167.925	102.515	751.300
195.039	208.695	103.827	749.996
158.895	262.702	104.720	748.880
125.129	321.010	105.634	749.214
91.514	378.090	106.259	749.663
68.404	423.086	106.257	750.285
44.381	465.741	106.391	751.388
26.773	491.637	105.291	749.753
15.650	514.741	105.373	750.888
21.918	504.238	105.479	750.784
11.832	524.331	105.593	752.778

Table C1.5 : Experimental readings of double delta heat exchanger with round-to-round diffuser and S-fan blade angle set to 18°. (Configuration [v])

Δp_{sett} (Pa)	Δp_{bell} (Pa)	T (N.m)	N (rpm)
324.967	5.334	90.863	750.266
314.474	10.242	89.711	750.022
302.473	18.223	88.509	750.064
289.759	30.322	88.143	752.718
276.832	46.852	87.251	751.173
283.701	70.143	89.516	749.237
282.847	97.795	93.144	751.151
273.151	131.283	96.834	751.215
252.085	176.288	99.790	750.032
224.306	223.392	101.893	748.492
194.736	284.318	104.255	749.735
160.549	348.940	105.850	750.341
124.643	416.587	106.027	748.041
98.667	462.719	106.191	748.311
77.053	504.888	106.268	749.966
57.051	538.554	106.205	751.356
51.975	544.185	105.721	750.208
47.057	556.451	105.746	751.070
42.561	561.213	104.894	748.950

Table C1.6 : Experimental readings of double delta heat exchanger with blade angle set to 22°. (Configuration [vi])

Δp_{sett} (Pa)	Δp_{bell} (Pa)	T (N.m)	N (rpm)
313.964	5.325	115.587	719.365
311.213	9.318	115.386	728.294
305.016	18.398	115.525	741.658
295.549	30.779	115.182	749.593
283.578	47.443	113.324	750.896
275.580	67.415	113.531	748.348
268.604	95.257	115.912	748.249
248.183	124.520	116.642	741.160
221.767	165.481	116.765	733.947
194.680	206.253	116.639	727.181
159.614	261.730	117.052	720.235
121.735	319.251	117.434	713.535
91.920	367.700	117.210	708.535
64.392	415.612	117.098	704.145
47.066	443.260	116.359	700.914
34.222	468.161	116.124	698.481
25.669	478.837	115.452	695.803
18.565	493.354	114.931	693.363
13.497	496.166	114.159	691.423

Table C1.7 : Experimental readings of double delta heat exchanger with side walls removed and blade angle set to 22°. (Configuration [vii])

Δp_{sett} (Pa)	Δp_{bell} (Pa)	T (N.m)	N (rpm)
312.731	3.507	116.625	715.668
302.338	7.616	114.611	718.121
297.920	16.679	115.287	732.554
289.078	31.059	115.427	742.609
282.015	45.282	115.351	749.387
274.877	68.800	114.911	746.868
267.182	96.927	115.679	740.430
248.484	127.658	116.331	731.335
226.406	165.168	116.986	725.003
197.422	209.389	116.141	714.704
164.533	267.403	116.601	707.829
129.772	328.901	117.052	701.191
96.524	389.878	117.189	695.932
71.884	444.488	117.071	691.891
55.011	478.931	116.761	688.850
38.605	514.204	116.427	686.824
26.394	533.801	116.085	684.757
23.369	549.793	115.732	683.589

Table C1.8 : Experimental readings of double delta heat exchanger with round-to-round diffuser and blade angle set to 22°. (Configuration [viii])

Δp_{sett} (Pa)	Δp_{bell} (Pa)	T (N.m)	N (rpm)
301.826	4.451	112.474	712.150
298.063	10.899	111.941	717.582
290.138	15.332	111.673	723.470
281.548	28.368	111.522	728.854
270.703	43.822	111.047	732.411
248.017	64.879	110.801	736.538
240.444	89.403	109.077	737.434
246.800	124.879	109.092	725.867
234.808	172.293	109.349	706.613
209.253	219.115	109.455	692.473
171.451	279.595	109.548	681.131
137.383	341.611	109.360	673.247
105.427	398.541	109.385	667.697
77.248	450.621	109.218	663.969
58.232	483.989	108.929	662.665
42.019	510.314	108.682	661.890
31.760	537.163	108.550	660.604

Table C1.9 : Experimental readings of double delta heat exchanger with blade angle set to 26°. (Configuration [ix])

Δp_{sett} (Pa)	Δp_{bell} (Pa)	T (N.m)	N (rpm)
256.713	5.199	116.623	635.995
252.625	8.976	115.942	644.518
249.695	16.432	116.727	657.691
244.250	27.363	117.256	668.907
237.414	43.219	118.009	679.451
229.529	64.051	117.180	679.867
220.657	88.974	116.803	675.550
206.711	118.302	117.215	668.806
186.745	154.175	117.267	661.018
164.402	197.321	117.220	655.094
137.768	242.178	116.818	648.828
102.291	300.813	117.046	643.278
71.281	352.878	117.184	637.661
43.202	397.905	116.370	630.436
22.006	435.296	115.992	624.869
14.118	452.279	115.937	623.277
3.807	478.386	115.979	621.182
2.946	473.761	115.868	621.747
-5.119	485.701	115.754	620.644

Table C1.10 : Experimental readings of double delta heat exchanger with side walls removed and blade angle set to 26°. (Configuration [x])

Δp_{sett} (Pa)	Δp_{bell} (Pa)	T (N.m)	N (rpm)
252.722	5.650	119.096	666.358
246.846	8.608	117.671	670.460
243.404	17.562	117.448	677.418
236.374	27.021	116.954	681.597
230.434	44.242	117.191	689.132
225.016	63.353	116.310	687.330
219.347	88.916	116.466	681.501
209.659	120.223	117.041	674.754
190.774	158.049	117.394	666.662
171.712	199.945	117.397	660.562
144.400	247.332	117.189	655.136
109.749	314.930	117.584	649.143
83.582	372.748	117.856	643.351
64.347	421.209	117.162	636.531
41.451	457.061	117.226	632.500
30.871	488.245	117.268	629.559
23.062	498.607	116.573	626.886
16.395	509.422	116.225	625.238
15.998	520.993	116.140	623.660

Table C1.11 : Experimental readings of double delta heat exchanger with round-to-round diffuser and blade angle set to 26°. (Configuration [xi])

Δp_{sett} (Pa)	Δp_{bell} (Pa)	T (N.m)	N (rpm)
260.633	5.786	118.258	661.116
254.630	9.199	117.598	666.633
251.401	16.847	117.811	674.082
243.379	27.626	117.484	679.375
229.002	45.711	117.325	683.148
218.328	63.346	117.352	687.105
200.062	88.032	116.533	690.637
193.041	116.783	117.048	703.465
203.986	162.221	117.379	691.765
196.143	209.469	117.427	677.351
175.894	273.390	119.696	664.170
138.925	336.776	118.483	648.666
107.464	389.973	118.459	641.888
81.526	447.295	118.585	636.459
66.533	479.553	118.183	633.167
54.217	498.976	117.601	630.127
37.269	532.138	117.197	627.334
39.212	528.966	116.605	625.722
32.427	540.837	115.788	623.505

Table C1.12 : Experimental readings of double delta heat exchange with round-to-round diffuser, no side walls and blade angle set to 26°. (Configuration [xii])

Δp_{sett} (Pa)	Δp_{bell} (Pa)	T (N.m)	N (rpm)
252.242	5.234	116.836	651.145
251.125	9.994	116.792	657.091
246.754	16.701	116.717	663.410
238.327	27.731	116.783	669.811
231.310	43.155	116.688	673.680
216.717	62.820	116.323	677.994
199.476	86.779	116.150	683.598
196.079	114.919	116.473	694.403
211.549	163.726	117.464	685.795
210.997	217.719	119.282	673.070
185.409	287.119	118.680	650.534
154.158	355.733	119.569	642.843
125.587	415.041	118.848	634.099
100.120	480.878	118.944	628.925
82.740	522.520	118.572	625.495
65.720	553.815	117.828	621.427
56.687	577.773	117.323	619.472
50.392	589.295	116.734	617.824
44.712	608.796	116.412	616.428

Table C2.1 : Calculated fan system characteristics for double delta heat exchanger with the blade angle set to 18°. (Configuration [i])

V (m^3/s)	**Δp_{sFS} (Pa)**	**P (W)**	**η_{sFS} %**
2.528	341.472	7338.120	11.763
3.342	328.736	7217.389	15.224
4.221	313.981	7111.236	18.637
5.635	298.216	7123.319	23.593
6.911	291.741	7290.680	27.653
8.405	278.170	7450.616	31.379
9.856	260.307	7614.854	33.691
11.298	241.028	7758.220	35.101
12.936	219.627	7919.939	35.873
14.407	193.295	8065.400	34.528
16.217	160.294	8199.593	31.703
17.996	124.950	8297.213	27.101
19.464	94.193	8361.539	21.927
20.524	70.897	8401.206	17.320
21.520	45.014	8395.610	11.538
22.012	35.225	8371.038	9.263
22.706	19.336	8372.265	5.244
22.694	19.026	8363.371	5.163
22.690	17.111	8364.827	4.641

Table C2.2 : Calculated fan system characteristics for double delta heat exchanger with round-to rectangular diffuser, flow director, flow straightner and blade angle set to 18°. (Configuration [ii])

V (m^3/s)	**Δp_{sFS} (Pa)**	**P (W)**	**η_{sFS} %**
2.490	337.246	7186.635	11.684
3.071	330.780	7111.666	14.283
4.411	316.261	7007.106	19.910
5.750	299.334	6941.206	24.795
7.126	294.463	7102.301	29.544
8.554	285.123	7373.950	33.075
9.911	266.318	7563.938	34.897
11.301	246.924	7719.349	36.149
13.024	221.438	7908.553	36.467
14.527	196.158	8041.427	35.436
16.389	162.686	8182.154	32.585
18.203	133.097	8272.643	29.287
19.792	98.573	8320.622	23.448
21.119	69.353	8328.374	17.587
21.969	52.533	8307.098	13.893
22.585	39.103	8284.933	10.659
22.828	31.895	8259.676	8.815
23.288	20.303	8238.510	5.739

Table C2.3 : Calculated fan system characteristics for double delta heat exchanger with round-to-rectangular diffuser, flow director, and blade angle set to 18°. (Configuration [iii])

V (m^3/s)	Δp_{sFS} (Pa)	P (W)	η_{sFS} %
5.538	283.714	6951.725	22.604
6.945	280.916	7186.127	27.148
8.407	273.764	7427.783	30.984
9.850	260.474	7614.749	33.694
11.319	243.214	7774.184	35.411
12.976	221.235	7929.885	36.202
14.513	197.095	8061.858	35.481
16.438	165.268	8197.580	33.140
18.341	129.788	8273.687	28.772
19.965	100.571	8307.515	24.170
21.037	77.553	8302.144	19.651
21.956	58.616	8302.076	15.502
22.522	42.816	8258.492	11.676
22.916	31.683	8233.589	8.818
23.241	26.206	8222.522	7.407

Table C2.4 : Calculated fan system characteristics for double delta heat exchanger with round-to-rectangular diffuser, flow straightner and blade angle set to 18°. (Configuration [iv])

V (m^3/s)	Δp_{sFS} (Pa)	P (W)	η_{sFS} %
5.597	298.753	7126.073	23.463
6.974	290.629	7227.343	28.045
8.461	281.266	7489.904	31.775
10.018	267.888	7651.485	35.074
11.447	247.053	7817.324	36.175
13.052	220.114	7990.133	35.955
14.572	193.675	8118.364	34.762
16.367	157.976	8209.660	31.495
18.078	123.981	8271.078	27.099
19.602	90.194	8307.277	21.282
20.713	66.956	8291.451	16.727
21.695	42.851	8275.578	11.234
22.335	25.457	8224.339	6.913
22.817	14.296	8204.977	3.975
22.587	20.542	8216.023	5.647
22.970	10.434	8180.572	2.930

Table C2.5 : Calculated fan system characteristics for double delta heat exchanger with round-to-round diffuser and blade angle set to 18°. (Configuration [v])

V (m^3/s)	Δp_{sFS} (Pa)	P (W)	η_{sFS} %
2.339	325.660	7151.899	10.649
3.242	315.306	7065.034	14.467
4.323	303.183	6968.790	18.808
5.556	288.326	6890.261	23.250
6.920	276.520	6847.690	27.943
8.489	284.814	7062.315	34.236
9.998	282.442	7311.107	38.625
11.582	272.599	7598.747	41.551
13.440	252.185	7853.742	43.156
15.156	225.096	8050.081	42.380
17.065	194.502	8207.030	40.444
18.884	159.768	8316.273	36.279
20.689	124.407	8378.539	30.720
21.791	98.064	8383.320	25.490
22.708	75.884	8350.579	20.635
23.404	55.575	8313.163	15.646
23.561	50.655	8300.213	14.379
23.797	45.602	8282.755	13.102
23.965	41.338	8262.181	11.990

Table C2.6 : Calculated fan system characteristics for double delta heat exchanger with blade angle set to 22°. (Configuration [vi])

V (m^3/s)	Δp_{sFS} (Pa)	P (W)	η_{sFS} %
2.454	347.047	10035.165	8.487
3.206	335.602	9773.307	11.011
4.424	317.130	9435.056	14.871
5.661	300.756	9208.058	18.491
7.016	287.496	9027.022	22.343
8.391	281.219	9104.489	25.917
9.975	274.081	9297.236	29.405
11.511	257.967	9533.664	31.147
13.397	234.863	9729.648	32.338
15.091	209.816	9898.167	31.990
17.158	175.053	10122.207	29.673
19.121	135.656	10342.929	25.078
20.659	103.507	10466.290	20.431
22.095	72.961	10584.160	15.231
22.919	53.425	10612.739	11.538
23.633	38.705	10663.845	8.578
23.991	28.893	10682.983	6.489
24.436	20.626	10708.989	4.706
24.573	14.687	10696.313	3.374

Table C2.7 : Calculated fan system characteristics for double delta heat exchanger with side walls removed and blade angle set to 22°. (Configuration [vii])

V (m^3/s)	Δp_{sFS} (Pa)	P (W)	η_{sFS} %
1.976	340.456	9971.996	6.747
2.902	326.851	9731.998	9.748
4.210	309.473	9407.010	13.851
5.667	292.149	9164.270	18.067
6.780	279.824	8992.735	21.098
8.385	274.505	9018.294	25.524
10.039	271.386	9236.392	29.496
11.662	258.569	9519.186	31.677
13.378	239.551	9738.547	32.907
15.275	214.714	9945.940	32.976
17.424	182.131	10176.868	31.183
19.500	146.014	10407.017	27.359
21.384	109.817	10573.718	22.209
22.961	82.293	10684.158	17.685
23.935	63.134	10748.407	14.059
24.870	44.058	10779.187	10.165
25.412	29.785	10811.158	7.001
25.834	26.240	10814.883	6.268

Table C2.8 : Calculated fan system characteristics for double delta heat exchanger with round-to-round diffuser and blade angle set to 22°. (Configuration [viii])

V (m^3/s)	Δp_{sFS} (Pa)	P (W)	η_{sFS} %
2.234	330.752	9680.579	7.632
3.469	321.673	9489.106	11.760
4.081	308.008	9312.156	13.497
5.509	294.430	9161.884	17.704
6.813	280.275	9033.533	21.139
8.242	253.799	8910.743	23.475
9.662	245.368	8750.121	27.095
11.602	259.878	9033.076	33.380
13.998	260.736	9553.356	38.204
16.104	241.701	9954.557	39.101
18.487	204.324	10293.755	36.696
20.667	167.180	10514.593	32.860
22.501	129.987	10689.116	27.363
24.054	95.813	10790.010	21.359
24.973	72.061	10801.797	16.660
25.669	51.624	10800.769	12.269
26.384	38.708	10828.674	9.431

Table C2.9 : Calculated fan system characteristics for double delta heat exchanger with blade angle set to 26°. (Configuration [ix])

V (m^3/s)	Δp_{sFS} (Pa)	P (W)	η_{sFS} %
2.691	349.794	12481.299	7.543
3.490	335.154	12081.927	9.680
4.627	318.097	11680.979	12.600
5.870	300.763	11343.108	15.565
7.263	283.276	11063.640	18.595
8.835	273.448	10971.593	22.020
10.479	266.147	11075.545	25.181
12.203	254.241	11338.332	27.363
14.092	234.939	11609.936	28.517
16.083	210.352	11813.617	28.638
17.985	179.407	11998.401	26.893
20.211	135.083	12225.867	22.331
22.076	95.305	12453.060	16.895
23.704	58.468	12648.084	10.958
25.008	29.527	12829.950	5.755
25.555	18.453	12888.461	3.659
26.368	3.795	12978.926	0.771
26.216	2.579	12942.843	0.522
26.589	-8.963	12975.037	-1.837

Table C2.10 : Calculated fan system characteristics for double delta heat exchanger with side walls removed and S-fan blade angle set to 26°.

V (m^3/s)	Δp_{sFS} (Pa)	P (W)	η_{sFS} %
2.696	317.891	11766.452	7.283
3.307	306.685	11483.185	8.832
4.675	296.192	11226.777	12.333
5.763	284.073	11042.128	14.825
7.293	270.844	10823.208	18.250
8.749	265.794	10797.762	21.537
10.453	263.456	10997.353	25.042
12.275	256.753	11272.696	27.959
14.243	239.140	11580.654	29.412
16.165	219.023	11793.613	30.020
18.122	186.952	11965.275	28.316
20.631	144.274	12224.087	24.350
22.642	111.405	12470.755	20.226
24.322	87.156	12661.965	16.741
25.491	56.231	12828.096	11.174
26.467	41.769	12951.485	8.536
26.858	31.014	12983.765	6.415
27.218	21.636	13012.449	4.525
27.595	21.136	13068.777	4.463

Table C2.11 : Calculated fan system characteristics for double delta heat exchanger with round-to-round diffuser and blade angle set to 26°. (Configuration [xi])

V (m^3/s)	Δp_{sFS} (Pa)	P (W)	η_{sFS} %
2.754	334.045	11904.738	7.727
3.443	320.941	11642.402	9.492
4.608	309.875	11406.804	12.519
5.855	295.273	11197.726	15.438
7.488	274.675	11057.750	18.601
8.764	258.780	10932.143	20.745
10.276	234.584	10743.178	22.439
11.619	218.070	10399.915	24.364
13.928	238.212	10786.298	30.759
16.162	238.732	11253.940	34.285
18.827	222.363	11928.870	35.095
21.387	183.671	12374.678	31.744
23.250	144.627	12630.826	26.623
25.107	111.071	12857.622	21.688
26.127	91.193	12945.741	18.405
26.777	74.658	13004.924	15.372
27.770	51.127	13073.748	10.860
27.759	54.177	13075.105	11.502
28.167	44.763	13075.035	9.643

Table C2.12 : Calculated fan system characteristics for double delta heat exchanger with round-to-round diffuser, no side walls and fan blade angle set to 26°. (Configuration [xii])

V (m^3/s)	Δp_{sFS} (Pa)	P (W)	η_{sFS} %
2.638	328.042	11934.431	7.252
3.613	320.687	11714.873	9.889
4.625	309.097	11484.822	12.449
5.903	292.804	11271.822	15.333
7.321	280.862	11132.881	18.469
8.775	259.703	10955.719	20.801
10.227	235.017	10758.991	22.340
11.586	223.792	10455.325	24.799
14.005	247.475	10812.334	32.054
16.455	256.090	11398.698	36.968
19.546	240.535	12137.501	38.735
22.010	204.370	12518.926	35.931
24.095	170.657	12785.249	32.162
26.142	137.764	13003.727	27.696
27.396	114.660	13103.396	23.972
28.384	91.783	13189.984	19.751
29.080	79.318	13215.335	17.454
29.445	70.621	13218.331	15.732
29.995	62.644	13240.891	14.191

Table C3.1 : Dimensionless velocity distribution (v/v_{he}) downstream of double delta heat exchanger with blade angle set to 18°. (Configuration [i])

	1	**2**	**3**	**4**	**5**	**6**	**7**	**8**	**9**	**10**
A	3.135	2.318	2.339	1.815	-0.427	-0.133	3.409	3.141	3.519	4.194
B	3.329	2.831	2.220	1.742	0.059	-0.053	2.767	2.788	2.998	3.105
C	3.233	2.893	2.370	2.448	0.010	-0.032	1.363	2.002	3.045	3.681
D	3.430	3.660	3.153	2.860	0.139	0.044	1.521	1.959	3.219	3.534
E	3.687	3.177	2.681	2.420	0.196	-0.143	2.880	2.570	3.126	3.699
F	2.994	3.249	2.261	1.263	0.336	-0.047	3.125	3.555	3.092	3.751
G	3.850	2.596	2.219	1.713	-0.109	0.016	2.411	2.787	2.949	4.038

Table C3.2 : Dimensionless velocity distribution (v/v_{he}) downstream of double delta heat exchanger with round-to-rectangular diffuser, flow director, flow straightner and blade angle set to 18°. (Configuration [ii])

	1	**2**	**3**	**4**	**5**	**6**	**7**	**8**	**9**	**10**
A	3.516	2.476	2.170	1.231	-0.040	-0.227	2.895	2.982	3.270	4.374
B	3.084	2.947	2.162	1.553	0.027	-0.010	2.698	2.752	2.778	3.530
C	3.766	3.048	2.479	2.458	-0.085	-0.126	1.654	2.031	3.013	3.467
D	3.911	3.429	3.379	3.532	0.060	0.097	1.371	2.791	2.854	3.817
E	3.618	3.302	2.446	2.655	0.571	0.669	2.494	3.397	3.367	3.597
F	3.449	2.650	2.411	1.800	0.092	-0.111	2.738	3.216	3.101	3.546
G	3.936	2.976	2.722	1.842	0.139	0.064	2.297	3.329	3.456	3.677

Table C3.3 : Dimensionless velocity distribution (v/v_{he}) downstream of double delta heat exchanger with round-to-rectangular diffuser, flow director and blade angle set to 18°. (Configuration [iii])

	1	**2**	**3**	**4**	**5**	**6**	**7**	**8**	**9**	**10**
A	3.255	2.693	1.955	1.251	-0.199	-0.132	3.055	3.015	3.539	4.207
B	3.493	3.068	2.096	1.588	0.073	-0.067	2.606	2.621	2.781	3.619
C	3.644	3.032	2.375	2.380	0.013	-0.082	1.557	2.024	2.847	3.412
D	4.046	3.522	3.102	3.237	0.063	0.079	1.383	2.478	3.491	3.977
E	3.563	3.632	2.559	2.341	0.037	-0.017	2.347	3.175	3.791	3.806
F	3.226	2.813	2.301	1.668	-0.014	-0.141	2.954	3.025	3.351	3.555
G	4.124	3.034	2.613	1.867	0.027	0.085	2.510	3.337	3.571	3.545

Table C3.4 : Dimensionless velocity distribution (v/v_{he}) downstream of double delta heat exchanger with round-to-rectangular diffuser, flow straightner and blade angle set to 18°. (Configuration [iv])

	1	**2**	**3**	**4**	**5**	**6**	**7**	**8**	**9**	**10**
A	3.550	2.137	2.367	1.134	0.004	-0.206	2.714	3.038	3.501	3.830
B	3.074	2.794	2.254	1.443	-0.053	-0.073	2.520	2.811	3.048	3.423
C	3.315	3.064	2.800	2.238	-0.115	-0.077	1.492	2.417	2.989	3.429
D	3.706	3.492	3.520	3.220	0.104	0.123	1.430	2.387	2.829	3.561
E	3.560	2.943	3.079	2.050	-0.065	-0.008	2.167	3.337	3.325	3.401
F	2.778	3.120	2.057	1.522	-0.175	0.048	2.968	3.403	3.156	3.623
G	3.684	3.179	2.407	2.065	-0.103	0.120	2.489	3.220	3.438	3.803

Table C3.5 : Dimensionless velocity distribution (v/v_{he}) downstream of double delta heat exchanger with round-to-round diffuser and blade angle set to 18°. (Configuration [v])

	1	**2**	**3**	**4**	**5**	**6**	**7**	**8**	**9**	**10**
A	3.091	2.519	2.280	1.336	-0.257	-0.127	3.007	3.005	4.279	3.613
B	3.677	3.049	1.982	1.649	0.004	0.040	2.524	2.565	3.107	3.635
C	3.831	3.161	2.571	2.345	0.001	-0.016	1.510	1.886	2.736	3.580
D	3.858	3.443	3.070	2.779	0.072	0.021	1.203	2.018	3.146	3.621
E	3.747	2.873	2.772	2.451	-0.025	-0.016	2.199	3.185	3.549	4.022
F	3.443	2.904	2.204	1.257	-0.101	0.040	2.569	3.074	3.392	3.539
G	3.905	3.308	2.113	1.967	-0.038	0.068	2.130	2.730	3.048	3.742

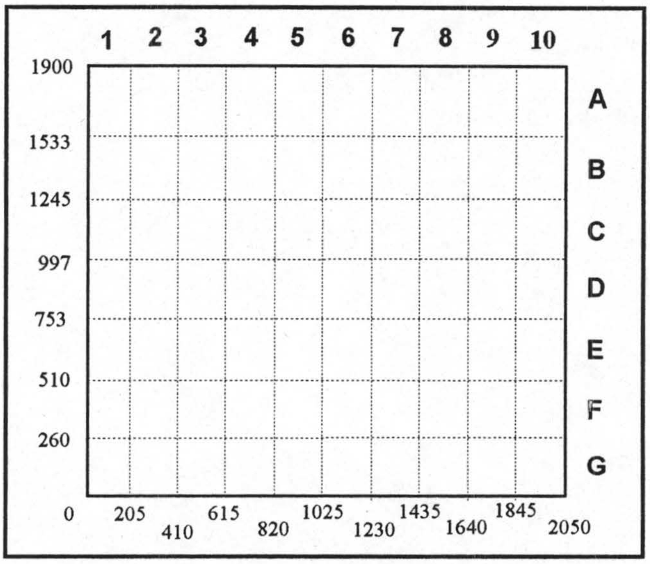

Figure C1.1 : Velocity traverse grid downstream of double delta heat exchanger (dimensions in mm).

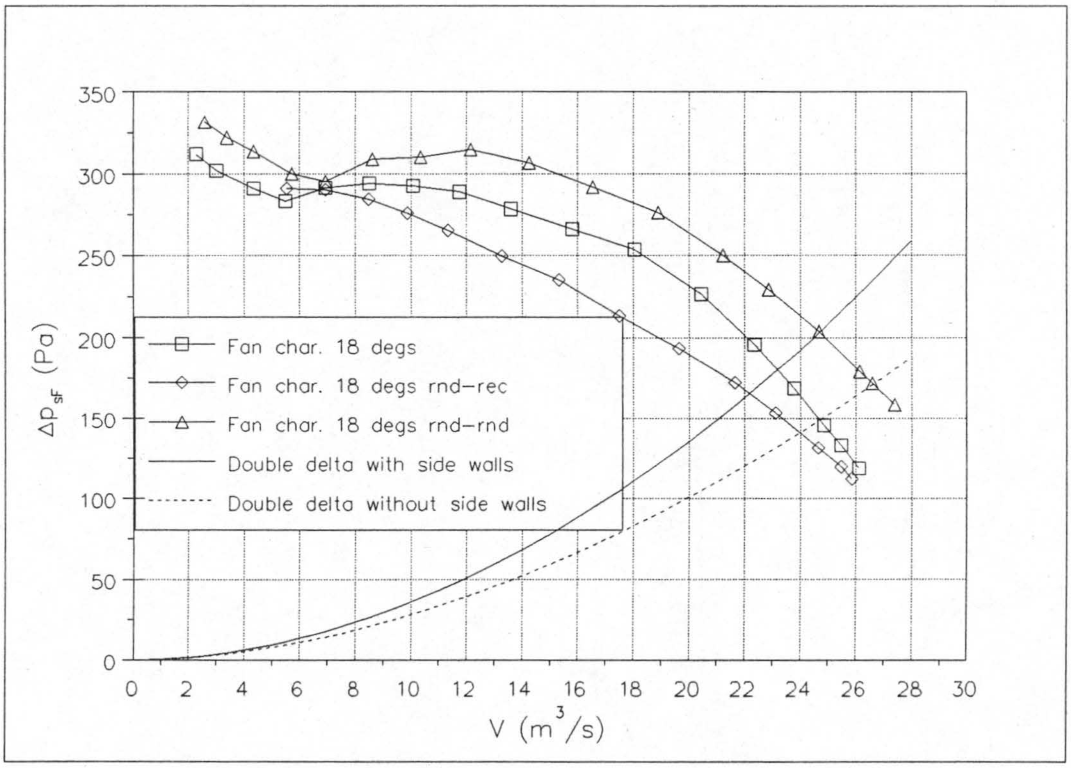

Figure C1.2 : Total pressure across double delta heat exchanger and S-fan static pressure rise characteristic for a blade angle of 18°.

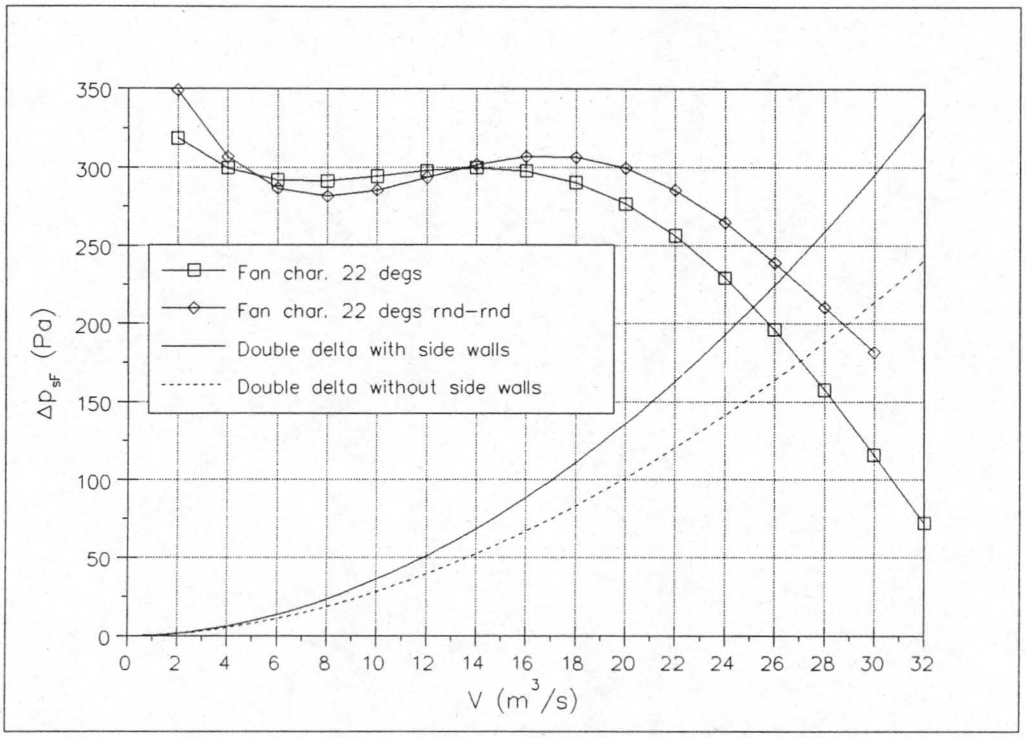

Figure C1.3 : Total pressure drop across double delta heat exchanger and S-fan static pressure rise characteristic for blade angle of 22°.

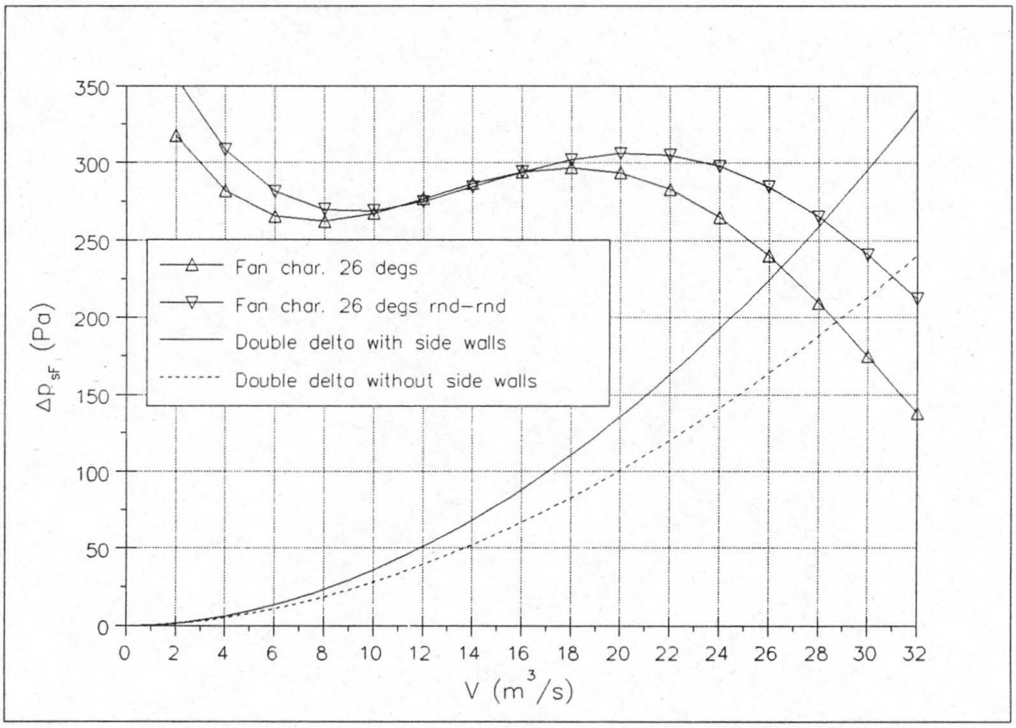

Figure C1.4 : Total pressure drop across double delta heat exchanger and S-fan static pressure rise characteristic for blade angle of 18°.

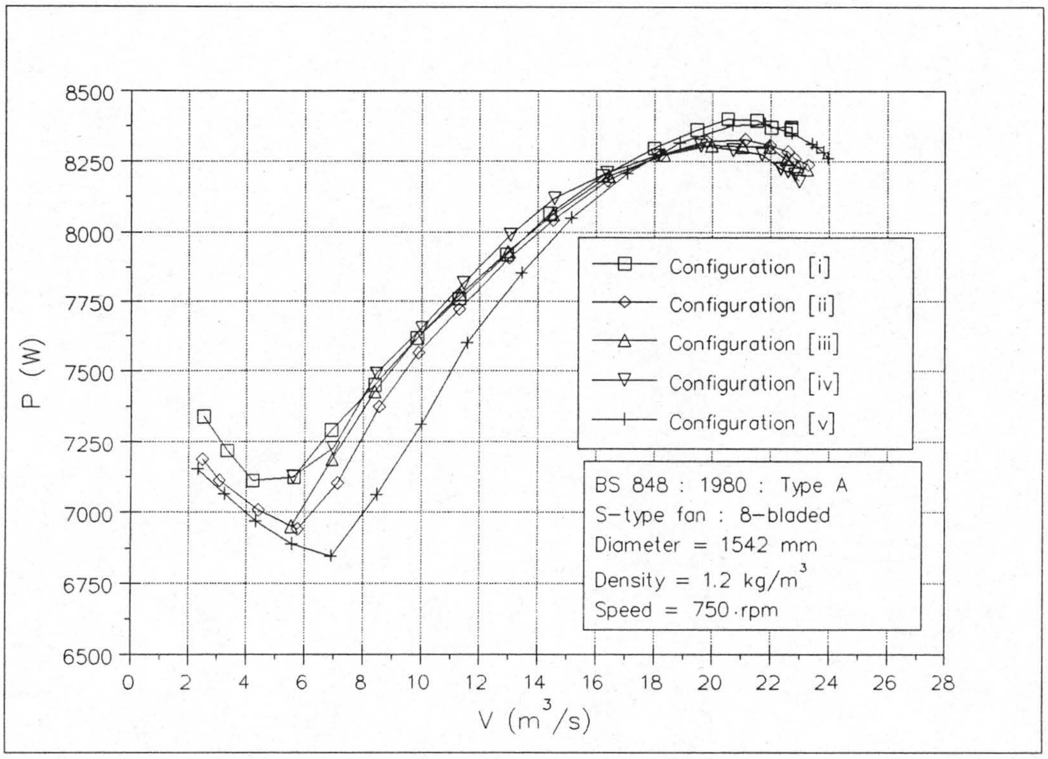

Figure C2.1 : P versus V for double delta heat exchanger with blade angle set to 18°.

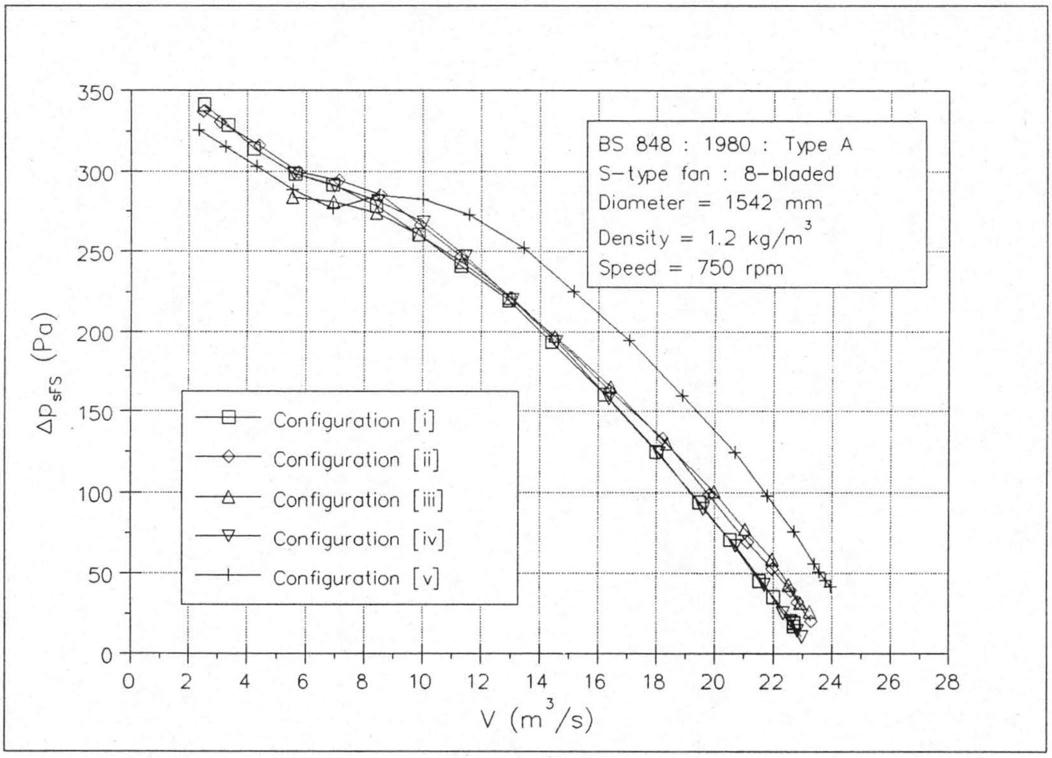

Figure C2.2 : Δp_{SFS} versus V for double delta heat exchanger with blade angle set to 18°.

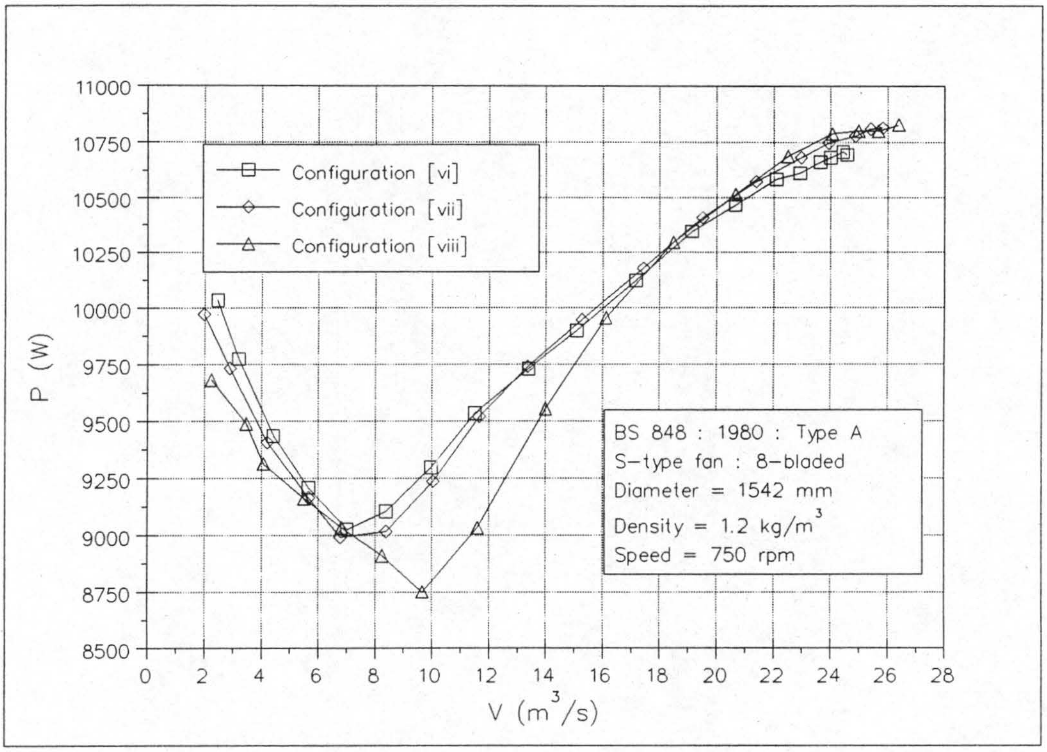

Figure C2.3 : P versus V for double delta heat exchanger with blade angle set to 22°.

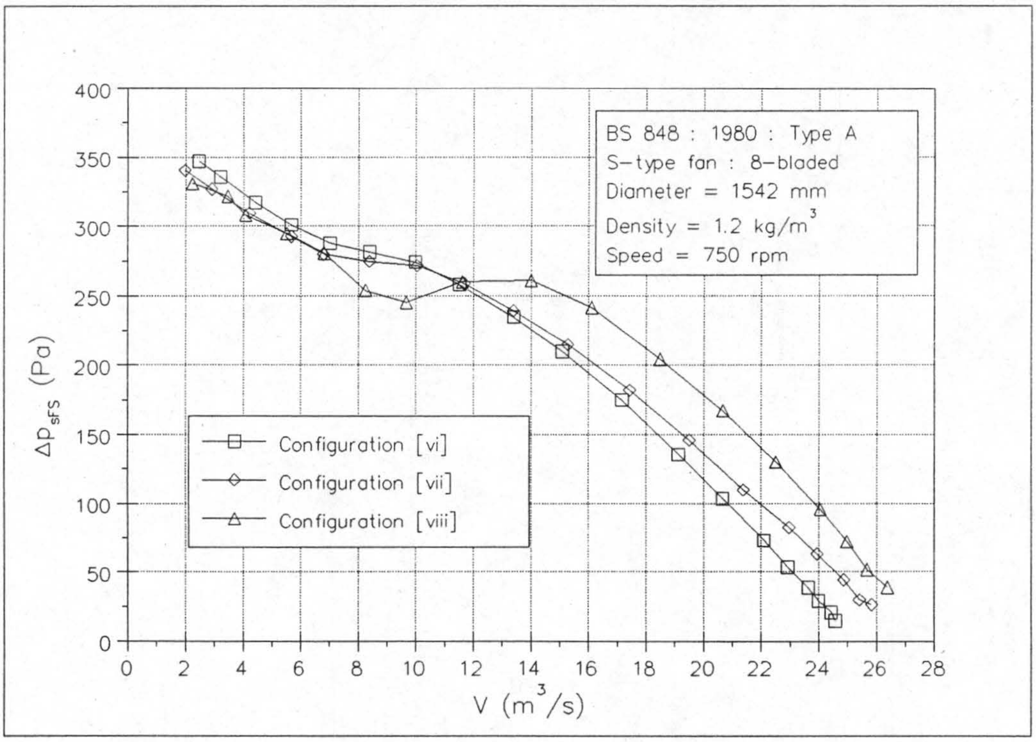

Figure C2.4 : Δp_{sFS} versus V for double delta heat exchanger with blade angle set to 22°.

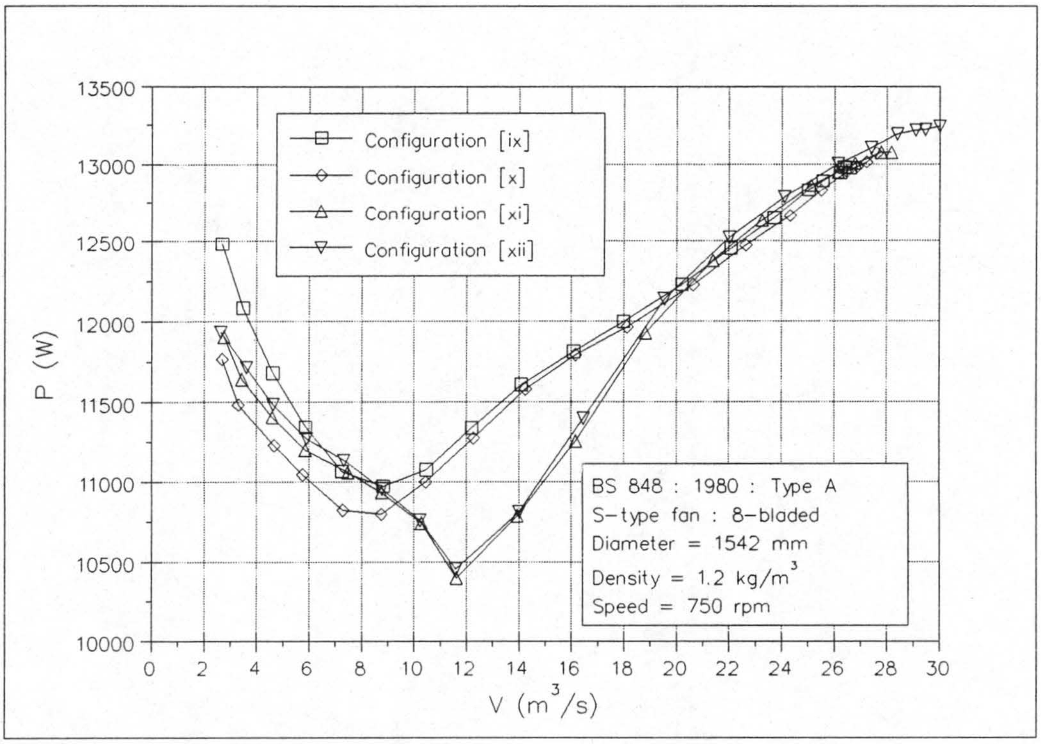

Figure C2.5 : P versus V for double delta heat exchanger with blade angle set to 26°.

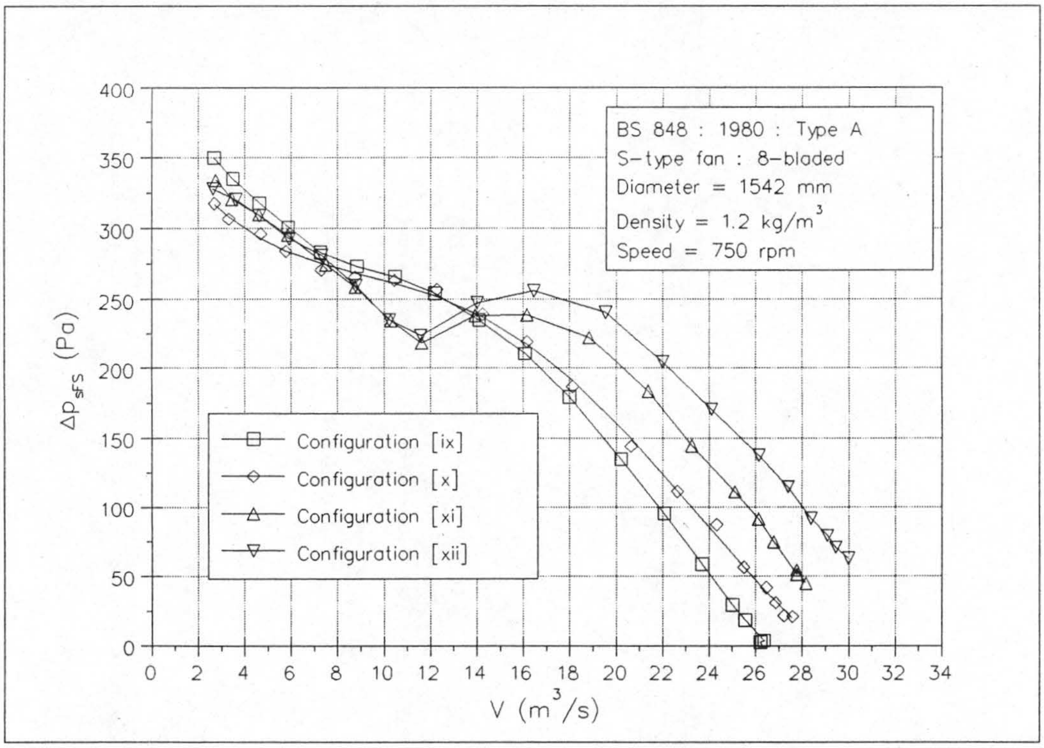

Figure C2.6 : Δp_{sFS} versus V for double delta heat exchanger with blade angle set to 26°.

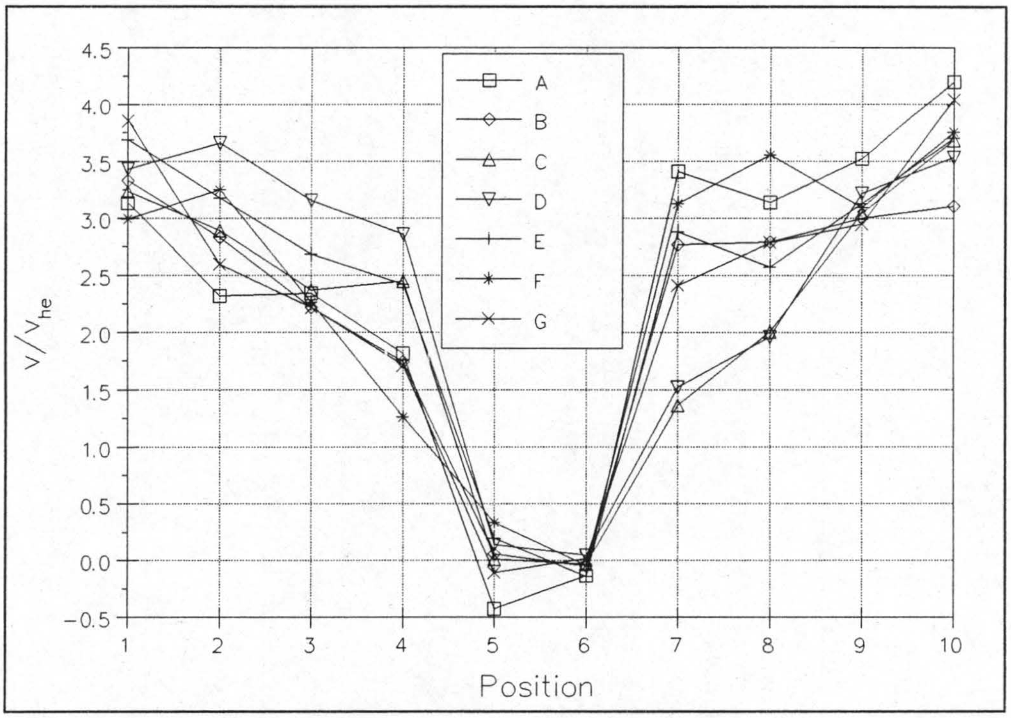

Figure C3.1 : Velocity distribution downstream of double delta heat exchanger with blade angle set to 18°. (Configuration [i])

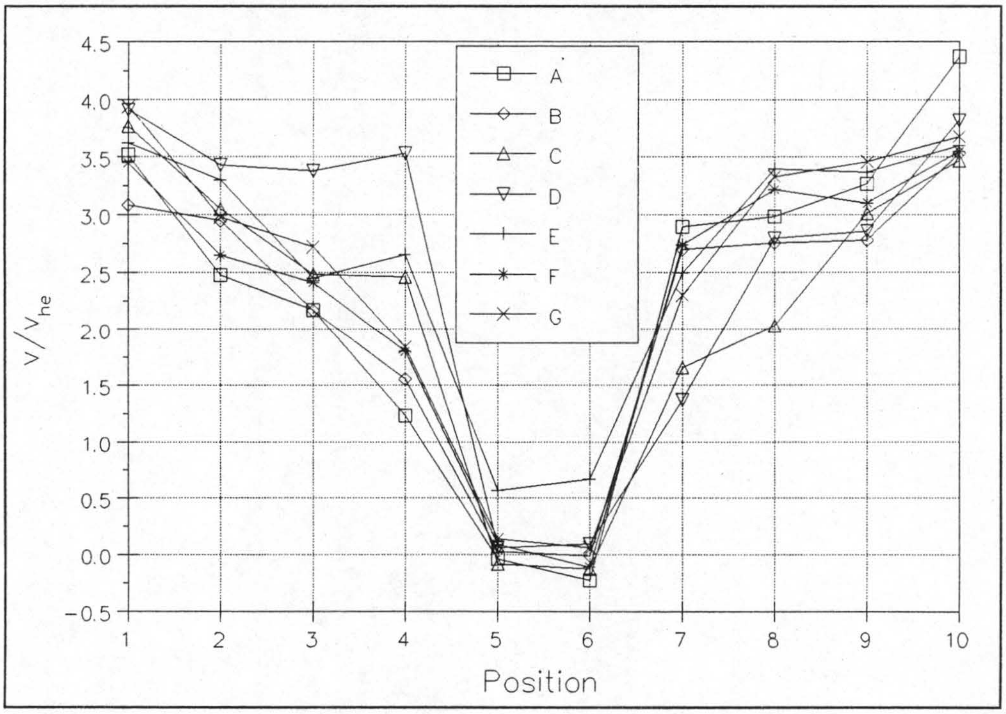

Figure C3.2 : Velocity distribution downstream of double delta heat exchanger with round-to-rectangular diffuser, guide vanes, flow straightner and blade angle set to 18°. (Configuration [ii])

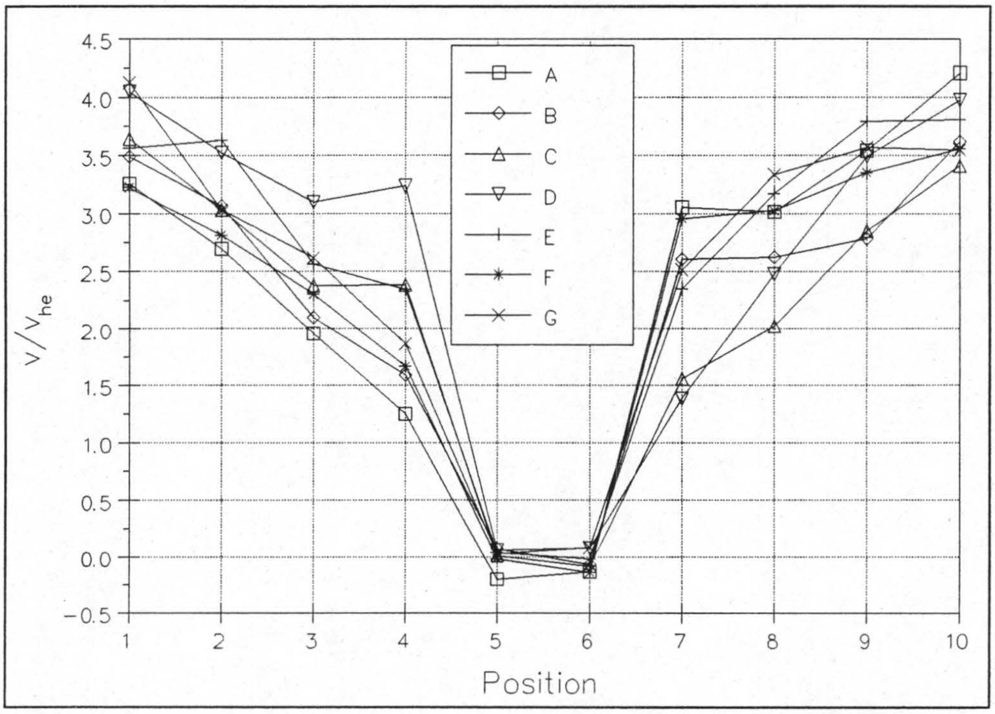

Figure C3.3 : Velocity distribution downstream of double delta heat exchanger with round-to-rectangular diffuser and guide vanes. (Configuration [iii])

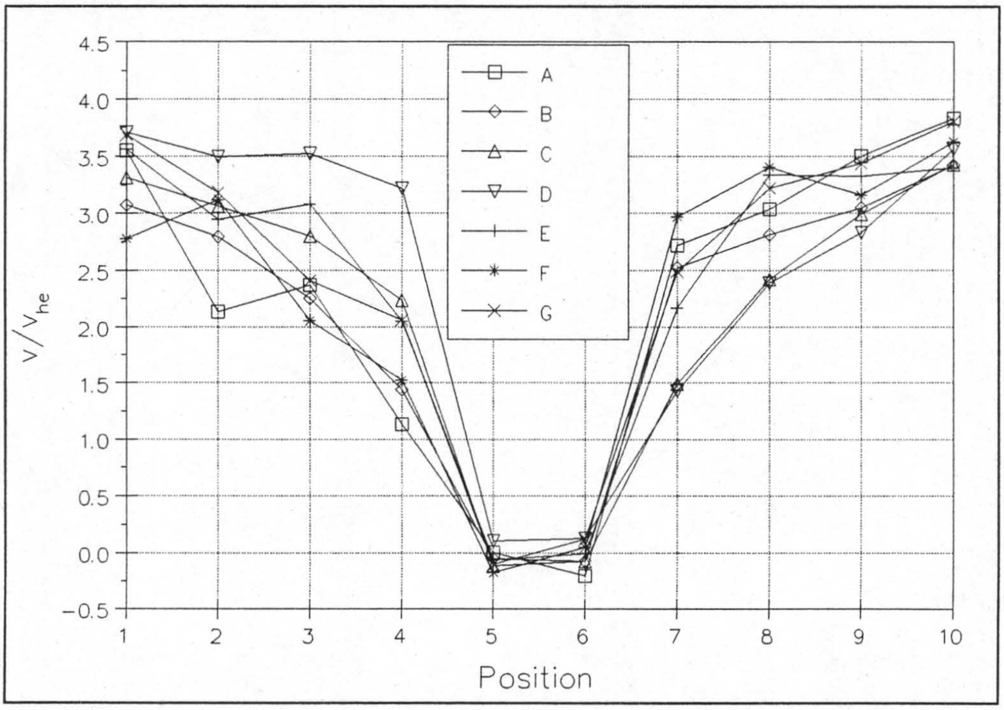

Figure C3.4 : Velocity distribution downstream of double delta heat exchanger with round-to rectangular diffuser, flow straightner and blade angle set to 18°. (Configuration [iv])

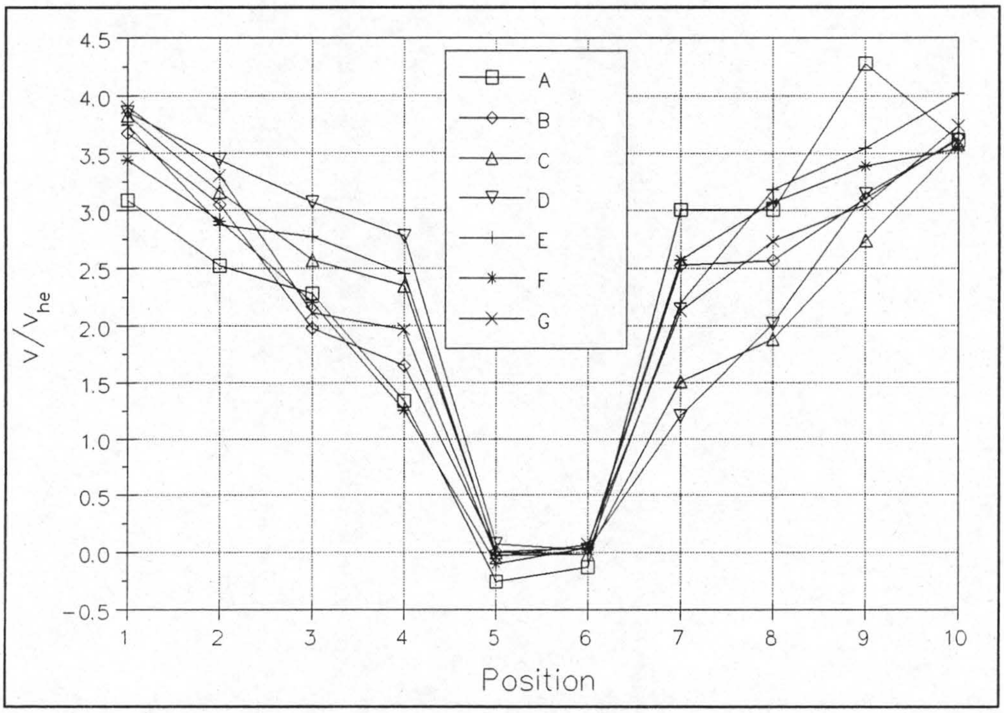

Figure C3.5 : Velocity distribution downstream of double delta heat exchanger with round-to-round diffuser and blade angle set to 18°. (Configuration [v])

Appendix D

Fan and Diffuser Characteristics

In order to predict the system operating points and to determine the plenum loss coefficients of the various fan systems investigated in this study, it is necessary that the fan characteristics of the S-fan be known. As many of the configurations tested make use of either the round-to-round diffuser or the round-to-rectangular diffuser it is also necessary to determine how these diffusers affect the fan characteristics. Section D.1 presents the S-fan's characteristics. The fan characteristics with the round-to-round diffuser and the round-to-rectangular diffuser attached downstream of the S-fan are presented in sections D.2 and D.3 respectively.

D.1 S-fan Characteristics

Tables D1.1.1 to D1.1.7 list the raw data readings taken to determine the S-fan characteristics for blade angles of 10°, 12°, 14°, 16°, 18°, 22° and 26°, where the blade angle is set at the tip of the blade. The calculated fan characteristics are listed in tables D1.2.1 to D1.2.7 and are presented in graphical form in figures D1.1 to D1.3. Tests conducted with the S-fan blade angle set to 22° or 26° could not be conducted at 750 rpm as the fan power requirements at this speed exceeds the maximum power available from the hydraulic motor driving the fan rotor. Thus the tests were conducted at the highest possible fan speed and the results were then extrapolated for a fan speed of 750 rpm using the fan laws. A sample calculation showing how the fan characteristics are determined is given in Appendix F.

Table D1.1.1 : Experimental readings for S-fan characteristics with blade angle set to 10°.

Δp_{sett} (Pa)	Δp_{bell} (Pa)	T (N.m)	N (rpm)
304.407	5.539	54.499	748.943
292.073	9.362	55.262	748.772
285.546	17.986	56.967	750.837
278.173	29.199	57.920	747.441
271.736	45.015	59.566	748.856
262.533	65.924	60.846	748.338
255.306	92.719	62.454	750.707
240.253	126.741	63.269	748.734
226.991	167.893	64.209	749.038
205.018	215.768	64.314	747.880
172.980	276.960	63.932	749.026
136.581	337.662	61.964	748.799
104.048	391.508	59.331	748.070
73.124	437.759	55.660	745.337
50.623	479.388	53.146	749.341
30.464	512.061	50.739	750.739
31.309	514.632	50.190	751.362

Table D1.1.2 : Experimental readings for S-fan characteristics with blade angle set to 12°.

Δp_{sett} (Pa)	Δp_{bell} (Pa)	T (N.m)	N (rpm)
312.729	5.968	64.565	750.632
303.354	10.400	65.187	750.923
293.598	16.686	66.725	751.784
287.612	29.342	67.854	751.212
283.520	46.687	69.309	750.974
277.513	69.055	70.918	752.213
268.098	96.170	71.623	749.505
257.287	130.724	73.019	750.731
241.699	177.427	73.976	749.814
225.711	225.184	74.602	749.546
198.976	292.656	74.707	750.733
165.678	354.735	73.362	750.439
130.858	414.953	70.832	749.438
101.947	466.973	67.968	748.808
79.982	512.531	66.003	753.438
58.903	541.522	62.569	748.745
52.854	559.434	62.407	753.165

Table D1.1.3 : Experimental readings for S-fan characteristics with blade angle set to 14°.

Δp_{sett} (Pa)	Δp_{bell} (Pa)	T (N.m)	N (rpm)
308.867	5.866	71.235	748.733
298.732	10.148	71.414	748.534
287.403	18.646	72.935	748.506
284.336	29.315	73.359	745.202
287.937	46.166	76.075	749.856
282.920	69.781	77.757	748.893
276.372	96.552	78.892	748.381
266.947	130.492	80.471	747.529
254.273	175.608	82.141	747.845
240.741	227.046	83.460	747.463
218.136	297.078	84.572	747.792
187.719	371.372	84.523	749.178
155.750	430.713	82.782	747.818
125.291	492.690	80.822	748.273
101.004	537.973	78.279	748.431
90.139	557.619	76.471	747.433
73.281	591.659	74.319	747.936

Table D1.1.4 : Experimental readings for S-fan characteristics with blade angle set to 16°.

Δp_{sett} (Pa)	Δp_{bell} (Pa)	T (N.m)	N (rpm)
327.235	6.534	84.507	750.887
309.173	9.783	83.861	750.622
304.682	17.038	84.120	750.517
297.102	29.223	85.348	751.669
297.594	47.335	86.710	750.625
293.460	71.999	88.389	749.493
287.590	99.806	89.674	748.822
281.276	137.266	91.461	749.908
266.564	187.250	93.596	745.393
256.471	238.693	95.626	749.476
240.776	316.881	97.759	750.415
211.481	398.644	98.872	747.747
177.769	476.535	99.321	746.869
152.678	533.484	98.175	746.644
124.122	589.190	95.908	745.141
111.330	621.370	94.602	746.705
101.425	644.087	94.784	747.262
84.233	678.737	94.065	746.301

Table D1.1.5 : Experimental readings for S-fan characteristics with blade angle set to 18°.

Δp_{sett} (Pa)	Δp_{bell} (Pa)	T (N.m)	N (rpm)
310.617	5.094	91.953	748.048
300.689	8.826	90.986	748.135
290.167	18.349	91.469	748.276
283.013	29.490	93.699	749.076
290.463	46.867	94.284	748.389
293.017	70.540	95.879	747.939
292.597	99.161	98.203	749.170
287.346	134.033	99.786	747.067
277.422	179.757	102.535	747.624
266.032	243.920	105.471	748.442
254.664	318.921	108.145	749.639
227.061	407.677	109.305	748.469
196.223	486.493	108.920	747.268
170.110	553.555	108.153	749.083
147.113	605.185	105.832	749.162
134.780	635.548	104.879	749.366
120.585	669.276	103.970	749.739

Table D1.1.6 : Experimental readings for S-fan characteristics with blade angle set to 22°.

Δp_{sett} (Pa)	Δp_{bell} (Pa)	T (N.m)	N (rpm)
285.732	5.209	113.018	711.491
286.982	9.526	113.560	720.340
286.926	17.756	115.243	734.100
281.270	28.479	114.735	736.057
281.137	45.890	115.272	738.996
287.100	70.223	115.409	735.209
287.344	99.161	115.790	730.826
284.196	135.119	116.039	726.152
278.506	184.846	117.298	721.814
268.438	250.428	117.474	712.409
250.433	326.595	118.038	703.832
225.051	407.488	118.755	696.188
193.334	496.112	119.069	690.540
170.277	555.418	118.578	686.818
141.538	627.966	117.813	684.154
124.126	665.936	116.179	681.077
115.344	683.710	115.555	680.915
117.189	684.014	115.736	680.972
105.349	712.894	115.240	681.314

Table D1.1.7 : Experimental readings for S-fan characteristics with blade angle set to 26°.

Δp_{sett} (Pa)	Δp_{bell} (Pa)	T (N.m)	N (rpm)
230.796	6.307	117.856	662.883
227.886	10.693	117.307	670.274
224.637	17.382	117.254	677.283
221.840	26.574	117.576	684.330
215.961	42.030	117.240	681.657
204.076	60.883	117.047	677.586
220.067	86.233	116.641	676.401
231.431	122.414	116.533	674.378
230.489	167.068	116.834	670.851
231.253	223.241	117.437	665.575
223.191	303.752	118.570	658.516
206.413	389.225	119.420	651.375
177.007	466.205	118.533	637.703
151.483	536.201	118.862	632.284
132.622	589.680	118.698	629.501
120.534	620.625	118.185	626.913
105.192	662.309	117.862	625.557

Table D1.2.1 : Fan characteristics for S-fan with blade angle set to 10°.

V (m^3/s)	Δp_{sF} (Pa)	P (W)	η_{sF} %
2.362	299.746	4214.974	16.800
3.071	287.688	4275.411	20.667
4.245	279.675	4382.889	27.089
5.433	274.888	4496.452	33.215
6.733	267.456	4606.465	39.091
8.153	258.680	4711.536	44.761
9.637	249.889	4805.215	50.118
11.296	236.268	4892.866	54.545
12.994	222.902	4960.877	58.384
14.750	201.753	4983.368	59.716
16.680	169.428	4937.042	57.243
18.417	133.529	4786.231	51.380
19.844	101.573	4590.310	43.910
21.054	71.501	4336.590	34.713
21.909	48.548	4095.737	25.970
22.597	28.578	3894.902	16.580
22.635	29.350	3846.399	17.272

Table D1.2.2 : Fan characteristics for S-fan with blade angle set to 12°.

V (m^3/s)	Δp_{sF} (Pa)	P (W)	η_{sF} %
2.452	307.883	4992.532	15.121
3.235	298.383	5036.307	19.167
4.093	288.082	5142.794	22.926
5.431	282.592	5237.520	29.303
6.853	278.694	5352.963	35.677
8.320	271.820	5458.916	41.428
9.853	264.405	5552.551	46.918
11.467	252.797	5641.735	51.384
13.374	237.897	5728.741	55.538
15.070	222.144	5780.411	57.914
17.148	194.940	5768.768	57.947
18.881	162.130	5667.458	54.012
20.441	128.036	5484.782	47.716
21.696	99.548	5270.327	40.980
22.585	76.786	5054.204	34.312
23.356	56.861	4850.445	27.380
23.598	50.250	4781.035	24.803

Table D1.2.3 : Fan characteristics for S-fan with blade angle set to 14°.

V (m^3/s)	Δp_{sF} (Pa)	P (W)	η_{sF} %
2.457	310.572	5625.937	13.561
3.232	300.499	5642.456	17.211
4.380	289.071	5762.429	21.973
5.516	288.492	5847.289	27.217
6.880	288.502	5988.967	33.142
8.469	284.132	6136.780	39.211
9.968	277.849	6234.505	44.424
11.600	268.871	6373.209	48.940
13.450	255.733	6499.187	52.923
15.299	242.191	6609.347	56.061
17.489	218.988	6690.030	57.246
19.511	187.421	6659.460	54.912
21.044	155.724	6543.895	50.078
22.487	124.729	6379.295	43.967
23.487	100.146	6174.495	38.094
23.941	89.416	6047.382	35.399
24.640	72.250	5868.254	30.337

Table D1.2.4 : Calculated fan characteristics for S-fan with blade angle set to 16°.

V (m^3/s)	Δp_{sF} (Pa)	P (W)	η_{sF} %
2.558	320.168	6494.144	12.610
3.130	302.647	6447.888	14.693
4.131	298.304	6469.331	19.050
5.402	289.941	6543.183	23.937
6.885	291.187	6666.126	30.073
8.503	287.939	6815.475	35.925
10.020	282.600	6926.542	40.881
11.733	275.485	7043.692	45.890
13.785	264.075	7294.647	49.903
15.477	251.152	7371.130	52.735
17.808	234.939	7515.542	55.669
20.039	207.486	7653.237	54.328
21.928	174.428	7703.498	49.651
23.203	149.569	7617.321	45.559
24.426	121.681	7469.356	39.792
25.029	108.451	7335.893	37.002
25.461	98.462	7338.342	34.162
26.166	81.629	7300.192	29.258

Table D1.2.5 : Fan characteristics for S-fan with blade angle set to 18°.

V (m^3/s)	Δp_{sF} (Pa)	P (W)	η_{sF} %
2.288	311.849	7250.956	9.838
3.010	301.772	7172.278	12.666
4.339	291.049	7206.930	17.524
5.495	283.219	7366.300	21.127
6.934	291.190	7426.502	27.188
8.512	294.055	7561.367	33.103
10.076	292.600	7719.232	38.192
11.746	288.865	7887.423	43.020
13.592	278.325	8091.893	46.750
15.814	266.113	8304.444	50.675
18.051	253.695	8486.885	53.960
20.435	226.547	8602.372	53.818
22.353	196.026	8596.967	50.968
23.780	168.757	8492.962	47.251
24.856	145.576	8307.003	43.558
25.461	133.090	8226.762	41.191
26.112	118.698	8146.228	38.047

Table D1.2.6 : Fan characteristics for S-fan with blade angle set to 22°.

V (m^3/s)	Δp_{sF} (Pa)	P (W)	η_{sF} %
2.422	314.502	9770.650	7.795
3.235	308.158	9577.857	10.408
4.334	296.636	9358.873	13.736
5.473	289.200	9267.568	17.080
6.920	286.725	9237.055	21.481
8.605	295.792	9344.064	27.240
10.287	299.533	9487.758	32.477
12.085	299.974	9630.607	37.643
14.219	297.361	9851.938	42.918
16.767	294.009	10127.970	48.675
19.378	280.713	10424.202	52.183
21.877	257.454	10716.401	52.559
24.329	224.323	10917.698	49.988
25.876	199.337	10988.341	46.941
27.613	166.465	10999.419	41.789
28.559	146.953	10943.227	38.351
28.942	136.422	10888.621	36.261
28.947	138.614	10904.095	36.797
29.533	124.189	10845.129	33.819

Table D1.2.7 : Fan characteristics for S-fan with blade angle set to 26°.

V (m^3/s)	Δp_{sF} (Pa)	P (W)	η_{sF} %
2.882	297.326	11925.415	7.186
3.711	287.117	11609.276	9.179
4.683	277.167	11364.681	11.421
5.730	268.073	11162.162	13.762
7.234	262.956	11217.018	16.959
8.758	251.388	11332.162	19.429
10.443	272.019	11334.304	25.063
12.481	287.723	11393.118	31.521
14.658	289.433	11542.907	36.753
17.078	294.847	11787.191	42.719
20.133	290.402	12156.428	48.095
23.036	274.101	12511.457	50.468
25.744	244.726	12952.920	48.640
27.839	212.524	13209.055	44.791
29.318	187.266	13305.317	41.264
30.198	171.294	13355.749	38.730
31.258	149.701	13375.108	34.986

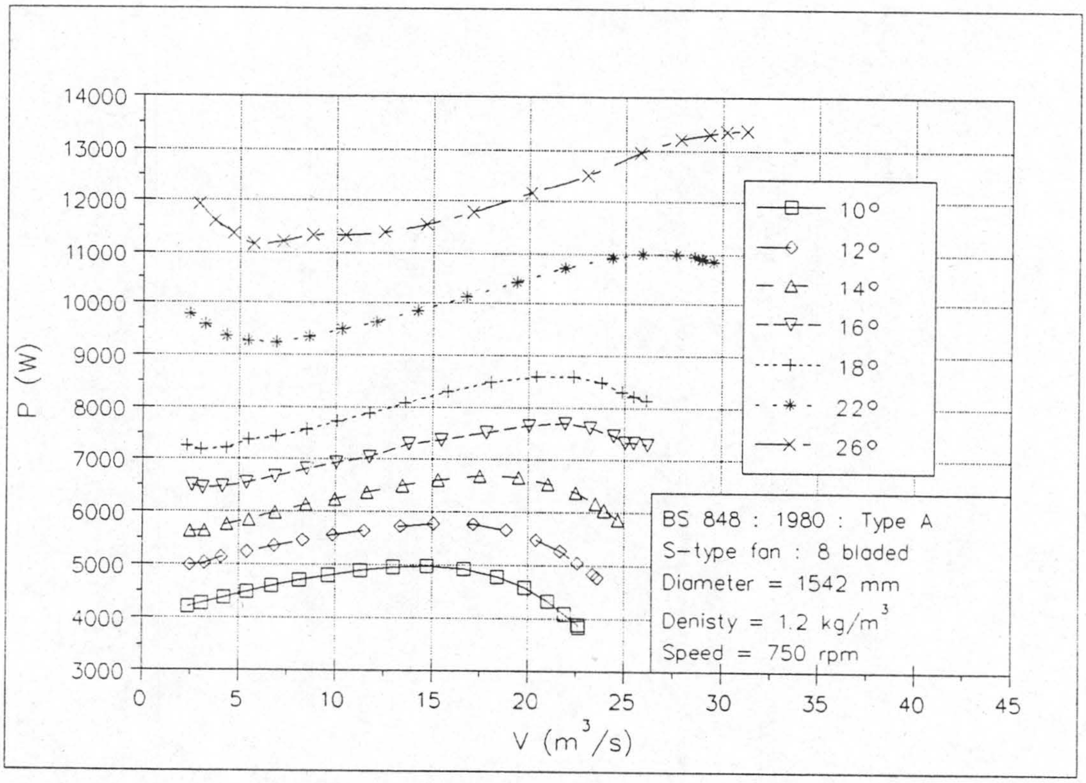

Figure D1.1 : P versus V for S-fan.

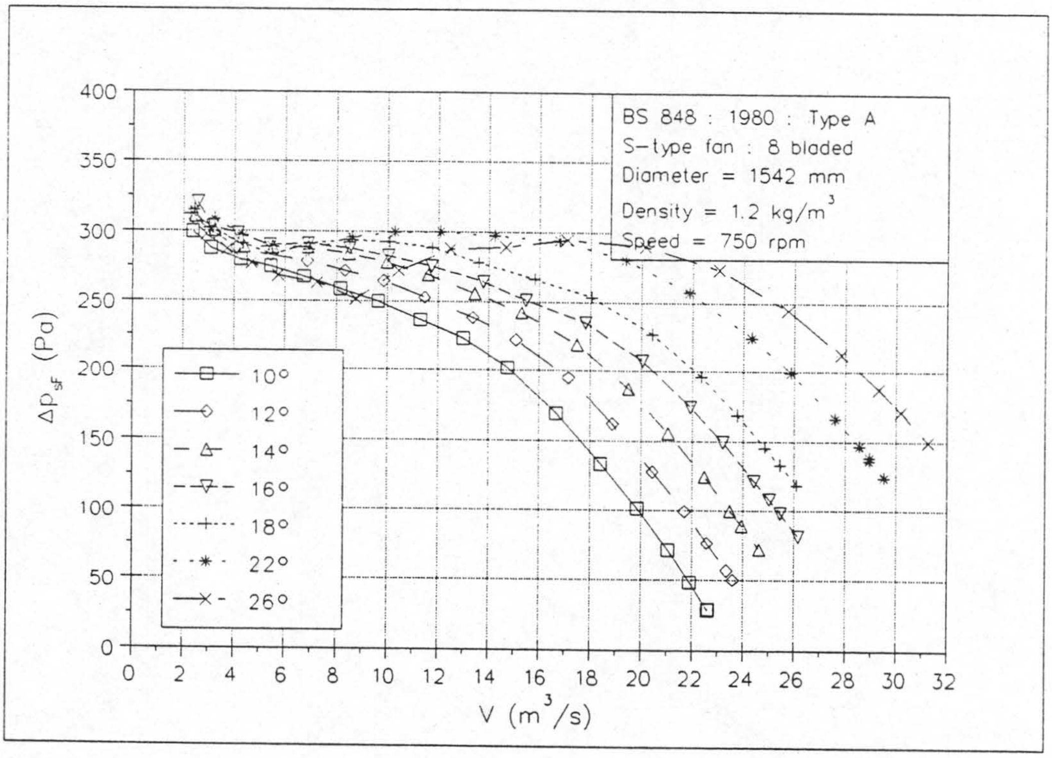

Figure D1.2 : Δp_{sF} versus V for S-fan.

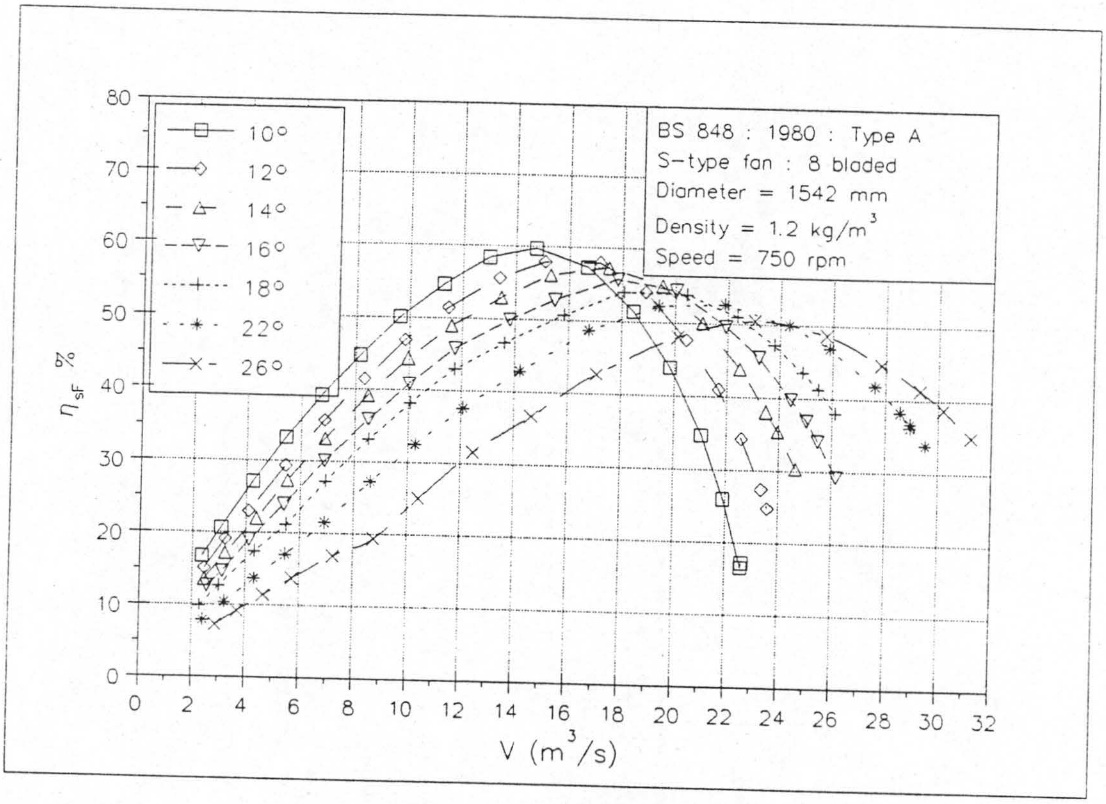

Figure D1.3 : η_{sF} versus V for S-fan.

D.2 S-fan with Round-to-Round Diffuser

Tables D2.1.1 to D2.1.7 list the experimental readings taken to determine the fan characteristics of the S-fan with the round-to-round diffuser attached downstream for blade angles of 10°, 12°, 14°, 16°, 18°, 22° and 26°. The calculated fan characteristics are listed in tables D2.2.1 to D2.2.7 and are presented in graphical form in figures D2.1 to D2.3. Tests conducted with the blade angle set to 22° and 26° could not be performed at 750 rpm as the fan rotor power requirements exceed the maximum power output of the hydraulic motor driving the fan rotor. Thus tests were conducted at the highest possible fan speed and the results were then extrapolated for a fan speed of 750 rpm using the fan laws.

Figure D2.4 shows the increase in the fan static pressure rise obtained by placing the round-to-round diffuser downstream of the S-fan, where the increase in the fan static pressure rise is given by

$$\Delta p_{sF} \text{ increase} = \Delta p_{sF \text{ with diffuser}} - \Delta p_{sF \text{ without diffuser}}$$

Also shown in figure D2.4 is the static pressure recovery as predicted by Wallis [83WA1]. Wallis gives the static pressure recovered by a diffuser as

$$p_{so} - p_{si} = \eta_D \cdot \frac{1}{2} \cdot \rho \cdot v_i^2 \left[1 - \left(\frac{A_i}{A_o} \right)^2 \right]$$

where p_{so} is the static pressure at the diffuser outlet.

p_{si} is the static pressure at the diffuser inlet.

A_i is the cross-sectional area at the diffuser inlet.

A_o is the cross-sectional area the diffuser outlet.

η_D is the diffuser efficiency.

v_i is the mean velocity at the diffuser inlet and is given by $v_i = V/A_i$

According to Wallis $\eta_D = 0.85$ for a round-to-round diffuser with an included angle of 14°. Note that the data provided by Wallis is for airflow entering the diffuser with a uniform axial velocity.

ESDU [73ES1] suggest a static pressure recovery coefficient, c_{pr}, of 0.4 for a round-to-round having an area ratio of 1.547 and L/d = 1 (as is the case with the diffuser tested here). The staic pressure recovery is then given by :

$$p_{so} - p_{si} = c_{pr} \cdot \frac{1}{2} \cdot \rho \cdot v_i^2 = 0.2 \cdot \rho \cdot v_i^2$$

This correlation is also plotted in figure D2.4 and it can be seen that ESDU gives more conservative values for static pressure recovery than Wallis.

As can be seen from figure D2.4, for small blade angles (10°, 12° and 14°), the actual static pressure recovery is generally slightly greater than the expected pressure recovery predicted by both Wallis and ESDU. This is especially so at the higher volume flow rates.This could be due to the fact that the airflow leaving the fan still has tangential and radial components and that these components help prevent flow separation from occurring along the walls of the diffuser and thus increases the diffuser efficiency of the round-to-round diffuser.

For higher blade angles (16°, 18°, 22° and 26°) the actual pressure recovery is less than the expected pressure recovery. This discrepancy between the actual and predicted (using Wallis' data) pressure recovery decreases as the volume flow rate increases. In most cases the discrepancy is acceptable at the high volume flow rate at which the diffuser will be operating at in the heat exchanger configurations investigated in this study. In general the static pressure recovery as predicted by Wallis is in good agreement with the experimental results, whilst ESDU tends to be mildly conservative.

Table D2.1.1 : Experimental readings for characteristics of S-fan with round-to-round diffuser and blade angle set to 10°.

Δp_{sett} (Pa)	Δp_{bell} (Pa)	T (N.m)	N (rpm)
305.129	11.820	54.777	751.249
294.903	19.449	55.606	750.122
297.860	30.092	55.404	752.386
282.362	47.021	56.237	751.536
274.934	73.027	58.263	750.673
266.417	101.720	60.776	751.529
255.142	133.317	62.038	749.688
238.810	175.058	63.201	749.599
222.961	220.066	63.033	750.199
194.448	281.974	61.297	750.306
159.857	353.726	58.349	751.263
129.967	415.029	54.485	751.625
101.852	473.624	50.593	754.408
77.632	510.854	45.895	748.213
70.458	535.883	45.002	754.218

Table D2.1.2 : Experimental readings for characteristics of S-fan with round-to-round diffuser and blade angle set to 12°.

Δp_{sett} (Pa)	Δp_{bell} (Pa)	T (N.m)	N (rpm)
317.267	8.945	62.479	749.957
304.937	16.853	62.770	749.717
312.495	29.755	64.469	753.579
300.478	48.093	65.040	751.352
295.968	73.559	66.996	752.564
294.699	101.437	70.154	751.448
279.568	136.554	72.413	749.039
263.776	186.349	74.252	751.383
243.152	248.149	74.519	750.298
218.275	314.507	73.890	752.337
187.585	384.330	71.361	750.247
156.463	455.720	67.536	749.820
127.089	523.174	63.529	751.056
102.605	572.678	59.251	749.975
87.613	613.185	57.103	753.831
82.991	629.015	55.852	753.203

Table D2.1.3 : Experimental readings for characteristics of S-fan with round-to-round diffuser and blade angle set to 14°

Δp_{sett} (Pa)	Δp_{bell} (Pa)	T (N.m)	N (rpm)
322.093	8.928	71.053	750.066
310.045	13.561	70.479	748.774
307.562	25.518	72.330	749.576
314.221	45.401	73.468	751.780
309.511	68.727	75.156	750.722
306.431	100.981	78.361	750.619
299.306	137.157	82.059	749.479
285.320	187.822	84.735	749.982
266.278	247.264	86.183	749.712
242.256	322.225	86.239	748.493
214.557	407.238	85.276	748.514
181.484	490.728	82.686	750.465
158.505	543.608	79.757	748.115
132.675	616.194	76.243	751.713
120.409	655.970	74.437	754.423
104.982	686.961	71.128	752.081
97.742	691.666	70.112	749.498

Table D2.1.4 : Experimental readings for characteristics of S-fan with round-to-round diffuser and blade angle set to 16°.

Δp_{sett} (Pa)	Δp_{bell} (Pa)	T (N.m)	N (rpm)
323.886	11.930	80.199	748.418
313.391	19.210	79.496	749.261
305.124	31.101	79.561	748.701
313.919	49.376	81.297	749.262
314.687	72.287	82.794	750.060
316.314	102.462	86.151	747.276
306.930	146.365	90.203	748.303
297.783	196.220	93.115	749.902
281.908	257.949	95.021	749.086
256.664	339.527	95.972	748.971
233.612	422.386	95.785	749.344
202.369	511.549	93.762	748.627
175.058	586.422	91.095	749.056
156.817	641.878	88.750	750.547
138.443	681.859	85.550	746.959
129.843	714.329	84.727	751.001

Table D2.1.5 : Experimental readings for characteristics of S-fan with round-to-round diffuser and blade angle set to 18°.

Δp_{sett} (Pa)	Δp_{bell} (Pa)	T (N.m)	N (rpm)
338.913	6.647	95.957	750.194
328.232	11.380	94.911	749.176
320.069	18.908	93.943	749.634
305.095	32.488	92.297	748.395
301.280	47.844	91.931	749.246
316.676	74.374	94.761	750.862
314.507	105.988	96.130	746.824
321.772	147.340	100.866	749.880
312.507	202.263	105.019	748.483
297.725	272.630	108.121	748.668
282.171	355.144	110.096	748.520
255.694	448.756	110.773	748.371
235.966	522.682	110.718	749.884
211.015	611.580	109.527	751.418
183.303	678.847	105.658	746.962
176.257	702.270	104.800	747.254
164.306	752.442	103.783	750.839

Table D2.1.6 : Experimental readings for characteristics of S-fan with round-to-round diffuser and blade angle set to 22°.

Δp_{sett} (Pa)	Δp_{bell} (Pa)	T (N.m)	N (rpm)
303.422	6.881	116.586	723.840
300.884	10.055	116.148	729.403
298.731	18.628	116.297	736.421
290.145	30.283	114.774	738.117
282.922	47.636	115.296	745.626
272.906	67.748	114.407	748.535
269.716	95.671	113.212	752.505
295.763	140.286	115.352	742.558
297.220	190.562	116.037	728.470
289.341	261.177	118.290	718.488
258.799	333.109	116.829	702.215
244.283	419.046	117.541	697.408
221.068	509.699	117.667	693.654
198.322	605.936	117.285	692.517
179.801	663.612	116.448	691.445
169.359	714.794	115.751	692.027

Table D2.1.6 : continued

Δp_{sett} (Pa)	Δp_{bell} (Pa)	T (N.m)	N (rpm)
162.028	728.226	115.009	690.704
155.776	755.621	114.732	691.240
150.605	780.920	114.886	693.847

Table D2.1.7 : Experimental readings for characteristics of S-fan with round-to-round diffuser and blade angle set to 26°.

Δp_{sett} (Pa)	Δp_{bell} (Pa)	T (N.m)	N (rpm)
246.584	6.378	117.731	659.867
240.020	9.734	115.569	659.374
238.912	17.507	116.752	668.425
236.874	27.199	116.117	673.185
230.908	41.929	115.919	676.842
223.699	61.778	115.893	683.110
217.362	87.184	116.263	692.163
219.819	119.255	116.818	704.079
240.554	172.097	117.536	687.557
248.345	234.433	118.842	674.545
237.577	314.946	118.065	652.208
222.090	399.987	119.307	644.067
198.458	492.828	119.080	635.582
177.453	572.028	118.873	630.619
162.006	635.589	118.499	628.753
154.500	675.700	118.169	627.836
143.585	722.126	117.648	626.594
138.576	742.369	117.499	626.112
131.881	767.729	117.195	625.970

Table D2.2.1 : Fan characteristics for S-fan with round-to-round diffuser and blade angle set to 10°.

V (m^3/s)	Δp_{sF} (Pa)	P (W)	η_{sF} %
2.770	306.506	4187.781	20.276
3.446	299.519	4223.505	24.435
4.426	290.303	4299.819	29.881
5.489	291.436	4258.596	37.563
6.868	276.812	4331.770	43.888
8.568	270.066	4497.837	51.446
10.100	261.009	4680.698	56.320
11.590	251.079	4800.867	60.613
13.280	234.906	4891.253	63.779
14.876	218.798	4869.702	66.836
16.831	190.497	4732.837	67.745
18.821	155.871	4492.222	65.305
20.371	126.268	4189.483	61.396
21.675	97.853	3860.511	54.940
22.692	75.452	3559.349	48.102
23.054	67.221	3434.511	45.122

Table D2.2.2 : Fan characteristics for S-fan with round-to-round diffuser and blade angle set to 12°.

V (m^3/s)	Δp_{sF} (Pa)	P (W)	η_{sF} %
2.996	311.223	4813.889	19.372
4.114	299.263	4838.857	25.442
5.439	303.539	4919.356	33.557
6.934	293.519	4991.838	40.771
8.561	288.107	5125.135	48.126
10.068	287.655	5382.648	53.806
11.718	274.508	5590.894	57.532
13.643	257.214	5696.319	61.606
15.764	237.561	5732.142	65.330
17.694	211.836	5651.640	66.321
19.608	182.744	5486.955	65.306
21.358	152.236	5197.206	62.560
22.839	122.854	4871.309	57.601
23.924	99.096	4555.322	52.044
24.625	83.454	4344.704	47.301
24.961	79.068	4256.457	46.367

Table D2.2.3 : Fan characteristics for S-fan with round-to-round diffuser and blade angle set to 14°.

V (m^3/s)	Δp_{sF} (Pa)	P (W)	η_{sF} %
2.997	316.757	5488.394	17.299
3.700	305.914	5462.204	20.723
5.070	302.778	5593.516	27.445
6.743	307.498	5648.631	36.710
8.308	303.672	5794.502	43.541
10.072	300.646	6043.078	50.108
11.755	294.438	6347.077	54.531
13.745	280.129	6544.343	58.834
15.773	261.403	6659.711	61.912
18.031	238.310	6684.149	64.286
20.264	210.704	6607.303	64.622
22.180	176.898	6371.265	61.582
23.412	155.165	6182.816	58.756
24.801	128.229	5852.538	54.338
25.494	115.301	5672.224	51.822
26.166	100.871	5453.047	48.403
26.344	94.434	5411.863	45.969

Table D2.2.4 : Fan characteristics for S-fan with round-to-round diffuser and blade angle set to 16°.

V (m^3/s)	Δp_{sF} (Pa)	P (W)	η_{sF} %
3.474	320.178	6227.230	17.862
4.403	309.055	6158.101	22.097
5.606	301.299	6171.928	27.367
7.059	309.506	6297.690	34.692
8.532	309.552	6400.047	41.267
10.196	313.409	6709.349	47.627
12.168	303.138	7004.992	52.657
14.058	292.697	7199.654	57.150
16.133	277.481	7361.939	60.807
18.507	252.401	7436.017	62.819
20.627	229.184	7412.444	63.777
22.715	198.507	7267.521	62.044
24.300	171.135	7050.783	58.980
25.368	152.393	6840.755	56.512
26.267	135.536	6656.465	53.483
26.738	125.565	6521.083	51.484

Table D2.2.5 : Fan characteristics for S-fan with round-to-round diffuser and blade angle set to 18°.

V (m^3/s)	**Δp_{sF} (Pa)**	**P (W)**	**η_{sF} %**
2.580	331.558	7373.267	11.601
3.380	321.937	7311.930	14.881
4.353	313.502	7227.887	18.883
5.715	299.747	7123.755	24.047
6.927	295.280	7079.105	28.895
8.620	309.025	7266.790	36.656
10.345	310.153	7451.577	43.060
12.149	314.668	7755.623	49.291
14.259	306.582	8104.333	53.943
16.549	291.705	8338.407	57.892
18.888	276.306	8492.828	61.451
21.231	250.114	8546.175	62.135
22.862	229.587	8505.872	61.709
24.674	204.087	8377.967	60.105
26.143	179.009	8176.452	57.236
26.578	171.865	8103.185	56.371
27.377	158.439	7947.220	54.579

Table D2.2.6 : Fan characteristics for S-fan with round-to-round diffuser and blade angle set to 22°.

V (m^3/s)	**Δp_{sF} (Pa)**	**P (W)**	**η_{sF} %**
2.745	324.697	9799.195	9.095
3.293	317.072	9613.846	10.859
4.439	308.805	9443.374	14.515
5.646	298.497	9276.105	18.168
7.009	285.168	9130.948	21.891
8.326	272.860	8989.357	25.272
9.841	266.756	8801.541	29.827
12.080	300.398	9212.137	39.391
14.352	313.545	9628.925	46.733
17.034	313.552	10089.699	52.934
19.677	293.244	10429.120	55.326
22.218	280.295	10636.345	58.550
24.631	255.988	10760.792	58.594
26.894	229.936	10758.641	57.477
28.183	208.751	10713.128	54.916

Table D2.2.6 : continued.

$V\ (m^3/s)$	Δp_{sF} (Pa)	P (W)	η_{sF} %
29.222	196.026	10629.963	53.888
29.549	188.121	10601.515	52.435
30.075	180.416	10558.896	51.388
30.458	172.969	10493.313	50.206

Table D2.2.7 : Fan characteristics for S-fan with round-to-round diffuser and blade angle set to 26°.

$V\ (m^3/s)$	Δp_{sF} (Pa)	P (W)	η_{sF} %
2.913	320.824	12031.176	7.768
3.601	312.719	11827.107	9.521
4.764	302.876	11626.672	12.410
5.896	296.025	11400.331	15.309
7.280	285.396	11257.551	18.457
8.755	271.355	11048.647	21.503
10.264	256.723	10795.175	24.410
11.802	250.832	10482.905	28.239
14.521	287.782	11062.589	37.775
17.276	308.531	11622.220	45.863
20.708	315.393	12349.307	52.887
23.628	301.942	12794.690	55.761
26.571	276.545	13110.484	56.048
28.846	250.683	13291.705	54.404
30.492	229.800	13326.618	52.580
31.483	219.537	13327.334	51.861
32.608	204.491	13319.869	50.061
33.086	197.494	13322.842	49.045
33.651	187.815	13293.490	47.544

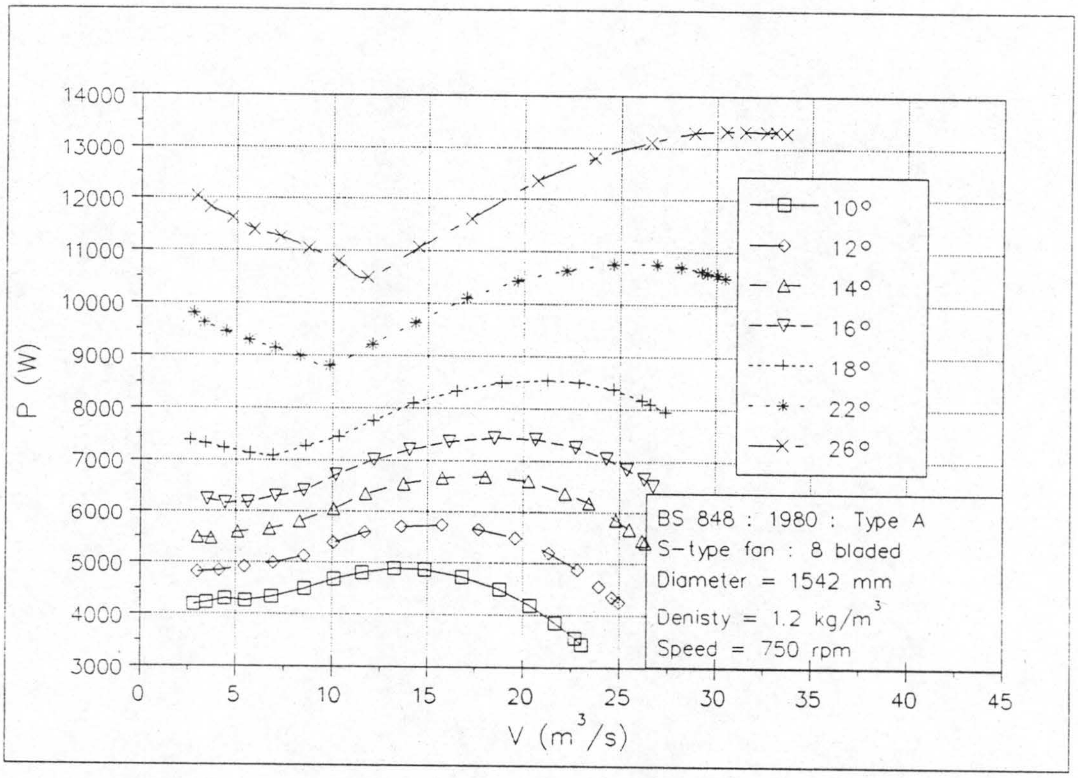

Figure D2.1 : P versus V for S-fan with round-to-round diffuser.

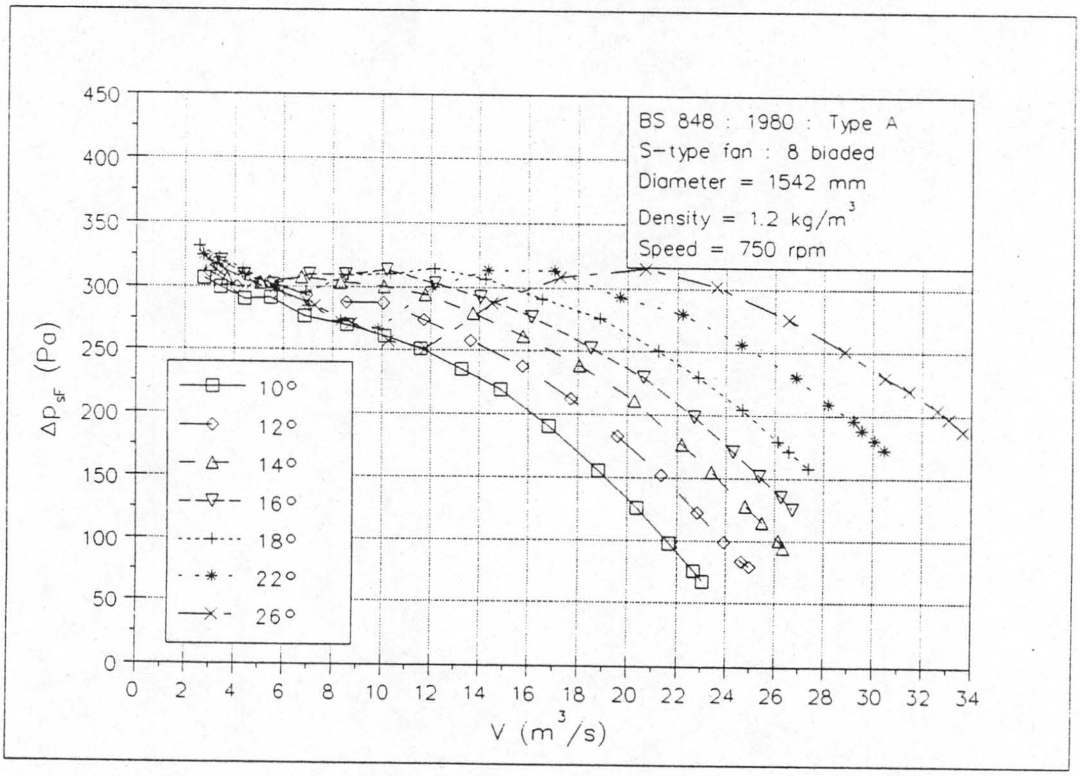

Figure D2.2 : Δp_{SF} versus V for S-fan with round-to-round diffuser.

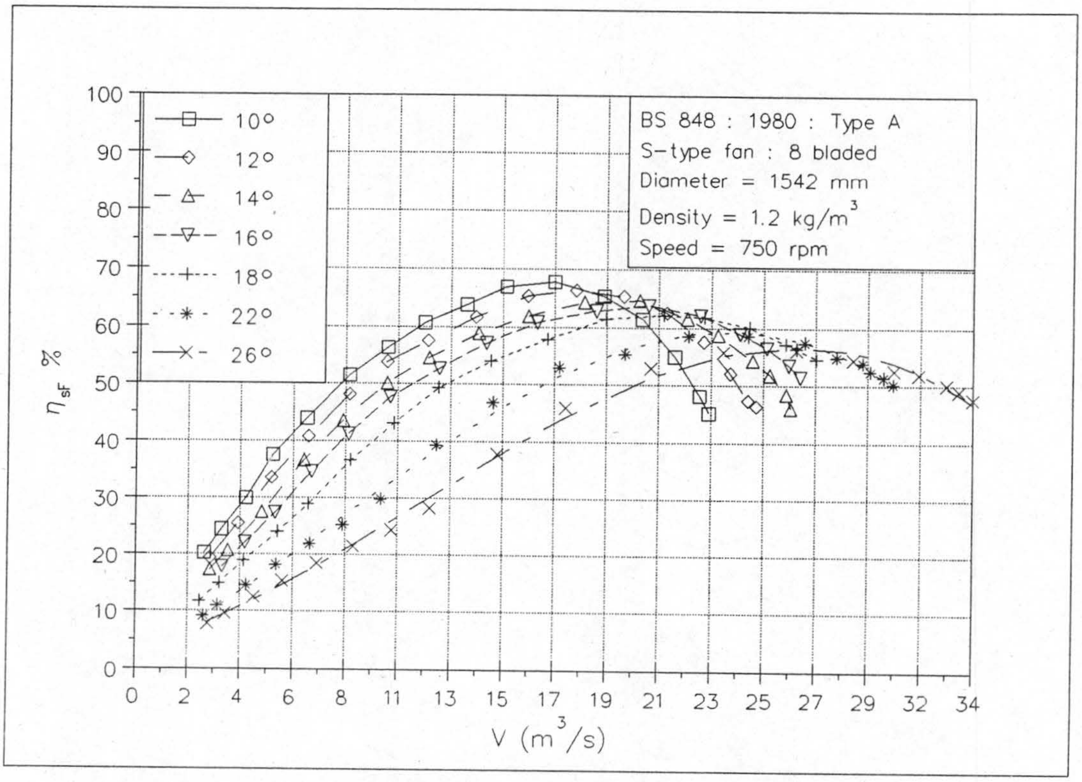

Figure D2.3 : η_{sF} versus V for S-fan with round-to-round diffuser.

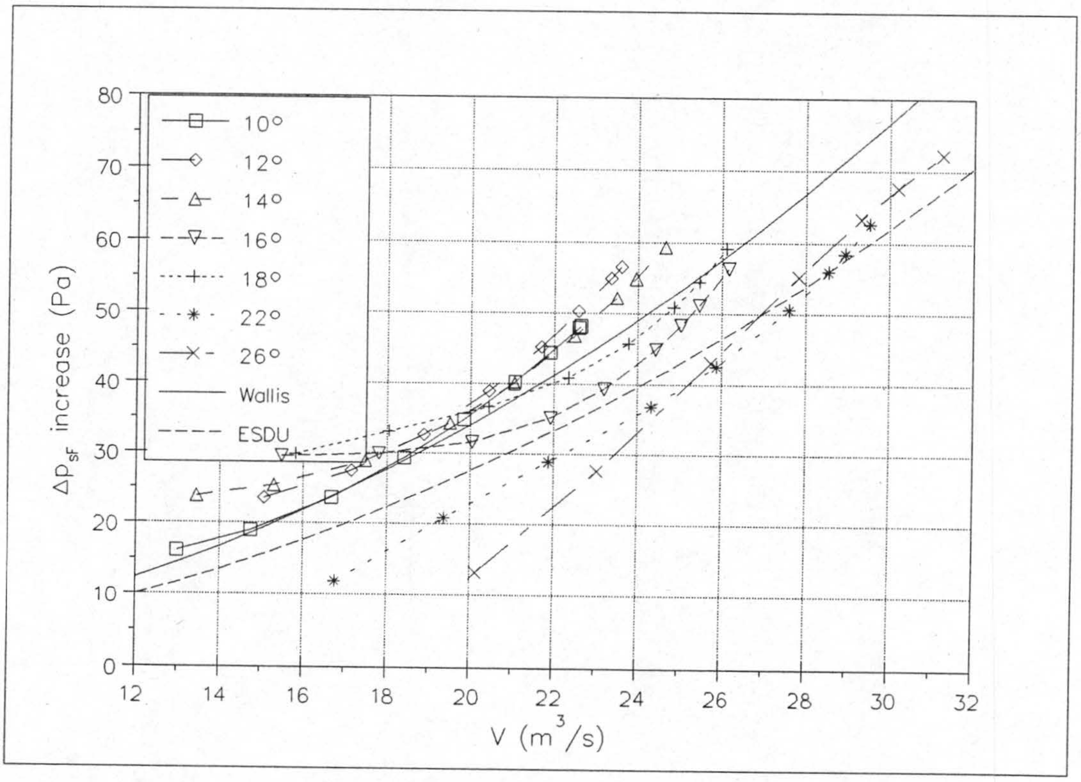

Figure D2.4 : Increase in fan static pressure obtained with round-to-round diffuser.

D.3 S-Fan with Round-to-Rectangular Diffuser

Tables D3.1.1 to D3.1.5 list the experimental readings taken to determine the fan characteristics of the S-fan with the round-to-rectangular diffuser attached downstream and the blade angle set to 18°. Tests were also conducted with the flow director and flow straightner installed in the round-to-rectangular diffuser. The calculated fan characteristics are listed in tables D3.2.1 to D3.2.5 and are shown in graphical form in figures D3.1 to D3.3. Appendix F provides a sample calculation of how the fan characteristics are determined.

Figure D3.4 shows the increase (or ,as in this case, the decrease) in static pressure obtained by attaching the round-to-rectangular diffuser downstream of the S-fan. As can be seen from the graph, the round-to-rectangular diffuser is a very poor diffuser; it in fact causes a decrease in the available static pressure. This poor performance could be due to the fact that it has a fairly high included angle of 28° between the two vertical side walls which could cause substantial flow separation to occur.

Table D3.1.1 : Experimental readings for characteristics for S-fan with round-to-rectangular diffuser and blade angle set to 18°.

Δp_{sett} (Pa)	Δp_{bell} (Pa)	T (N.m)	N (rpm)
278.761	28.684	85.722	747.169
277.734	44.842	88.832	746.630
272.664	67.193	91.653	747.070
265.223	91.616	93.835	748.175
255.527	121.137	95.653	748.964
240.724	165.874	97.740	748.939
226.353	220.674	99.553	747.715
206.127	288.235	100.801	748.605
186.762	362.348	101.219	747.318
166.482	441.073	101.109	748.014
148.738	503.779	100.391	748.357
128.301	573.813	98.738	748.899
116.791	611.874	97.698	748.532
110.412	634.916	97.638	750.966

Table D3.1.2 : Experimental readings for characteristics of S-fan with round-to-rectangular diffuser, flow straightner and blade angle set to 18°.

Δp_{sett} (Pa)	Δp_{bell} (Pa)	T (N.m)	N (rpm)
323.437	5.385	90.354	748.652
313.877	9.115	88.819	747.931
299.010	18.114	87.184	748.333
283.444	30.697	85.700	748.015
285.090	46.625	89.113	747.795
278.595	67.817	91.954	748.812
265.804	93.501	93.709	747.229
251.568	122.703	95.650	748.154
237.714	166.949	97.916	748.789
224.934	216.762	99.578	749.100
202.964	287.246	101.120	747.693
186.176	363.575	102.328	749.505
166.234	440.323	101.825	747.821
145.185	524.279	101.225	750.307
132.031	567.931	99.736	749.330
122.200	604.671	98.784	749.338
113.543	633.111	97.740	749.322

Table D3.1.3 : Experimental readings for characteristics of S-fan with round-to-rectangular diffuser, flow directors and blade angle set to 18°

Δp_{sett} (Pa)	Δp_{bell} (Pa)	T (N.m)	N (rpm)
310.333	5.837	91.016	748.424
306.934	9.871	90.494	748.868
293.383	16.306	88.983	749.331
285.213	29.452	88.265	749.179
287.280	47.677	92.216	751.179
283.443	64.535	94.919	748.959
278.340	95.608	97.614	749.587
268.391	128.630	100.076	750.368
254.147	176.102	101.718	748.680
238.127	235.942	104.092	749.232
217.332	309.929	105.644	749.089
196.610	393.833	106.383	749.583
173.574	479.989	106.340	750.011
156.766	557.355	104.104	746.558
135.288	625.714	103.534	749.238
130.294	654.108	103.419	752.742
140.323	720.234	101.243	750.578
123.265	718.354	100.193	747.716

Table D3.1.4 : Experimental readings for characteristics of S-fan with round-to-rectangular diffuser,flow director, low straightner and blade angle set to 18°.

Δp_{sett} (Pa)	Δp_{bell} (Pa)	T (N.m)	N (rpm)
343.681	4.778	94.418	748.766
333.766	8.267	93.179	750.028
316.909	17.618	91.161	749.111
301.842	28.566	89.819	747.203
300.154	47.761	92.176	749.482
291.548	69.705	95.487	747.641
281.607	96.366	98.262	748.987
269.684	131.433	100.661	750.148
252.460	177.001	102.592	748.675
236.361	231.431	104.813	748.985
214.699	306.581	106.695	748.795
193.468	391.985	107.852	749.145
174.094	470.334	107.748	749.342
151.513	552.756	106.559	749.251
131.474	616.654	105.109	749.963
113.126	687.589	102.927	750.603

Table D3.2.1 : Fan characteristics for S-fan with round-to-rectangular diffuser and blade angle set to 18°.

V (m^3/s)	**Δp_{sF} (Pa)**	**P (W)**	**η_{sF} %**
5.534	290.888	7027.233	22.907
6.924	290.191	7292.575	27.552
8.470	284.485	7514.953	32.065
9.875	275.819	7670.531	35.509
11.342	265.068	7801.952	38.535
13.271	249.564	7971.559	41.547
15.330	235.239	8144.806	44.275
17.495	213.448	8225.653	45.399
19.646	193.772	8286.577	45.940
21.651	172.080	8260.526	45.102
23.124	153.299	8192.924	43.268
24.656	131.671	8044.666	40.356
25.470	119.740	7966.853	38.281
25.860	112.321	7909.878	36.721

Table D3.2.2 : Fan characteristics for S-fan with round-to-rectangular diffuser flow straightner and blade angle set to 18°.

V (m^3/s)	**Δp_{sF} (Pa)**	**P (W)**	**η_{sF} %**
2.384	333.480	7317.005	10.864
3.104	324.207	7205.933	13.965
4.373	308.449	7064.587	19.091
5.694	292.561	6949.210	23.970
7.019	294.399	7230.304	28.580
8.453	286.838	7440.047	32.590
9.946	274.723	7613.281	35.888
11.378	259.245	7750.636	38.056
13.258	244.393	7919.754	40.913
15.099	230.887	8046.414	43.326
17.410	208.848	8199.963	44.343
19.537	190.370	8256.511	45.046
21.544	170.426	8251.293	44.498
23.426	147.487	8146.661	42.410
24.410	134.233	8046.762	40.720
25.184	124.029	7968.950	39.197
25.768	115.062	7884.436	37.605

Table D3.2.3 : Fan characteristics for S-fan with round-to-rectangular diffuser, flow director and blade angle set to 18°.

V (m^3/s)	Δp_{sF} (Pa)	P (W)	η_{sF} %
2.440	309.291	7124.670	10.591
3.171	305.520	7075.200	13.692
4.072	291.615	6947.501	17.092
5.473	283.554	6893.725	22.513
6.946	284.054	7164.105	27.539
8.104	281.872	7417.643	30.796
9.856	276.242	7615.036	35.752
11.418	265.701	7790.134	38.945
13.389	252.570	7952.538	42.522
15.483	236.094	8124.887	44.992
17.745	215.289	8247.440	46.322
19.986	194.196	8292.528	46.805
22.047	170.894	8277.770	45.516
23.863	155.454	8177.532	45.364
25.189	132.826	8072.905	41.443
25.633	126.607	7988.689	40.623
26.977	137.116	7866.519	47.022
27.041	121.147	7843.342	41.766

Table D3.2.4 : Fan characteristics for S-fan with round-to-rectangular diffuser, flow director, flow straightner and blade angle set to 18°.

V (m^3/s)	Δp_{sF} (Pa)	P (W)	η_{sF} %
2.194	338.476	7303.541	10.170
2.882	327.566	7182.719	13.141
4.211	311.709	7043.217	18.636
5.375	298.336	6974.014	22.993
6.929	294.815	7113.459	28.716
8.390	287.694	7404.620	32.600
9.847	276.791	7591.737	35.901
11.480	264.129	7752.131	39.116
13.347	248.065	7930.550	41.748
15.253	231.863	8094.282	43.692
17.556	210.448	8242.056	44.827
19.838	189.148	8321.942	45.089
21.720	169.808	8307.896	44.395
23.544	147.449	8216.398	42.252
24.839	127.359	8087.650	39.115
26.202	109.011	7904.797	36.134

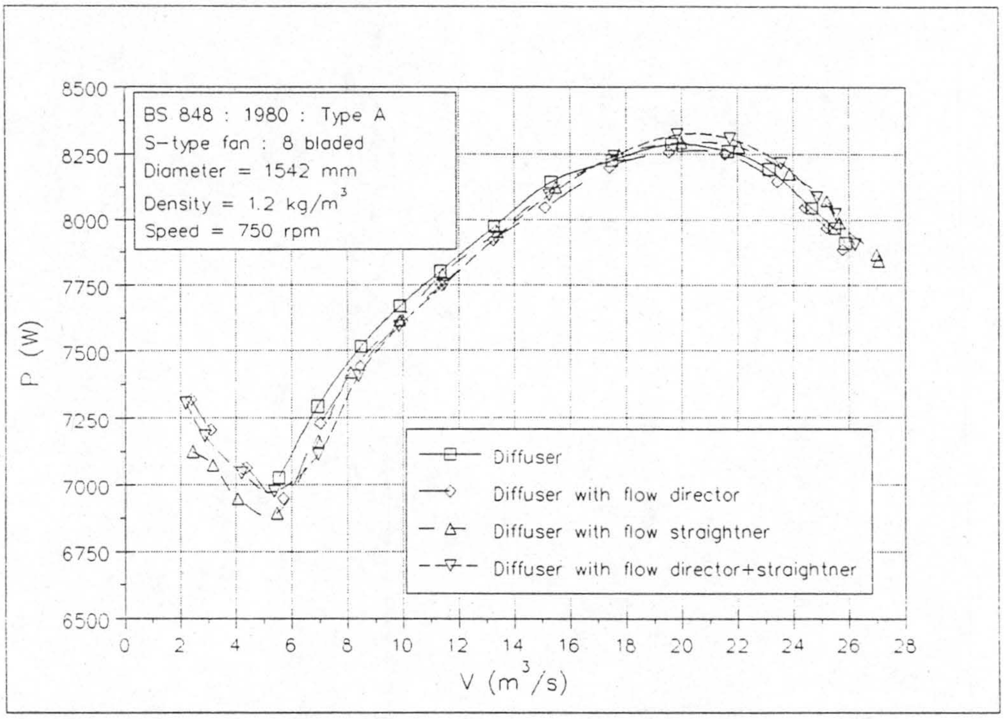

Figure D3.1 : P versus V for S-fan with round-to-rectangular diffuser and blade angle set to 18°.

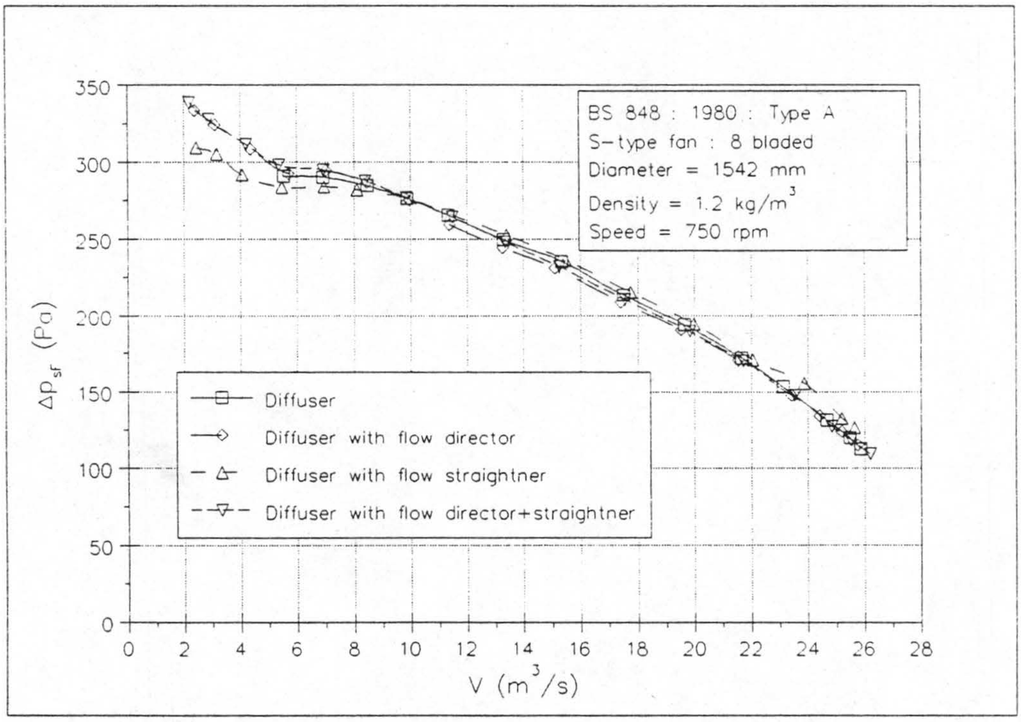

Figure D3.2 : Δp_{SF} versus V for S-fan with round-to-rectangular diffuser and blade angle set to 18°.

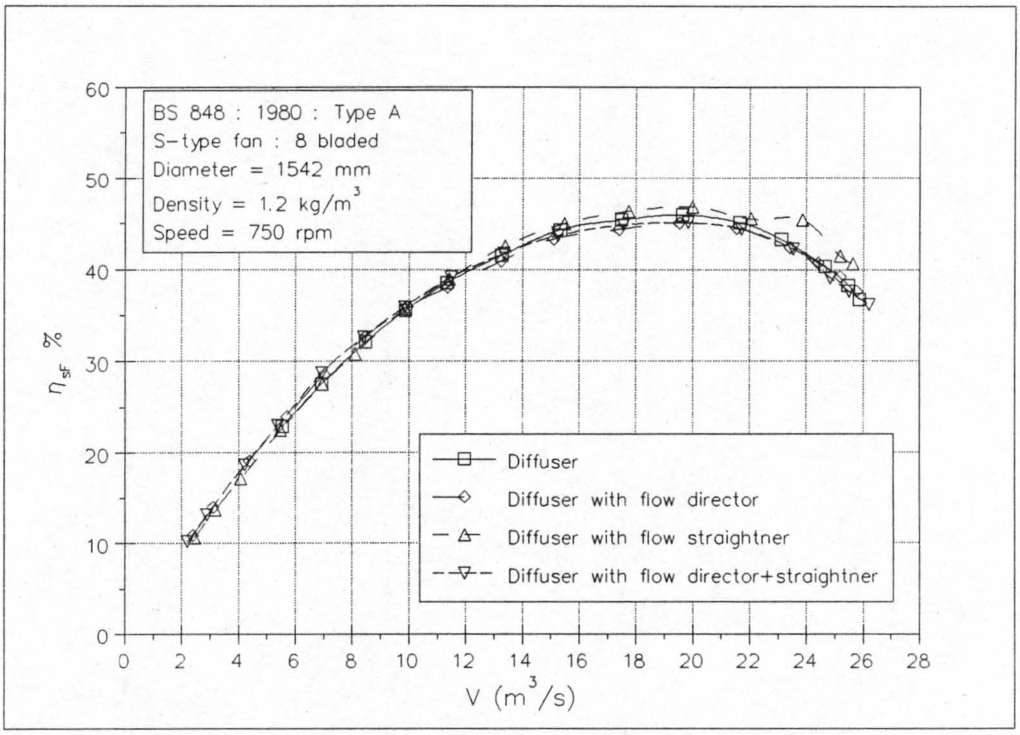

Figure D3.3 : η_{sF} versus V for S-fan with round-to-rectangular diffuser with blade angle set to 18°.

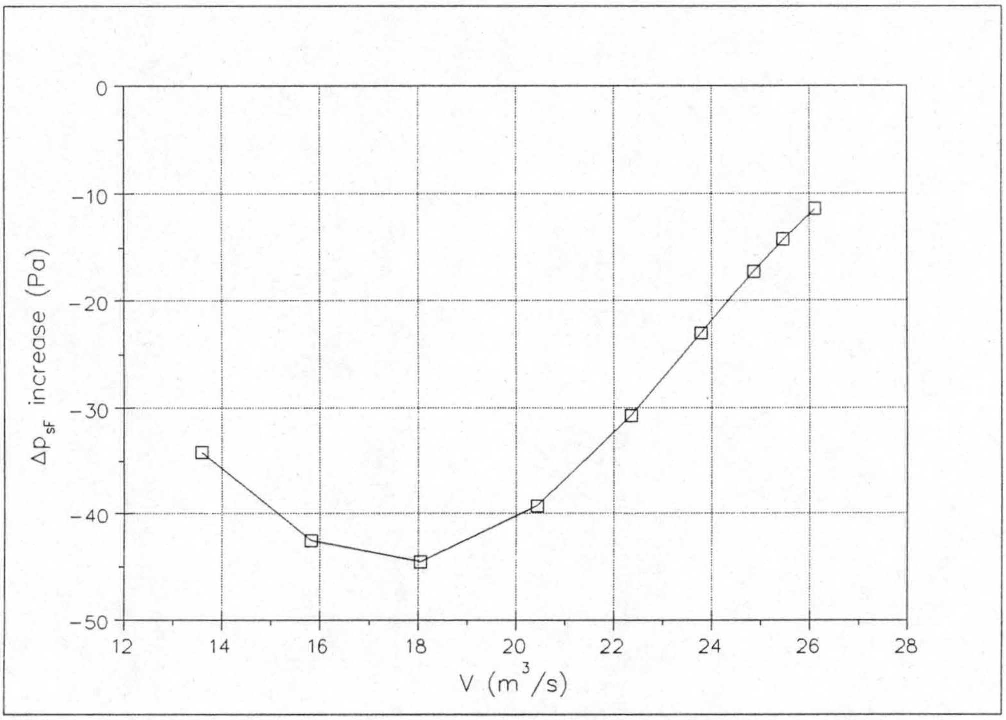

Figure D3.4 : Increase in fan static pressure obtained with round-to-rectangular diffuser.

Appendix E

K-values of Heat Exchangers

E.1 K-values of Normal Flow Heat Exchanger

In order to determine the predicted operating point of the plenum configurations tested using the normal flow heat exchanger, it is necessary to know what the static pressure drop over the heat exchanger is for varying volume flow rates. This is can be expressed in terms of a heat exchanger pressure drop coefficient, K_{he}, which is defined as :

$$K_{he} = \frac{\Delta p_t}{\frac{1}{2} \cdot \rho \cdot v_{he}^2}$$

where Δp_t is the total pressure drop over the heat exchanger and v_{he} is the average velocity through the heat exchanger.

In order to determine K_{he} for the normal flow heat exchanger, a rectangular duct having a cross-sectional area of 1.6 m x 1.9 m is attached to the outlet of settling chamber of the code tunnel as shown in figure E.1.1. The heat exchanger is placed in the duct. The code tunnel's auxiliary fan is then used to blow air through the heat exchanger. The volume flow rate can be varied by adjusting the louvres.

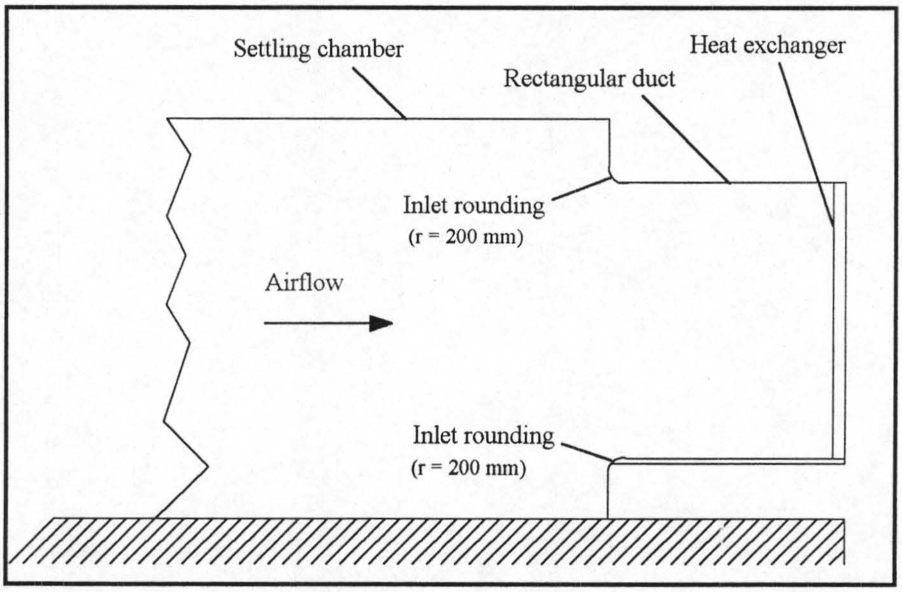

Figure E.1.1 : Experimental set-up for determination of K_{he} for normal flow heat exchanger.

By measuring the static pressure differential over the inlet bellmouth (Δp_{bell}) and between the settling chamber and atmosphere (Δp_{sett}), K_{he} for the heat exchanger can be determined. Tables E1.1 and E1.2 list all the experimental readings and calculated results whilst figure E1.2 shows the results in graphical form.

Example

For the purpose of an illustrative example of how K_{he} is calculated, K_{he} will be determined for data point number 13 in table E1.1. The following raw data is given : $\Delta p_{bell} = 126.353$ Pa, $\Delta p_{sett} = 175.487$ Pa and $\rho = 1.235$ kg/m^3.

The mean velocity of the air passing through the inlet bellmouth is given by :

$$v_{bell} = \alpha\varepsilon\sqrt{\frac{2 \cdot \Delta p_{bell}}{\rho}} = 0.9802\sqrt{\frac{2 \cdot 126.353}{1.235}} = 14.021 \text{ m/s} \tag{E1.1}$$

Hence the volume flow rate through the system is

$$V = A_{bell} \cdot v_{bell} = \frac{\pi}{4} \cdot 1.008^2 \cdot 14.021 = 11.189 \text{ m}^3\text{/s} \tag{E1.2}$$

The velocity in the settling chamber is thus

$$v_{sett} = \frac{V}{A_{sett}} = \frac{11.189}{16} = 0.699 \text{ m/s} \tag{E1.3}$$

The average velocity through the heat exchanger is

$$v_{he} = \frac{V}{A_{he}} = \frac{11.189}{1.6 \cdot 1.9} = 3.681 \text{ m/s} \tag{E1.4}$$

The pressure drop coefficient for the heat exchanger is given by

$$\begin{aligned} K_{he} &= \frac{\Delta p_t}{\frac{1}{2} \cdot \rho \cdot v_{he}^2} = \frac{\Delta p_{sett} + \frac{1}{2} \cdot \rho \cdot v_{sett}^2 - \frac{1}{2} \cdot \rho \cdot v_{he}^2}{\frac{1}{2} \cdot \rho \cdot v_{he}^2} = \frac{\Delta p_{sett} + \frac{1}{2} \cdot \rho \cdot v_{sett}^2}{\frac{1}{2} \cdot \rho \cdot v_{he}^2} - 1 \\ &= \frac{175.487 + \frac{1}{2} \cdot 1.235 \cdot 0.699^2}{\frac{1}{2} \cdot 1.235 \cdot 3.681^2} - 1 \\ &= 20.010 \end{aligned} \tag{E1.5}$$

It will be noted that in the above equation, the inlet contraction losses of the rectangular duct have been neglected. The mean velocity in the rectangular duct is

$v_{duct} = v_{he} = 3.681$ m/s

and the equivalent hydraulic radius of the rectangular duct is given by

$$d_h = 4 \cdot \frac{\text{cross-sectional area}}{\text{wetted perimeter}} = 4 \cdot \frac{1.6 \cdot 1.9}{2 \cdot (1.6 + 1.9)} = 1.737 \text{ m}$$

Idelchik [89ID1] gives the inlet contraction loss coefficient, K_c, for entry from a larger conduit and for a ratio of $r/d_h = 0.2/1.737 = 0.115$ as being 0.09. Hence the pressure loss due to the flow contraction is

$$\Delta p_c = K_c \cdot \frac{1}{2} \cdot \rho \cdot v_{he}^2 = 0.09 \cdot 0.5 \cdot 1.235 \cdot 3.681^2 = 0.753 \text{ Pa}$$

This is negligible when compared to $\Delta p_{sett} = 175.487$ Pa and is thus not included when determining K_{he}.

The loss coefficient is expressed in terms of a characteristic flow parameter which is defined as follows :

$$Ry = \frac{G_{he}}{\mu} = \frac{\rho \cdot v_{he}}{\mu} = \frac{1.235 \cdot 3.681}{1.785017 \text{x} 10^{-5}} = 254677 \text{ m}^{-1} \qquad \text{(E1.6)}$$

Table E1.1 : Experimental readings and calculated results for determining K_{he} for normal flow heat exchanger. (P_{atm} = 101580 Pa, T_{atm} = 286.65K, ρ = 1.235 kg/m^3 and μ = 1.785017x10^{-5} kg/sm)

No	Δp_{sett} (Pa)	Δp_{bell} (Pa)	v_{bell} (m/s)	V (m^3/s)	v_{sett} (m/s)	v_{he} (m/s)	Ry (m^{-1})	K_{he}
1	4.292	2.577	2.003	1.598	0.100	0.526	36364	24.192
2	33.738	21.127	5.734	4.576	0.286	1.505	104119	23.156
3	46.523	30.653	6.907	5.512	0.344	1.813	125415	21.960
4	61.943	42.801	8.161	6.513	0.407	2.142	148197	20.895
5	75.260	51.491	8.952	7.144	0.446	2.350	162546	21.113
6	93.665	64.096	9.988	7.970	0.498	2.622	181354	21.108
7	108.109	75.134	10.813	8.629	0.539	2.839	196350	20.769
8	125.558	88.351	11.726	9.357	0.585	3.078	212921	20.501
9	141.235	100.055	12.478	9.958	0.622	3.276	226585	20.357
10	156.276	111.444	13.170	10.509	0.657	3.457	239133	20.216
11	164.074	116.901	13.488	10.764	0.673	3.541	244918	20.235
12	170.920	122.458	13.805	11.017	0.689	3.624	250672	20.118
13	175.487	126.353	14.023	11.190	0.699	3.681	254627	20.014
14	177.236	128.849	14.161	11.300	0.706	3.717	257130	19.812
15	180.132	131.628	14.313	11.422	0.714	3.757	259888	19.706
16	178.553	129.053	14.172	11.309	0.707	3.720	257333	19.934

Table E1.2 : Experimental readings and calculated results for determining K_{he} for normal flow heat exchanger. (P_{atm} = 101610 Pa, T_{atm} = 288.15K, ρ = 1.229 kg/m^3 and μ = 1.792009x10^{-5} kg/sm)

No	Δp_{sett} (Pa)	Δp_{bell} (Pa)	v (m/s)	Q (m^3/s)	v_{sett} (m/s)	v_{he} (m/s)	Ry (m^{-1})	K_{he}
1	13.450	8.095	3.558	2.839	0.177	0.934	64040	24.132
2	22.133	14.064	4.690	3.743	0.234	1.231	84411	22.806
3	32.476	21.285	5.770	4.604	0.288	1.515	103844	22.082
4	45.198	30.558	6.913	5.517	0.345	1.815	124425	21.376
5	58.834	38.916	7.801	6.226	0.389	2.048	140414	21.871
6	75.115	51.719	8.994	7.177	0.449	2.361	161871	20.973
7	92.165	64.133	10.015	7.992	0.500	2.629	180254	20.742
8	108.292	76.258	10.921	8.715	0.545	2.867	196557	20.485

Table E1.2 : continued

No	Δp_{sett} (Pa)	Δp_{bell} (Pa)	v (m/s)	Q (m^3/s)	v_{sett} (m/s)	v_{he} (m/s)	Ry (m^{-1})	K_{he}
9	123.147	86.470	11.629	9.280	0.580	3.053	209304	20.547
10	138.343	99.429	12.470	9.951	0.622	3.273	224441	20.052
11	152.142	109.735	13.100	10.454	0.653	3.439	235786	19.977
12	160.608	118.670	13.623	10.872	0.679	3.576	245197	19.478
13	168.762	122.086	13.818	11.027	0.689	3.627	248701	19.915
14	170.413	125.666	14.019	11.187	0.699	3.680	252321	19.518
15	177.035	129.455	14.229	11.355	0.710	3.735	256097	19.692
16	176.266	130.048	14.261	11.381	0.711	3.744	256683	19.508
17	178.380	130.254	14.273	11.390	0.712	3.747	256886	19.721

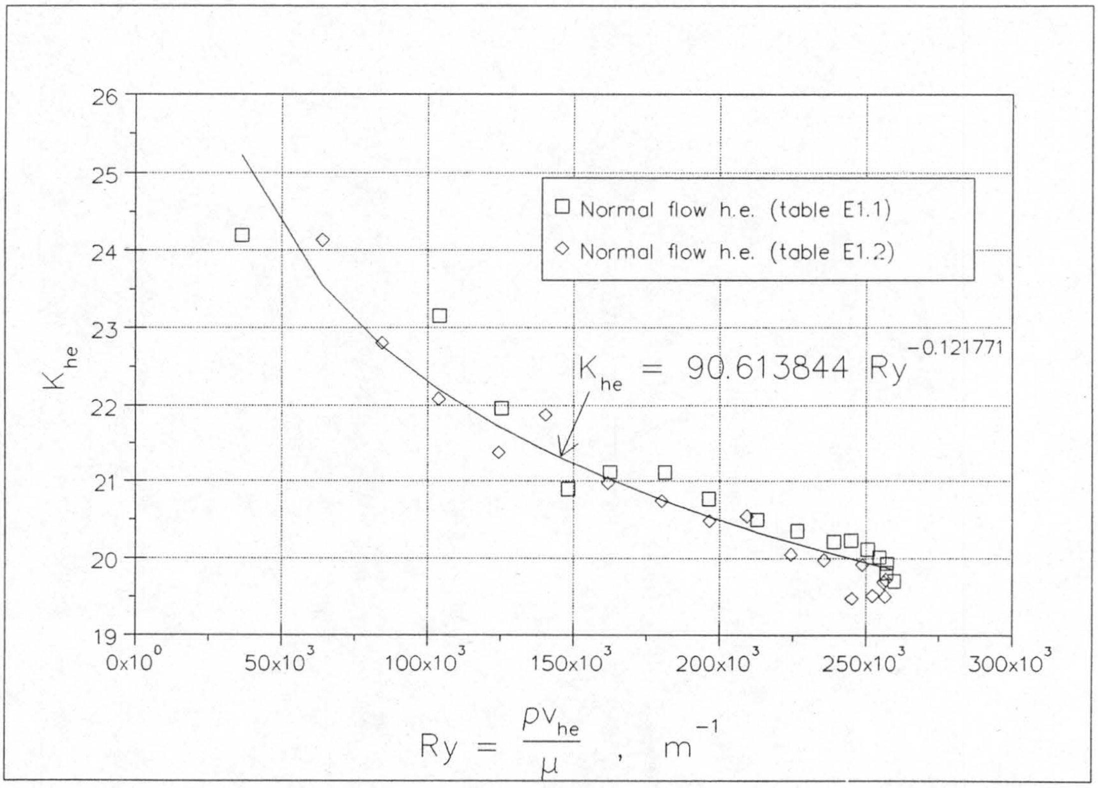

Figure E1.2 : K_{he} for normal flow heat exchanger.

E.2 K-values of Delta Heat Exchanger

In order to predict the operating point of the various configurations tested using the delta heat exchanger, it is necessary to know what the total pressure drop over the heat exchanger is for varying volume flow rates. This can be expressed in terms of the total oblique flow isothermal loss coefficient, K_θ, which is defined as follows :

$$K_\theta = K_{i\theta} + K_f + K_e + K_{dj} + K_o \tag{E2.1}$$

where : $K_{i\theta}$ = the inlet loss due to oblique flow

K_f = frictional losses through the heat exchanger

K_e = exit losses though the heat exchanger

K_{dj} = jetting losses in the downstream region

K_o = the outlet kinetic energy loss

The various components of K_θ are illustrated in figure E2.1

In order to experimentally determine K_θ for the delta heat exchanger, a rectangular duct having a cross-sectional area of 1.8 m x 1.9 m is attached to the outlet of the settling chamber of the code tunnel as shown in figure E2.1. The delta heat exchanger is placed in the duct. The auxiliary fan is then used to blow air through the heat exchanger. By changing the setting of the louvres, the volume flow rate through the system can be varied. The side walls of the rectangular duct can be removed in order to determine the K_θ values of the delta heat exchanger without side walls present.

By measuring the static pressure drop over the inlet bellmouth (Δp_{bell}) and the static pressure differential between the settling chamber and atmosphere (Δp_{sett}), K_θ can be calculated for the delta heat exchanger. The experimental readings and calculated results for the delta heat exchanger with side walls present are listed in tables E2.1 and E2.2 whilst those for the delta heat exchanger without side walls present are listed in tables E2.3 and E2.4. The results are shown in graphical form in figure E2.2.

Example

For the purpose of an illustrative example as to how K_θ is calculated, K_θ will be determined for data point number 15 in table E2.2. The following raw data is given : $\Delta p_{bell} = 212.072$ Pa, $\Delta p_{sett} = 115.660$ Pa and $\rho = 1.220$ kg/m^3.

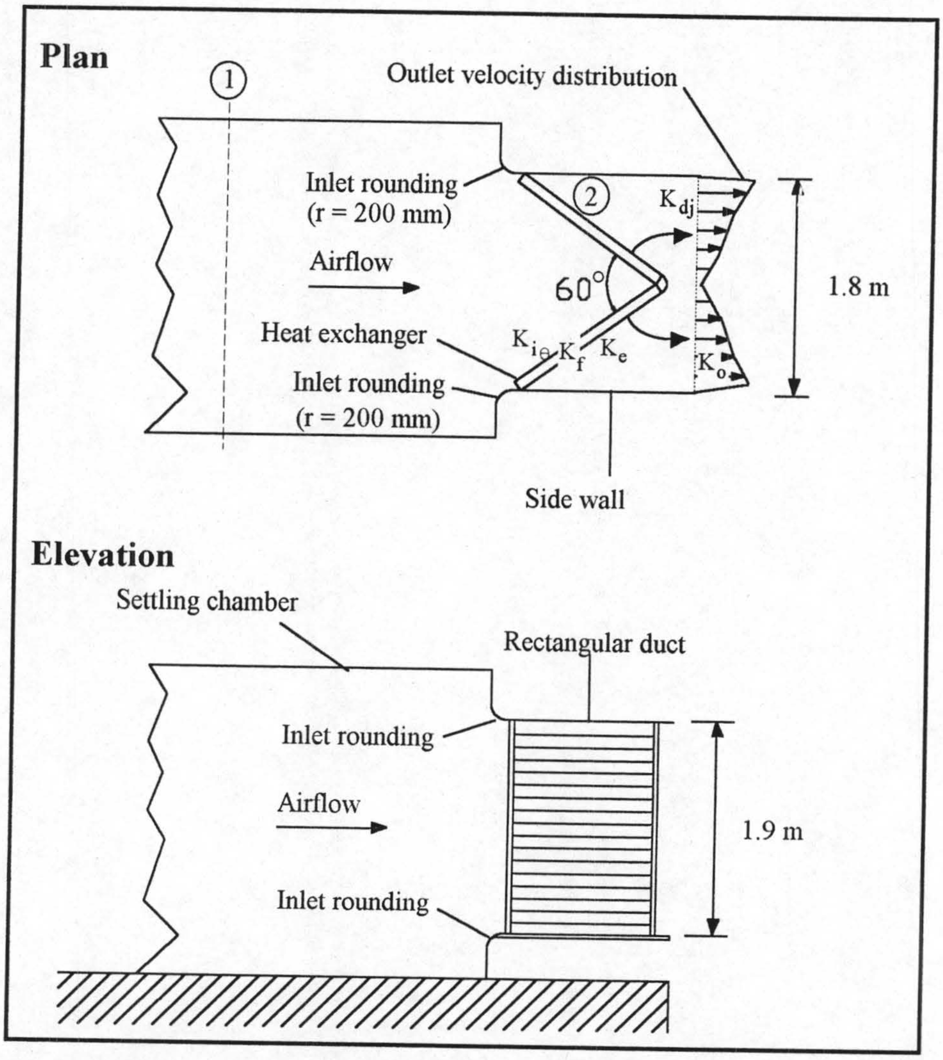

Figure E2.1 : Experimental set-up for determination of K_θ for delta heat exchanger.

The mean velocity of the air passing through the inlet bellmouth is given by :

$$v_{bell} = \alpha\varepsilon\sqrt{\frac{2 \cdot \Delta p_{bell}}{\rho}} = 0.9802\sqrt{\frac{2 \cdot 212.072}{1.220}} = 18.276 \text{ m/s} \qquad \text{(E2.2)}$$

Hence the volume flow rate through the system is

$$V = A_{bell} \cdot v_{bell} = \frac{\pi}{4} \cdot 1.008^2 \cdot 18.276 = 14.585 \text{ m}^3/\text{s} \tag{E2.3}$$

The velocity in the settling chamber is thus

$$v_{sett} = \frac{V}{A_{sett}} = \frac{14.585}{16} = 0.912 \text{ m/s} \tag{E2.4}$$

The average velocity through the heat exchanger is given by

$$v_{he} = \frac{V}{A_{he}} = \frac{14.585}{2 \cdot 1.6 \cdot 1.9} = 2.399 \text{ m/s} \tag{E2.5}$$

The oblique flow loss coefficient is expressed in terms of a characteristics flow parameter which is defined as follows :

$$Ry = \frac{G_{he}}{\mu} = \frac{\rho \cdot v_{he}}{\mu} = \frac{1.220 \cdot 2.399}{1.792008\text{x}10^{-5}} = 163324 \text{ m}^{-1} \tag{E2.6}$$

The total oblique flow loss coefficient , K_θ, is defined as

$$K_\theta = \frac{p_{t1} - p_a}{\frac{1}{2} \cdot \rho \cdot v_{he}^2} = \frac{\left(p_a + \Delta p_{sett} + \frac{1}{2} \cdot \rho \cdot v_{sett}^2\right) - p_a}{\frac{1}{2} \cdot \rho \cdot v_{he}^2} = \frac{\Delta p_{sett} + \frac{1}{2} \cdot \rho \cdot v_{sett}^2}{\frac{1}{2} \cdot \rho \cdot v_{he}^2}$$

$$= \frac{115.660 + \frac{1}{2} \cdot 1.220 \cdot 0.912^2}{\frac{1}{2} \cdot 1.220 \cdot 2.399^2} \tag{E2.7}$$

$$= 33.090$$

It will be noted that in the above equation, the inlet contraction losses of the rectangular duct have been neglected. The mean velocity in the rectangular duct is

$v_{duct} = V/A_{duct} = 14.585/(1.8 \text{ x } 1.9) = 4.265$ m/s

and the equivalent hydraulic radius of the duct is given by

$$d_h = 4 \cdot \frac{\text{cross-sectional area}}{\text{wetted perimeter}} = 4 \cdot \frac{1.8 \cdot 1.9}{2 \cdot (1.8 + 1.9)} = 1.849 \text{ m}$$

Idelchik [89ID1] gives the inlet contraction loss coefficient, K_c, for entry from a larger conduit and for a ratio of $r/d_h = 0.2/1.849 = 0.108$ as being 0.11. Hence the pressure loss due to the flow contraction is

$$\Delta p_c = K_c \cdot \frac{1}{2} \cdot \rho \cdot v_{duct}^2 = 0.11 \cdot 0.5 \cdot 1.220 \cdot 4.265^2 = 1.221 \text{ Pa}$$

This is negligible when compared to $\Delta p_{sett} = 115.660$ Pa and is thus not included when determining K_θ.

The above procedure is also used to calculate the value of K_θ for the delta heat exchanger without side walls present. However, the value of K_θ so calculated no longer contains a jetting loss component and is made up of the following components :

$$K_\theta = K_{i\theta} + K_f + K_e + K_o \qquad \text{(E2.8)}$$

Van Aarde and Kröger [93VA1] provide correlations to predict the total oblique flow isothermal loss coefficients (K_θ) for A-frame finned tube heat exchangers given the geometry of the A-frame and the finned tubes and the isothermal heat exchanger loss coefficient under normal flow conditions. These predicted values for K_θ are compared to the experimentally determined values in figure E2.2.

As can be seen from figure E2.2, the predicted values and experimentally determined values of K_θ compare well with each other in the high volume flow rate region (high values of Ry) for the delta heat exchanger with the side walls present. In the low volume flow rate region (low values of Ry) the scatter of the experimentally determined values increases but are fairly equally distributed on both sides of the predicted values. As the delta heat exchanger will typically be operating between 20 m^3/s and 26 m^3/s ($2.169 \times 10^5 \leq Ry \leq 2.820 \times 10^5$), this increased scatter in the low flow rate region does not warrant further attention.

The predicted values of K_θ for the delta heat exchanger without side walls present are consistently lower than the experimentally determined values. The difference between the two increases as Ry (and hence the volume flow rate) decreases. In the high flow rate region the difference between the two is less than 2% and hence quite acceptable. Once again, as the delta heat exchanger will invariably be operating in the high flow rate region, the increase in the difference between the predicted K_θ and experimentally determined K_θ does not warrant further attention.

Example

A numerical example of how Van Aarde and Kröger's method is used to predict K_θ for data point number 15 in table E2.2 follows below.

Van Aarde and Kröger [93VA1] give the total oblique flow isothermal loss coefficient as being

$$K_\theta = K_{he} + \left(\frac{1}{\sin\,\theta_m} - 1\right) \text{x} \left[2 \cdot K_c^{0.5} + \left(\frac{1}{\sin\,\theta_m} - 1\right)\right] + K_{dj} + K_o \qquad \text{(E2.9)}$$

In the above equation, K_{he} is the isothermal heat exchanger loss coefficient under normal flow conditions. θ_m is the mean angle of attack. K_c is the entrance contraction loss coefficient. K_{dj} is the jetting loss coefficient and K_o is the outlet kinetic energy loss

The empirical relation between the mean angle of attack (θ_m) and the semi-apex angle (θ) is given as

$$\theta_m = 0.0019\theta^2 + 0.9133\theta - 3.1558 \qquad \text{(E2.10)}$$

For a semi-apex angle of 30° equation (E2.10) yields

$$\theta_m = 0.0019 \cdot 30^2 + 0.9133 \cdot 30 - 3.1558 = 25.953°$$

The entrance contraction loss coefficient (K_c) is given by Kröger [89KR1] as 0.05 for typical industrial finned tubes.

Van Aarde and Kröger suggest the following correlation to determine the downstream jetting loss coefficient

$$\begin{aligned} K_{dj} &= \exp\left(2.36987 + 5.8601x10^{-2}\theta - 3.3797x10^{-3}\theta^2\right) \\ &= \exp\left(2.36987 + 5.8601x10^{-2} \cdot 30 - 3.3797x10^{-3} \cdot 30^2\right) \\ &= 2.962904 \end{aligned} \tag{E2.11}$$

The outlet kinetic energy loss coefficient is given by

$$K_o = \alpha_{e3}\left(\frac{L_b}{L_s}\right)^2 \tag{E2.12}$$

where α_{e3} is the kinetic energy flux coefficient at the outlet of the heat exchanger, L_b is the length of the bundle and L_s is the length of the process steam duct. L_b = 1.6 m and L_s = 0.9 m for the configuration tested. Van Aarde and Kröger suggest the following correlation to determine α_{e3}

$$\alpha_{e3} = 1.9874 - 3.02783\left(\frac{d_s}{2L_t}\right) + 2.0187\left(\frac{d_s}{2L_t}\right)^2 \tag{E2.13}$$

where d_s is the steam duct diameter and L_t is the total length of the duct. As there are no steam ducts in the configuration tested (d_s = 0) equation (E2.15) reduces to α_{e3} = 1.9864. Thus

$$K_o = 1.9874\left(\frac{1.6}{0.9}\right)^2 = 6.2811654$$

Hence equation (E2.9) becomes

$$\begin{aligned} K_\theta &= K_{he} + \left(\frac{1}{\sin\ 25.953} - 1\right) x \left[2 \cdot 0.05^{0.5} + \left(\frac{1}{\sin\ 25.953} - 1\right)\right] \\ &\quad + 2.962904 + 6.2811654 \\ &= K_{he} + 11.470 \end{aligned} \tag{E2.14}$$

The isothermal heat exchanger loss coefficient under normal flow conditions is given in figure E1.2 as

$$K_{he} = 90.613844\ Ry^{-0.121771}$$

Hence, equation (E2.16) becomes

$$K_\theta = 90.613844 \cdot Ry^{-0.121771} + 11.470 \qquad \text{(E2.15)}$$

If Ry is assigned the value of 163324, as calculated in equation (E2.6), equation (E2.15) yields :

$$K_\theta = 90.613844 \cdot 163324^{-0.121771} + 11.470 = 32.479$$

which compares well to the experimentally determined value of 33.090 from equation (E2.7).

With the side walls removed, $K_{dj} = 0$ and if it is assumed that K_o=1, equation (E2.9) becomes

$$\begin{aligned} K_\theta &= K_{he} + \left(\frac{1}{\sin\ 25.953} - 1\right) x \left[2 \cdot 0.05^{0.5} + \left(\frac{1}{\sin\ 25.953} - 1\right)\right] + 1 \\ &= 90.613844 \cdot Ry^{-0.121771} + 3.226 \end{aligned} \qquad \text{(E2.16)}$$

For Ry = 174199, equation (E2.16) gives K_θ = 24.070 which compares well to the experimentally determined value of 25.159.

Table E2.1 : Experimental readings and calculated results for determining K_θ for delta heat exchanger with side walls. (P_{atm} = 100390 Pa, T_{atm} = 287.15 K, ρ = 1.218 kg/m^3 and μ = 1.787348x10^{-5} kg/sm)

No	Δp_{sett} (Pa)	Δp_{bell} (Pa)	v_{bell} (m/s)	V (m^3/s)	v_{sett} (m/s)	v_{he} (m/s)	Ry (m^{-1})	K_θ
1	18.801	36.214	7.558	6.032	0.377	0.992	67611	31.510
2	26.311	47.743	8.678	6.925	0.433	1.139	77631	33.440
3	35.127	66.585	10.249	8.179	0.511	1.345	91678	32.017
4	46.797	83.554	11.481	9.162	0.573	1.507	102698	33.983
5	56.849	103.792	12.796	10.211	0.638	1.679	114462	33.236
6	68.118	124.636	14.022	11.190	0.699	1.840	125429	33.164
7	79.175	146.604	15.207	12.136	0.758	1.996	136035	32.773
8	93.122	166.212	16.192	12.922	0.808	2.125	144847	33.993
9	102.791	187.815	17.213	13.736	0.858	2.259	153972	33.210
10	109.442	208.151	18.120	14.460	0.904	2.378	162094	31.910
11	113.001	204.562	17.964	14.335	0.896	2.358	160690	33.519
12	117.063	213.956	18.371	14.661	0.916	2.411	164339	33.200
13	116.641	218.063	18.547	14.801	0.925	2.434	165908	32.461
14	119.989	221.580	18.696	14.920	0.932	2.454	167241	32.861

Table E2.2 : Experimental readings and calculated results for determining K_θ for delta heat exchanger with side walls. (P_{atm} = 100890 Pa, T_{atm} = 288.15 K, ρ = 1.220 kg/m^3 and μ = 1.792008x10^{-5} kg/sm)

No	Δp_{sett} (Pa)	Δp_{bell} (Pa)	v_{bell} (m/s)	V (m^3/s)	v_{sett} (m/s)	v_{he} (m/s)	Ry (m^{-1})	K_θ
1	5.903	8.616	3.684	2.940	0.184	0.484	32917	41.537
2	9.246	16.311	5.069	4.045	0.253	0.665	45291	34.392
3	15.542	25.512	6.339	5.059	0.316	0.832	56643	36.950
4	19.821	36.139	7.545	6.021	0.376	0.990	67415	33.281
5	27.431	49.871	8.863	7.073	0.442	1.163	79194	33.376
6	35.098	63.088	9.968	7.955	0.497	1.308	89073	33.756
7	45.730	82.593	11.406	9.102	0.569	1.497	101916	33.596
8	56.006	101.922	12.670	10.111	0.632	1.663	113215	33.343
9	66.974	121.171	13.815	11.025	0.689	1.813	123444	33.538

Table E2.2 : continued

No	$\Delta p'_{sett}$ (Pa)	Δp_{bell} (Pa)	v_{bell} (m/s)	V (m^3/s)	v_{sett} (m/s)	v_{he} (m/s)	Ry (m^{-1})	K_θ
10	77.104	140.297	14.866	11.863	0.741	1.951	132830	33.348
11	87.662	158.855	15.818	12.623	0.789	2.076	141342	33.484
12	96.779	176.185	16.659	13.294	0.831	2.186	148852	33.331
13	103.909	190.050	17.302	13.807	0.863	2.271	154598	33.177
14	105.743	191.516	17.368	13.860	0.866	2.280	155193	33.503
15	115.660	212.072	18.277	14.585	0.912	2.399	163310	33.094
16	116.415	214.723	18.391	14.676	0.917	2.414	164327	32.900
17	122.049	223.574	18.766	14.975	0.936	2.463	167680	33.126
18	121.514	222.380	18.716	14.935	0.933	2.456	167232	33.158

Table E2.3 : Experimental readings and calculated results for determining K_θ for delta heat exchanger without side walls. (P_{atm} = 100800 Pa, T_{atm} = 286.15 K, ρ = 1.227 kg/m^3 and $\mu = 1.782684 \times 10^{-5}$ kg/sm)

No	Δp_{sett} (Pa)	Δp_{bell} (Pa)	v_{bell} (m/s)	V (m^3/s)	v_{sett} (m/s)	v_{he} (m/s)	Ry (m^{-1})	K_θ
1	2.717	4.533	2.664	2.126	0.133	0.350	24074	36.357
2	4.904	9.173	3.790	3.024	0.189	0.497	34246	32.444
3	7.541	15.024	4.850	3.870	0.242	0.637	43828	30.469
4	11.189	22.956	5.995	4.784	0.299	0.787	54176	29.592
5	16.259	34.344	7.333	5.852	0.366	0.962	66264	28.747
6	21.366	46.574	8.539	6.814	0.426	1.121	77166	27.861
7	29.252	63.922	10.004	7.983	0.499	1.313	90402	27.792
8	37.904	85.653	11.580	9.241	0.578	1.520	104647	26.881
9	46.565	105.278	12.838	10.245	0.640	1.685	116018	26.867
10	55.394	127.660	14.137	11.282	0.705	1.856	127756	26.360
11	62.892	146.977	15.169	12.105	0.757	1.991	137082	25.997
12	72.867	170.841	16.354	13.051	0.816	2.147	147792	25.913
13	83.649	199.255	17.662	14.095	0.881	2.318	159610	25.508
11	90.235	214.962	18.345	14.640	0.915	2.408	165782	25.506
12	95.908	228.966	18.933	15.109	0.944	2.485	171096	25.451
13	95.861	229.691	18.963	15.133	0.946	2.489	171367	25.359
14	97.763	234.815	19.173	15.301	0.956	2.517	173268	25.298
15	98.270	237.346	19.277	15.383	0.961	2.530	174199	25.159

Table E2.4 : Experimental readings and calculated results for determining K_θ for delta heat exchanger without side walls. (P_{atm} = 100860 Pa, T_{atm} = 287.15 K, ρ = 1.224 kg/m^3 and μ = 1.787341x10^{-5} kg/sm)

No	**Δp_{sett} (Pa)**	**Δp_{bell} (Pa)**	**v_{bell} (m/s)**	**V (m^3/s)**	**v_{sett} (m/s)**	**v_{he} (m/s)**	**Ry (m^{-1})**	**K_θ**
1	1.621	2.740	2.074	1.655	0.103	0.272	18641	35.887
2	2.571	4.776	2.738	2.185	0.137	0.359	24611	32.668
3	4.703	8.696	3.695	2.949	0.184	0.485	33209	32.819
4	7.254	14.862	4.831	3.855	0.241	0.634	43414	29.633
5	10.972	23.340	6.054	4.831	0.302	0.795	54405	28.546
6	16.402	36.169	7.536	6.014	0.376	0.989	67727	27.542
7	22.450	49.874	8.849	7.062	0.441	1.161	79530	27.340
8	28.521	63.366	9.975	7.960	0.497	1.309	89644	27.338
9	36.875	83.517	11.451	9.138	0.571	1.503	102915	26.820
10	45.591	105.288	12.857	10.260	0.641	1.688	115553	26.306
11	55.933	126.654	14.102	11.253	0.703	1.851	126736	26.826
12	62.354	148.451	15.267	12.183	0.761	2.004	137209	25.521
13	70.934	170.700	16.371	13.065	0.817	2.149	147133	25.250
14	81.823	194.087	17.457	13.931	0.871	2.291	156888	25.615
15	83.468	198.498	17.654	14.088	0.881	2.317	158661	25.549
16	88.324	213.279	18.300	14.603	0.913	2.402	164462	25.164
17	93.495	226.650	18.864	15.054	0.941	2.476	169539	25.067
18	96.378	234.003	19.168	15.296	0.956	2.516	172267	25.028
19	98.396	238.514	19.352	15.443	0.965	2.540	173920	25.068

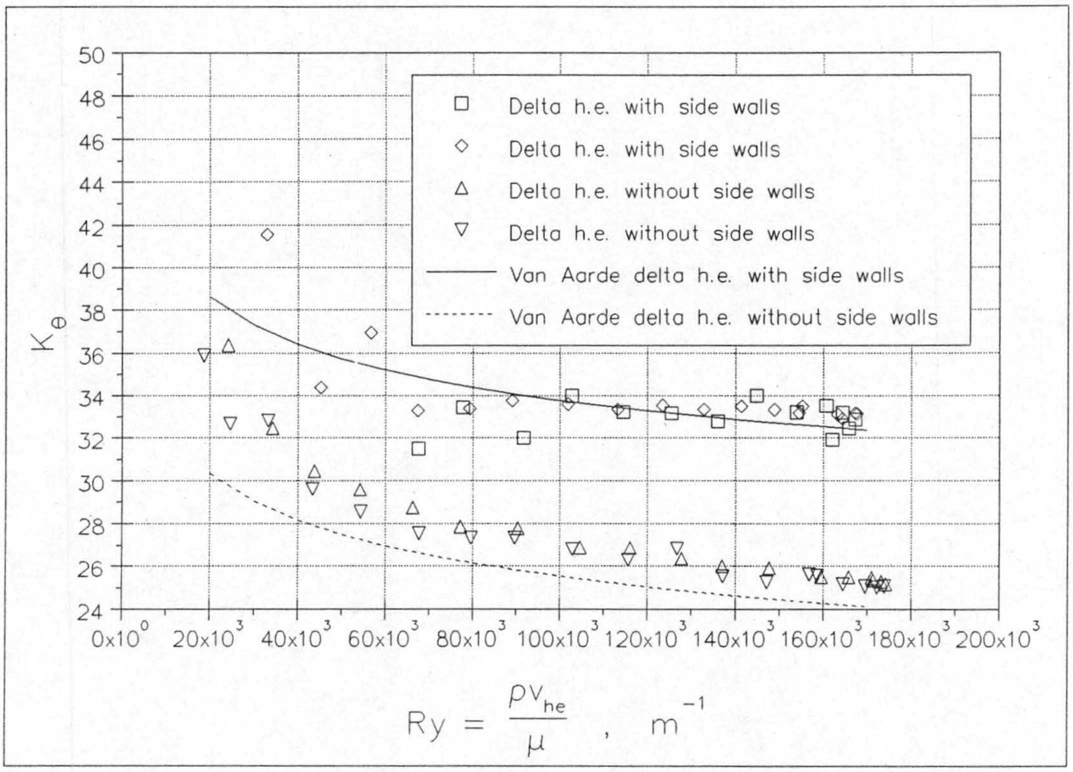

Figure E2.2 : K_θ for delta heat exchanger.

E.3 K-values of Double Delta Heat Exchanger

In order to predict the operating point of the various configurations tested using the double delta heat exchanger, it is necessary to know what the total pressure drop over the heat exchanger is for varying volume flow rates. This can be expressed in terms of the total oblique flow isothermal loss coefficient, K_θ, which is defined as follows :

$$K_\theta = K_{i\theta} + K_f + K_e + K_{dj} + K_o \quad \text{(E3.1)}$$

where : $K_{i\theta}$ = the inlet loss due to oblique flow

K_f = frictional losses through the heat exchanger

K_e = exit losses through the heat exchanger

K_{dj} = jetting losses in the downstream region

K_o = the outlet kinetic energy loss

Note that for the double delta, the downstream jetting losses include the jetting losses that occur between the secondary deltas as well as between the primary delta and the windwalls.

In order to experimentally determine K_θ for the double delta heat exchanger, a rectangular duct having a cross-sectional area of 2.05 m x 1.9 m is attached to the outlet of the settling chamber of the code tunnel as shown in figure E3.1. The double delta heat exchanger is placed in the duct. The auxiliary fan is then used to blow air through the heat exchanger. By changing the setting of the louvres, the volume flow rate through the system can be varied. The side walls of the rectangular duct can be removed in order to determine the K_θ values of the delta heat exchanger without side walls present.

By measuring the static pressure drop over the inlet bellmouth (Δp_{bell}) and the static pressure differential between the settling chamber and atmosphere (Δp_{sett}), K_θ can be calculated for the delta heat exchanger. The experimental readings and calculated results for the double delta heat exchanger with side walls present are listed in table E3.1 whilst those for the delta heat exchanger without side walls present are listed in tables E3.2 and E3.4. The results are shown in graph form in figure E3.2.

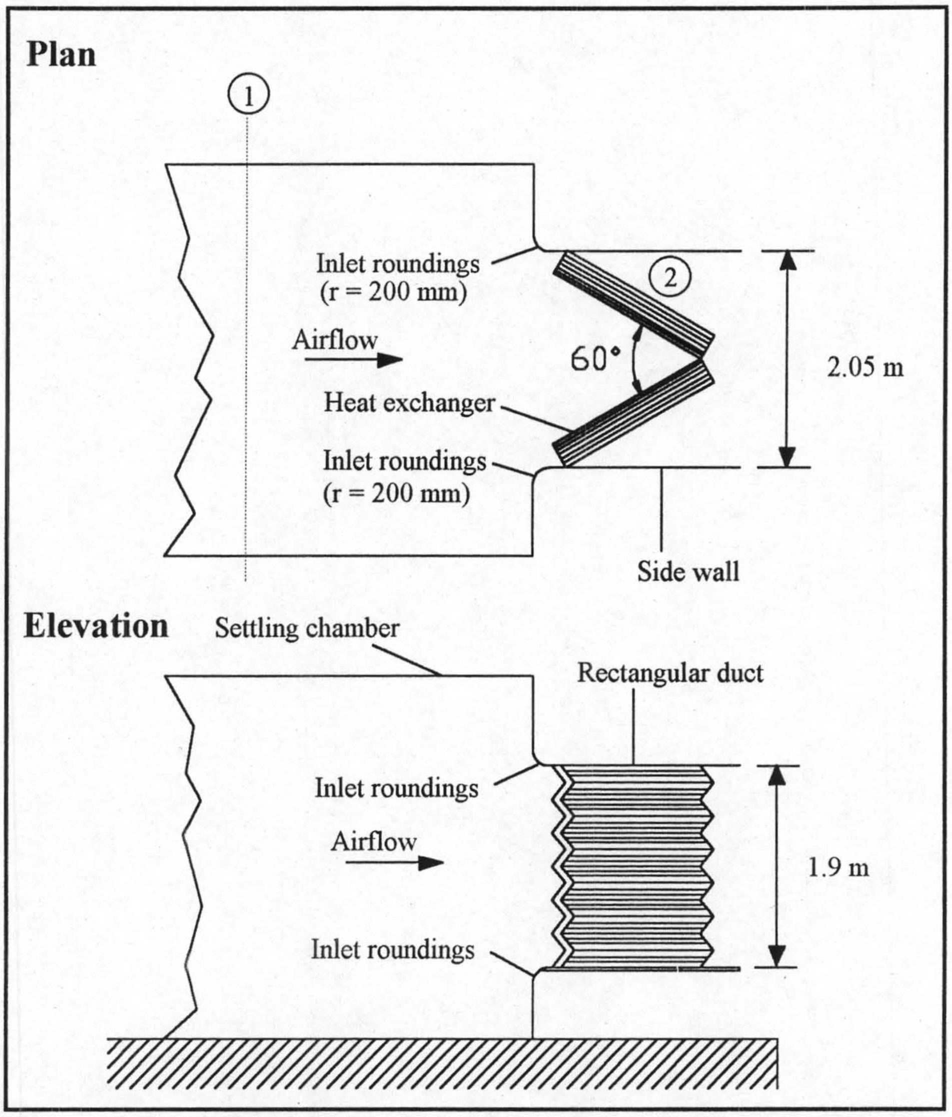

Figure E3.1 : Experimental set-up for determination of K_θ for double delta heat exchanger.

Example

As an illustrative example as to how to calculate K_θ for the double delta heat exchanger, K_θ will be determined for data point 17 in table E3.1. The following raw data is given : $\Delta p_{bell} = 259.007$ Pa, $\Delta p_{sett} = 90.649$ Pa and $\rho = 1.235$ kg/m^3.

The mean velocity of the air passing through the inlet bellmouth is given by :

$$v_{bell} = \alpha\varepsilon\sqrt{\frac{2 \cdot \Delta p_{bell}}{\rho}} = 0.9802\sqrt{\frac{2 \cdot 259.007}{1.235}} = 20.075 \text{ m/s} \tag{E3.2}$$

Hence the volume flow rate through the system is

$$V = A_{bell} \cdot v_{bell} = \frac{\pi}{4} \cdot 1.008^2 \cdot 20.075 = 16.020 \text{ m}^3/\text{s} \tag{E3.3}$$

The velocity in the settling chamber is thus

$$v_{sett} = \frac{V}{A_{sett}} = \frac{16.020}{16} = 1.001 \text{ m/s} \tag{E3.4}$$

The average velocity through the heat exchanger is given by

$$v_{he} = \frac{V}{A_{he}} = \frac{16.020}{24 \cdot 1.6 \cdot 0.252} = 1.656 \text{ m/s} \tag{E3.5}$$

The oblique flow loss coefficient is expressed in terms of a characteristics flow parameter which is defined as follows :

$$Ry = \frac{G_{he}}{\mu} = \frac{\rho \cdot v_{he}}{\mu} = \frac{1.235 \cdot 1.656}{1.78735\text{x}10^{-5}} = 114390 \text{ m}^{-1} \tag{E3.6}$$

The total oblique flow loss coefficient , K_θ, is defined as

$$K_\theta = \frac{p_{t1} - p_a}{\frac{1}{2} \cdot \rho \cdot v_{he}^2} = \frac{\left(p_a + \Delta p_{sett} + \frac{1}{2} \cdot \rho \cdot v_{sett}^2\right) - p_a}{\frac{1}{2} \cdot \rho \cdot v_{he}^2} = \frac{\Delta p_{sett} + \frac{1}{2} \cdot \rho \cdot v_{sett}^2}{\frac{1}{2} \cdot \rho \cdot v_{he}^2}$$

$$= \frac{90.649 + \frac{1}{2} \cdot 1.235 \cdot 1.001^2}{\frac{1}{2} \cdot 1.235 \cdot 1.656^2} \tag{E3.7}$$

$$= 53.896$$

It will be noted that in the above equation, the inlet contraction losses of the rectangular duct have been neglected. The mean velocity in the rectangular duct is

$v_{duct} = V/A_{duct} = 16.020/(2.05 \text{ x } 1.9) = 4.113$ m/s and the equivalent hydraulic radius for the duct is given by

$$d_h = 4 \cdot \frac{\text{cross-sectional area}}{\text{wetted perimeter}} = 4 \cdot \frac{2.05 \cdot 1.9}{2 \cdot (2.05 + 1.9)} = 1.972 \text{ m}$$

Idelchik [89ID1] gives the inlet contraction loss coefficient, K_c, for entry from a larger conduit and for a ratio of $r/d_h = 0.2/1.972 = 0.101$ as being 0.12. Hence the pressure loss due to the flow contraction is

$$\Delta p_c = K_c \cdot \frac{1}{2} \cdot \rho \cdot v_{duct}^2 = 0.12 \cdot 0.5 \cdot 1.235 \cdot 4.113^2 = 1.254 \text{ Pa}$$

This is negligible when compared to $\Delta p_{sett} = 90.649$ Pa and is thus not included when determining K_θ.

The above procedure is also used to calculate the value of K_θ for the double delta heat exchanger without side walls present. However, due to the fact that there are no side walls present the jetting component included in K_θ consists only of the jetting losses that occur between the secondary deltas.

Table E3.1 : Experimental readings and calculated results for determining K_θ for double delta heat exchanger with side walls. (P_{atm} = 101780 Pa, T_{atm} = 287.15 K, ρ = 1.235 kg/m^3 and μ = 1.787349x10^{-5} kg/sm)

No	Δp_{sett} (Pa)	Δp_{bell} (Pa)	v_{bell} (m/s)	V (m^3/s)	v_{sett} (m/s)	v_{he} (m/s)	Ry	K_θ
1	2.040	4.712	2.708	2.161	0.135	0.223	15429	66.624
2	3.696	9.223	3.788	3.023	0.189	0.312	21586	61.696
3	6.005	16.895	5.127	4.092	0.256	0.423	29216	54.762
4	9.213	24.406	6.162	4.918	0.307	0.508	35114	58.138
5	13.095	34.962	7.376	5.886	0.368	0.608	42028	57.688
6	17.398	47.088	8.560	6.831	0.427	0.706	48774	56.912
7	24.010	65.516	10.096	8.057	0.504	0.833	57532	56.452
8	31.152	85.782	11.553	9.219	0.576	0.953	65831	55.944
9	38.835	109.857	13.074	10.433	0.652	1.078	74499	54.467
10	47.039	130.728	14.262	11.381	0.711	1.176	81268	55.434
11	57.055	160.663	15.811	12.617	0.789	1.304	90093	54.715
12	64.783	183.160	16.881	13.472	0.842	1.392	96195	54.496
13	72.302	204.185	17.824	14.224	0.889	1.470	101566	54.558
14	77.663	220.332	18.515	14.776	0.923	1.527	105505	54.310
15	83.514	236.458	19.181	15.307	0.957	1.582	109298	54.418
16	88.939	251.958	19.800	15.800	0.988	1.633	112823	54.388
17	90.649	259.007	20.075	16.020	1.001	1.655	114391	53.929
18	93.481	268.508	20.440	16.311	1.019	1.686	116470	53.648

Table E3.2 : Experimental readings and calculated results for determining K_θ for double delta heat exchanger without side walls. (P_{atm} = 101880 Pa, T_{atm} = 289.15 K, ρ = 1.228 kg/m^3 and μ = 1.796664x10^{-5} kg/sm)

No	Δp_{sett} **(Pa)**	Δp_{bell} **(Pa)**	v_{bell} **(m/s)**	**V (m^3/s)**	v_{sett} **(m/s)**	v_{he} **(m/s)**	**Ry (m^{-1})**	K_θ
1	5.076	14.921	4.833	3.857	0.241	0.399	27232	52.430
2	7.113	23.343	6.045	4.824	0.301	0.498	34061	47.000
3	10.731	34.551	7.354	5.869	0.367	0.606	41439	47.898
4	14.134	49.515	8.804	7.025	0.439	0.726	49608	44.052
5	19.005	66.640	10.213	8.150	0.509	0.842	57551	44.012
6	24.412	87.301	11.690	9.328	0.583	0.964	65871	43.161
7	31.287	110.805	13.169	10.509	0.657	1.086	74210	43.579
8	37.766	135.365	14.556	11.616	0.726	1.200	82023	43.064
9	44.426	170.200	16.322	13.025	0.814	1.346	91974	40.313
10	53.415	196.298	17.529	13.988	0.874	1.446	98774	42.010
11	56.196	219.436	18.533	14.789	0.924	1.528	104433	39.559
12	64.989	250.862	19.816	15.813	0.988	1.634	111661	40.013
13	77.479	289.605	21.291	16.990	1.062	1.756	119974	41.310
14	79.959	300.729	21.696	17.314	1.082	1.789	122256	41.057
15	80.323	306.454	21.901	17.478	1.092	1.806	123415	40.479
16	79.474	309.472	22.009	17.563	1.098	1.815	124021	39.668

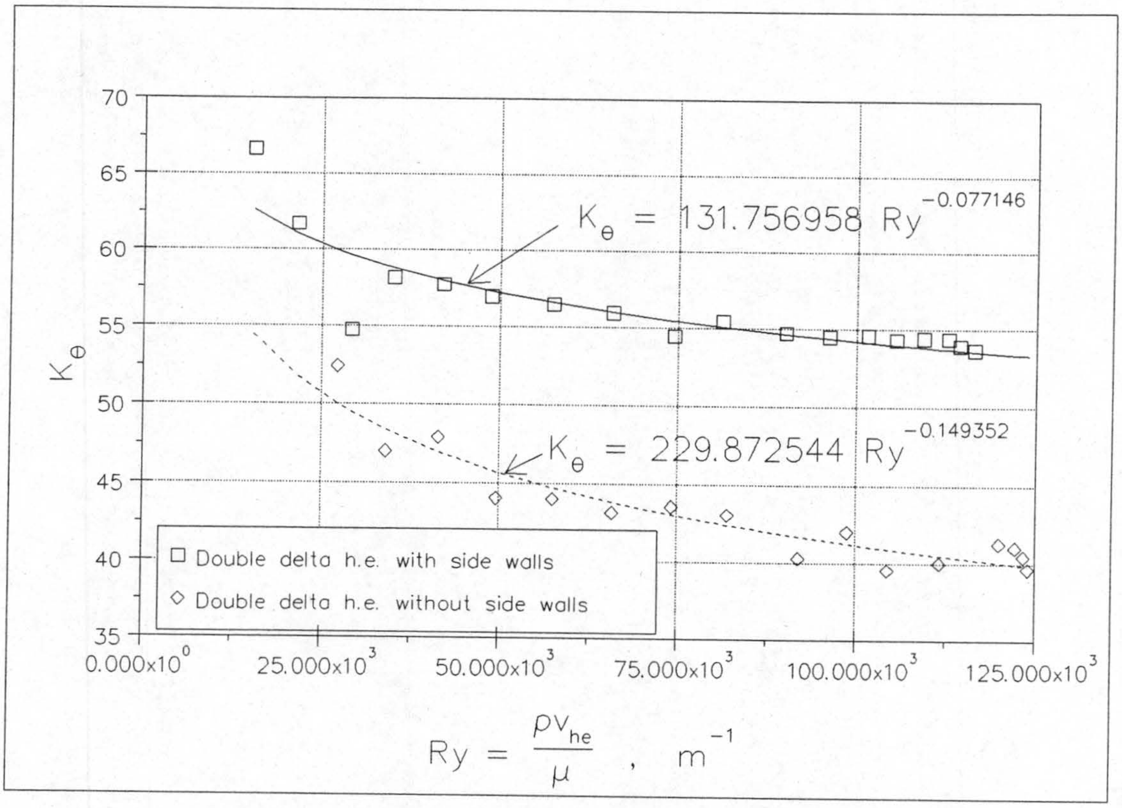

Figure E3.2 : K_θ for double delta heat exchanger.

Appendix F

Sample Calculations

F.1 Fan and Fan System Characteristic Calculations

This section gives a sample calculation of how the fan and fan system characteristics are determined from the measured data of the fan testing facility. For the purpose of this sample calculation the following data will be used :

Rotational speed	N	$= 746.644$ rpm
Input torque	T	$= 98.175$ N.m
Inlet bellmouth pressure differential	Δp_{bell}	$= 533.484$ Pa
Settling chamber pressure differential	Δp_{sett}	$= 152.678$ Pa
Barometric pressure	p_{bar}	$= 1016.2$ mbar
Temperature at barometer	T_{bar}	$= 15.5$ °C
Ambient temperature at testing facility inlet	T_{amb}	$= 14.5$ °C

According to the mercury barometer's instruction manual, the temperature corrected ambient pressure as measured by the mercury barometer is calculated as follows :

$$p_{amb} = p_{bar} - 0.000162 \cdot T_{bar} \cdot p_{bar} \qquad \text{with } T_{bar} \text{ in °C and } p_{bar} \text{ mbar}$$

$$= 1016.2 - 0.000162 \cdot 15.5 \cdot 1016.2$$

$$= 1013.648 \text{ mbar}$$

$$= 101364.8 \text{ Pa}$$

From the ideal gas law, the density of the ambient air is

$$\rho_{amb} = \frac{p_{amb}}{R \cdot T_{amb}} = \frac{101364.8}{287.04 \cdot 287.65} = 1.227 \text{ kg/m}^3$$

Assuming that the airflow through the bellmouth is incompressible, it follows from Bernoulli that :

$$\Delta p_{bell} = p_{amb} - p_{bell} = \frac{1}{2}\rho_{amb} \cdot v_{bell}^2$$

$$v_{bell} = \sqrt{\frac{2 \cdot \Delta p_{bell}}{\rho_{amb}}}$$

Now, the mass flow rate of air through the fan testing facility is

$$m = \rho_{amb} \cdot A_{bell} \cdot v_{bell} = A_{bell}\sqrt{2 \cdot \Delta p_{bell} \cdot \rho_{amb}} \quad \text{where} \quad A_{bell} = \frac{\pi}{4} d_{bell}^2$$

Due to frictional losses and non-uniform velocity distribution through the bellmouth, this becomes

$$m = \alpha\varepsilon \cdot \frac{\pi}{4} d_{bell}^2 \cdot \sqrt{2 \cdot \Delta p_{bell} \cdot \rho_{amb}}$$

The product of the flow coefficient (α) and the expansibility factor (ε) is known as the compound calibration constant. The compound calibration constant accounts for flow losses due to the actual flow conditions not being isentropic. It is determined by calibrating the inlet bellmouth against flow measurements using pitot static tube traverses. Venter [90VE1] determined it to be 0.9802 for the inlet bellmouth. Thus the mass flow rate through the fan testing facility is :

$$m = 0.9802 \cdot \frac{\pi}{4} 1.008^2 \cdot \sqrt{2 \cdot 533.484 \cdot 1.227} = 28.302 \text{ kg/s}$$

If it assumed that the air flows adiabatically through the fan testing facility, then the temperature in the settling chamber is $T_{sett} = T_{amb} = 287.65$ K.

Since $\Delta p_{sett} = p_{amb} - p_{sett}$, the pressure in the settling chamber is

$$p_{sett} = p_{amb} + \Delta p_{sett} = 101364.8 - 152.678 = 101212.1 \text{ Pa}$$

Thus the air density in the settling chamber is

$$\rho_{sett} = \frac{p_{sett}}{R \cdot T_{amb}} = \frac{101212.1}{287.04 \cdot 287.65} = 1.226 \text{ kg/m}^3$$

Hence, the air velocity and dynamic pressure in the settling chamber are :

$$v_{sett} = \frac{\dot{m}}{\rho_{sett} \cdot A_{sett}} = \frac{28.302}{1.226 \cdot 16} = 1.443 \text{ m/s}$$

Now

$$p_{d_{sett}} = 0.5 \cdot \rho_{sett} \cdot v_{sett}^2 = 0.5 \cdot 1.226 \cdot 1.443^2 = 1.276 \text{ Pa}$$

The volume flow rate is

$$V = v_{sett} \cdot A_{sett} = 1.443 \cdot 16 = 23.085 \text{ m}^3/\text{s}$$

The fan static pressure rise is

$$\begin{aligned} \Delta p_{sF} &= p_{amb} - (p_{sett} + p_{d_{sett}}) \\ &= 101364.8 - (101212.1 + 1.276) \\ &= 151.424 \text{ Pa} \end{aligned}$$

The power used by the fan is

$$P = T \cdot 2\pi \cdot N / 60 = 98.175 \cdot 2\pi \cdot 746.644 / 60 = 7676.144 \text{ W}$$

The fan static efficiency is given by

$$\eta_{sF} = \frac{\Delta p_{sF} \cdot V}{P} \cdot 100 = \frac{151.424 \cdot 23.085}{7676.144} \cdot 100 = 45.5 \text{ \%}$$

The final step is to scale the results to the standard air density ($\rho' = 1.2$ kg/m^3) and rotational speed (N' = 750 rpm). The fan laws are utilised to derive the following equations [73EC1, 77OS1, 78DA1, 80BS1].

$$V' = V \frac{N'}{N} = 23.085 \frac{750}{746.644} = 23.189 \text{ m}^3/\text{s}$$

$$\Delta p_{sF}' = \Delta p_{sF} \cdot (N'/N)^2 \cdot \frac{\rho'}{\rho_{sett}} = 151.424 \cdot (750/746.644)^2 \cdot \frac{1.2}{1.226} = 149.548 \text{ Pa}$$

$$P' = P \cdot (N'/N)^3 \cdot \frac{\rho'}{\rho_{sett}} = 7676.144 \cdot (750/746.644)^3 \cdot \frac{1.2}{1.226} = 7615.123 \text{ W}$$

$$\eta_{sF} = \eta_{sF}' = 45.5 \text{ \%}$$

The exact same calculation procedure is used to determine the fan system characteristics viz. the volume flow rate (V), the fan system static pressure rise ($\Delta p_{s_{FS}}$), the power consumption (P) and the fan system static efficiency ($\eta_{s_{FS}}$)

F.2 Heat Transfer Rate in a Normal Flow Heat Exchanger

To find the heat transfer rate in a practical forced draught air-cooled heat exchanger the distorted air velocity distribution through the heat exchanger must be considered. The following illustrates the procedure that is followed to evaluate the thermal performance of the heat exchanger and to show the influence of distorted flow for the case of a plenum length of 1.08 m for a normal flow heat exchanger.

Ganguli et al [85GA1] propose the following correlation for the air-side heat transfer coefficient (h_a) for an air-cooled heat exchanger having three or more rows of round finned tubes :

$$\frac{h_a \cdot d_r}{k_a} = 0.38 \cdot Re_a^{0.6} \cdot Pr_a^{0.333} \left(\frac{A_a}{A_r} \right)^{-0.15} \tag{F2.1}$$

The air-side Reynolds number (Re_a) is given by

$$Re_a = \frac{\rho_a \cdot v_c \cdot d_r}{\mu_a}$$

where v_c is the velocity of the air through the minimum open area in the heat exchanger core. The ratio of the total air-side area (A_a) to the root area (A_r) is given by

$$\frac{A_a}{A_r} = \frac{\frac{d_f^2 - d_r^2}{2} + d_f \cdot t_{f_t} + d_r \left(P_f - t_{f_r} \right)}{d_r \cdot P_f}$$

Figure F2.1 shows the nomenclature used in the above equation.

Solving for h_a we have :

$$h_a = 0.38 \cdot \frac{k_a}{d_r} \cdot Re_a^{0.6} \cdot Pr_a^{0.333} \cdot \left(\frac{A_a}{A_r} \right)^{-0.15} \tag{F2.2}$$

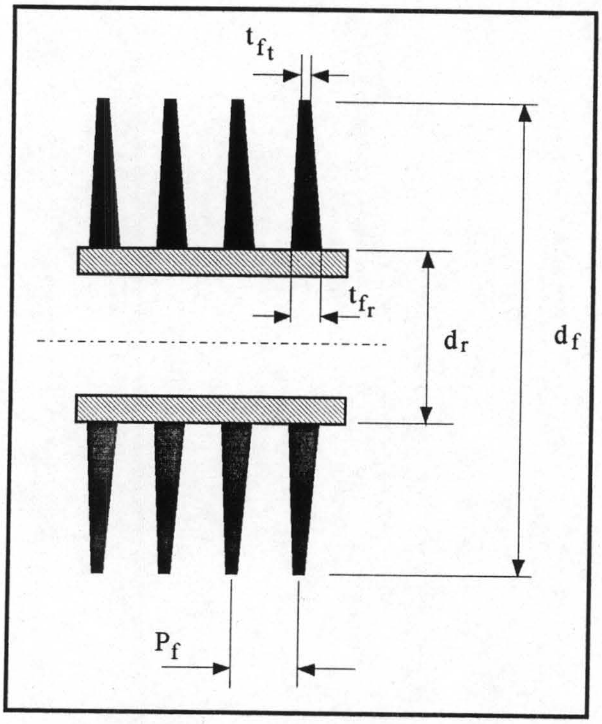

Figure F2.1 : Finned tube nomenclature.

Now, Schmidt [46SC1] proposes the following empirical relation for fin efficiency

$$\eta_f = \frac{\tanh(0.5bd_r\phi)}{0.5bd_r\phi} \tag{F2.3}$$

where $b = \sqrt{\dfrac{2h_a}{k_f t_f}}$ and $\phi = \left(\dfrac{d_f}{d_r} - 1\right)\left(1 + 0.35\ln\dfrac{d_f}{d_r}\right)$

Kröger [89KR1] gives the surface effectiveness of a finned tube heat exchanger as

$$e_f = 1 - \frac{A_f}{A_a}(1 - \eta_f) \tag{F2.4}$$

where the total area of the fins (A_f) and the total air-side area (A_a) are given by

$$A_f = n_r \cdot n_{tr} \cdot L_t \cdot \pi \frac{0.5\left(d_f^2 - d_r^2\right) + d_f \cdot t_{f_t}}{P_f}$$

$$A_a = A_f + \pi \cdot n_r \cdot n_{tr} \cdot L_t \cdot d_r \cdot \frac{(P_f - t_f)}{P_f}$$

Assuming that the air-cooled heat exchanger is a steam condenser and that the thermal resistances due to tube wall, fouling and thermal contact are negligible, the overall heat transfer coefficient is given by :

$$U_a = \left(\frac{1}{h_a \cdot e_f} + \frac{A_a}{h_c \cdot A_c} \right)^{-1} \tag{F2.5}$$

The condensate heat transfer coefficient (h_c) is usually of the order 250 times larger than the air-side heat transfer coefficient (h_a) and thus the term $A_a/(h_c.A_c)$ can be neglected in the above equation. Thus :

$$U_a = h_a \, e_f \tag{F2.6}$$

The NTU effectiveness is defined as

$$\varepsilon = \frac{T_{ao} - T_{ai}}{T_{he} - T_{ai}} \tag{F2.7}$$

but for a condenser Holman [89HO1] gives the NTU effectiveness as $\varepsilon = 1 - e^{\frac{-U_a A_a}{m_a c_{p_a}}}$

Hence equation (F2.7) can be rewritten as

$$T_{ao} = T_{ai} + \left(1 - \exp\left(\frac{-U_a \cdot A_a}{m_a \cdot c_{p_a}} \right) \right) (T_{he} - T_{ai}) \tag{F2.8}$$

Now, to determine the heat transfer rate from the heat exchanger, the following solution procedure is used :

1. Guess a value for the outlet air temperature T_{ao}
2. Determine the thermophysical properties of air at the arithmetic mean temperature $T_{am} = 0.5\,(T_{ai} + T_{ao})$
3. Calculate h_a from equation (F2.2)
4. Calculate η_f from equation (F2.3)
5. Calculate e_f from equation (F2.4)
6. Calculate U_a from equation (F2.6)

7. Calculate T_{ao} from equation (F2.7)
8. Repeat steps 2 through 8 until convergence of T_{ao} is obtained.
9. The heat flux is given by $Q = m_a c_{pa}(T_{ao} - T_{ai})$ where T_{ai} is the inlet air temperature.

When this solution procedure is used in conjunction with the velocity distributions measured, the total heat transfer (Q_{tot}) can be calculated by summing the individually calculated values of Q. To calculate the heat transfer rate that would be obtained with a uniform velocity distribution ($Q_{uniform}$), the total volume flow rate is divided by the frontal area (A_{fr}) to give a mean velocity. This mean velocity is then used in the calculations instead of the measured local velocity. Table 3.3.2 lists the total heat transfer rate (Q_{tot}) and uniform heat transfer rate ($Q_{uniform}$) calculated for the various plenum lengths.

Numerical Example

For the purpose of a numerical example, a heat exchanger bundle having dimensions similar to those of the normal flow test bundle and the same fan and a plenum length of 1.08 m will be considered. The velocity distribution listed in table A3.5 will thus be used to determine Q_{tot}. Other details are as follows :

Tube length	L_t	= 1.6 m
Bundle frontal area	A_{fr}	= 3.04 m^2
Number of finned tube rows	n_r	= 6
Number of finned tubes per row	n_{tr}	= 30
Transversal tube pitch	P_{tr}	= 63.5 mm
Longitudinal tube pitch	P_l	= 60.0 mm
Fin pitch	P_f	= 2.3 mm
Fin thickness	t_f	= 0.4 mm
Tube inside diameter	d_i	= 21.1 mm
Tube outside diameter	d_o	= 25.4 mm
Fin root diameter	d_r	= 25.4 mm

Fin diameter	d_f	= 57.15 mm
Thermal conductivity of fins	k_f	= 204 W/mK

It is assumed that the heat exchanger is a steam condenser having a steam temperature (T_{he}) of 333.15 K. Furthermore it is assumed that the pressure and the temperature of the steam remain essentially constant throughout the heat exchanger. Thermal contact resistances, fouling and tube wall thermal resistance are considered to negligible.

Specified operating conditions are as follows :

Inlet air dry bulb temperature	T_{ai}	= 293.150 K
Inlet air wet bulb temperature	T_{aiw}	= 288.150 K

By following an iterative procedure, the outlet air temperature is found i.e. T_{ao} = 326.876K

The thermophysical properties for air at the mean air temperature $T_{am} = 0.5(T_{ai} + T_{ao})$ = 310.013 K are as follows :

Density	ρ_a	= 1.145 kg/m^3
Specific heat	c_{pa}	= 1009.6 J/kg
Dynamic viscosity	μ_a	= 1.8789x10^{-5} kg/sm
Thermal conductivity	k_a	= 0.026781 W/mK
Prandtl number	Pr_a	= 0.708

From table A3.5 it can be seen that the local velocity at position A1 (v_{A1}) was measured as being 4.793 m/s. Figure A1.1 shows that the frontal area of position A1 (A_{A1}) is given by $A_{A1} = 0.367 \cdot 0.2 = 0.0734$ m^2.

To find the air-side heat transfer coefficient it is necessary to determine the air-side Reynolds number and the ratio of the total air-side area to the root area. For the heat exchanger bundles used in this calculation the ratio of frontal area to minimum open area in the core of the heat exchanger is 1.944, hence the air-side Reynolds number is given by :

$$\mathrm{Re}_a = \frac{\rho_a \cdot v_c \cdot d_r}{\mu_a} = \frac{1.145 \cdot 1.944 \cdot 4.793 \cdot 0.0254}{1.8789\mathrm{x}10^{-5}} = 14425.983$$

The ratio of the total air-side area (A_a) to the root area (A_r) is given by

$$\frac{A_a}{A_r} = \frac{\dfrac{d_f^2 - d_r^2}{2} + d_f \cdot t_{f_t} + d_r \cdot \left(P_f - t_{f_r}\right)}{d_r \cdot P_f}$$

$$= \frac{\dfrac{0.05715^2 - 0.0254^2}{2} + 0.05715 \cdot 0.0004 + 0.0254 \cdot (0.0023 - 0.0004)}{0.0254 \cdot 0.0023}$$

$$= 23.649$$

From equation (F2.2), the air-side heat transfer coefficient is

$$h_a = 0.38 \cdot \frac{0.026781}{0.0254} \cdot 14425.983^{0.6} \cdot 0.708^{0.333} \cdot 23.649^{-0.15}$$

$$= 69.553\ \mathrm{W/m^2K}$$

To determine the fin efficiency it follows from equation (F2.3) that

$$b = \sqrt{\frac{2 \cdot 69.553}{204 \cdot 0.0004}} = 41.288$$

$$\phi = \left(\frac{0.05715}{0.0254} - 1\right)\left(1 + 0.35 \ln \frac{0.05715}{0.0254}\right) = 1.605$$

$$\eta_f = \frac{\tanh(0.5 \cdot 41.288 \cdot 0.0254 \cdot 1.605)}{0.5 \cdot 41.288 \cdot 0.0254 \cdot 1.605} = 0.816$$

The surface effectiveness of a finned tube heat exchanger is given by equation (F2.4) as

$$e_f = 1 - \frac{A_f}{A_a}(1 - \eta_f)$$

The total finned area (A_{f_t}) of the heat exchanger is given by

$$A_{f_t} = n_r \cdot n_{tr} \cdot L_t \cdot \pi \cdot \frac{\frac{d_f^2 - d_r^2}{2} + d_f \cdot t_{f_t}}{P_f}$$

$$= 6 \cdot 30 \cdot 1.6 \cdot \pi \cdot \frac{0.5 \cdot \left(0.05715^2 - 0.0254^2\right) + 0.05715 \cdot 0.0004}{0.0023}$$

$$= 524.513 \text{ m}^2$$

Hence the finned area (A_f) in block A1 is given by :

$$A_f = A_{f_t} \cdot \left(\frac{A_{A1}}{A_{fr}}\right) = 524.513 \cdot \left(\frac{0.0734}{3.04}\right) = 12.664 \text{ m}^2$$

The total air-side area (A_{a_t}) is given by

$$A_{a_t} = A_{f_t} + \pi \cdot n_r \cdot n_{tr} \cdot L_t \cdot d_r \cdot \frac{P_f - t_f}{P_f}$$

$$= 524.513 + \pi \cdot 6 \cdot 30 \cdot 1.6 \cdot 0.0254 \cdot \frac{0.0023 - 0.0004}{0.0023}$$

$$= 543.498 \text{ m}^2$$

Hence the air-side area (A_a) in block A1 is

$$A_a = A_{a_t} \cdot \left(\frac{A_{A1}}{A_{fr}}\right) = 543.498 \cdot \left(\frac{0.0734}{3.04}\right) = 13.123 \text{ m}^2$$

Thus with A_a, A_f and η_f known, the surface effectiveness is calculated to be

$$e_f = 1 - \frac{12.664}{13.123}(1 - 0.816) = 0.822$$

The total heat transfer coefficient is given by equation (F2.6)

$$U_a = 69.553 \cdot 0.822 = 57.172 \text{ W/m}^2\text{K}$$

The air mass flow rate is

$$m_a = \rho_a . A_{A1} \cdot v_{A1} = 1.14578 \cdot 0.0734 \cdot 4.793 = 0.403 \text{ kg/s}$$

From equation (F2.8), the new value for T_{ao} is

$$T_{ao} = 293.15 + \{1 - \exp[-57.172 \cdot 13.088 / (0.403 \cdot 1009.6)]\}(333.15 - 293.15)$$

$$= 326.792 \text{ K}$$

The heat transfer rate for block A1 is thus

$$Q_{A1} = m_a c_{pa}(T_{ao} - T_{ai}) = 0.403 \cdot 1009.6 \cdot (326.792 - 293.15) = 13687.880 \text{ W}$$

This procedure is repeated until convergence of T_{ao} is obtained. This is done for each point of the velocity distribution and the heat transfer rates for each point are summed to give the total heat transfer rate of the bundle (Q_{tot}). For the case of a plenum length of 1.08 m, Q_{tot} = 499.566 kW.

To calculate $Q_{uniform}$ the total volume flow rate is divided by the heat exchanger area A_{he} to give a mean velocity. This mean velocity is then used in the calculations instead of the measured local frontal velocity (v_{A1}). Integrating the velocity distribution of table A3.5 it is found that the volume flow rate is 13.003 hence the mean velocity is 13.003/3.04 = 4.277 m/s. Thus, it can be shown that $Q_{uniform}$ is calculated to be 501.747 kW. Hence $Q_{tot}/Q_{uniform}$ = 0.996 and it can thus be seen that the distorted air velocity distribution does not adversely affect the thermal performance of the heat exchanger.

Appendix G

Calibration of Instrumentation

G.1 Calibration of the Pressure Transducers

The two Höttinger type PD1 pressure transducers used to measure the pressure drop over the inlet bellmouth and the pressure differential between the settling chamber and atmosphere are calibrated using a Betz micromanometer with an accuracy of 2 Pa. The positive pressure tapping points of both pressure transducers and the Betz manometer are joined by means of plastic tubing and T-pieces to a common valve (as shown in figure G.1.1). The negative pressure tapping points are all at atmospheric pressure.

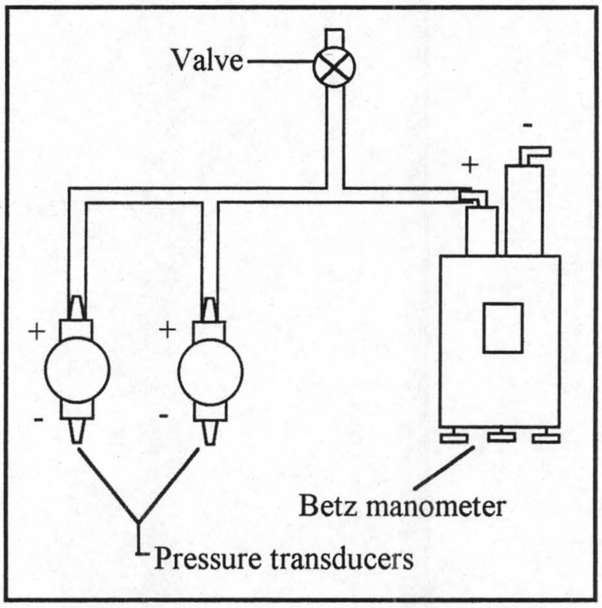

Figure G.1.1 : Experimental set-up for calibration of pressure transducers.

The air pressure on the positive pressure tappings is increased by blowing air through the valve and then closing it. Once the pressure reading on the Betz manometer has stabilised, voltage readings are taken from both pressure transducers. This procedure is repeated to obtain several data points. Table G.1.1 lists the data points obtained and figure G.1.2 shows these data points as well as the linear regression applied to each pressure transducer's readings.

Table G.1.1 : Pressure transducers' calibration points.

Betz (Pa)	E_{sett} (V)	E_{bell} (V)
24	0.239	0.241
51	0.515	0.536
102	1.047	1.104
151	1.558	1.650
202	2.093	2.218
250	2.595	2.747
301	3.136	3.314
354	3.697	3.902
400	4.181	4.407
456	4.777	5.025
501	5.259	5.528
557	5.583	6.145
606	6.380	6.687
652	6.875	7.198

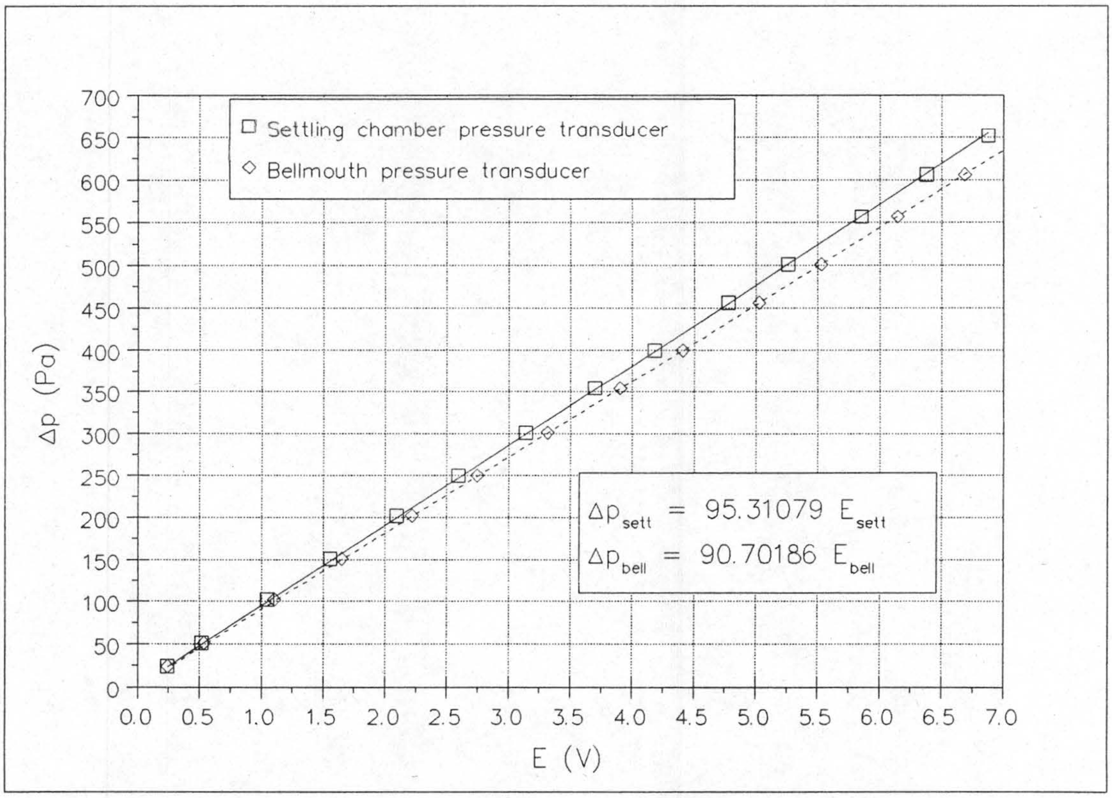

Figure G.1.2 : The pressure transducers' calibration data.

G.2 Calibration of the Torque Transducer

The Höttinger type T2 torque transducer, used to measure the torque transmitted by the hydraulic motor to the test fan's rotor, is calibrated using a torque arm and a shaft break. The torque arm, having an effective arm of 510 mm, is placed on the end of the drive shaft of the hydraulic motor whilst the shaft break is placed behind the torque transducer (as shown in figure G.2.1).

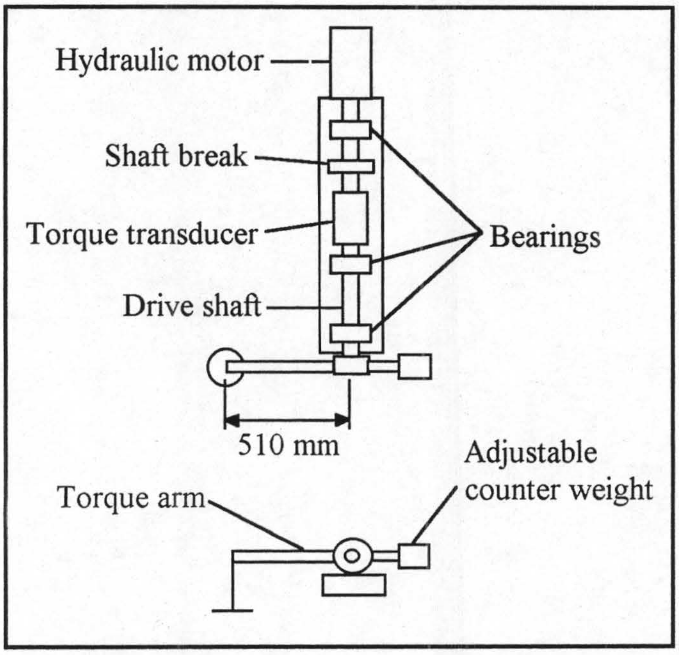

Figure G.2.1 : Experimental set-up for torque transducer calibration.

By varying the mass placed at the end of the torque arm, the amount of torque applied to the drive shaft is varied. The torque transducer's output voltage is measured with several different masses placed at the end of the torque arm. Table G.2.1 lists the experimental and calculated results. The torque transmitted (T) is calculated by :

$T = M \cdot g \cdot l$

where :M is the mass (in kg)

g is gravitational acceleration (9.7981 m/s^2)

l is the length of the torque arm (0.51 m)

Figure G.2.2 shows the calibration data points as well as the linear regression applied to these data points.

Table G.2.1 : Experimental and calculated results of torque transducer calibration.

m (kg)	E (V)	T (N.m)
0.000	-0.006	0.000
4.930	-0.877	24.635
9.670	-1.700	48.321
14.523	-2.544	72.572
19.473	-3.314	97.307
14.523	-2.507	72.572
9.670	-1.673	48.321
4.930	-0.858	24.635
0.000	0.027	0.000

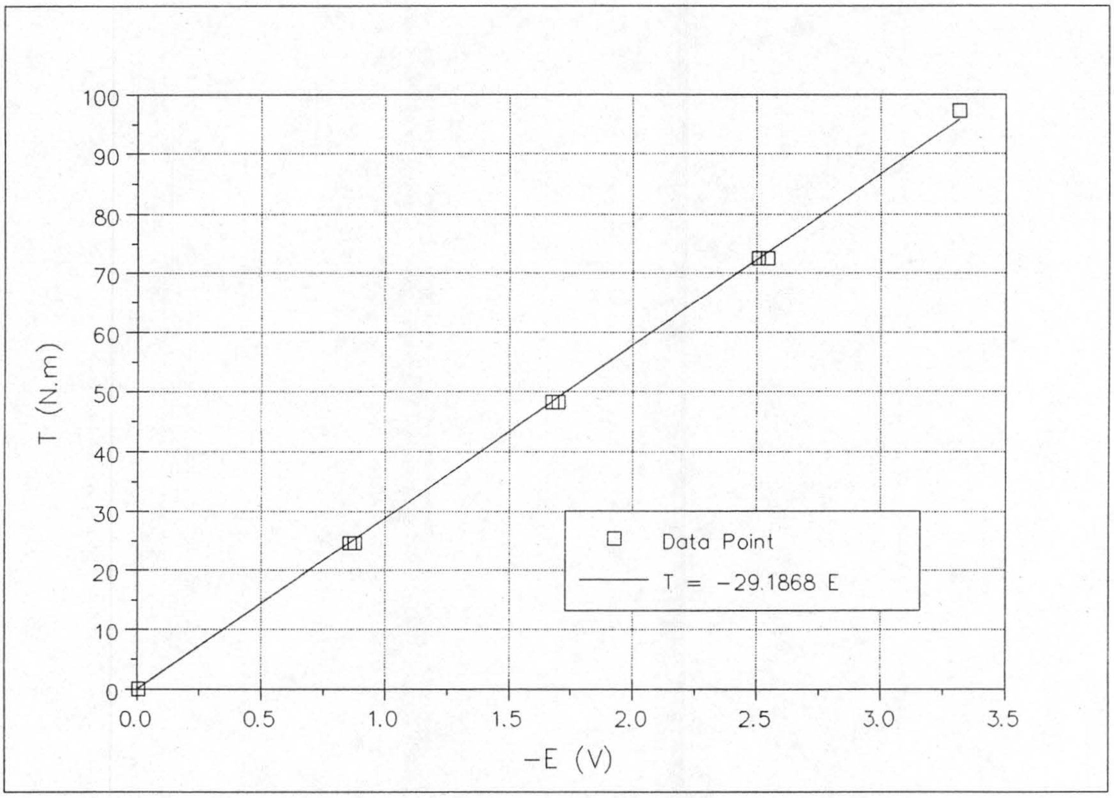

Figure G.2.2 : Torque transducer's calibration data.

G.3 Calibration of the Propeller Anemometers

The seven propeller anemometers, used to perform velocity traverses at the heat exchanger outlet, are individually calibrated using the apparatus shown in figure G.3.1. The 220 mm diameter propeller anemometer is placed in the throat of the inlet bellmouth which delivers air to the settling chamber. A standard 50 mm short radius flow nozzle at the exit of the settling chamber is used to determine the volume flow rate through the system. The volume flow rate through the system is regulated by the ball valve placed between the flow nozzle and the centrifugal fan which is used to draw air through the system.

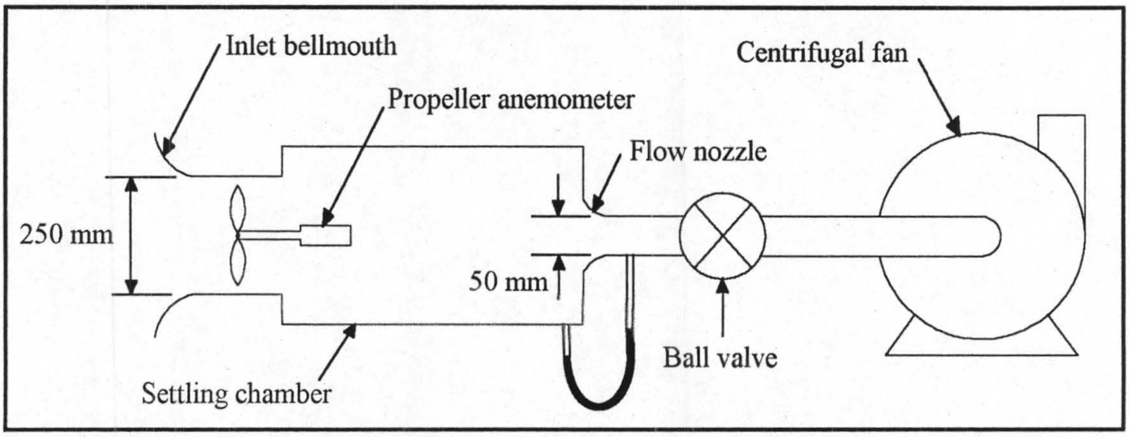

Figure G.3.1 : Apparatus used for the calibration of the propeller anemometers.

For various volume flow rates, the pressure drop over the flow nozzle and the voltage output of the propeller anemometer are measured. The volume flow rate through the system is calculated as follows :

$$V = \sqrt{\frac{2 \cdot \Delta p_{nozzle}}{\rho}} \cdot \pi \cdot 0.025^2$$

The velocity (v) measured by the anemometer is then

$$v = \frac{V}{\pi \cdot 0.125^2} = 0.04\sqrt{\frac{2 \cdot \Delta p_{nozzle}}{\rho}}$$

Table G.3.1 lists the experimental as well as the calculated values for each of the anemometers. Figures G.3.2 to G.3.8 show calibration data for each of the anemometers as well as a linear regression of the data.

Table G.3.1 : Propeller anemometer calibration data.

Anemometer	Δp_{nozzle} (Pa)	E (V)	v (m/s)
1	0	0.000008	0.000
1	89	0.032156	0.483
1	226	0.054300	0.770
1	374	0.067752	0.990
1	630	0.092276	1.286
1	847	0.102851	1.491
1	1508	0.142315	1.989
1	2347	0.181768	2.481
1	4083	0.234293	3.273
2	0	0.000005	0.000
2	88	0.028215	0.480
2	240	0.052583	0.793
2	382	0.068378	1.001
2	694	0.095611	1.349
2	834	0.105671	1.479
2	1506	0.142875	1.988
2	2355	0.178328	2.485
2	4054	0.235130	3.261
3	0	0.000001	0.000
3	100	0.030018	0.512
3	212	0.048359	0.746
3	383	0.062911	1.002
3	617	0.088477	1.272
3	826	0.099535	1.472
3	1502	0.138469	1.985
3	2346	0.173368	2.481
3	4032	0.224911	3.252
4	0	0.000002	0.000
4	96	0.014604	0.502
4	222	0.028822	0.763
4	371	0.043638	0.987
4	615	0.063039	1.270
4	834	0.079040	1.479
4	1510	0.117666	1.990
4	2320	0.153905	2.467
4	3372	0.183414	2.974
4	4070	0.203248	3.267

Table G3.1 : continued

Anemometer	Δp_{nozzle} (Pa)	E (V)	v (m/s)
5	0	0.000002	0.000
5	90	0.029036	0.487
5	216	0.048369	0.754
5	368	0.063078	0.985
5	612	0.084360	1.270
5	835	0.101467	1.483
5	1522	0.137954	2.003
5	2338	0.172226	2.482
5	3388	0.206561	2.988
5	4030	0.225312	3.259
6	0	0.000001	0.000
6	91	0.031594	0.488
6	217	0.049227	0.754
6	371	0.068191	0.986
6	850	0.105788	1.492
6	1520	0.142272	1.995
6	2330	0.176201	2.470
6	4090	0.228400	3.272
7	0	0.000000	0.000
7	86	0.020670	0.475
7	214	0.042555	0.750
7	377	0.064987	0.995
7	613	0.085465	1.269
7	840	0.098609	1.485
7	1482	0.133463	1.972
7	2342	0.175798	2.480
7	3306	0.206760	2.946
7	4048	0.229456	3.260

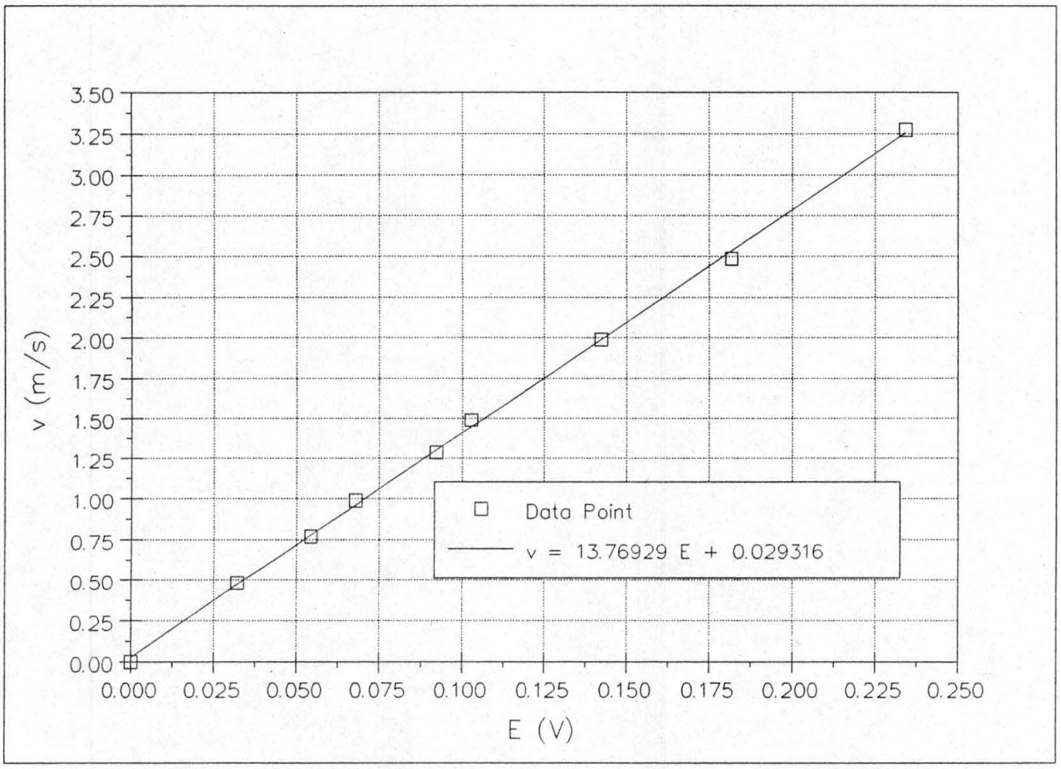

Figure G.3.2 : Calibration data for propeller anemometer number 1.

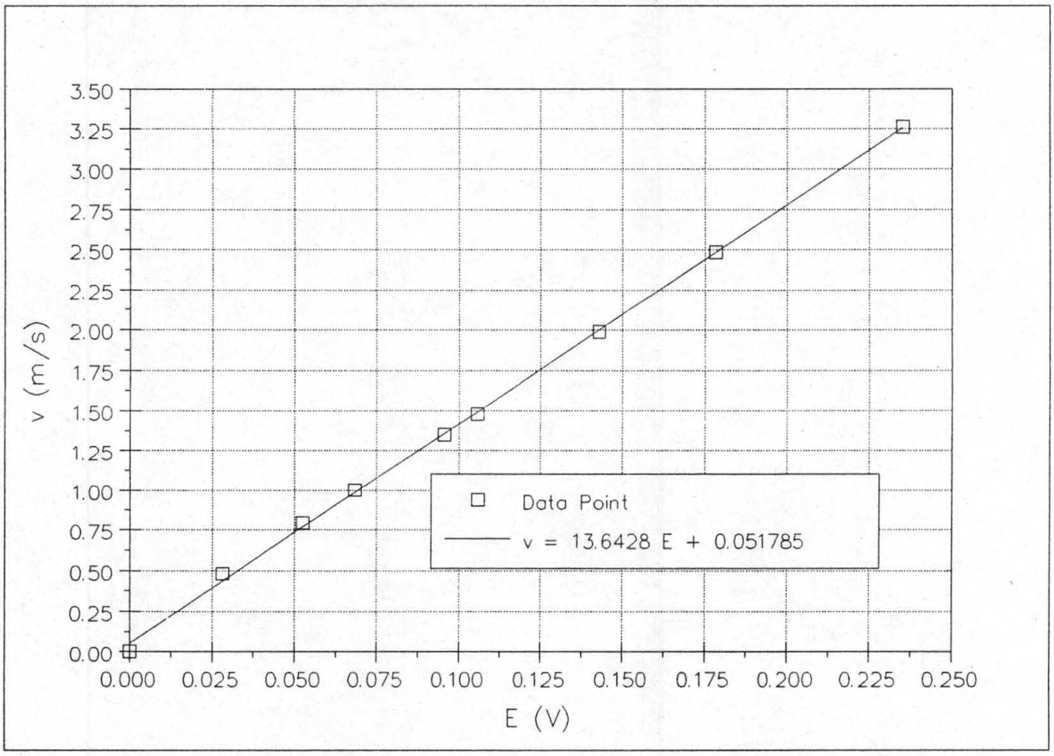

Figure G.3.3 : Calibration data for propeller anemometer number 2.

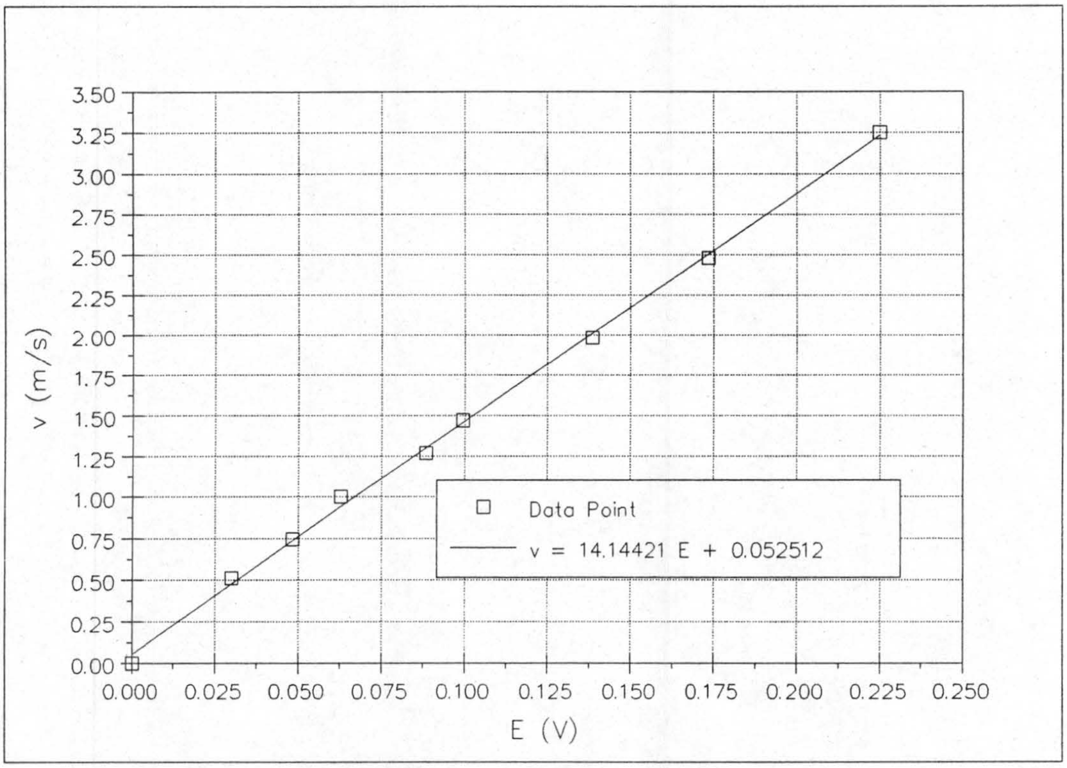

Figure G.3.4 : Calibration data for propeller anemometer number 3.

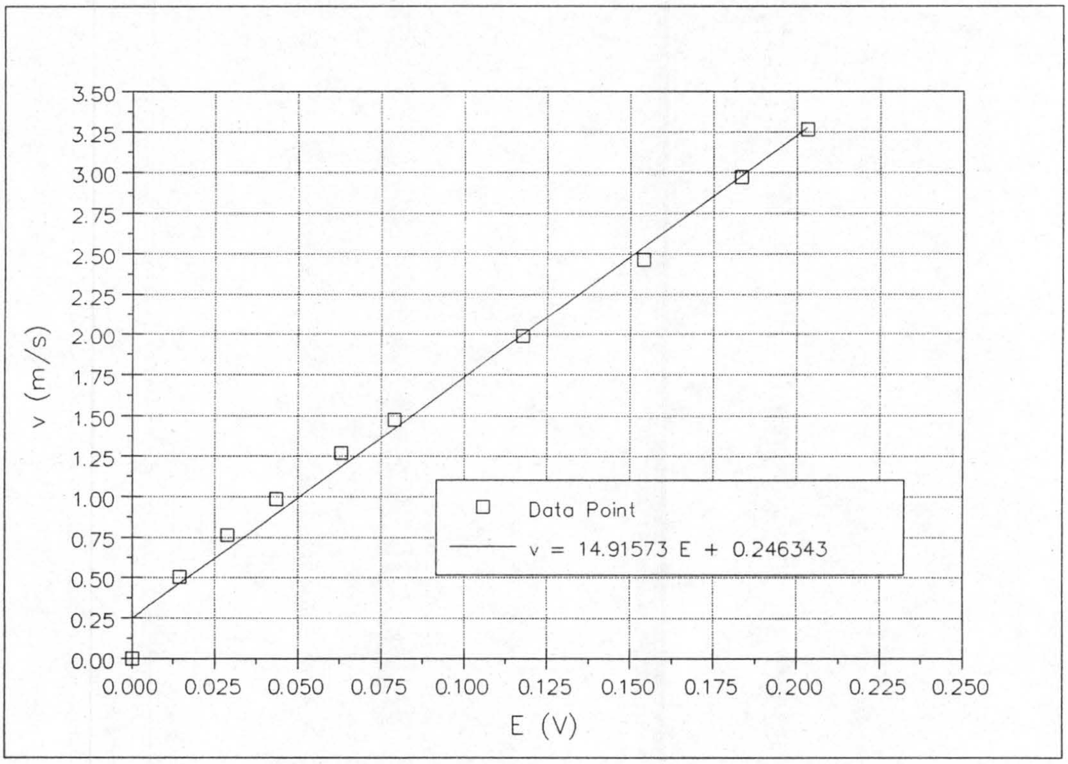

Figure G.3.5 : Calibration data for propeller anemometer number 4.

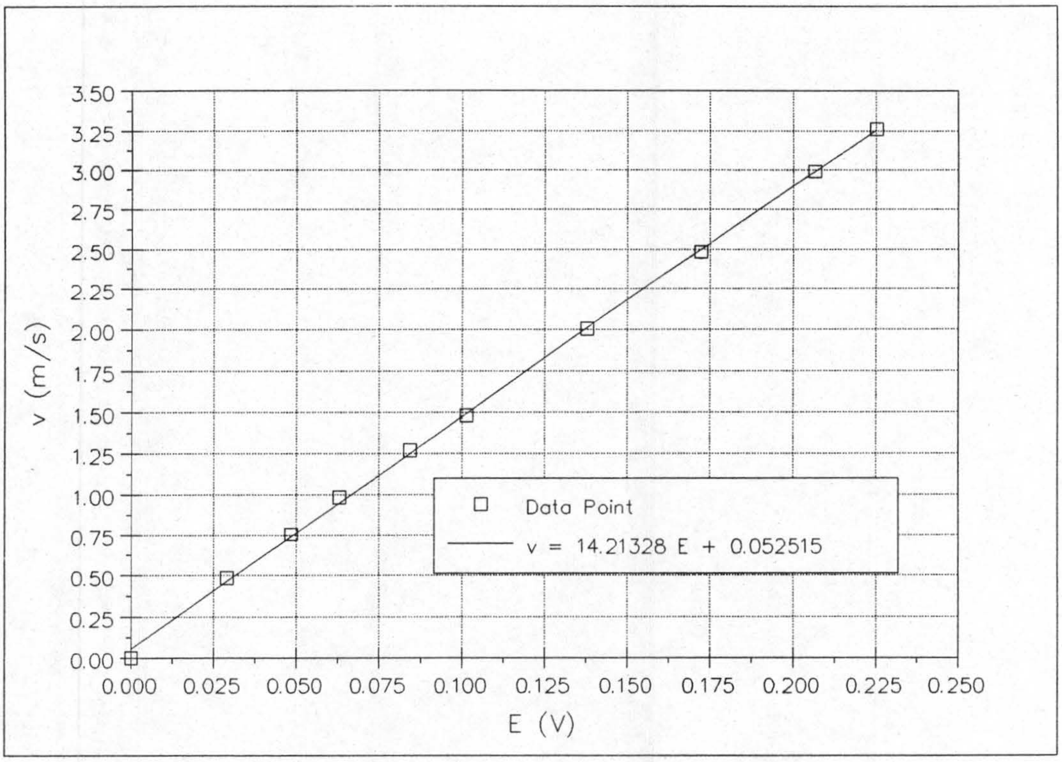

Figure G.3.6 : Calibration data for propeller anemometer number 5.

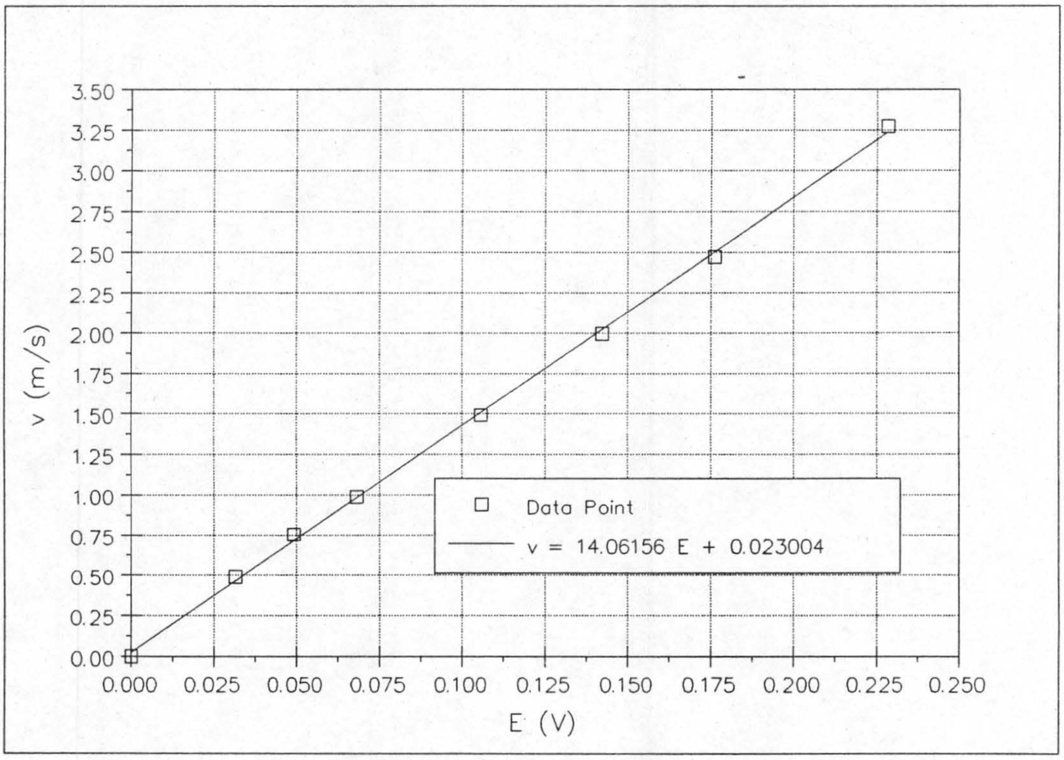

Figure G.3.7 : Calibration data for propeller anemometer number 6.

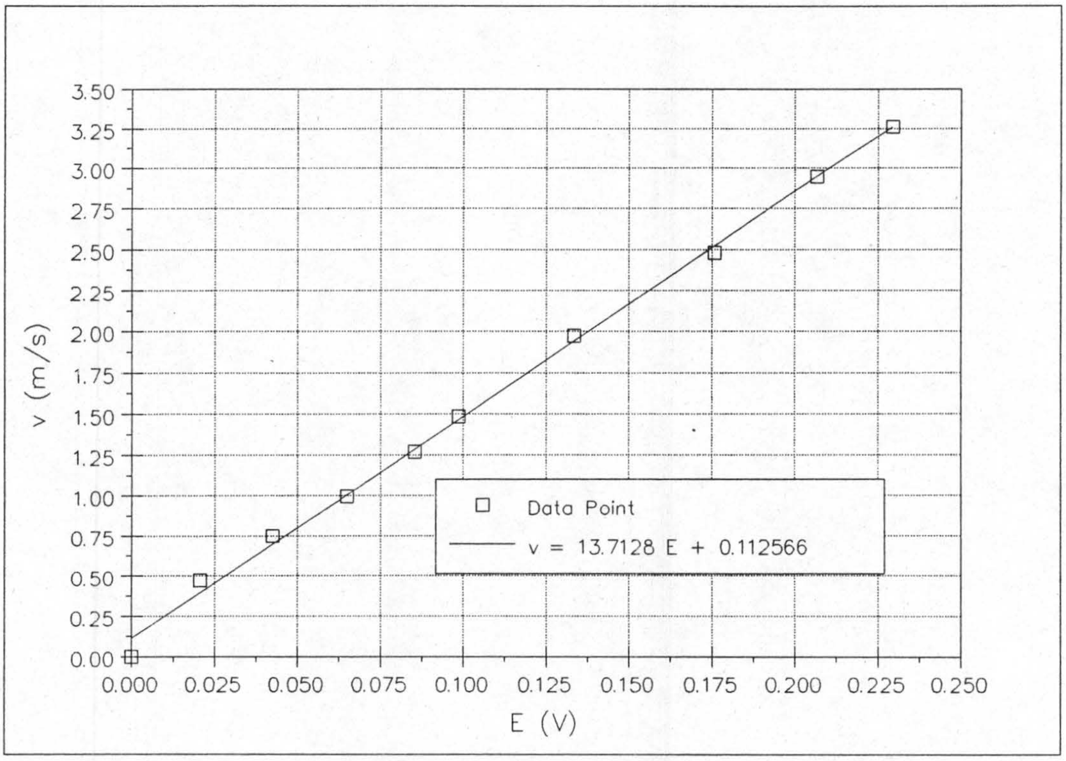

Figure G.3.8 : Calibration data for propeller anemometer number 7.